

Kurdistan Region-Iraq  
Ministry of higher education and scientific researches  
University of Sulaimani  
College of Science / Department of Geology



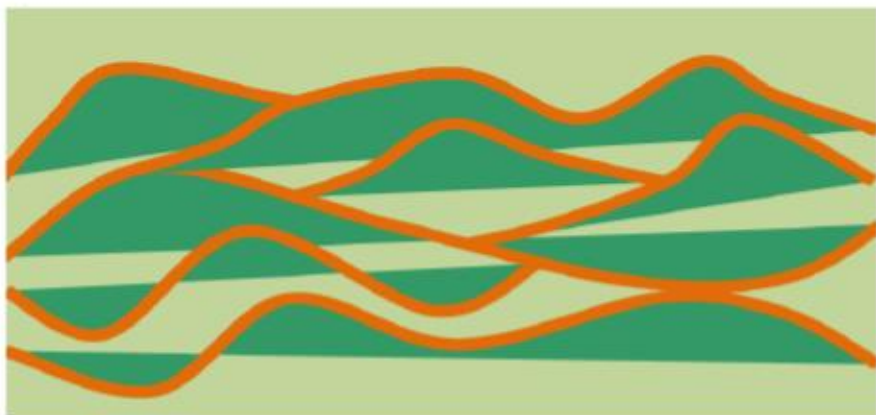
# Introduction to the Seismic Exploration

Hamid N. AISadi (PhD in Geophysics)

Ezzadin N. Baban (Professor; PhD in Geophysics)

Revised by

Bakhtiar Kadir Aziz (Professor; PhD in Geophysics)



First Edition, 2020

*Published by Sulaimani University, Kurdistan Region, Iraq*

---

**Kurdistan Regional Government, Iraq  
Ministry of Higher Education and Scientific Research  
University of Sulaimani  
College of Science / Department of Geology**



# **Introduction to the Seismic Exploration**

**Hamid Nasar Al-Sadi**  
*Expert; PhD in Geophysics*

**Ezzadin N. Baban**  
*Professor in Geophysics*

*Revised by*  
**Bakhtiar Kadir Aziz**  
*Professor in Geophysics*

***Published by University of Sulaimani, Sulaimaniyah, Kurdistan Region, Iraq.  
First Edition, 2020***

---

Copyright 2020 University of Sulaimani Publications, Sulaimaniyah,  
Kurdistan Region- Iraq.

All rights reserved. This publication or part hereof may not be reproduced or transmitted in any form or by any means, electronic or mechanical, including photocopy, recording, scanning or any information storage and retrieval system, without the prior written permission of the publisher and the copyright owner.

ISBN 978-9922-20-599-1

Recording No. at General Library of Sulaimaniyah: 1425

Introduction to the seismic exploration  
Hamid Nasar Alsadi, Ezzadin N. Baban

---

## PREFACE

Naturally, science is continuously advancing as the years pass by. Seismic Exploration is no exception to this rule. During the past three decades, great developments in the seismic exploration technology have taken place. These developments have occurred in all of the three exploration phases; acquisition, processing and interpretation techniques. The most prominent advances that took place during the past thirty years are the wide-spread implementation of the 3D surveying, pre-stack migration and seismo-stratigraphy.

This book is written primarily as an introductory comprehensive treatise covering the basic aspects of the 2D seismic-exploration techniques. Presentation of the subject matter is started with the basic theoretical background followed by the field acquisition techniques, data processing, and interpretation. It is addressing audiences in both of the academic and industrial establishments. The subject matter is presented in as clear and simple language as possible, avoiding excessive descriptions and unnecessary lengthy comments, using numerous illustration figures.

The book consists of eight chapters. The first four chapters cover the theoretical aspect of the subject including basic principles of the seismic field generation and associated propagation phenomena as reflection, diffraction, transmission, and refraction. The following three chapters are devoted to the 2D field acquisition techniques, seismic signal properties, and data processing procedures, normally applied to the field data. The last chapter is devoted for interpretation.

We would like to express our gratitude to all contributors.

**Hamid N. Alsadi & Ezzadin N. Baban**

---

## **ACKNOWLEDGMENT**

We have to start by great thanks to our awesome wives, sons and daughters.

We would like to express my gratitude to the all people who support, offered comments, evaluation and assisted in the editing, and proofreading saw us through this book;

We would like to thank professors; Prof. Dr. Fadhil Ali Ghaib at department of geology, college of science, University of Salahaddin-Erbil and Assist. Prof. Dr. Omer Qadir Ahmed at department of geology, college of science, University of Sulaimani for their scientific evaluation and Mrs. Najat Ismael Sayakhan, Department of English language, college of Basic Education, University of Sulaimani for language's evaluation and their feedback on this book.

We wish to extend our sincere thanks to all staffs of the Central Committee for books approving and publishing at Sulaimani University for invaluable help, comments and approving in preparation of the book.

We would like to thank Presidency of Sulaimani University, College of Science and Geology Department for enabling us to publish this book.

Thanks to everyone on our publishing team.

---

# Contents

<b>1.</b>	<b>INTRODUCTION.....</b>	<b>1</b>
	1.1 Historical Review .....	1
	1.2 The Geophysical Exploration Project.....	1
	1.3 Geophysical Exploration Methods.....	2
	1.3.1 The Seismic Method .....	2
	1.3.2 The Gravity Method.....	3
	1.3.3 The Magnetic Method .....	4
	1.3.4 The Electrical Method.....	6
	1.3.5 The Radioactivity Method.....	10
	1.4 Oil-Well Drilling .....	10
	1.4.1 Drilling of the Exploration-Well .....	11
	1.4.2 The Oil-Well Rotary Drilling .....	12
	1.4.3 The Drill-Hole and Well Casing .....	12
	1.5 Well Geophysical Logging .....	14
	1.5.1 Electrical Logging .....	15
	1.5.2 Radioactivity Logging .....	18
	1.5.3 Acoustic Logging .....	22
	1.5.4 Log Interpretation.....	25
	1.6 Well Completion.....	26
<b>2.</b>	<b>SEISMIC WAVES .....</b>	<b>29</b>
	2.1 Theory of Elasticity.....	29
	2.2 Stress.....	29
	2.3 Strain.....	30
	2.3.1 Common Types of Strain.....	30
	2.3.2 The Longitudinal Strain.....	31
	2.3.3 The Shear Strain.....	32
	2.3.4 The Cubical Dilatation .....	33
	2.3.5 Stress-Strain Relationship .....	34
	2.4 The Elastic Moduli.....	35
	2.5 Classification of Common Elastic Waves.....	37
	2.5.1 Body Waves .....	38
	2.5.2 Surface Waves .....	40
	2.5.3 Seismic Noise .....	41
	2.6 Propagation of Seismic Waves.....	43
	2.6.1 The Seismic Field.....	43

---

---

2.6.2 Concepts of Wave-Fronts and Rays .....	43
2.6.3 Huygens' Principle .....	44
2.6.4 Concept of the Interface .....	45
2.6.5 Changes of Propagation Direction at Interfaces .....	46
2.6.6 Wave Conversion at Interfaces .....	48
2.7 <i>Effect of the Medium on Wave Energy</i> .....	48
2.7.1 Geometrical Spreading .....	49
2.7.2 Inelastic Attenuation .....	50
2.8 <i>The Seismic Trace</i> .....	50
2.9 <i>Seismic Energy Measurement and the DB Unit</i> .....	51
<b>3. SEISMIC WAVE REFLECTION AND DIFFRACTION .....</b>	<b>53</b>
3.1 <i>The Commonly-Recorded Seismic Events</i> .....	53
3.2 <i>The Seismic Wave Reflection</i> .....	54
3.2.1 Reflection Coefficient at Normal Incidence .....	54
3.2.2 Geometry of Reflection from Horizontal Reflectors .....	56
3.2.3 Reflection from Multiple Reflectors .....	56
3.3 <i>The Normal Move-Out (NMO) Concept</i> .....	58
3.3.1 NMO in Case of Horizontal Reflector .....	58
3.4. <i>CDP, CRP, and CMP in Case of Horizontal Reflector</i> .....	59
3.5 <i>The Seismic Wave Diffraction</i> .....	60
3.5.1 The Point-Diffractor .....	60
3.5.2 Diffraction Travel-Time Function .....	61
3.5.3 The Diffraction Hyperbola .....	62
<b>4. SEISMIC REFRACTION .....</b>	<b>65</b>
4.1 <i>Introduction</i> .....	65
4.2 <i>Advantages and disadvantages Seismic Refraction</i> .....	66
4.3 <i>Wave Refraction and Snell's Law</i> .....	66
4.4 <i>Seismic ray Paths in the subsurface layers</i> .....	70
4.4.1 Case of horizontal reflectors: .....	71
4.4.2 Case of Dipping refractors (layers) .....	77
4.2.3 Faulted Planar Interface .....	81
<b>5. 2D SEISMIC REFLECTION SURVEYING .....</b>	<b>83</b>
5.1 <i>The Shot-point</i> .....	83
5.2 <i>Seismic Trace Modes of Display</i> .....	83
5.3 <i>The Spread Configuration</i> .....	85

---

5.4	<i>The CDP Concept</i> .....	86
5.5	<i>The Seismic Profiling Technique</i> .....	86
5.6	<i>The Coverage Diagram</i> .....	87
5.7	<i>The Fold of Coverage</i> .....	89
5.8	<i>Seismic Reflection Data Acquisition</i> .....	90
5.9	<i>Seismic Energy Sources</i> .....	90
5.9.1	<i>Land Seismic Sources</i> .....	90
5.9.2	<i>Marine Seismic Sources</i> .....	95
5.10	<i>Seismic Detectors</i> .....	95
5.11	<i>The Seismic Data Recording</i> .....	97
5.12	<i>Field Measures for Signal Enhancement</i> .....	97
5.13	<i>Determination of the LVL Properties</i> .....	99
5.14	<i>The Seismic Field Crew</i> .....	101
<b>6.</b>	<b>3D SEISMIC REFLECTION SURVEYING</b> .....	<b>103</b>
6.1	<i>Nature is Three Dimensional</i> .....	103
6.2	<i>1D - 2D - 3D Terminology</i> .....	104
6.3	<i>Merits of the 3D Technique</i> .....	105
6.4	<i>3D Field Surveying</i> .....	107
6.5	<i>The CDP-Bin Concept</i> .....	108
6.6	<i>The Seismic Data Volume</i> .....	111
6.7	<i>Types of 3D Spread</i> .....	112
6.7.1	<i>Marine 3D Surveying Spreads</i> .....	112
6.7.2	<i>Land 3D Surveying Spreads</i> .....	113
6.7.3	<i>The Spread Template</i> .....	114
6.7.4	<i>The Swath Shooting Technique</i> .....	115
6.8	<i>3D Data Display</i> .....	116
<b>7.</b>	<b>REFLECTION DATA PROCESSING</b> .....	<b>119</b>
7.1	<i>Processing Definition and Objectives</i> .....	119
7.2	<i>Main Processing Activities</i> .....	121
7.3	<i>The Processing Sequence</i> .....	122
1.	<i>The Final Product</i> .....	124
	<i>The Input Raw Data</i> .....	124
7.4	<i>Data Re-Organization</i> .....	124

---

---

7.5 Pre-Stack Processing .....	127
7.6 Stack and Post-Stack Processing .....	135
7.7 Parameter Optimization.....	139
<b>8. SEISMIC REFLECTION DATA INTERPRETATION .....</b>	<b>141</b>
8.1 The Two Interpretation Tools .....	141
8.2 Structural Interpretation Sequence.....	142
8.3 Stratigraphic Interpretation Sequence .....	143
8.4 Interpretation Example .....	144
8.5 Seismic Attributes.....	150
<b>9. CASE STORIES .....</b>	<b>155</b>
9.1 Seismic study of a regional line in the Western Desert of Iraq.....	155
9.1.1 Introduction .....	155
9.1.2 Geology and Tectonic setting .....	156
9.1.3 Constructing of the regional line .....	157
9.1.4 Interpretation of the seismic regional line .....	159
9.1.5 Conclusions .....	169
9.2 Study of subsurface structures using seismic reflection data for Kalar– Khanaqin area / Kurdistan region, Iraq.....	171
9.2.1 Introduction.....	171
9.2.2 Geology and tectonic setting.....	171
9.2.3 Seismic data and methodology.....	172
9.2.4 Interpretation and discussion .....	174
9.2.5 Possibility of hydrocarbon occurrences.....	187
9.2.6 Conclusions .....	187
<b>REFERENCES.....</b>	<b>189</b>
<b>INDEX</b>	<b>199</b>

---



# 1. INTRODUCTION

## 1.1 Historical Review

The principles of seismic exploration techniques were used in Earthquake Seismology as early as the mid-nineteenth century. The actual seismic exploration by use of seismic waves was first applied in the early 1920s when Mintrop Seismos Company carried out seismic refraction surveys in Mexico and Gulf Coast areas of the United States of America. These surveys were mainly aiming at locating salt domes. By the early 1930s, the reflection surveying-method began to replace refraction techniques in exploring deeper geological structures. The first break-through in the surveying technique was the introduction in 1952 of the analogue magnetic recording and play-back recording. At about this time (in 1953) Vibroseis and Weight-dropping were introduced as energy generators. In the mid-1960s digital recording and processing were introduced. About ten years later, 3D seismic reflection surveying became in common use.

A full coverage and detailed account on the historical development of the exploration seismology is given by (Sheriff and Geldart, 1995, pp.3-32).

## 1.2 The Geophysical Exploration Project

A geophysical exploration-project normally follows a sequence of activities starting with field work and ending up with production of the subsurface geological model of the project area. An exploration project passes through a sequence of three phases, normally executed in sequence. The starting phase of a survey is collecting the field raw data through standard field procedures by which the geophysical measured values are recorded, usually on magnetic tapes. After completing the acquisition work, the recorded data are passed on to a processing center where it is subjected to certain processing steps for purpose of certain corrections and enhancing of the geophysical signal. The third and last phase of the project is to interpret the final processed data to extract the subsurface geological model of the area under exploration. The three phases of exploration work are summarized in Figure 1.1.

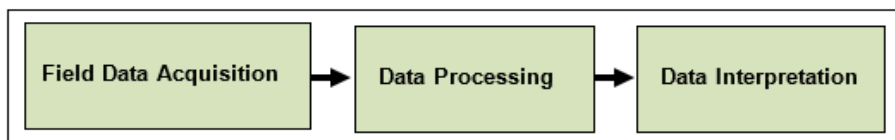


Figure 1.1 The three phases of the seismic exploration project; Data acquisition, processing, and interpretation.

---

### 1.3 Geophysical Exploration Methods

The main exploration methods employing geophysical principles are:

- (i) Seismic
- (ii) Gravity
- (iii) Magnetic
- (iv) Electrical
- (v) Radioactivity
- (vi) Electromagnetic

Seismic method is by far the most widely applied method in the exploration of oil and gas deposits. Gravity, magnetic, electrical, and radioactivity methods provide support data in the oil exploration and also applied as the main tools for other mineral exploration. Geophysical techniques which are using the earth geophysical potential fields (as gravity and magnetic fields) are often called Potential Methods. These methods are defined as follows:

#### 1.3.1 The Seismic Method

This method is based on generating seismic waves by a mechanical energy source at a point on, or just below, the ground surface and recording the arrival at another surface point of the reflected (or refracted) waves. From the travel-time measurements of these waves and wave motion-velocity, the structural variation of subsurface geological layers is mapped. Under favorable conditions, study of the seismic wavelet can provide information on the stratigraphic nature and hydrocarbon contents of the traversed rocks. The raw seismic data (normally recorded on magnetic tapes), are passed through a sequence of processing steps followed by a set of certain interpretation procedures in order to obtain the final result, which is a model of the subsurface geological structure. Detailing of this technique is the subject of this monograph.

There are two main techniques involved by the seismic method; the reflection and the refraction methods (Figure. 1.2).

In a seismic experiment, there are generally four types of wave arrivals that can be detected by a receiver placed at an offset-distance from the seismic source. These are:

- Reflection Arrivals
- Refraction Arrivals
- Diffraction Arrivals
- Direct (Transmission) Arrivals

These four types of seismic wave arrivals can be considered to be the main seismic exploration-tools involved in any seismic exploration project.

---

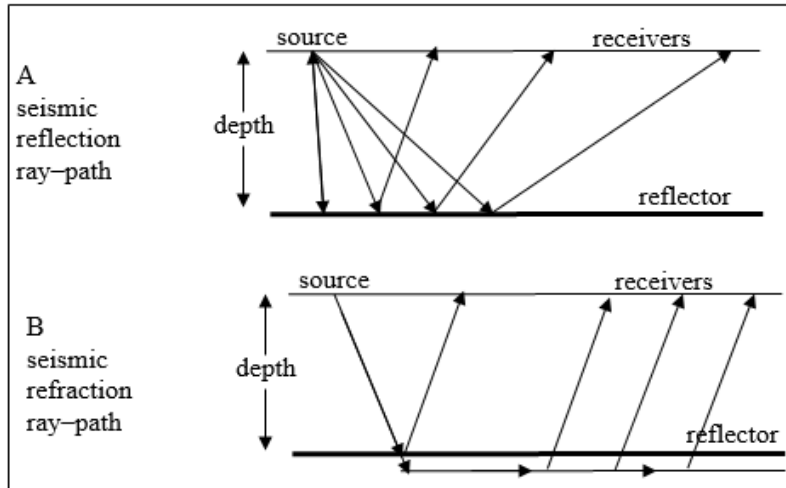


Figure 1.2 Essence of the two seismic techniques; reflection (A) and refraction (B).

### 1.3.2 The Gravity Method

In this method the acceleration due to the earth gravitational force is measured at a grid of points distributed over the survey area. The observed gravity values are reduced to what they would be, had they been measured at a fixed datum level (normally fixed at the sea level). The so-corrected gravity values are contoured to show the variation of the gravity values (in acceleration units) throughout the area.

It is known that gravity changes depend on changes in density as well as on the depth of the causing geological anomaly. Thus, as the density increases (relative to the host medium), the gravity attraction (or acceleration value) of a rock mass at a given depth increases. If, however, a constant-density rock mass exists at different depths, the corresponding gravity values are different. Gravity values of deeper rocks are less than those for shallower rocks. A typical example for this case is the gravity changes normally exhibited over an anticline, where the gravity change (called the gravity anomaly) is greater over the anticline axis falling to lower values over the flanks. A structural feature showing relative density-deficiency (such as a salt dome) gives an inverted bell-shaped anomaly normally referred to as negative anomaly which is of opposite shape to that exhibited by the relatively denser-rock geological anomaly (positive anomaly). The principle is shown in (Figure 1.3).

The measuring instrument normally used in gravity surveying are called the gravity meters (or gravimeters) they are designed to measure gravity variations rather than absolute gravity values. These instruments are capable of measuring gravity changes to less than a tenth of a milligal. The gravity unit (the gal) is defined to be equal to  $1 \text{ cm/sec}^2$ . Thus, the gravimeter is capable of measuring gravity variations to within about ten-millionth of the earth's total gravity field which is about 1000 gal.

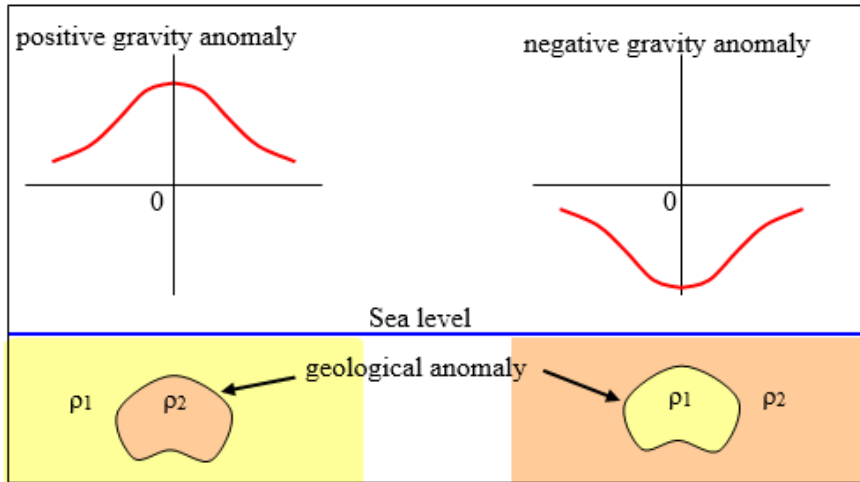


Figure 1.3 Dependence of the gravity-anomaly sign on density contrast ( $\rho_2 - \rho_1$ ) of the geological anomaly. Positive sign ( $\rho_2 > \rho_1$ ) for density surplus and negative sign ( $\rho_2 < \rho_1$ ) for density deficiency.

Gravity surveying is ideally suited to map subsurface rock layers or mineral deposits that show density or depth variations such as folded strata, salt domes, heavy mineral deposits, and subsurface cavities. Because of the two factors affecting the measured gravity change (density and depth), interpretation of the gravity data suffers from ambiguity in the determination of the real geological anomaly responsible for creating the gravity anomaly. For this reason, an additional tool or information is needed to determine the true causal geological anomaly.

Details of this method can be found in many standard geophysical publications. A simplified monograph on the subject that can be referred to is Alsadi and Baban, 2014.

### 1.3.3 The Magnetic Method

As often stated in the geophysical literature, the magnetic method is considered to be the oldest method applied in geophysical exploration. The Magnetic Phenomenon is force of attraction or repulsion due to electron arrangement in certain substances having magnetic properties. The magnetic body (magnet) is made up of small parts called magnetic domains which are lined up in the same direction. Unlike the case of gravity, the magnetic body has always two poles (dipole-body); one has attraction effect and the other has repulsion effect. An end-point of a long bar magnet can be considered as an isolated magnetic pole for certain computational purposes. The concept of line-force representing the magnetic field and the convention used in force direction relative to the magnetic poles are shown in Figure 1.4.

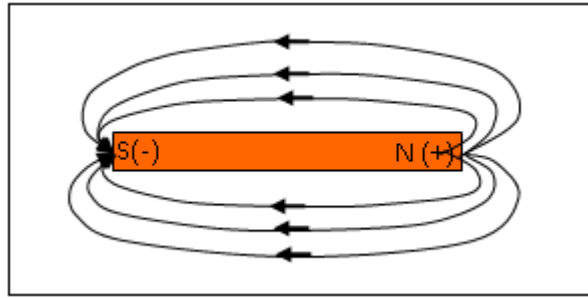


Figure 1.4 Magnetic poles of a magnetic body, are two points near magnet ends to which force lines are pointing; the North (+N) and South (-S) poles. Arrows indicate the conventional movement-direction of a unit positive pole placed in the magnetic field.

Magnetic surveying, basically depends on the variation in the body-ability of being magnetized when exposed to a magnetic field. This property called the magnetic susceptibility, which, differs with different materials. Sedimentary rocks are generally of small susceptibility values compared with metamorphic or igneous rocks. For this reason, magnetic surveying is normally carried out to explore magnetized materials, such as iron-ore deposits, igneous intrusions, and surfaces of basement rocks. Rocks which have high-susceptibility mineral contents, acquire magnetic intensity by magnetic induction process creating a magnetic field which is added to the already existing Earth ambient magnetic field.

As a result of this phenomenon a magnetic anomaly of a value proportional to the intensity of magnetization (of the causing geological anomaly) is created. After certain processing measures these anomalies are interpreted to reveal the causal geological structure.

The unit of magnetic-field measurement is the Oersted, where one Oersted is equal to one dyne per unit magnetic pole. In practice, another smaller unit ( $\gamma = 10^{-5}$  Oersted) is used. More recently an SI unit called nanotesla where 1 nanotesla is equal to 1 gamma. The SI (System International) uses MKS measurement units. The total magnetic field of the Earth is about half an Oersted.

In petroleum exploration, aeromagnetic surveying is usually conducted to delineate major structural changes of areas such as sedimentary basins, and regional geological changes including mapping of sedimentary basins and major rift zones. On smaller scales, magnetic surveying can be used to detect magnetic minerals such as magnetite and other iron ore deposits. The method is used to explore near-surface geological changes (such as dykes) and buried archaeological objects.

As it is the case with all of the other exploration potential methods, the magnetic method suffers from the ambiguity problem in the interpretation process. The degree of uncertainty due to this problem is reduced by using additional independent geological information.

### 1.3.4 The Electrical Method

This method is based on the relationship between the electrical conductivity (or electrical resistivity) property and electrical current (or electrical voltage). Some electrical surveys are based on artificially-generated electrical currents while others are using the earth naturally-generated electrical currents. These are summarized in the table 1.1:

Table 1.1 shows artificial and natural electrical field methods

Artificial Electrical Field Methods	Natural Electrical Field Methods
Electrical Resistivity	Self-Potential (SP)
Induced Polarization (IP)	Telluric Currents
Equipotential & Electromagnetic (EM)	Magnetotelluric

Electrical methods are mainly used for the exploration of ore-bodies, minerals, ground water resources and for relatively shallow geological anomalies. Because of lack of deep penetration its use for oil exploration is limited. Most of the methods are effective only for shallow depths (300 m – 500 m).

#### Artificial-Source Electrical Methods

##### (i) Electrical Resistivity Surveying:

In the electrical resistivity method, a DC electric current (or very low frequency AC) is introduced into the ground. From the voltage drop measured over a defined distance, the effective (apparent) resistivity is mapped and then interpreted in terms of geological changes. The simplest field technique, called Wenner configuration, consists of two current electrodes and two voltage measuring electrodes as shown in Figure 1.5.

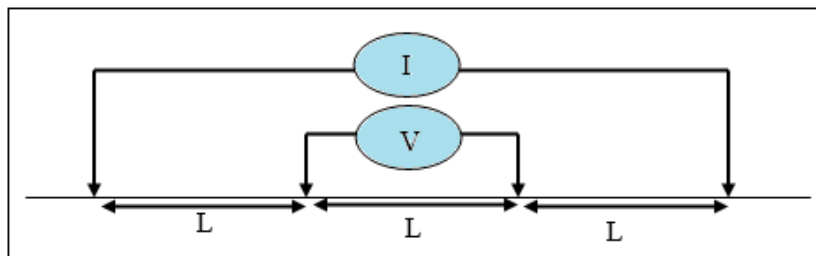


Figure 1.5 Principle of the Wenner configuration used in electrical resistivity surveying.

The two approaches (forward and inverse) modeling processes are applied in interpreting resistivity data. The more widely used method is done by applying a trial-

and-error method (model-analysis method). By comparing the observed data with curves computed for defined geological models, a subsurface geological model is determined.

Resistivity surveying is particularly effective in exploring discontinuities as in determination of layering, faults, sills and dykes, especially when these are not too deep features. The method is usually applied in engineering geophysical studies, as in determining of the water table and other ground-water investigations.

### ***(ii) Induced Polarization Surveying***

The Induced Polarization method (IP method) uses the decay time of an electric potential, induced after an electric current fed to the ground, is switched off. The phenomenon is associated with electrochemical reactions activated by the electric current which disturbs the ion distribution in the affected ground material which gets back to normal state after the applied electric current is stopped at an instant,  $t_0$  (Figure 1.6).

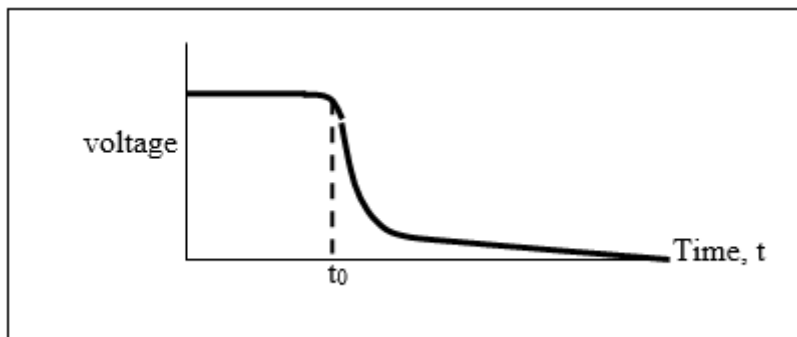


Figure 1.6 Voltage drop after the applied electric current is switched off at time ( $t_0$ ), the procedure used in the IP method.

The method is used mainly for purposes of metallic minerals and ground water exploration. For the field surveying, the same electrode set up for resistivity is also used. Thus, using four electrodes (called dipole-dipole array) is used in IP surveying. The polar dipole system is preferred where the voltage electrode spacing is decreased to minimize the effect of wire-currents.

### ***(iii) Equipotential and Electromagnetic Surveying***

The equipotential method uses the electric potential field generated by a fixed electric-current electrode while the electric potential is mapped by a moving electrode. Instead of using DC-electrodes, another method (called the Electromagnetic method) uses an electric AC of few hundred-to-few kilohertz, induced into the ground by a source-coil and received by another coil, the receiver-coil. The transmitter coil induces an alternating (primary) magnetic field, while the receiver coil senses the ground-

generated alternating (secondary) magnetic field combined with the primary. The combined magnetic fields induce AC in the secondary coil. This current is then measured and converted into the combined magnetic field at the location of the receiver. From comparison of the combined magnetic field with the primary magnetic field (which is known), the contribution of the anomalous body is determined and then interpreted into geological information.

In addition to ground surveying, there is the airborne EM surveying where the transmitter coil is fixed to the aircraft and receiver is mounted in a "bird" trailed behind. The EM method is used for exploring base-metals and ground water accumulations.

### ***Natural-Source Electrical Methods***

There is another less commonly applied electrical group of methods which are dependent on measurements of the earth natural electric field. Self-potential (SP), Telluric Current and magneto-telluric methods are typical examples of such techniques. These methods are used to determine large-scale crustal structural variations as sedimentary basins and regional-scale geological variations.

#### ***(i) Self Potential (SP) Surveying***

Mineralized zones found in the upper part of the Earth crust and some ore bodies found at shallow depths, develop their own natural electric fields. In particular, a metallic sulfide body, which has part of it above the water table and the other below, shows such a phenomenon. It acts as a natural battery where ions, (due to differential oxidation) move from one part of the body to the other. The electrical currents are formed as a result of chemical reaction that takes place with the aid of the electrolytes present in the host medium.

The potential difference measured on the surface will map the potential anomaly (Figure 1.7).

---

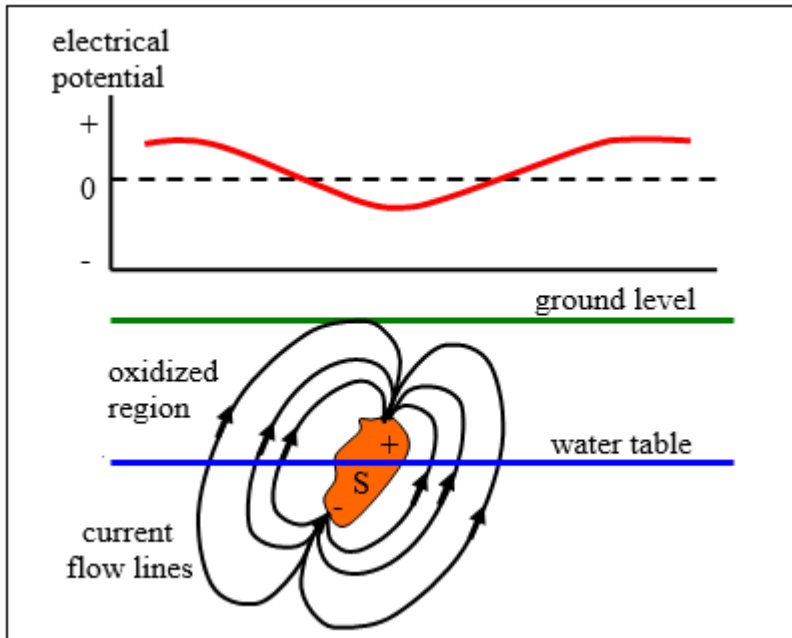


Figure 1.7 Sulfide body (S) acting as a natural battery, causing abnormality in the generated electrical potential.

The SP method is typically used to map the electrochemical potential generated by buried sulfide bodies.

### (ii) Telluric Currents Surveying

The term *telluric current* is used for the natural electric currents that flow horizontally in the upper part of the Earth crust. Variation of the current-density, over the earth surface, is governed by the rock-resistivity changes. Thus, if a salt dome, for example, is found imbedded within relatively high conductivity-formations, the lines of currents flow will by-pass the salt body causing distortions in the potential gradient in the overlying surface cover. From the detected anomalous potential gradient, the causing geological change is then interpreted.

### (iii) Magneto-telluric Currents Surveying

Another related method, the so-called magneto-telluric method, involves simultaneous measurements of both voltages created by the telluric currents and the magnetic field induced by these currents. From plots of the alternating voltage and that of the associated magnetic field (as function of frequency), information on the resistivity as function of depth can be given.

**(iv) Audio-Frequency Magnetic Surveying**

There is still another closely related method which uses the audio-frequency variations in the electric field to study the earth resistivity. It is called Audio-Frequency Magnetic method, termed (AFMAG) method.

**1.3.5 The Radioactivity Method**

Some naturally occurring substances, such as Uranium and Thorium, emit particles and radiation energy, as a result of atomic disintegration. These chemical elements are called *radioactive elements*, and the phenomenon of the radiation, emitted in the form of particles and rays, is called *radioactivity*. Three types of radiation (Alpha, Beta, and Gamma) are released in this process. Radiation and energy characteristics of these types of radiation are summarized in the table 1.2, (Maton et al, 1995, p 269).

Table 1.2 Radiation types and radiation and energy characteristics

Radiation type	Radiation characteristics	Energy characteristics
Alpha particles	Positively-charged protons	Can be stopped by a sheet of paper
Beta particles	Negatively-charged electrons	Can pass through as much as 3 millimeters of aluminum
Gamma rays	High-frequency electromagnetic waves	Can pass through several centimeters of lead

All of the three types of radiation have the ionizing ability when colliding with atoms. This effect is the basis of radioactivity detection.

A detection instrument (the Geiger counter) was designed by Hans Geiger in 1928. It consists of a tube filled with an inert gas (helium or argon) at a reduced pressure. When radiation enters the tube, it removes electrons from the atoms of the gas, making them positively charged ions. The electrons move to wire in the tube, setting up an electric current which is amplified and fed into the recording device. The current produces a clicking sound that pulsates at a rate which is depending on the radiation strength. A counter, attached to the wire, measures the current which gives the radioactivity-reading accordingly.

**1.4 Oil-Well Drilling**

Drilling of the oil exploration well is considered to be the last phase of any oil exploration project. This work provides the direct information as regards geological and geophysical properties of the subsurface rock medium. The obtained drilling data give direct recognition of the rock formations and their mineral and fluid contents (hydrocarbons and water). Associated with the drilling process, are certain activities which help in getting these useful data. Most important of these are laboratory analyses

---

of the rock cuttings and from well cores. Also, drilling parameters and the well geophysical logging give valuable geological and geophysical information.

The common way followed in drilling is what is known the rotary drilling which is done by use of the drilling rig, especially designed to carry out this operation. A photo of typical oil-well rig is shown in Figure 1.8.



Figure 1.8 A typical rotary drilling rig, set up for oil-well drilling operation.

### 1.4.1 Drilling of the Exploration-Well

Since the first 69-foot oil-well (drilled by Drake in Pennsylvania, USA in 1859), drilling technology has witnessed great advances in the capability of drilling deep wells and in the control on the direction of the drilled well. Inclined wells and even horizontal drilling are now in common application.

Drilling of the first oil well after completing the geophysical exploration activities is called *Exploration drilling* or *Wildcat drilling*. There are other types of drilling labeled according to the purpose of the drilled well. For instance, it is called Production drilling when the well is designed for normal oil production, and Observation drilling for monitoring the behavior of the oil reservoir. Water or gas injection drilling is special for injecting water or gas to enhance the reservoir pressure.

An exploration well provides the following useful information:

- Drilling parameters (like drilling rate) give indications on the physical nature of rocks penetrated by the drilling process.
-

- Rock cuttings and cores provide direct information on the rock lithology and thicknesses of the penetrated rock formations.
- From the circulating drilling mud, cores, and cuttings presence of hydrocarbon matter can be readily seen.
- From the analyses of the well logs (as electrical logs, radioactivity logs, and sonic logs) valuable information are obtained on the geological specifications and on the hydrocarbon contents.

### 1.4.2 The Oil-Well Rotary Drilling

The common technique applied in drilling oil wells is what is called *Rotary Drilling*. The drilling process is done by rotating a column of steel pipes, with a drilling head (called the Bit) attached to its end. The rotating bit carves a hole through the rocks and in this way a drill-hole is made. Drilling mud is pumped through the pipe, returning to surface via the space between the drill pipe and well wall. Mud circulation will carry rock cuttings to surface and provide cooling and lubrication to the drilling process.

Drilling operation is done by the drilling rig, which is a mechanical steel structure designed in the form of a tower of height of (120 ft – 150 ft). A schematically representation of a typical oil-well drilling rig, with its principal parts, is shown in Figure 1.9.

The drilling rig, shown above, is made up of the drill tower (called derrick), drill pipes, drilling floor (Kelly Bush), and used other facilities to provide energy for rotating the pipe column and to circulate the drilling mud. The grinding process is executed by the rotating bit attached to the end of the drill pipe.

The more common types of bits are the *grinding bits* which produce rock cuttings that are removed by the circulating mud, and the coring tubular bits producing rock-cores.

### 1.4.3 The Drill-Hole and Well Casing

During the drilling process, drilling mud is circulating carrying with it the produced rock cuttings. According to the extent of penetration into the well wall of drill-fluid, three types of zones are recognized (Figure 1.10).

---

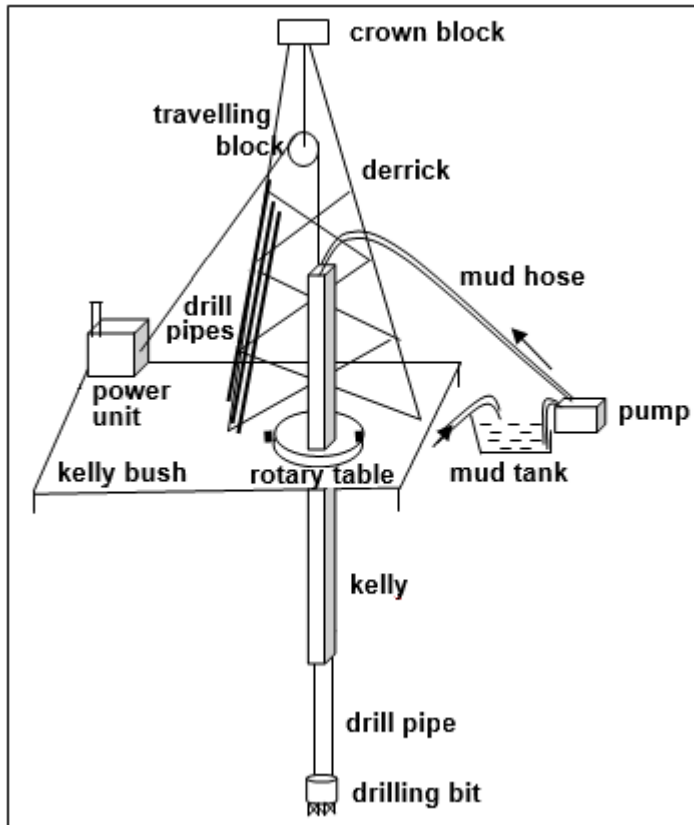


Figure 1.9 A Simplified sketch showing the main parts of a rotary drilling rig.

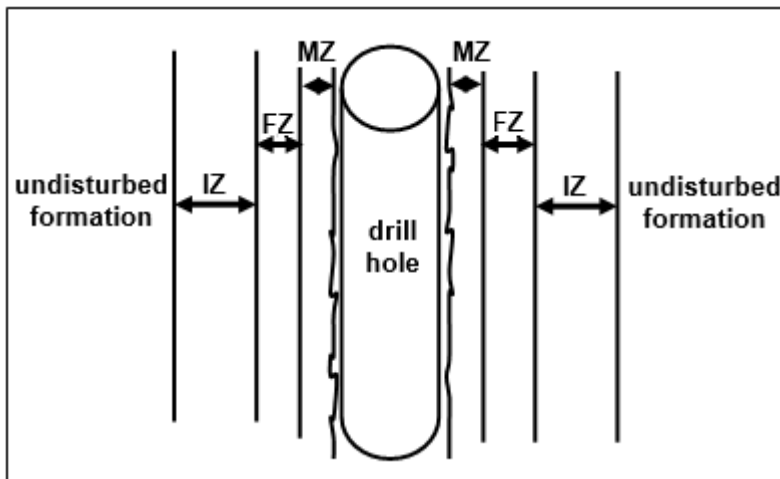


Figure 1.10 Mud invasion-zones into the well wall, labeled: mud-cake zone (MZ), flushed zone (FZ), and invasion zone (IZ).

### **Mud-Cake Zone (MZ)**

This is a thin coating of the well-wall which is of few tenths of an inch.

### **Flushed Zone (FZ)**

Natural fluid is completely replaced by the drilling fluid (several inches).

### **Invasion Zone (IZ)**

Drilling fluid infiltrated into the region surrounding the well (few inches as in shale to several feet as in porous sandstone).

After removing drill-pipes, a pipe column is lowered into the well, then cement is pumped-in to hold it tight in place. Casing prevents caving and fluid seeping. However, to allow oil and water to flow into the well, the casing is later on perforated at the appropriate places.

Electric logs cannot usually be run with casing, and sonic logging is severely disturbed. In general, all logging processes are carried out in uncased (open-hole) wells.

## **1.5 Well Geophysical Logging**

After completion of the drilling operations of a well, a group of technical activities (well logging) are done to extract direct information on the rock formations penetrated by the drilling process. Study of the penetrated rock formations (commonly referred to as formation evaluation) includes examination of its contents of rock cuttings, detection of hydrocarbon matter, and documentation of lithological and paleontological changes. The greater bulk of activities done at this stage is the geophysical logging of the drilled well which is always done as a concluding stage of the drilling operation of drilled exploration wells. Well logging give direct determination of petrophysical properties of the penetrated rock formations, which are essential in the formation evaluation and reservoir characterization processes.

The well log (or wireline log, as it is often referred to) is recorded by a special well logging tool (called sonde), carrying sensors which are lowered into the hole by a cable. The standard procedure is to start the measurements at the bottom of the hole and move upwards through the borehole. Measurement of a certain geophysical parameter is done either continuously or at discrete points. The output is recorded and normally produced as charts showing the measured value as a function of the well-depth (Figure 1.11).

---

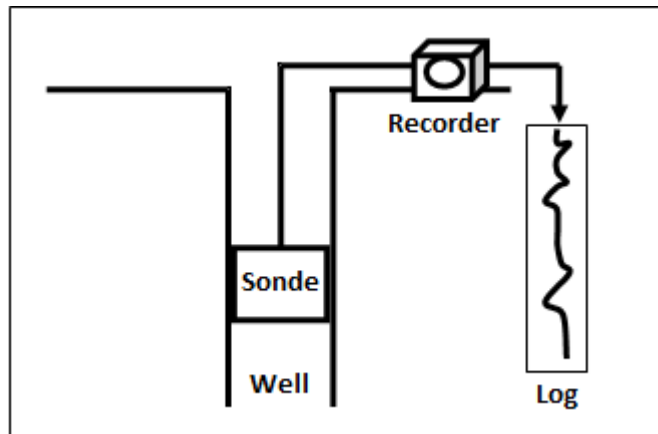


Figure 1.11 Principles of well logging.

The well logging process results in measurements-data normally plotted as charts called *well logs*. Since it was introduced by C & M. Schlumberger in 1928, the geophysical well logging technique has vastly developed into an indispensable formation-evaluation tool for the rocks penetrated by drill-holes. Logging methods can be divided into the three principal methods; electrical-, radioactivity-, and acoustic-logging.

### 1.5.1 Electrical Logging

Basically, electrical logging involves measurements of the variations of electrical resistivity and natural potential of rocks down the drilled well. Depending on the applied electrode configuration, the following techniques are in common use.

#### (i) Electrical Resistivity Logging

This type of electrical logging is based on a configuration whereby a DC (or low frequency AC) source electrode is lowered down the drill-hole and measuring the potential drop across a set of potential electrodes. The output is a continuous record of the variation of the electrical potential (or the corresponding apparent resistivity) with depth. This method must be applied in uncased wells.

There are two types of configurations, the normal-sonde and the lateral-sonde logging (Figure 1.12).

The resistivity log expresses measurements of the electrical resistivity in the usual (ohm units) for the rock medium surrounding the drill-hole. Penetration distance of the electric field in the penetrated rocks depends on the electrode spacing-distance. The larger the electrode spacing, the greater is the penetration distance.

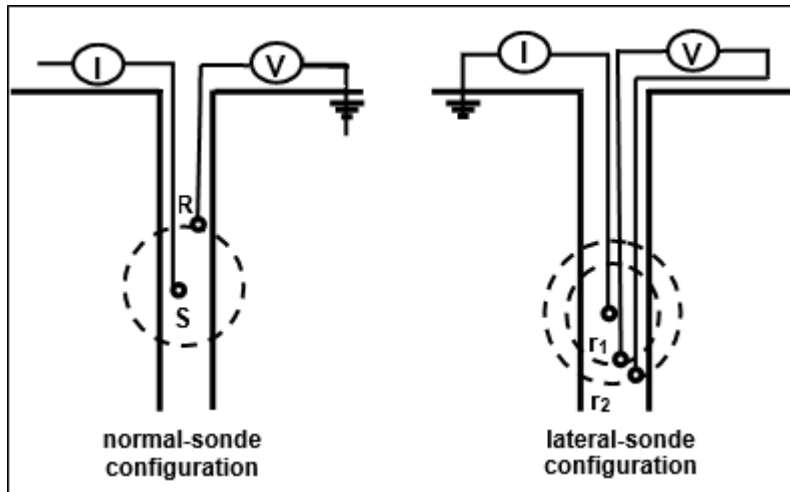


Figure 1.12 The two types of electrode configurations

The normal sonde electrode-configuration includes two electrodes; one source and one receiver spaced few feet apart. The instrument reading which is given in apparent resistivity units reflects the properties of the region near the source-electrode. The other type (the lateral-sonde configuration) is equipped with three electrodes; one source and two receivers. A variation was made on the lateral sonde whereby the current rays spread out horizontally (focused rays) rather than radially (unfocussed) spreading. This modified procedure is called *laterologging* and the produced resistivity chart is called *laterolog*. The lateral logs give more accurate and sharper boundary detection, in addition to reduction of effects of the mud and hole-diameter variations.

Resistivity logs help in the diagnosis of types and boundaries of formations. For example, low resistivity indicates higher porosity and permeability of water saturated formations, whereas increase of resistivity can reflect existence of oil and gas. In general, low-porosity rocks (as shale) and porous rocks saturated with salty water exhibit low resistivity. On the other hand, porous rocks saturated with low-salt fresh water, or saturated with oil will exhibit high resistivity. On this basis, resistivity logs serve as important and effective indicators for presence of oil.

### (ii) Electrical Induction Logging

The logging sonde uses coils instead of electrodes. A primary coil carrying an AC current, creates an alternating magnetic field which is inducing currents into the rock formations. These currents, in turn, create secondary magnetic field which induces, in receiving secondary coil, an AC which varies with the resistivity of the formations. The coil-sondes configuration is shown in Figure 1.13.

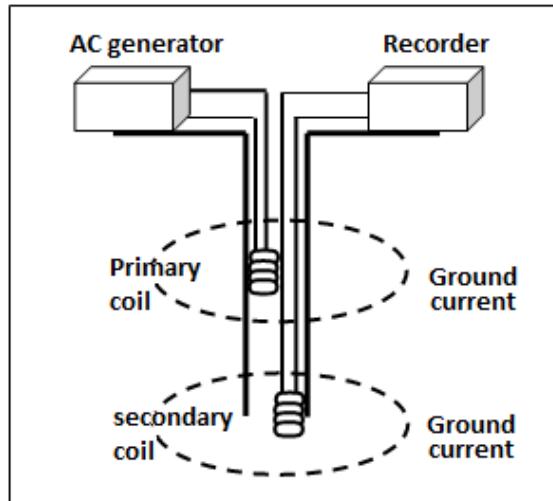


Figure 1.13 Coil-sondes configuration used in induction logging

Like lateral logging, there is a variation made on induction logging to give focused current radiation, for getting sharper boundary indication. Induction logging is used in wells filled with conducting, or no-conducting, drilling-mud.

### (iii) Spontaneous Potential (SP) Logging

This logging method depends on measurements of the natural electric potential (in millivolt units) of the rock medium surrounding the surveyed well. It is normally referred to as self-potential or spontaneous potential (SP) logging. It is used only in uncased hole filled with conductive mud. The measuring sonde is of simple configuration. It consists of only two electrodes; one is lowered into the well by an insulated cable and the other is fixed at the ground surface (Figure 1.14).

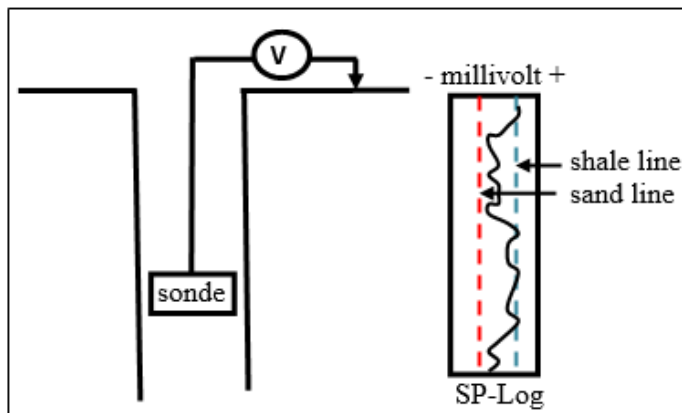


Figure 1.14 Configuration used in spontaneous potential logging with schematic representation of the SP log

This method, which needs no artificial current, can detect natural potential differences which develop at formation boundaries. Compared with resistivity logs, the SP logs give more sharp changes and hence more accurate formation-boundaries. Like lateral logging mentioned above, there is a variation made on induction logging to give focused current radiation for getting sharper boundary indication.

Interpretation of the SP logs depends on the manner of the electrical potential variation. As a general rule, changing of the log values towards positive potentials is considered as an indicative of impermeable rocks as shale or tight limestone or tight sandstones. When the change is towards negative potential, it is interpreted as being due to porous sandstones or porous limestone. In this way, the SP logs give useful indications on lithology, water salinity and help in determining of formation boundaries. In particular, it shows the boundaries of formations in sand-shale sequences.

These are determined with the help of drawing lines (sand and shale base-lines) in the produced SP log (shown in the figure above). It is commonly observed that shale beds give the same level of SP-readings allowing for drawing a straight line indicating shale SP-value. This is called the *shale line*. Similarly, a sand line can be drawn for sandstone SP-value. The inflection points in the SP-log indicate formation boundaries.

### 1.5.2 Radioactivity Logging

Radioactivity is the phenomenon of emission of particles and photons of electromagnetic energy from an atom. This radiation process occurs either naturally from unstable nuclii or induced by bombarding of stable nuclii by photons or particles.

Examples of such radioactive elements are uranium, thorium rubidium and potassium 40 which are most commonly found in shale and clay and less in sandstone and limestone.

There are three types of radiation; Alfa particles formed of charged helium nuclii, Beta particles formed of high-speed electrons, and Gamma rays of electromagnetic wave-energy. Out of these, only gamma ray is used in well radioactivity logging. The detection instrument is a Geiger or more usually is the scintillation counter which consists of a special crystal (like sodium iodide), which emits flashes of light as they absorb gamma-ray photons, hence the name (scintillation counter). A photoelectric tube converts these flashes into electric currents which are displayed in the form of a continuous chart (the radioactivity log).

Radio activity logs provide important information on rock lithological types, especially on those containing certain concentrations of radioactive minerals. Thus, these methods are ideal indicators of shales and clays which are, by nature, contain radioactive minerals in their makeup.

---

Three methods of gamma radioactivity logging are in common use. These are: natural Gamma-ray, Gamma-ray rock-density, and neutron Gamma-ray Logging methods.

**(i) Natural Gamma-Ray Logging**

This method uses a detector mounted on a sonde to measure the naturally emitted gamma rays from the radioactive minerals existing in the rock formations. Unlike electrical logging, gamma-ray logging can be run in cased wells, as well as in uncased wells, with detection penetration of few feet from the well walls.

The resolution power of formations boundaries is affected by the counting time of the instrument and sonde logging speed. Reasonable results are obtained with a counting time of 2 seconds and sonde speed of 150 mm per second. Measurements can be made in cased wells, but the intensity of radiation is reduced by about 30% in this case (Kearey and Brook, 2002, p.244).

In general, log values are interpreted as increase of the shale percentage, while the fall in the log values is interpreted as indication for sandstones and limestone rocks. To aid interpretation, it is possible to draw shale-lines and sand-lines on the log chart. An advantage of the gamma log is its capability of differentiating between shale and sandstones independent of the porosity and permeability characteristics of the rocks.

**(ii) Gamma-Ray Rock-Density Logging**

The sonde contains a gamma-ray source and a scintillation counter to detect the gamma ray which is back-scattered from the formations and received by a detector fixed at a certain distance from the source. It is also called gamma-gamma logging method.

The gamma-ray photons collide with the electrons of the elements in the formation resulting in loss of photon energy and back scattering of gamma-ray which has a wavelength different from that of natural gamma-rays. This is called *Compton Scattering Effect*. The collision rate and the back-scattered (secondary radiation) are proportional to electron density which is, in turn, proportional to rock-formation density. The principle of the Gamma-gamma logging is shown in Figure 1.15.

In practice, the gamma-ray detector is shielded to record only the secondary radiation, and the sonde is firmly pressed to well-wall and moved slowly (less than 30 feet/min) in order to maintain good contact. The produced chart (gamma-gamma log) expresses the formation-density log.

---

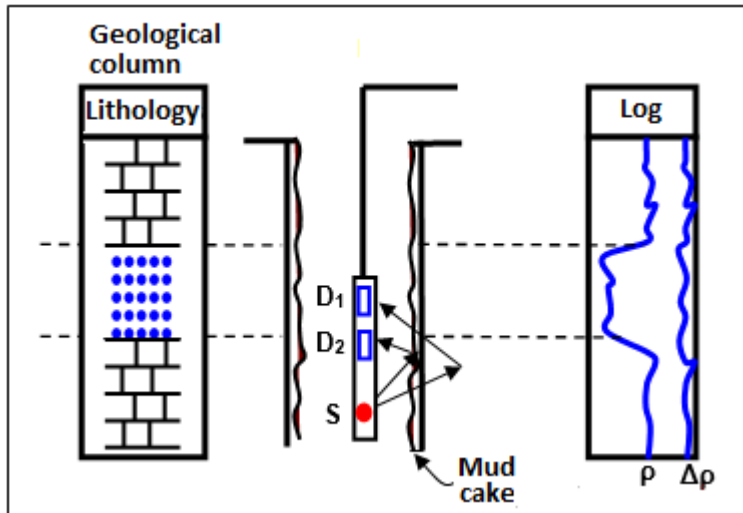


Figure 1.15 Principle of gamma-gamma log recording. Detectors, ( $D_1$ ) and ( $D_2$ ) record secondary and mud-cake radiations respectively. The symbol ( $S$ ) represents the source.

A variation to the method is introduced to provide corrections for mud-cake effect. As shown in the figure, above, a secondary detector  $D_2$  is included in the sonde which is responding to mud-cake and small wall irregularities. The resulting log (called Compensated Density Log) shows both of the bulk density ( $\rho$ ) and the density-correction log ( $\Delta\rho$ ).

Interpretation of the density log is based on the direct proportionality existing between the recorded scattered gamma ray intensity and the number of electrons found in the scattering rocks. The number of the scattered electrons is, in turn, proportional to rock bulk density.

This type of log can be used in computing porosity ( $\phi$ ) by using the following relationship:

$$\phi = (\rho_m - \rho_l) / (\rho_m - \rho_f)$$

where, ( $\rho_m$ ), ( $\rho_l$ ), and ( $\rho_f$ ) represent matrix density, log read-density, and pore fluid density respectively.

### (iii) Neutron Gamma-Ray Logging

The sonde consists of a neutron source and detecting scintillation counter placed at a fixed distance apart. The source is a small radioactive body (such as plutonium-beryllium) which emits neutrons during the process of radioactive decay.

When the source-generated neutron collides with a hydrogen nucleus (which is of a matching mass) its kinetic energy is reduced to an extent that it can be captured by a large nucleus (as the hydrogen nucleus) causing emission of a secondary gamma

radiation (capture gamma radiation). The principle of the logging is sketched in Figure 1.16.

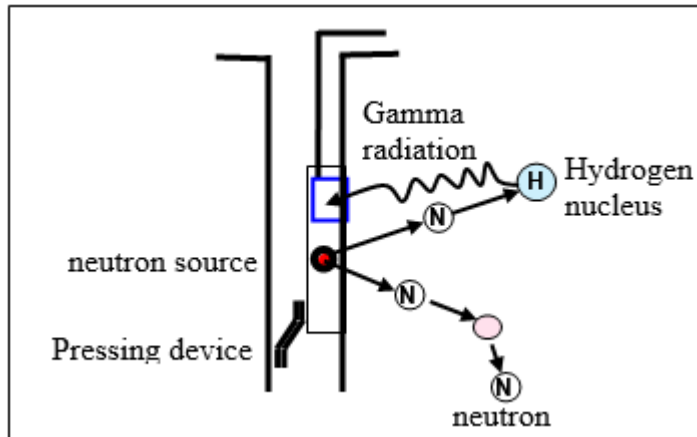


Figure 1.16 Principle of Neutron Gamma-Ray logging.

In the logging process, the sonde is moved at a speed of 30 ft/min with 2 seconds for the counting time. A skid (pressing device) is provided to keep the sonde in close contact to wall. The gamma radiation, generated by the capturing-phenomenon, comes from the material surrounding the drill-hole. The produced log (which can be run in cased or non-cased well) is displayed in the appropriate measuring units or in porosity percentages.

The intensity level of measured radiation is proportional to concentration of hydrogen, which exists in water, in hydrocarbon, and in hydrous minerals such as silicate-clays, micas, amphiboles, and gypsum. Thus, in carbonates and sandstones, hydrogen source is water and hydrocarbon found in the pores of the rock.

In shale however, mica and clay minerals contribute to hydrogen content as well as from pore water. In this case other types of logs (e.g. gamma-ray logs) are needed to distinguish shale from water-saturated porous sandstones or limestones. In general neutron logs are best in following up the porosity variation of porous rocks using the direct proportionality between porosity and gamma-ray intensity-level.

In short, neutron log, depend on the gamma ray generated from neutron bombardments of hydrogen atoms. The generated gamma ray, which is proportional to concentration of the hydrogen element in the penetrated rocks, is dependent on the water and hydrocarbon fluids in the rocks. This also means that high log values indicate high porosity.

It is useful to note that in case of presence of hydrocarbon gas in high porosity formations, density logs (gamma ray rock density log) is expected to give low log values compared with the neutron log vales at the same zone, where the neutron

readings expected to be relatively high. This means that both of the logs (density and neutron logs) are necessary in order to detect hydrocarbons (oil or gas).

### 1.5.3 Acoustic Logging

The purpose of this type of logging is basically for getting information on velocity of propagating acoustic (seismic) waves. Sonic logging, well velocity surveying (well shooting) and VSP surveying are included in this type of well-logging.

#### (i) Sonic Logging

The logging sonde, in its standard form, consists of two receivers about one foot apart and a source at about three feet from the nearest receiver. To correct for tilting and hole-irregularities effects, a dual source sonde is used, making what is called a borehole-compensated sonde (Figure 1.17).

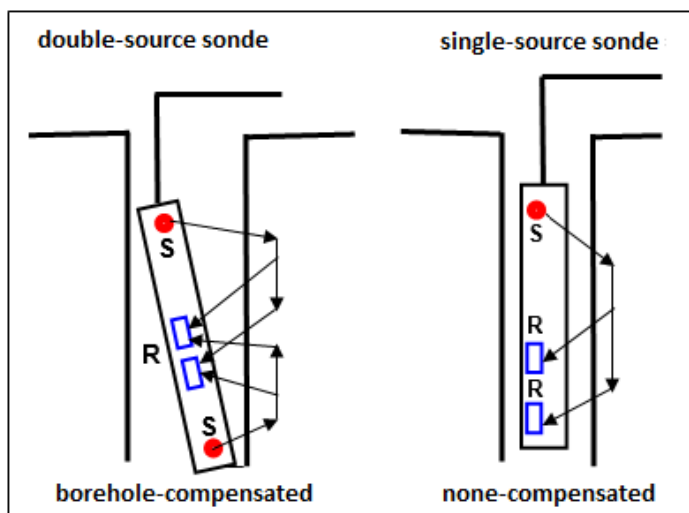


Figure 1.17 Configuration of source (S) and receiver (R) of the sonde employed in sonic logging.

The electronic structure of the sonde is designed in such a way, that the output is made to be the difference in the travel-times to the two receivers. The time difference, measured in time-units per one-foot, called *interval transit time*, is plotted (normally in micro seconds) against depth to give the continuous wiggly curve known as the *sonic log*. In the compensated sonic logging, seismic pulses are emitted alternately from the two sources and the transit times from the two oppositely traveling refracted P-waves are averaged electronically. The output (transit time) is plotted against depth, giving the borehole-compensated (BHC) sonic log (Figure 1.18).

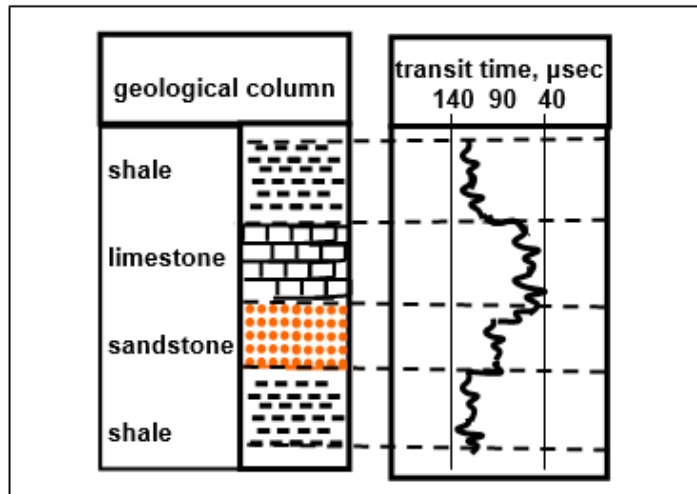


Figure 1.18 Sketch sonic log of a hypothetical geological column

The borehole compensated sonde (BHC) gives an average interval transit time which is plotted on a paper strip. The produced log in this case is normally referred to as BHC sonic log which is used to identify lithologies, determine formation boundaries, and in computing synthetic seismograms. The interval transit time can be integrated down the well to give the total travel time. This type of logging can only be run in an open (uncased) hole.

Sonic logs provide the interval transit time which represent travel-time (usually in microsecond units) of the P-wave in covering a distance (usually one foot). This parameter (the interval transit time) is useful in computing the porosity ( $\emptyset$ ) by using the following relationship:

$$\emptyset = (\Delta t_l - \Delta t_m) / (\Delta t_f - \Delta t_m)$$

where,  $(\Delta t_m)$ ,  $(\Delta t_f)$ , and  $(\Delta t_l)$ , represent transit times of matrix material, of pore fluid, and log read-transit time respectively.

### (ii) Well Velocity Surveying

A hydrophone-type detector is lowered down the well which is filled with the drilling fluid. The travel time of the seismic wave generated by a surface-placed shot and received by a detector placed at a formation boundary is recorded. The full log is obtained by repeating the recording at each boundary traversed by the well. From the measured travel time of direct arrivals, the average velocity and interval velocity are plotted as function of well-depth. The velocity survey is also called *check-shot survey*. Principle of the velocity survey setup and velocity-depth plot is shown in Figure 1.19.

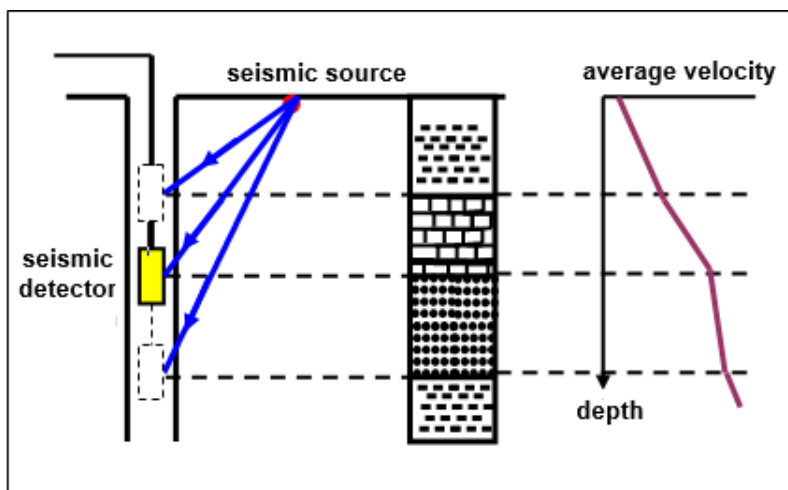


Figure 1.19 Principle of the well velocity surveying and a typical velocity-depth plot obtained from the survey.

The obtained velocity information is used to calibrate the sonic log and check the sonic-log integrated time (hence the name, check-shot surveying).

### (iii) Vertical Seismic Profiling (VSP)

Basically, the measurement set-up is the same as the check-shot recording system. The difference is in the recording duration time which is here extended to allow recording reflected waves as well as the direct arrivals. At each detector stop-location (normally at 25 m spacing), the recorded seismic trace is allowed to include events from up going reflected waves in addition to the first arrival (direct wave) event. The terms *down-going* wave and *up-going* wave are normally applied to refer to the direct and reflected waves respectively. The ray paths of the VSP shooting and the corresponding travel-time plot of the recorded waves are schematically shown in Figure 1.20.

A seismic pulse is generated on the surface from dynamite explosion or from an air gun submerged in a water filled hole. This is repeated at all of the hydrophone positions, normally positioned at 25 m-spacing down the well.

With an appropriate processing sequence, the final corrected VSP section is produced. Processing includes, data editing, correction to vertical time and velocity filtering for separating unwanted events. It is evident from the VSP section that downward events (primary and multiples) increase in time with depth, and the upward events (primary and multiples) decrease in time with increasing depth. By arranging the produced seismic traces (25 m spaced down the hole) a seismic VSP section is obtained. Each seismic trace of a VSP section contains events from down-going waves (direct and multiples arrival) and from up-going waves (reflections and multiples).

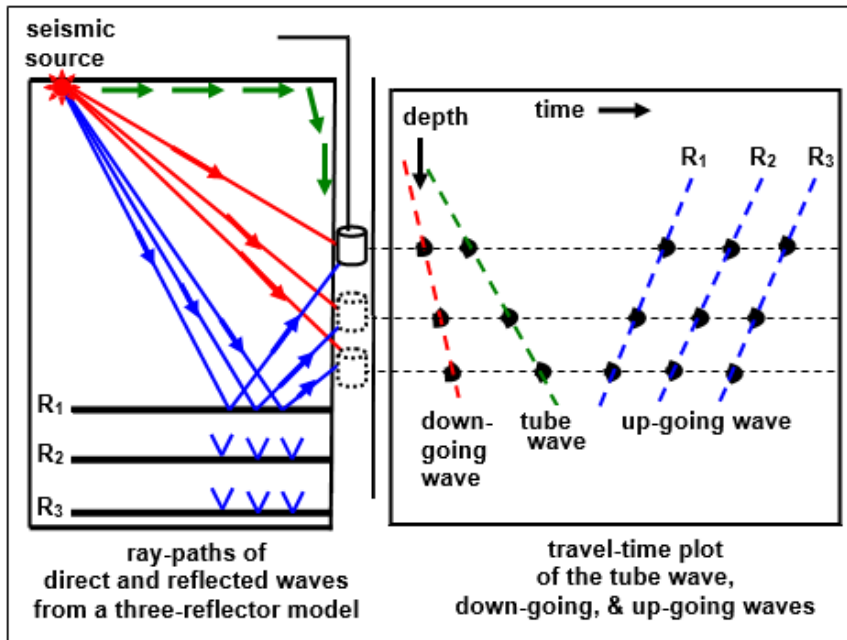


Figure 1.20 Ray-path diagram and the corresponding travel time plot of a VSP survey of a geological model made up of three reflectors.

The main application of VSP is providing seismic section of reflectors which have not been reached by the drilling. In fact, the VSP data are equivalent to both the check-shot data and the sonic-derived synthetic seismogram.

#### (iv) Other Logging Techniques

Some logs are used to give geometrical information on the deviation from the vertical (hole-drift angle) as well as the azimuth of the deviation. Other logs are made to give the bedding dip (dip-meter logs) and measurements of the well-hole diameter (caliper logs).

On more limited scale of application, other types of well logging have been used. Specially modified borehole-gravimeters, magnetometers, and thermometers are examples of such tools. Geothermal prospecting is applied to detect geological features which affect heat flow such as shallow salt domes, faults and dykes. Also ground water is investigated by this method.

### 1.5.4 Log Interpretation

The process of analysis and interpretation of well logs is sometimes called *Formation Evaluation*. Normally all the logs obtained for a well and their analysis-

results are presented in one combined display called the *composite log*. This comprehensive log usually contains all or most of the following log data:

1. Geological column showing lithological and paleontological information
2. Borehole compensated sonic log
3. Gamma-ray and Neutron logs
4. Resistivity and SP logs
5. Drilling information (drilling rate, mud density variation)
6. Caliper and dip-meter logs.

The main information which can be obtained from well logs can be summarized as in the following table 1-3.

Table 1-3 shoe the log type and its applications

Log Type	Application	Comment
Electrical Logs - Resistivity - Induction - Spontaneous Potential	- Fluid-type identification - Porosity evaluation - Boundary determination - Shale and sand lines	Logging is done in uncased wells
Radioactivity Logs - Natural gamma-ray - Gamma-ray Density - Neutron gamma-ray	- Shale/sandstone - Formation density - Porosity - Fluid type	Logging is done in cased wells
Acoustic Logs - Sonic logs - Well velocity - VSP	- Lithology type - Boundaries - Synthetic seismic -Seismic-velocity -Reflection identification	Logging is done in cased and in uncased wells

## 1.6 Well Completion

Well completion in petroleum production, is the process of making a drilled well ready for production (or fluid injection). This principally involves preparing the bottom of the hole to the required specifications, running in the central production tubing and its associated down-hole tools as well as perforating and stimulating as required. Sometimes, the process of pipes running-in and cementing the casing is considered as an integral part of the completion process.

To prevent caving in of the well walls, drilling is stopped at various depths. and a steel pipe (casing) is lowered into the well and fixed in position by pumping cement mixture in the space between the casing pipes and the well walls (cementing process). According to the planned drilling program, drilling after casing being cemented is

---

continued with a different (usually smaller) bit-size. At this stage, the drilled hole is lined by the appropriate casing which is likewise cemented in. The drill-casing-and-cementing phases are repeated until the final planned total depth is reached. The end result of the casing operations is a set of concentric pipes each of which is ending at the surface.

When the planned total depth is reached, all used drill pipes including the attached drilling bit, are withdrawn. The next operation is perforation of the parts of the casing facing the oil-bearing formations. The so-produced holes are made to allow the oil to seep inside the central production tubing of the well. The last stage in preparing the well for the production process is fixing of a group of flanges which provide a sealing structure connecting together all the surface ends of the casing tubes. This part of the well which contains pressure equipment in addition to the mechanical system that provide the blowout prevention (BOP) is called the well head which is also equipped with an assembly of valves that controls flow, and any other possible interventions. This assembly is normally referred to as the Christmas tree.

---



# 2. SEISMIC WAVES

## 2.1 Theory of Elasticity

Two main concepts are governing the propagation of seismic waves in an elastic medium; the (stress) and the (strain). Stress represents the external force applied to the elastic medium, and strain is the resulting changes in volume and in shape. The theory of elasticity deals with analysis of these two effects; stress and strain.

## 2.2 Stress

In the broad sense, stress is represented by a force called *traction* which is acting on a finite area occupying an arbitrary position within the medium. However, for more precise definition, the stress ( $\mathbf{T}$ ) is defined to be a limiting value of the ratio of a force ( $\mathbf{F}$ ) acting on an elementary area ( $\Delta\mathbf{A}$ ) which is diminishing to zero. That is:

$$\mathbf{T} = \lim_{\Delta\mathbf{A} \rightarrow 0} (\mathbf{F}/\Delta\mathbf{A})$$

In general, the stress ( $\mathbf{T}$ ) is a vector that can be resolved into components parallel and perpendicular to the area ( $\Delta\mathbf{A}$ ). The normal component ( $\mathbf{T}_z$ ) is called the normal stress or dilatational or pressure stress as it is sometimes called. The other two components ( $\mathbf{T}_x$  and  $\mathbf{T}_y$ ) which are in the plane of the elementary area, are called tangential or shearing stresses (Figure 2.1).

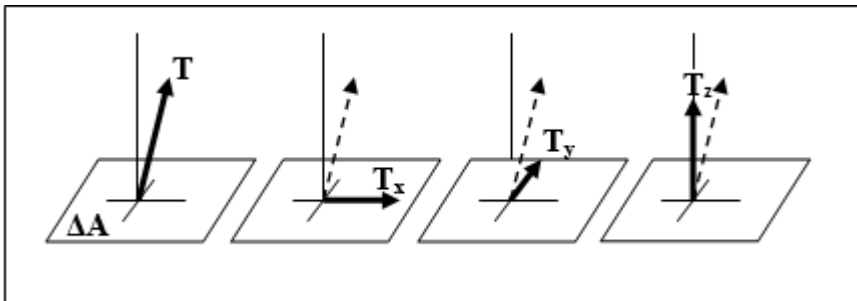


Figure 2.1 Stress ( $T$ ) and its components ( $T_x$ ,  $T_y$ ,  $T_z$ ) acting on the elementary area ( $\Delta A$ ).

The stress system within a body is completely defined if, at each point in that body, the normal stress and the two shearing stresses are all determined for three mutually perpendicular plane areas. It follows, therefore, that nine stress components

are needed to completely define the stress at a given point. This nine-component set constitutes what is known as the (stress tensor) at that point.

For the simple one-dimensional case, when a force ( $\mathbf{F}$ ) is acting uniformly at the cross-sectional area ( $\mathbf{A}$ ) of a bar or a metal wire, stress is defined as the force per unit area of the cross-sectional area, ( $\mathbf{F}/\mathbf{A}$ ). This stress is called tensile stress when the force is a pull-force and it is called compressive stress when it is a push-force.

Units of stress is the same as those used in measuring pressure (force per unit area), and in the SI unit system the unit is Newton per square meter ( $\text{N}/\text{m}^2$ ) which is called Pascal, where one Pascal is equal to one  $\text{Newton}/\text{m}^2$ .

### 2.3 Strain

Let us consider two points located within an unstressed body, where the first point ( $\mathbf{P}_1$ ) is located at  $(\mathbf{x}, \mathbf{y}, \mathbf{z})$  and the second point ( $\mathbf{P}_2$ ) at  $(\mathbf{x} + \mathbf{dx}, \mathbf{y} + \mathbf{dy}, \mathbf{z} + \mathbf{dz})$ . Now, we let this body to deform as a result of a stress system created within it. If the two points ( $\mathbf{P}_1$  &  $\mathbf{P}_2$ ) were displaced from their original positions by equal displacements ( $\mathbf{D}$ , say), then it is considered that there is no strain taking place. Strain occurs only when there is variation of displacement of any point (within that medium) with respect to other points. In the language of mathematics, we say that strain depends on the derivatives of the displacement-components with respect to the chosen coordinates  $(\mathbf{x}, \mathbf{y}, \& \mathbf{z})$ .

In general, when a body is subjected to elastic stress, both of its size and shape will change. As it is mentioned above, the resulting changes represent elastic strains when each point of the stressed body experiences a displacement of its own which is different from the displacements experienced by the other points of the body. This implies that there are two types of strains, namely the “volume strain” and the “shape strain” (Figure 2.2).

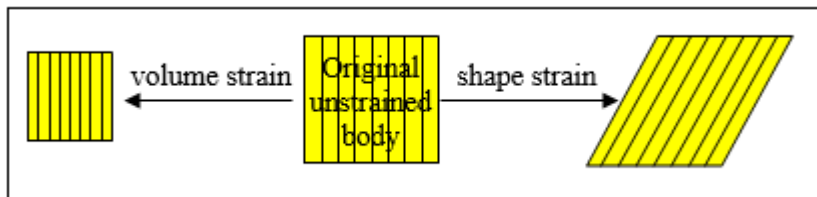


Figure 2.2 The two types of strain; “volume” and “shape” strains.

#### 2.3.1 Common Types of Strain

Common types of strain are cases of compression, bulk contraction, tension, and shear strains. Rigid body-translation and rotation represent cases of no strain, since no volume and no shape deformation are involved. In the following figure (Figure 2.3), an

---

elementary cube (shown here in plan) is used to show simple types of elastic deformation (strain) and no-strain changes.

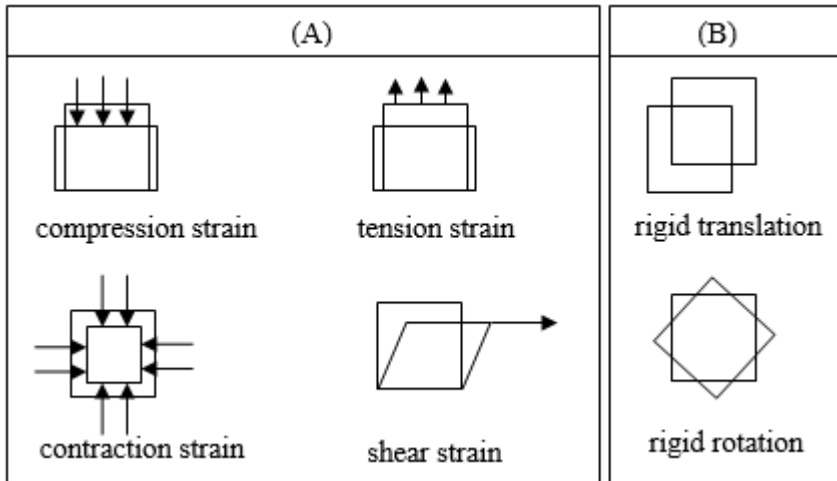


Figure 2.3 Types of simple strains (A) and no-strain changes (B).

In general, an elastic body under stress can experience two types of distortions; changes in volume and changes of shape. These changes which occur as a result of stress, express the physical property (the elastic strain) of a stressed body. In its simple form, elastic strain can be divided into two main types. These are: the longitudinal strain (expressing the change in volume) and the shear strain (expressing the change in shape).

### 2.3.2 The Longitudinal Strain

The longitudinal strain ( $\epsilon$ ) is defined to be the change in length in a certain dimension, of a body under stress relative to its original length. For a rectangular lamina of dimensions ( $\Delta x$  by  $\Delta y$ ), the longitudinal strains ( $\epsilon_x$  and  $\epsilon_y$ ) in the  $x$  and  $y$  directions are defined (Figure 2.4):

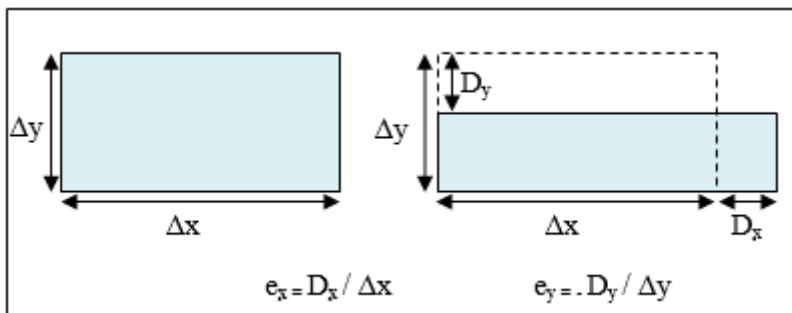


Figure 2.4 Definition of the longitudinal strain as applied for a rectangular lamina of dimensions ( $\Delta x$  by  $\Delta y$ ).

The longitudinal strains can be extensional (tensile strain) or compressional (contraction strain). Longitudinal strains ( $e_x$  and  $e_y$ ) in the directions ( $x$  and  $y$ ) are defined as:

$$e_x = D_x / \Delta x$$

$$e_y = - D_y / \Delta y$$

where ( $D_x$  and  $D_y$ ) are the changes in length in  $x$  and  $y$  directions respectively.

The minus sign that appeared in the  $e_y$  expression is entered to denote that the change ( $D_y$ ) is in opposite direction to the change ( $D_x$ ) in the  $x$ -direction.

### 2.3.3 The Shear Strain

As longitudinal strain gives expression for the volume changes resulting from stress application, the shear strain gives the corresponding measure for the shape deformation. Using the example above ( $\Delta x$  by  $\Delta y$  rectangular lamina). The shear strain (also called angular strain) is considered to be the average of the two angles by which two neighboring sides rotate as a result of the shearing stress. Thus, the shear strain ( $e_{xy}$ ) is defined as:

$$e_{xy} = (\alpha + \beta) / 2$$

where ( $\alpha$  and  $\beta$ ) represent the angles of rotation of the two sides ( $\Delta x$  and  $\Delta y$ ) brought about by the shear stress (Figure 2.5).

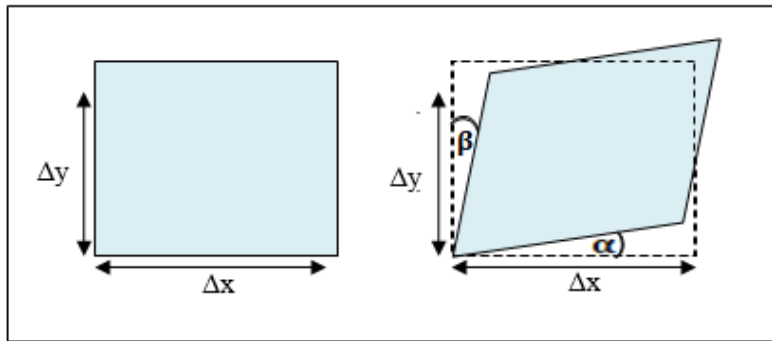


Figure 2.5 Concept of shear or angular strain,

Since these two angles are very small (usually so, in seismic-field conditions), they can be represented by their corresponding tangents, giving

$$e_{xy} = (\alpha + \beta) / 2 = (D_x / \Delta y + D_y / \Delta x) / 2$$

where the angles ( $\alpha$  &  $\beta$ ) are in radians.

---

It should be emphasized that strain occurs only if the body particles experience unequal displacements. When the displacements are equal a body may experience pure translation (rigid body-translation) or pure rotation (rigid body-rotation). Such changes of bodies are not considered as elastic strains.

It should be emphasized that strain occurs only if the body particles experience unequal displacements. When the displacements are equal a body may experience pure translation (rigid body-translation) or pure rotation (rigid body-rotation). Such changes of bodies are not considered as elastic strains (Figure 2.6).

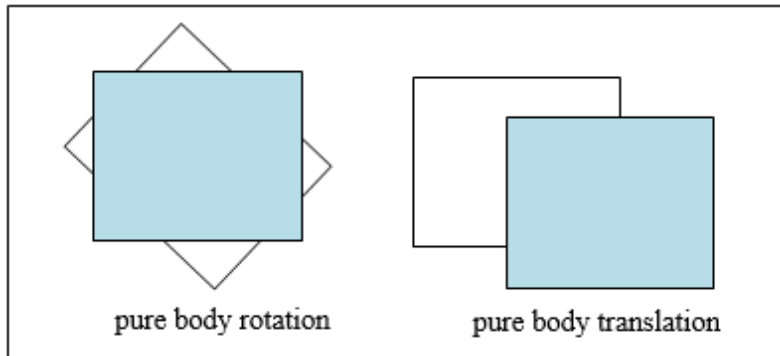


Figure 2.6 Pure rotation and pure translation changes of a body, are not considered to be elastic strains.

### 2.3.4 The Cubical Dilatation

A parameter, closely related to longitudinal strain and of special importance in the theory of elasticity is the Cubical Dilatation ( $\theta$ ). At a certain point within a strained medium, this is defined as the fractional change in a unit volume surrounding that point. Thus, for a three-dimensional body with longitudinal strains ( $e_{xx}$ ,  $e_{yy}$ ,  $e_{zz}$ ), the cubical dilatation can be computed as follows:

$$\theta = (1+e_{xx})(1+e_{yy})(1+e_{zz}) - 1$$

For small strains  $e_{xx}$ ,  $e_{yy}$ ,  $e_{zz}$  (which is the case in seismic-field conditions), the products of these terms may be neglected giving the result:

$$\theta = e_{xx} + e_{yy} + e_{zz} = D_x / \Delta x + D_y / \Delta y + D_z / \Delta z$$

The sign convention of ( $\theta$ ) is negative for compression and positive for expansion strains.

### 2.3.5 Stress-Strain Relationship

It is a common experience that a body under stress, undergoes deformation of a form and value depending on the applied load and on the physical properties of that body. Bodies of the type which, under stress, exhibit a proportional strain are called elastic bodies. When the proportionality is linear, these are called perfectly elastic bodies.

Normally, bodies, under increasing stress, exhibit linear stress-strain behavior up to a certain limit, beyond which the material may still be elastic but with no more linear relationship. Usually there is a point (the elastic limit) after which the deformation becomes irrecoverable and in this case the body behavior is described to be plastic. An increase of stress beyond the elastic limit produces large increase in strain, and it does so even with decreasing stress. With further increase of an extensional stress (tensile loading) for example, a point is reached where the body can no longer sustain the applied stress. At this point (called the rupture point) the body breaks up. Behavior of a ductile solid-body under an increasing extensional stress is shown in Figure 2.7.

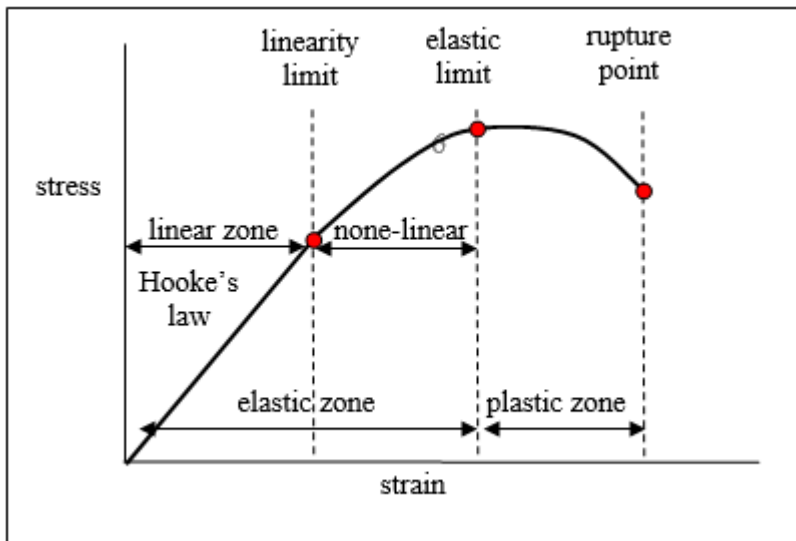


Figure 2.7 Elastic and plastic zones shown by a solid ductile body under an increasing tensile stress

For an isotropic body (physical properties are independent of direction) and for an elastic body, under small strain, strain varies linearly with the applied stress. This linear stress-strain relationship is governed by a well-known mathematical equation, which is the Hooke's law, which simply states that the strain is linearly proportional to the applied stress. It is applicable to the behavior of stressed bodies when stresses are sufficiently small.

---

## 2.4 The Elastic Moduli

The elastic modulus of a body is the proportionality constant of the stress-strain linear relationship. It expresses an important physical property which is the extent of resistance of that body to the applied stresses. Moduli of important practical applications are Young's Modulus, bulk modulus, and shear modulus. These are defined in the following discussions.

### (i) Young's Modulus and Poisson's Ratio

Let a simple tensile stress ( $\mathbf{T}_x$ ) be applied to an isotropic bar placed along the x-axis. This will cause the bar to experience a longitudinal extension ( $\mathbf{e}_x$ ) in the x-direction and, at the same time, it experiences lateral contractions along y- and z-directions. Being an isotropic body, the contractions in the y- and z-directions ( $\mathbf{e}_y$ , &  $\mathbf{e}_z$ ) are equal. These changes (expressed by the strains  $\mathbf{e}_x$ ,  $\mathbf{e}_y$ , &  $\mathbf{e}_z$ ) are governed by the elastic coefficients of the stressed body. The coefficients which govern the stress-strain relation, in the presence of the tensile stress ( $\mathbf{T}_x$ ), are Young's modulus ( $\mathbf{Y}$ ) and Poisson's ratio ( $\sigma$ ).

For a one-dimensional stress action on a body obeying Hooke's law, Young's modulus ( $\mathbf{Y}$ ) is the proportionality constant in the linear relation that connects stress ( $\mathbf{T}_x$ ) with strain ( $\mathbf{e}_x$ ). The relationship is:

$$\mathbf{T}_x = \mathbf{Y} \mathbf{e}_x$$

In the case of a rectangular rod of length ( $\mathbf{L}$ ), cross-sectional area ( $\Delta\mathbf{A}$ ) stretched by ( $\Delta\mathbf{L}$ ) due to force ( $\mathbf{F}$ ), Young's modulus ( $\mathbf{Y}$ ) is given by Figure 2.8:

$$\mathbf{Y} = \mathbf{T}_x / \mathbf{e}_x = (\mathbf{F} / \Delta\mathbf{A}) / (\Delta\mathbf{L} / \mathbf{L})$$

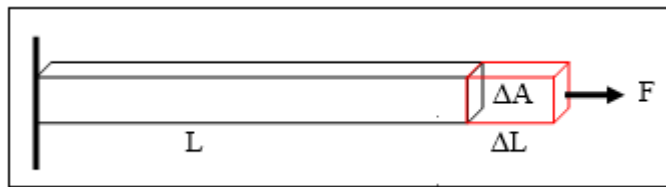


Figure 2.8 An elastic rectangular rod under extension force.

Young's modulus is measured by pressure units (as psi, dyne/cm<sup>2</sup> or Newton/m<sup>2</sup>).

The Poisson's ratio ( $\sigma$ ), on the other hand, is defined as the ratio of transverse strain ( $\mathbf{e}_y$  or  $\mathbf{e}_z$ ) to longitudinal strain ( $\mathbf{e}_x$ ). For an isotropic body, this is given by:

$$\sigma = - \mathbf{e}_y / \mathbf{e}_x = - \mathbf{e}_z / \mathbf{e}_x$$

The minus sign is used to indicate that ( $\mathbf{e}_y$ ) and ( $\mathbf{e}_z$ ) are contractions for elongation ( $\mathbf{e}_x$ ).

**(ii) The Bulk Modulus**

The Bulk modulus (**B**) is defined to be the ratio of change in hydrostatic pressure ( $\Delta P$ ), acting on a solid body of volume (**V**), to the relative decrease in its volume ( $\Delta V/V$ ). For a cube of volume (**V**) under hydrostatic pressure-change ( $\Delta P$ ), the bulk modulus (**B**) is given by Figure 2.9:

$$B = - \Delta P / (\Delta V/V) = - V \cdot (\Delta P/\Delta V) = - \Delta P/\theta$$

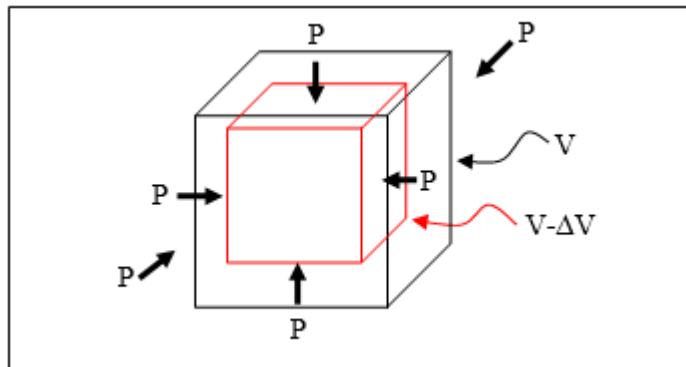


Figure 2.9 An elastic cube under hydrostatic compression forces.

The minus sign is entered to denote volume decrease for increase in compression and ( $\theta$ ) is the cubical dilatation:

The Bulk Modulus (**B**) is a measure for the body resistance to uniform compression. Its SI unit is the pressure measuring unit (the pascal) sometimes called *Incompressibility* and its inverse ( $1/B$ ) is called *Compressibility*.

An equivalent expression for the bulk modulus can be given in terms of density change ( $\Delta \rho$ ) instead of the volume change. Thus, the definition becomes:

$$B = + \rho (\Delta P/\Delta \rho)$$

The plus sign is entered to denote density increase for increase in compression.

**(iii) The Shear Modulus**

The shear modulus, ( $\mu$ ), which expresses the relationship between shearing stress and shearing strain, is defined as the ratio of the shear stress ( $T_{xy}$ ) and the shearing strain ( $e_{xy}$ ) represented by the resulting angular change. For tangential force (**F**) acting on the face of a rectangular block of area ( $\Delta A$ ), the shear modulus ( $\mu$ ) is defined as follows (Figure 2.10):

$$\mu = T_{xy} / e_{xy} = (F / \Delta A) / (\Delta x / h)$$

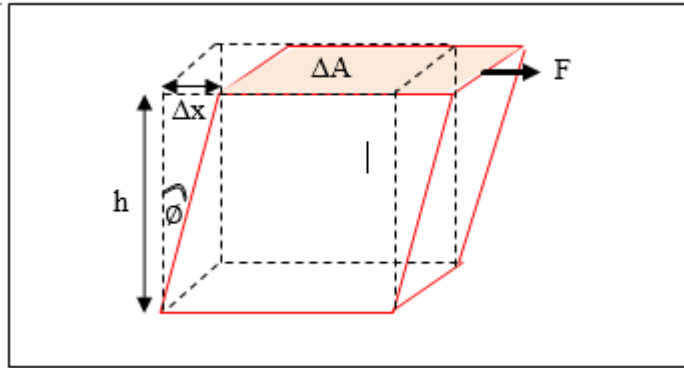


Figure 2.10 An elastic rectangular block under shearing force ( $F$ ) acting on area ( $\Delta A$ ).

The strain ( $\mathbf{e}_{xy}$ ) in this case is tangent of the angle of shear ( $\phi$ ), or the angle in radians for small value of the angle ( $\phi$ ). That is,

$$\mu = T_{xy} / \phi$$

The angle ( $\phi$ ) is normally called angle of shear and the coefficient ( $\mu$ ) is the shear modulus or rigidity modulus as it is sometimes called. Measurement unit of the shear modulus is pressure units as in the case of Young's modulus.

It is to be noted here that ( $\mu$ ) serves as measure for the resistance of an elastic solid body to shearing deformation (i. e. to shape changes) and that is why it is called rigidity modulus. For this reason, it is equal to zero for a fluid medium as it has zero-resistance to shape-changes.

For most rocks, values of the moduli ( $\mathbf{Y}$ ,  $\mathbf{B}$ , &  $\mu$ ) lie in the range ( $2 \times 10^{10}$  –  $12 \times 10^{10}$ )  $\text{N/m}^2$ , with ( $\mathbf{Y}$ ) being the largest and ( $\mu$ ) the smallest of these three (Sheriff & Geldart, 1995, p. 38). Table of values of elastic moduli of rocks have been published by Birch, 1966.

## 2.5 Classification of Common Elastic Waves

From the analysis of stress and strain we have seen that strain is, in general, made up of two types of elastic disturbance; the cubic dilatation and the shear strain. Solution of the equation of motion showed that each of these types of deformation travels through the medium with its own velocity. The first type of disturbance represents the moving “volume” strain and the second type involves the “shape” strain. The first type is called *Longitudinal*, *Compressional*, or *Primary* wave (or just P-wave) which travels faster than the second type which is called *Transverse*, *Shear*, or *Secondary* wave (or just S-wave).

These two types of waves (P- and S-waves) belong to a class of waves (called body waves) to differentiate them from another class of waves which move on and near

the free surface of the medium (called surface waves) which includes Rayleigh- and Love-waves. Classification of the common elastic (seismic) waves is shown in Figure 2.11.

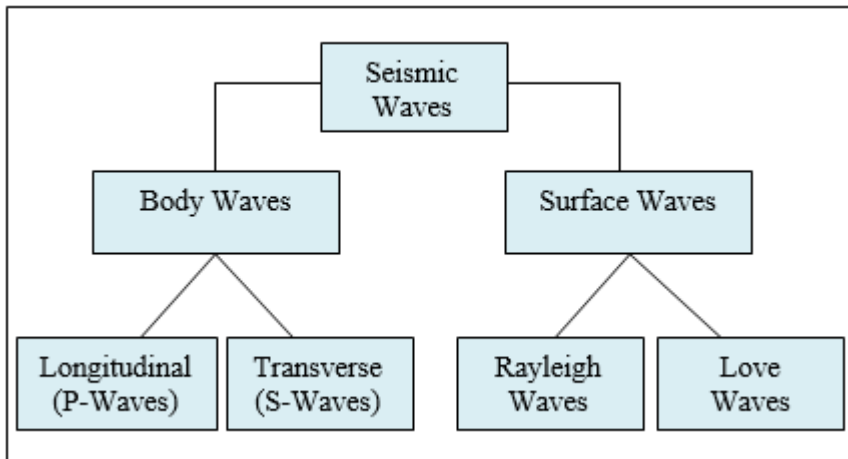


Figure 2.11 Classification of the common seismic waves.

### 2.5.1 Body Waves

Body waves are waves that can travel through an elastic materialistic medium in any direction. As they move, the waves may experience changes in their energy level and in their travel-path geometry subject to the physical properties of the medium. There are two sub-types of these waves; the longitudinal and the transverse waves (Figure 2.12).

#### (i) Longitudinal Waves

This type of waves is also known as compressional, Primary, or just P-wave. The travelling disturbance in this case is “volume” deformation expressed by the cubical dilatation ( $\theta$ ) as defined above (Figure 2.12).

The particles of the medium, traversed by a plane P-wave, vibrate about their neutral positions in the direction of the wave propagation. The travel path consists of a sequence of alternating zones of compressions and rarefactions. This is the type of wave which is commonly employed in seismic reflection and refraction prospecting work.

P-wave is the fastest wave for a given medium and, therefore, its arrival at a certain observation point is the earliest among the seismic wave-types. This is a common observation of seismologists working on analysis of earthquake seismograms. Propagation velocity ( $v_p$ ) of P-wave depends on the medium density ( $\rho$ ) and elastic properties ( $\lambda$  &  $\mu$ ) and it is given by the expression  $v_p = [(\lambda+2\mu)/\rho]^{1/2}$ .

---

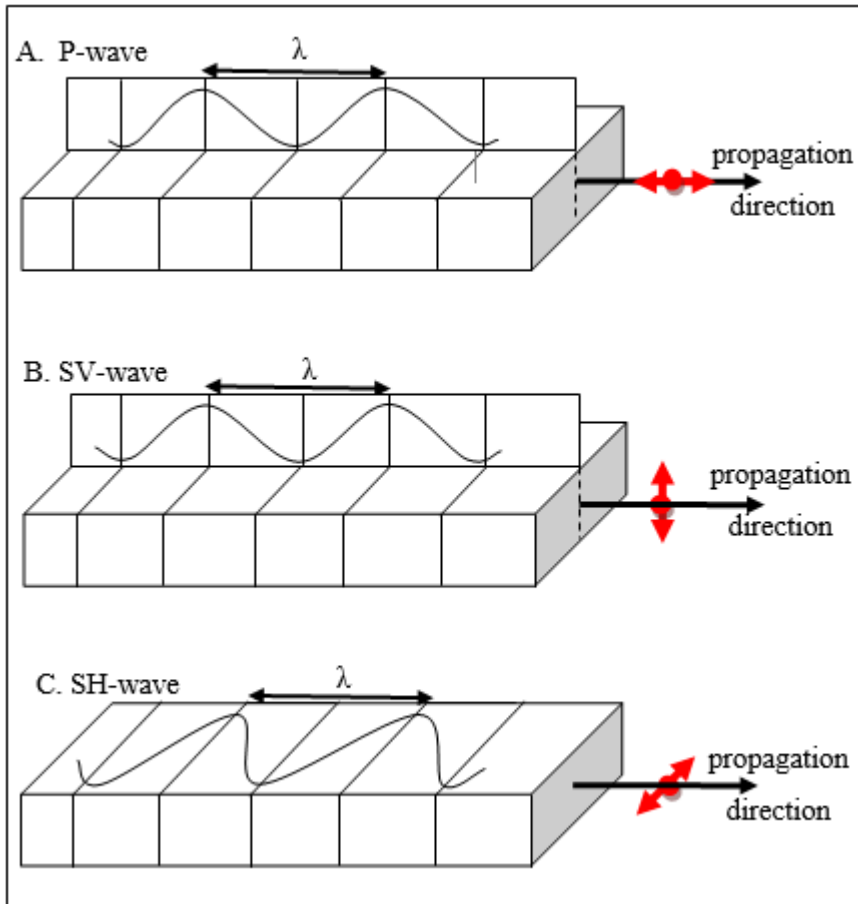


Figure 2.12 Particle displacement-mode of a medium traversed by plane body-waves,  $\lambda$  is wavelength. A. P-wave, B. SV-wave, C. SH-wave.

### (ii) Transverse Waves

The travelling disturbance in this case is the shear strain or “shape” deformation. The medium which is traversed by this type of waves experiences no volume changes. A consequence of the shear strain (rotation of part of the medium) is the transverse displacement of the path particles relative to the propagation direction. They are also called *shear waves* or *Secondary*, or just *S-waves*.

A horizontally moving S-wave, which is so polarized that the particle motion is confined to vertical plane, is known as SV-wave (Figure 2.12 B). When the polarization plane is horizontal, it is called SH-wave (Figure 2.12 C). The velocity of S-waves,  $v_s$  is given by  $v_s = [\mu/\rho]^{1/2}$ . In liquid-media, where ( $\mu=0$ ), S-waves do not propagate.

### 2.5.2 Surface Waves

As it is implied by its name, surface waves are waves that move on the free surface of the earth. The main features common among all surface waves, observed on earthquake seismograms, are their relatively large amplitudes (high energy content) and low frequencies when compared with the body waves. In addition to that, they move with velocity which is generally slower than body waves moving in the same medium. It is a common observation that the dispersion phenomena are more prominent in surface waves due to dependence of the velocity on the frequency of individual harmonic component.

The main sub-types of surface waves are Rayleigh waves and Love waves (Figure 2.13).

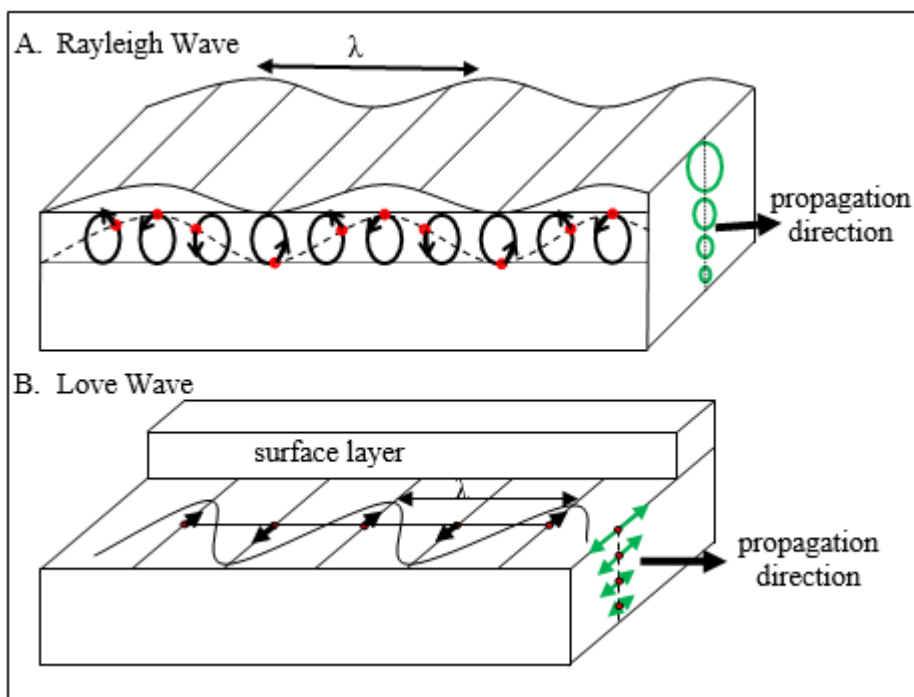


Figure 2.13 Particle displacement-mode of a medium traversed by plane surface-waves, ( $\lambda$ ) is wavelength. (A) Rayleigh Wave, (B) Love Wave. S

#### (i) Rayleigh Waves

Rayleigh waves, which were discovered by Lord Rayleigh in 1885, are usually developing at the free surface of a semi-infinite solid medium. Its wave amplitude decays rapidly with increasing depth. The travelling disturbance in this case is a sort of combination of particle-motions of both P- and SV-waves. The particle motion, which has a retrograde elliptical orbit, takes place in a vertical plane parallel to propagation direction (Figure 2.13A). The minor axis of the elliptical orbit is parallel to wave

motion direction and it is equal to two-thirds of its major axis. Rayleigh waves travel on the surface of a solid medium with velocity of 0.92 of the velocity of S-waves moving in that medium (Bullen, 1965, p 90).

In the case where the semi-infinite medium is overlain by a low-velocity surface layer, Rayleigh waves exhibit a phenomenon known as *dispersion*. Harmonic components of longer periods (lower frequencies) travel faster. Consequently, the Rayleigh wave seismograms would, in general, show decrease in period along the wave-train.

Components of too-long wavelengths (too long compared with the thickness of the surface layer) penetrate deeper and travel with velocity of about 0.9 times the S-wave velocity in the subsurface material. The short wavelengths travel mainly in the surface layer with velocity of about 0.9 times the S-wave velocity in the surface layer.

Surface waves, normally seen on shot records, obtained in seismic reflection surveys, are commonly called (ground roll) and these are identified to be of Rayleigh-wave type. Sometimes, these are called pseudo-Rayleigh waves (Sheriff, 2002). Ground-roll waves are considered to be unwelcomed noise and efforts are usually made to get rid of them or at least minimize their masking effect caused to the seismic reflection signal.

### **(ii) Love Waves**

This is the second sub-type of surface waves which was presented in 1911 by a geophysicist named A. E. H. Love (1863-1940). It develops only in cases where a solid elastic semi-infinite medium is overlain by a horizontal low-velocity layer. Like SH-wave vibration mode, the particle movement is transverse and is confined to the horizontal plane (Figure 2.13 B). Love waves travel by multiple reflections between the top and bottom boundary-planes of the surface layer. The propagation velocity approaches S-wave velocity in the subsurface medium for very long wavelengths and to that of the surface layer for short wavelengths (Dobrin, 1960, p23). Love waves always exhibit dispersion. As in the case of Rayleigh waves, Love waves propagation velocity increases with the period of the harmonic component. Again, the vibration amplitude decays exponentially with depth in the lower medium.

Since they possess no vertical component, Love waves are not detected by the geophone or by any such-like vertical-component sensing instrument.

### **2.5.3 Seismic Noise**

Broadly speaking, the term *noise* used in seismology, is applied to all types of disturbance which may interfere with (and impose masking effects to) the seismic signal of interest. In this way, the concept of seismic noise bears a relative implication. Thus, when the interest is focused on reflected body waves, surface waves and other non-reflection waves (as direct and refraction arrivals) are considered to be the

---

unwanted troublesome noise. If the interest is in the refraction arrivals, reflection arrivals become the unwanted noise. In the strict sense, however, the ambient seismic disturbances (usually of random energy distribution which form the background of a distinct travelling signal) are considered to be the seismic noise.

Seismic noise has destructive effects on the seismic signals of interest. A signal recorded amid a background of noise is distorted and weakened because of the interfering noise. Signal resolution is badly affected with noise development. A measure for the signal resolution, called the *signal-to-noise ratio* (S/N ratio) is usually applied. It is defined to be the ratio between signal amplitude detectable amid a background seismic noise.

In exploration seismology, seismic noise is divided into two main types; coherent and incoherent noise (Figure 2.14).

**(i) Coherent Noise**

Coherent noise is a seismic event characterized by a distinct apparent velocity and well-defined onset. In reflection seismology, coherent noise which appears on shot records, are source-generated seismic events. They are made up mainly of surface waves (ground roll) and air-waves which are of fairly narrow bandwidth with low frequency range. Frequency content of this type of noise is typically below 20 Hz (Figure 2.14).

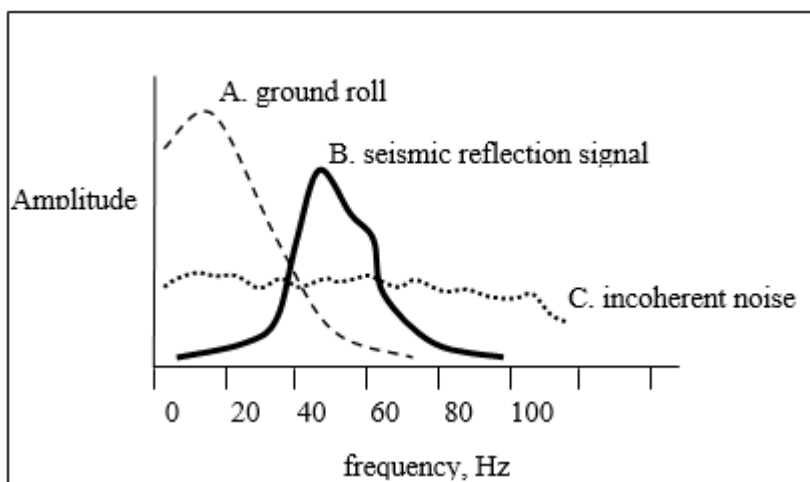


Figure 2.14 Sketch showing amplitude spectra of common coherent noise, ground roll (A), and incoherent noise, random noise (C), in relation to that of the reflection signal (B).

**(ii) Incoherent Noise**

Unlike coherent noise, the incoherent noise consists of seismic events with unpredictable amplitude and onset. This type of noise, which is basically of random nature, forms the seismic-energy background of any seismic shot-record. In earthquake

---

seismology, it is commonly known as *microseisms*, and in prospecting seismology it is called *incoherent background noise*, or *ambient noise* as it is sometimes referred to. In addition to the randomness nature, the incoherent noise is characterized by a broad amplitude spectrum that covers a wide range of frequencies compared with the nearly limited bandwidth of reflection signals or coherent noises (Figure 2.14). In the geophysical literature we sometimes meet terms like white noise indicating wide-band noise, and red noise for low-frequency random noise.

Because of seismic noise which is unavoidable seismic events which get recorded alongside the objective signal, the signal-to-noise-ratio (S/N) becomes an important parameter in signal detection studies. The S/N ratio is used as measure for the signal quality-level.

Signal clarity (S/N enhancement) is a central objective, aimed at, in seismic data acquisition. Several ways and means are followed in the field-acquisition stage or in the following data-processing stage to get enhanced S/N ratio. Suitable measures are applied to the parameters of the seismic source and detectors as well as those measures applied in processing work, in order to attenuate these noises.

## **2.6 Propagation of Seismic Waves**

Seismic waves are generated from a sudden change in the internal strain occurring inside an elastic medium. The generating source may be natural as in the case of earthquakes or artificial, like exploding a charge of dynamite, as normally done in seismic exploration. All parameters of an advancing seismic wave (waveform, speed, and travel-path geometry) may change during the wave propagation. Form and magnitude of these changes depend on the physical properties of the host medium.

### **2.6.1 The Seismic Field**

Whether the source is natural or artificial, a seismic field is created when a sudden pressure pulse is initiated. The generated seismic energy moves away from the source zone in a form of a wave motion propagation. Under these conditions (seismic energy source within an elastic medium), the seismic wave spreads out from the source zone in every possible direction. A travel ray-path, in a particular medium, is defined once the locations of both the source-point and detector-point are defined.

### **2.6.2 Concepts of Wave-Fronts and Rays**

From a mechanical energy-source, (such as a mechanical pressure pulse), a seismic wave spreads out into the three-dimensional space of the host medium. If the medium is homogeneous, the seismic energy would advance in every possible direction with constant velocity. This means that after any given travel-time the energy would

---

have reached points of equal distances from the source. These points fall on a spherical surface which is marking the wave front.

At any point in the wave-field, the line which is perpendicular to the wave front at a certain instant represents a (**ray**). The ray is an imaginary line normal to the wave front at a certain point which indicates the motion-direction of the advancing wave at that point. Near the source point, the wave fronts of seismic waves travelling through a homogeneous medium are of spherical shapes and thus the rays are straight lines radiating in all directions from the source point. At very large distances, the wave fronts are approximating to planes and the rays, in this case, become parallel straight lines perpendicular to the plane wave-fronts.

The familiar example is the wave which develops on the surface of water when a small solid object (a pebble, say) is dropped vertically into it. The crests and troughs of the generated wave spread out from the source-point in the form of concentric circles. In fact, these circles are depicting the surface expression of the spherical wave-fronts which are advancing through the three-dimensional space of the medium. By definition, the ray at any point on the wave front is a line drawn normal to the spherical wave-front (circles on the surface plane) at that point. Concepts of the wave-front and rays are shown in Figure 2.15 for a case of dropping a pebble into a still pond.

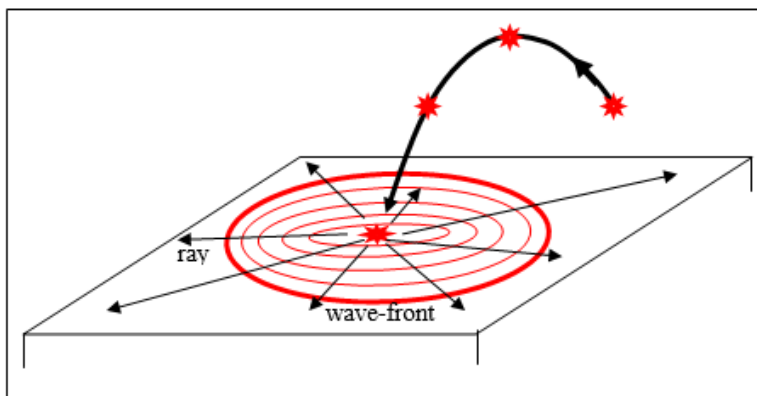


Figure 2.15 Concepts of the wave fronts and rays as seen when a water wave is created from dropping a pebble into a still pond.

### 2.6.3 Huygens' Principle

Huygens' Principle states that each point on a wave-front acts a source of a new wave which, in a homogeneous medium, generates a secondary spherical wave-front, the envelope of which defines the position of a wave generated at some later time.

Huygens' model of wave propagation requires that the secondary wave-fronts are active only at the points where the envelope touches their surfaces. The wave energy is spreading out from the primary source-points in all directions, but their mutual interactions make the resultant disturbance zero everywhere except at the points

---

where they touch the common envelope. Applying the principle on plane-wave propagation in a homogeneous, and in an inhomogeneous medium, is shown in Figure 2.16.

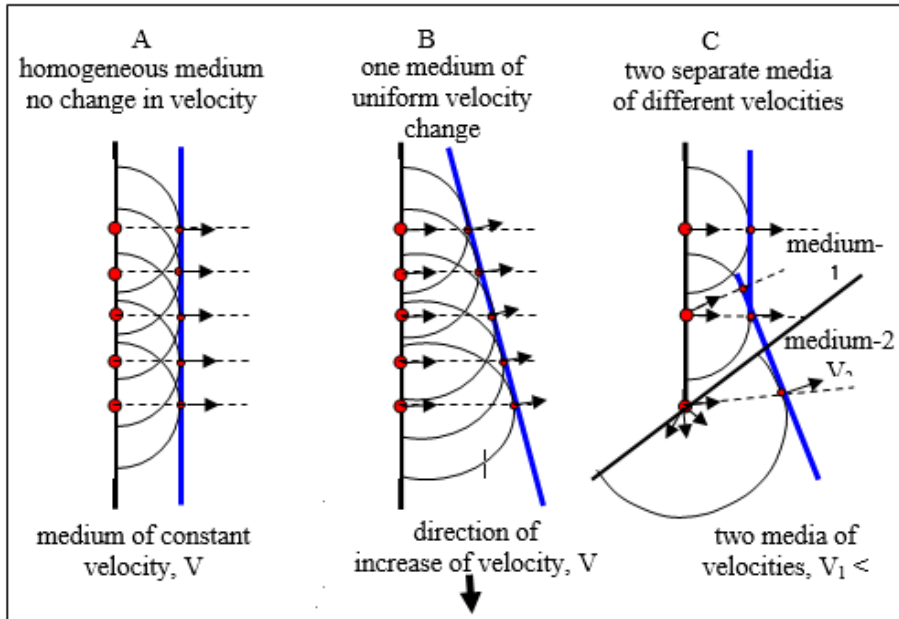


Figure 2.16 Plane-wave propagation according to Huygens' Principle. (A) through a homogeneous medium where velocity is constant. (B) Inhomogeneous medium of velocity which is uniformly changing across the propagation direction. (C) Two media of different velocities.

#### 2.6.4 Concept of the Interface

The Interface is that boundary-surface separating two different media. As far as the changes (changes in spectral structure and propagation direction) of seismic waves are concerned, two media are considered to be different if both of the wave propagation velocity and the medium bulk density are different. Since velocity is function of elastic coefficients, it can be said that density and elastic properties are the factors which control the specific characters of the media. The parameter which expresses the combined effect of velocity and density is called (acoustic impedance) which is defined to be the product of velocity by the density.

To clarify the concept of the interface and the roll of the acoustic impedance waves hitting an interface let us consider a two-layer model which consists of two adjacent media ( $M_1$  &  $M_2$ ) of velocities and densities ( $v_1$  &  $\rho_1$ ) for medium ( $M_1$ ) & ( $v_2$  and  $\rho_2$ ) for medium ( $M_2$ ). The acoustic impedances ( $z_1$  &  $z_2$ ) for the two layers are ( $z_1 = \rho_1 v_1$ ) and ( $z_2 = \rho_2 v_2$ ) as shown in Figure 2.17.

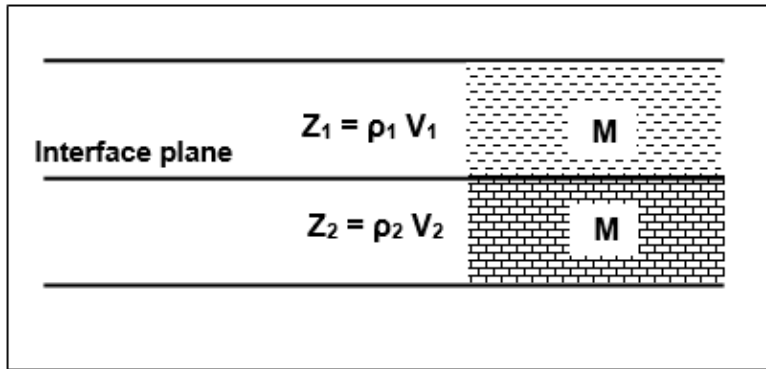


Figure 2.17 Concept of the Interface and definition of the Acoustic Impedance,  $z (= \rho v)$ .

In analogy to the role of electrical impedance in the flow of electrical current, the acoustic impedance expresses the extent of resistance the seismic energy meets when traversing a medium. The higher the acoustic impedance, the lower the particle vibration-velocity will be, and vice versa. Acoustic impedance is measured by  $(\text{kg s}^{-1} \text{m}^2)$  or by the equivalent  $(\text{Ns m}^3)$  units.

At an interface, an incident seismic wave (normally a P-wave in seismic exploration work) would, under certain geometrical conditions, give rise to wave conversion in addition to reflection, refraction, and diffraction. These cases shall be dealt with in some details in the following discussions.

### 2.6.5 Changes of Propagation Direction at Interfaces

In an idealized homogenous and elastic medium, a seismic wave propagates with no changes taking place on ray-path direction or on the waveform of the travelling seismic pulse. In nature, however, the medium is far from this idealized form. In the solid crust of the Earth, it is commonly made up of rock layers of varying physical properties and varying geometrical forms and sizes.

In such inhomogeneous environments a moving seismic wave would suffer from a number of changes whenever it meets a change in the properties of the medium. In particular, changes in energy content, waveform (spectral structure), propagation velocity, direction of motion, and new wave generation are generated at the interface planes forming the layer bounding surfaces (Figure 2.18).

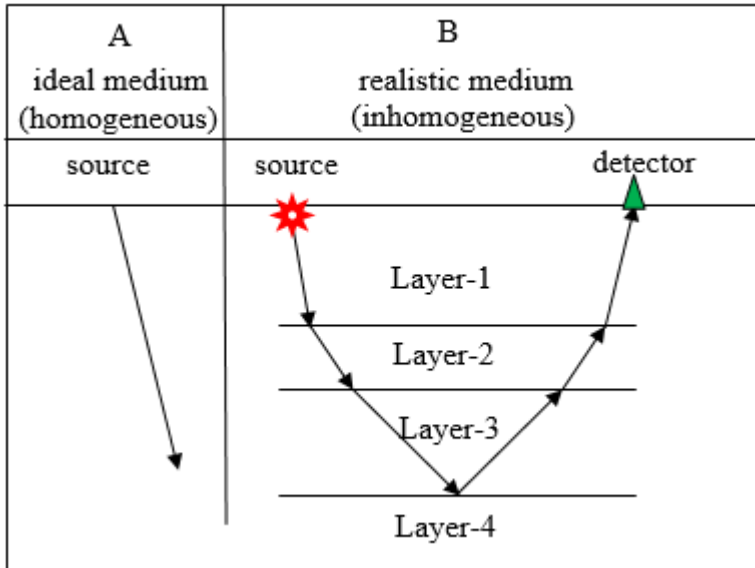


Figure 2.18 A-Infinite, elastic homogeneous medium showing straight ray-path. B-Inhomogeneous (layered) medium showing changes in ray-path direction.

The common changes in ray-path direction, which are of significance to exploration seismology, are reflection, refracted transmission (refraction), and diffraction. These shapes of the moving wave ray-path occur at the boundaries of media having different seismic propagation velocities (Figure 2.19).

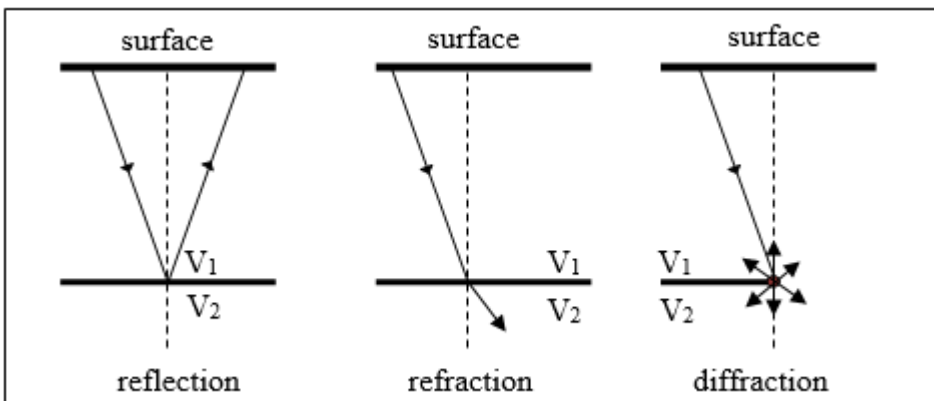


Figure 2.19 Ray-path geometry of the three most common wave propagation changes: reflection, refraction, and diffraction.

### 2.6.6 Wave Conversion at Interfaces

When a seismic wave impinges on an interface separating two media, which differ in acoustic impedances, the incident seismic energy is partly reflected and partly transmitted with certain waveform changes. When the ray-path of an incident seismic wave is oblique, that is inclined with respect to an interface, new waves are generated. If, for example, the incident wave is P-wave (or SV-wave) separating two solid media of different density and elastic properties, four new wave phases are generated; reflected and refracted P- and SV-waves. If, however the incident is SH-wave, the generated waves are only reflected and refracted SH-wave. The SV-waves, generated from an incident P-wave, (or P-waves generated from an incident SV-wave) are called (converted waves), (Figure 2.20).

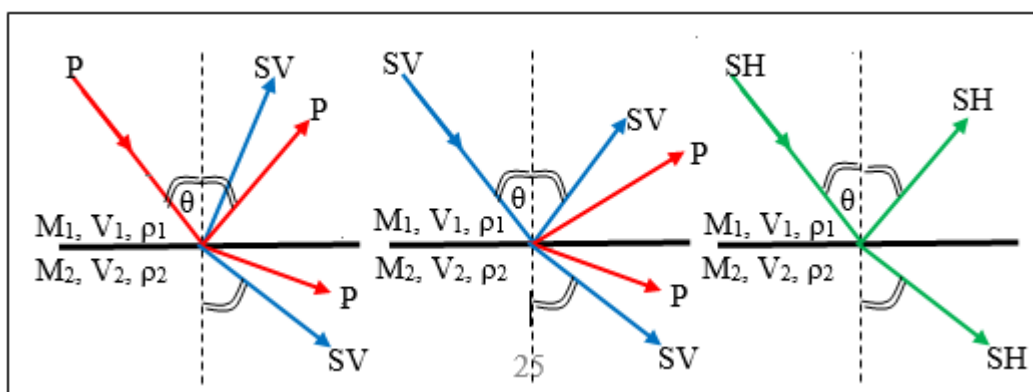


Figure 2.20 Wave conversion at an interface for three types of incident waves (P, SV, and SH waves). The symbol ( $\theta$ ) denotes angle of incidence.

An incident seismic wave onto an interface will be partly reflected and partly transmitted across the interface. In general, the interface will bring about wave conversion, reflection, transmission, and diffraction at a terminating interface. It should be noted here that refraction is a special case of transmission. Refraction (ray-path bending) occurs only in the case of inclined incidence.

### 2.7 Effect of the Medium on Wave Energy

Due to the earth filtering effect and other causes, the wavelet generated by the source energy, is changed from its initial high-energy, impulsive form into a lower energy and stretched-form wavelet when observed at the end of its travel-path. Taking the case of reflection, the main factors bringing about the changes in the shape and energy content of the travelling seismic signal, are reflection coefficient, geometrical spreading and inelastic attenuation.

### 2.7.1 Geometrical Spreading

In case of a homogeneous medium, seismic energy generated at the source, spreads out as spherical wave fronts concentric at the source point. Due to expansion of the advancing wave-front, wave energy is distributed over increasing wave-front surfaces. Mechanism of reduction of the wave energy level with travel-distance can be presented as follows (Figure 2.21):

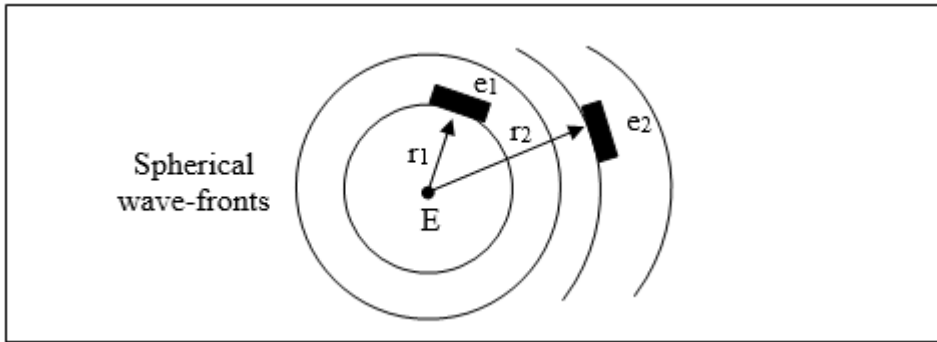


Figure 2.21 Wave-fronts generated by a point source are spreading out as spherical wave-fronts in a homogenous medium

Referring to Figure 2.21, let a source energy ( $\mathbf{E}$ ) be generated at the source point, then, after travelling distances ( $\mathbf{r}_1$ ) and ( $\mathbf{r}_2$ ) the corresponding energy-density of the spherical wave fronts will be ( $\mathbf{e}_1$ ) and ( $\mathbf{e}_2$ ) respectively. Since the same energy quantity ( $\mathbf{E}$ ) was distributed over the wave-fronts of radii ( $\mathbf{r}_1$  and  $\mathbf{r}_2$ ), we can write:

$$\mathbf{E} = 4\pi (\mathbf{r}_1)^2 \cdot \mathbf{e}_1 = 4\pi (\mathbf{r}_2)^2 \cdot \mathbf{e}_2$$

giving,

$$\mathbf{e}_1/\mathbf{e}_2 = (\mathbf{r}_2)^2/(\mathbf{r}_1)^2$$

or, (since energy is function of the square of amplitude,  $\mathbf{a}$ ),

$$\mathbf{a}_1/\mathbf{a}_2 = \mathbf{r}_2/\mathbf{r}_1$$

This result has shown that amplitude attenuation due to spreading of the wave-fronts (called geometrical spreading) is proportional to the travelled distance. The amplitude value is related to the travelled distance ( $\mathbf{r}$ ) according to inverse relation. Thus, ( $\mathbf{a}$ ) is proportional to ( $1/\mathbf{r}$ ), or to ( $1/\mathbf{v}(\mathbf{t}, \mathbf{t})$ ), where  $\mathbf{v}(\mathbf{t})$  is the velocity expressed as function of travel-time ( $\mathbf{t}$ ).

For a medium made up of parallel layers, it was shown (Newman, 1973) that geometrical spreading depends on ( $1/\mathbf{v}^2(\mathbf{t}, \mathbf{t})$ ) and not on ( $1/\mathbf{v}(\mathbf{t}, \mathbf{t})$ ), that was derived for homogeneous media.

Geometrical spreading (sometimes called spherical divergence) is independent of frequency.

### 2.7.2 Inelastic Attenuation

Due to friction between the vibrating particles of a medium traversed by a propagating seismic signal, some of the vibration energy is lost as a result of being converted into heat. The amount of loss increases with the increase of distance from source ( $\mathbf{r}$ ). Experimentally, this is found to take an exponential function of the form:

$$\mathbf{a}(\mathbf{r}) = \mathbf{a}_0 e^{-\alpha r},$$

or,

$$\mathbf{a}(\mathbf{t}) = \mathbf{a}_0 e^{-\alpha \cdot v(\mathbf{t}) \cdot t}$$

where,  $\mathbf{a}(\mathbf{r})$  is the amplitude at distance ( $\mathbf{r}$ ), ( $\mathbf{a}_0$ ) is the initial amplitude, ( $\alpha$ ) is the attenuation coefficient (expressing amplitude reduction due to absorption), ( $v$ ) propagation velocity, ( $t$ ) travel-time, and ( $e$ ) is constant representing the base of natural logarithm, where. ( $e = 2.71828$ ).

### 2.8 The Seismic Trace

A seismic pulse incident at an interface is partly reflected and partly transmitted into the following layer. In a multi-layer medium this is repeated at each interface present in the way of the advancing wave. A detector placed on the surface receives sequentially, the reflected wavelets, at time-intervals depending on the depths of the reflectors. The source pulse reaches the detector after being affected by the various types of modifications (as discussed above) including the process of reflection in which amplitude and polarity are governed by the reflection coefficient of the reflector. From each reflector a wavelet representing the source wavelet scaled by the reflection coefficient will arrive at the detection point. Thus, a series of such wavelets, shifted in time, are superimposed on each other to form a record, the seismic trace (Figure 2.22).

This process, which involves multiplication of the source wavelet, time shifting and superposition, is similar to the mathematical convolution process taking place between the source function, in this case, and the reflection-coefficient series. This is the construction mechanism model which is accepted by geophysicists for the formation of the seismic trace. This model (called the convolutional model) is applied in working out synthetic seismograms

---

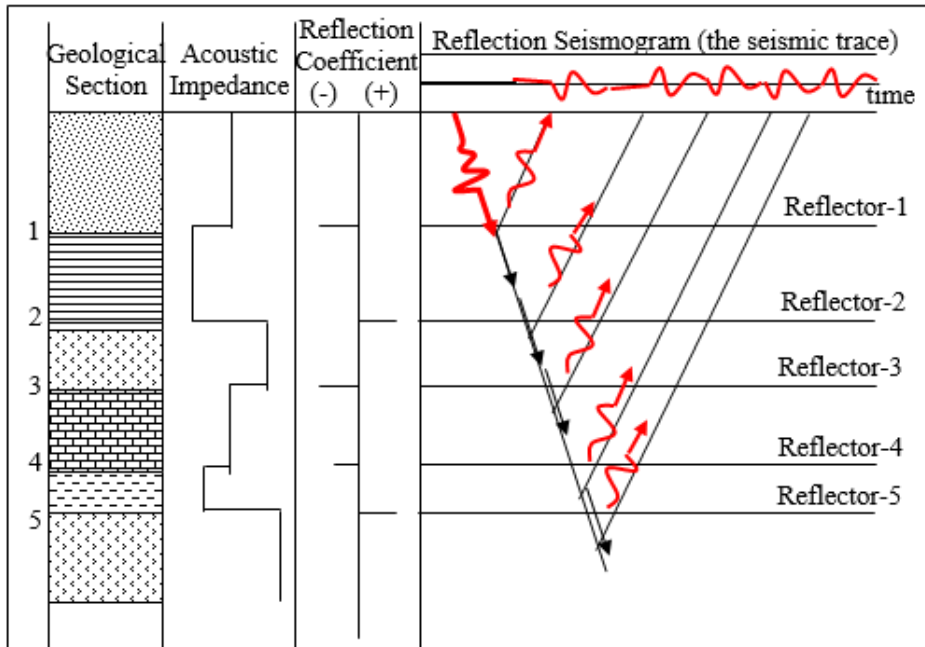


Figure 2.22 Sketch of the convolutional model of the seismic trace (Al-Sadi, 1980, p.192).

## 2.9 Seismic Energy Measurement and the DB Unit

We are all familiar with the units with which physical quantities are measured. Common examples are: gram for measuring mass, meter for lengths, and seconds for time. Ratios, on the other hand have no units as such. The decibel unit (or db), which is one-tenth of the bell unit, is introduced for measuring values of ratios in just the same way as in measuring masses, lengths, and other physical quantities.

The db unit seems to have been developed in connection with measuring energy- or power-ratios of sound-wave intensity expressed by its wave energy or by its wave amplitude. Likewise, the db-unit is usually used in measuring seismic wave energy.

The decibel is defined to be the unit of measuring a power (energy) ratio ( $E$ ), expressed in logarithmic domain to the base 10, hence,

$$[E]_{db} = 10 \log_{10} E = 20 \log_{10} A$$

where the power quantity ( $E$ ) is related to the square of amplitude ( $A$ ),

From this definition, it is apparent that the ratio expressed in decibels is positive when  $E > 1$ , and negative for  $E < 1$ , and it is zero when  $E = 1$ . Another useful note is that ratios (in the db-domain) are added or subtracted corresponding to multiplication or division of the original ratios. For example, the ratio of (2/1) in db units, is  $20 \log (2)$  which is equal to (6 db), and that of the ratio (1/2), it is (-6 db), and so on.



# 3. SEISMIC WAVE REFLECTION AND DIFFRACTION

In this chapter, discussion shall deal with the reflection and diffraction of seismic waves since they are physically more closely related to each other. Transmission with its special case, the refracted transmission (refraction) shall be dealt with separately in the following chapter.

## 3.1 The Commonly-Recorded Seismic Events

A seismic event on a shot record may be created as a result of a certain type of wave arrival (direct, refracted, reflected, or diffracted) depending on the nature of the involved interface and on the detector position. All of these four types of seismic events play important roles in seismic exploration activities. In normal seismic reflection records, these events are diagnosed by their recorded wave-arrivals as shown in Figure 3.1.

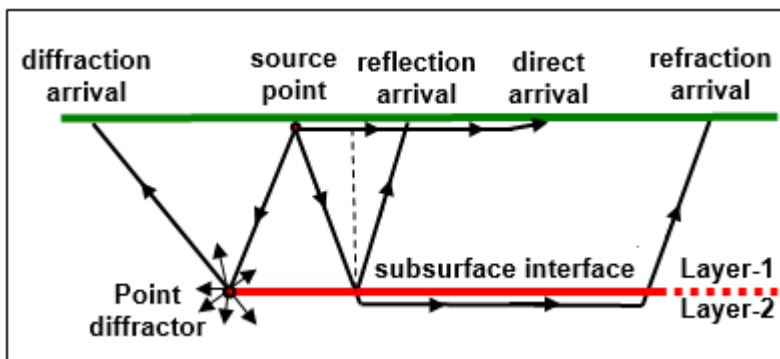


Figure 3.1 The four principal types of wave arrivals (direct, reflection, refraction, and diffraction) representing the commonly recorded seismic events.

A diffraction event bears a marked relation with reflection events since both are types of seismic energy generated from an intervening interface. A plane-surface (surface-reflector) causes reflection whereas point-obstacle (point-reflector) causes diffraction.

### 3.2 The Seismic Wave Reflection

The reflection process involves two main types of changes. These are: change in the propagation direction and change in the energy content (Figure 3.2).

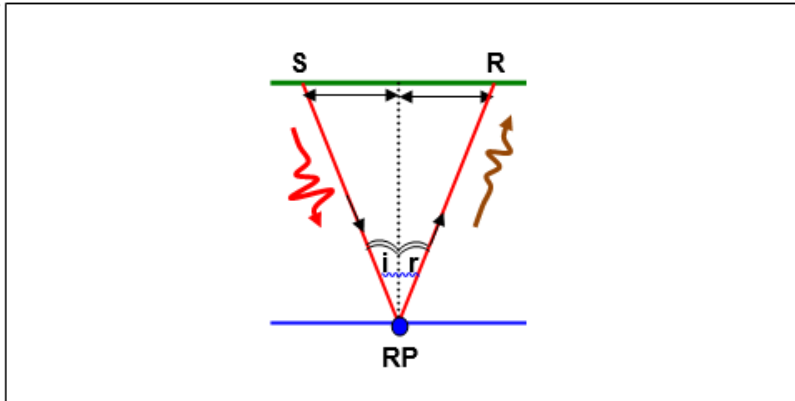


Figure 3.2 Reflection of a seismic wave from an interface. Travel path from the source point (S) to receiver (R) via the reflection point (RP). Change in travel-path direction and reduction in energy content.

The two types of changes occurring in the reflection phenomenon are:

**(i) Change in Energy content:**

In the process of reflection, the energy content of the incident wave is shared among all of the reflected and transmitted waves. Consequently, the amplitude of any of the reflected waves is always less than that of the incident wave. Distribution of the incident seismic energy is governed by a measurement parameter, the reflection coefficient.

**(ii) Change in Propagation Direction:**

At the interface, part of the incident seismic energy is reflected following a travel path defined by the law of reflection which states that angles of incidence and reflection are equal provided that these are of the same wave types. The geometry of the reflection travel-paths are normally expressed by certain adequate mathematical functions.

These two types of changes are dealt with in the following discussions

#### 3.2.1 Reflection Coefficient at Normal Incidence

A P-wave hitting an interface in the direction of the normal to the plane of the interface (angle of incidence equals zero) will give rise to only reflected and

---

transmitted P-waves. No wave conversion and no refraction shall take place in this case (Figure 3.3).

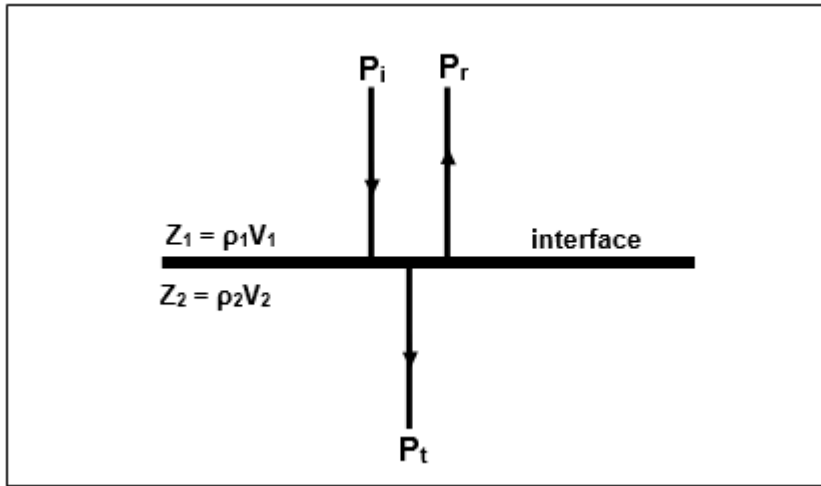


Figure 3.3 Reflection in case of normal incidence of P-wave at an interface. The incident, reflected, and transmitted waves are  $P_i$ ,  $P_r$  and  $P_t$  respectively.

The efficiency of an interface in reflecting seismic energy is expressed by the reflection coefficient which is defined by the ratio of reflected amplitude ( $A_r$ ) to the incident amplitude ( $A_i$ ). Sometimes, the reflection coefficient is defined in terms of energy ratios instead of amplitude ratios. With this approach, the coefficients are expressed by squares of the amplitudes. The reflection coefficient ( $R = A_r / A_i$ ) and transmission coefficient ( $T = A_t / A_i$ ) for the case of normal incidence, are given in terms of the contrast in the acoustic impedance ( $Z$ ) of the two media on either side of the interface, thus:

$$R = A_r / A_i = (\rho_2 v_2 - \rho_1 v_1) / (\rho_2 v_2 + \rho_1 v_1) = (Z_2 - Z_1) / (Z_2 + Z_1)$$

$$T = 1 - R = A_t / A_i = C/A = 2\rho_1 v_1 / (\rho_2 v_2 + \rho_1 v_1) = 2 Z_1 / (Z_2 + Z_1)$$

It is evident from these equations (case of normal incidence) that the reflection coefficient depends only on the contrast in the acoustic impedance ( $Z_2 - Z_1$ ). The greater the contrast, the larger reflection coefficient will be. This implies that no reflection occurs from an interface across which the acoustic impedance assumes the same value, even if either velocity or density varies individually across the interface.

The reflection coefficient ranges in value from (-1) to (+1) depending on the acoustic impedances ( $Z_1$  &  $Z_2$ ). When the acoustic impedance ( $Z_2$ ) in the second medium (medium in which transmission occurs) is greater than that in the first medium (medium of incident wave,  $Z_1$ ) a compression displacement is reflected as compression, and the reflection coefficient is positive. In the opposite case, that is when ( $Z_1 > Z_2$ ), a compression is reflected as rarefaction (phase change =  $\pi$ ) and the reflection coefficient becomes negative. Reflection coefficient is zero when the two

acoustic impedances ( $Z_1$  &  $Z_2$ ) are equal, which means that there is no interface existing in the way of the incident wave.

Another useful feature which may be deduced from the reflection coefficient expression is the case where the acoustic impedance in one of the two adjacent media is approaching zero or infinity. Thus, when ( $Z_1$ ) is very small compared with ( $Z_2$ ), that is when ( $Z_1$ ) approaches zero, ( $R$ ) approaches unity ( $R=1$ ). In this case, the interface is considered to be ideal reflector since this means that all of the incident energy is reflected and no part of it is transmitted through. A good approximation of this kind of situation is the earth free-surface which is an interface between the upper air-medium and the lower rock-medium. Because of the vast difference between the acoustic impedances of these two media, the reflection coefficient approaches the value of (+1) for a source located in the air and (-1) for a source located inside the rock-medium. The interface in both cases is equally efficient in the reflecting process, but in the second case there occurs a polarity reversal, or phase change of ( $\pi$ ) for an incident sine wave.

### 3.2.2 Geometry of Reflection from Horizontal Reflectors

For a horizontal reflector the travel-time function is obtained by putting ( $\theta = 0$ ) in the function for the dipping reflector, giving:

$$T_x = (x^2/V^2 + 4z^2/V^2)^{1/2}$$

This is also a hyperbola having its apex located at the point ( $0, 2z/V$ ) which is symmetrical about the time-axis. Using ( $z = VT_0/2$ ), this becomes:

$$T_x = (x^2/V^2 + T_0^2)^{1/2}$$

As in the previous case, this equation can be expressed in an approximate form by using the binomial expansion. The reflection function in this case becomes:

$$T_x \approx x^2/2T_0V^2 + T_0$$

Ray path and the corresponding travel-time curve of reflection from a horizontal interface, is shown in the following figure (Figure 3.4).

### 3.2.3 Reflection from Multiple Reflectors

It is possible that a seismic wave arrives at a point on the surface after being reflected several times from a number of interfaces. The first arrival (called the primary reflection) is the strongest, followed by other arrivals (the multiple reflections) which are of less energy. A well-known type of multiple is the *ghost reflection* which occurs when a wave travels upwards from a source-point located at a certain depth and is reflected by the free earth surface or by the base of a low-velocity surface layer (the weathering zone).

---

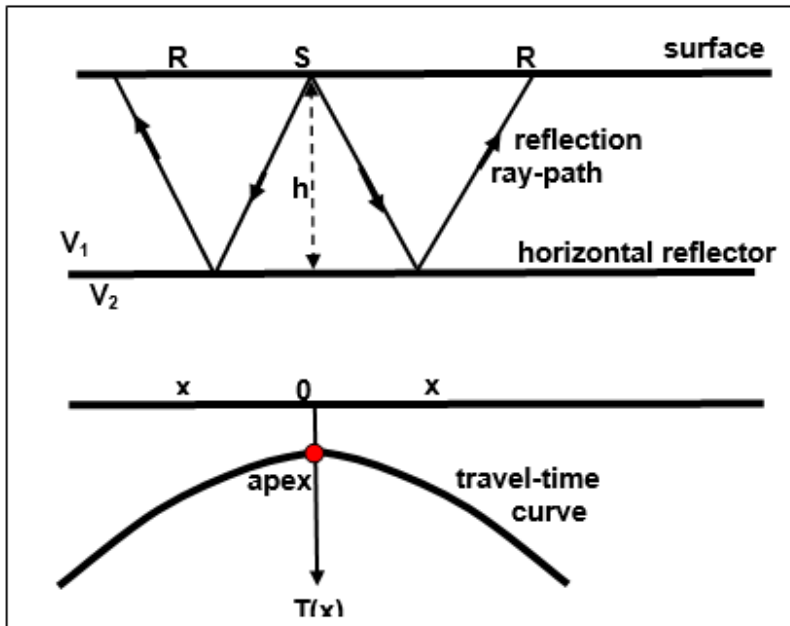


Figure 3.4 Ray-path and travel-time curve of a seismic wave reflected from a horizontal interface.

Because of the short extra travel path, the multiple arrives at a short time-interval after the primary reflection. On the seismic section it appears as a weak reflection event which is closely following the stronger primary reflection, and for this appearance it was named ghost reflection. Some of the commonly known types of multiples are shown in Figure 3.5.

Several other types of multiples may occur depending on the structural form of the medium. Multiple reflections include also reflected refraction or refracted reflection. Identification of these wave arrivals is very important, since mistaking a multiple for a primary reflection introduces a serious error in the interpretation results.

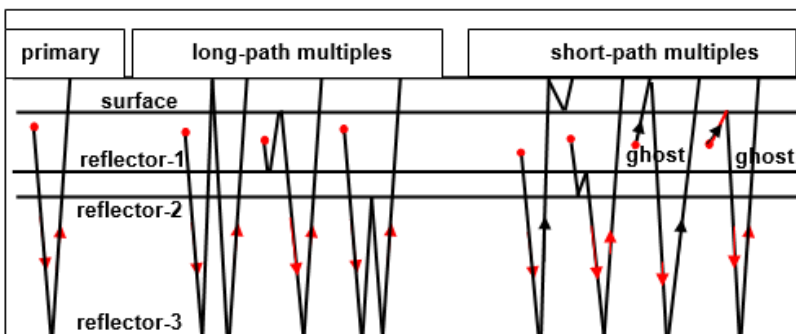


Figure 3.5 Types of multiple reflections

### 3.3 The Normal Move-Out (NMO) Concept

A parameter which plays a fundamental role in seismic reflection-data processing is the Normal Move-Out (NMO). It is defined as the difference ( $\Delta T$ ) between reflection travel-time ( $T_x$ ) and the two-way vertical travel-time ( $T_0$ ). For a single horizontal reflector found at the base of a homogenous layer (of constant velocity), the NMO ( $\Delta T$ ) is given by (Figure 3.6):

$$\Delta T = T_x - T_0$$

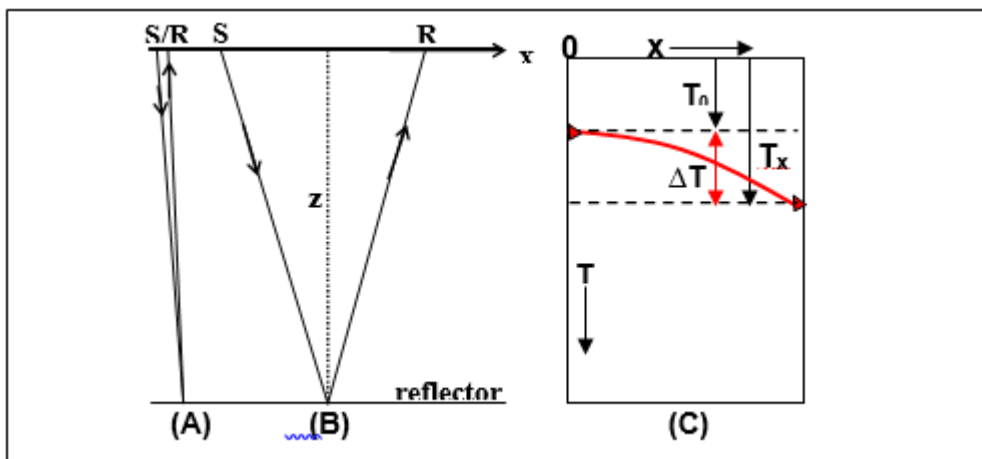


Figure 3.6 The NMO concept. (A) Two-way vertical ray-path, (B) Two-way slant ray-path, (C) Reflection arrival times corresponding to the ray-paths of A and B. The NMO ( $\Delta T$ ) is shown as the difference, ( $T_x - T_0$ ).

#### 3.3.1 NMO in Case of Horizontal Reflector

For a horizontal reflector, the NMO equation takes the following form:

$$\Delta T = T_x - T_0 = [(x/V)^2 + T_0^2]^{1/2} - T_0$$

This equation can be expressed in another form, using the binomial expansion (with truncation of the resulting series after the first term). This form gives:

$$\Delta T = x^2/2T_0V^2$$

This is considered accepted approximation since  $(x/VT_0 \ll 1)$ , which is usually the case in seismic reflection exploration. In this mathematical process, the exact form of ( $\Delta T$ ) is transformed from its hyperbolic function to the approximate form which is a parabolic function.

Both forms of these two equations show that ( $\Delta T$ ) is function of three variables; the receiver offset ( $x$ ), velocity ( $V$ ), and the two-way vertical time ( $T_0$ ). The proportionality is direct with ( $x^2$ ) and inverse with both ( $V$ ) and ( $T_0$ ). These changes are shown as follows (Figure 3.7):

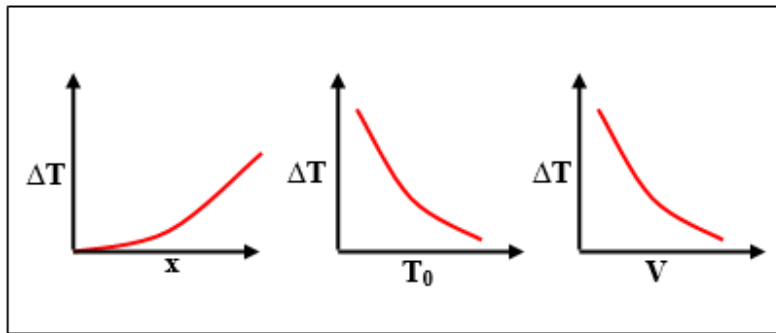


Figure 3.7 NMO ( $\Delta T$ -function) direct variation with ( $x$ ) and inverse variation with both  $T_0$  and  $V$ .

For a given offset ( $x$ ), the time ( $T_x$ ) can be readily measured for a certain reflection event appearing on the seismic trace recorded at that offset. From these data, the NMO ( $\Delta T$ ) can be accurately calculated (from the given NMO equations) provided that the velocity ( $V$ ) is known.

### 3.4. CDP, CRP, and CMP in Case of Horizontal Reflector

By use of certain source-receiver layout, it is possible to shoot a number of shots such that the reflection points resulting from this number of shots coincide on each other, that is one point-location will serve as common point to all of the implemented shots. In this type of repeated shooting-spread, the reflection point becomes known as common depth point, common reflection point, or common mid-point. These are normally abbreviated as CDP, CRP, CMP respectively (Figure 3.8).

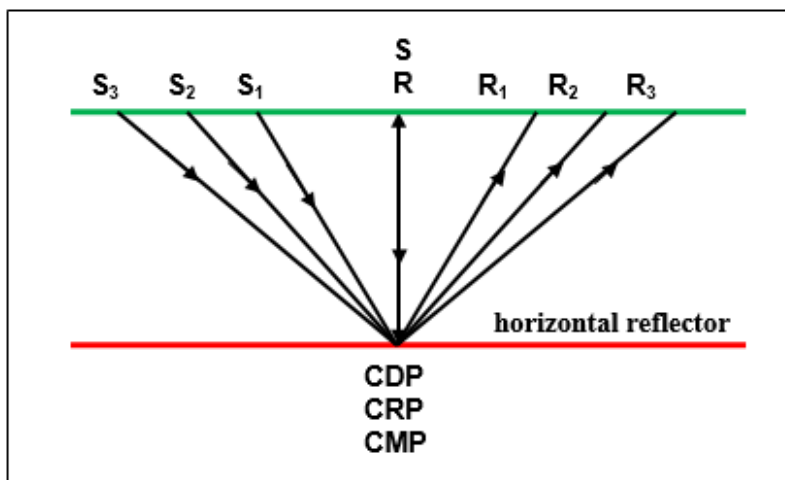


Figure 3.8 Definition of the common points (CDP), (CRP), and (CMP), which coincide on each other in case of horizontal reflector

The four reflections ray-paths, shown in this figure, have one common depth point (the CDP), and each produces a *seismic trace*. These traces belong to the same depth point (CDP) and thus they form a group of traces called the (CDP-Gather). In this case (case of horizontal reflector) the CDP and the other points (CRP and CMP) will coincide on each other. However, these points do not fall at one location-point when the reflector is dipping. For details see (Alsadi, 2017, p. 80-81).

### 3.5 The Seismic Wave Diffraction

A part of a seismic wave-energy is reflected when the wave hits a continuous plane interface surface. However, when the interface is not a continuous plane but of curvature which is large in comparison with the curvature of the incident wave-front, the change in propagation direction does not follow the known laws of reflection. If the intervening obstacle, to an advancing seismic wave, is of size approaching to a “point-reflector”, the wave radiates from that obstacle, in every possible direction giving a phenomenon called (diffraction) and the wave which leaves the obstacle after incidence is called (diffracted wave).

A closely related term is (wave scattering) which is used to describe diffracted wave-field caused by small structural irregularities, as for example found with seismic energy reflected from rugged basement surfaces.

#### 3.5.1 The Point-Diffractor

A structural obstacle, having radius of curvature which is shorter than the incident wavelength, acts as a diffraction-generating point (or diffraction point). This is normally referred to as the point diffractor.

The diffraction phenomenon can be explained by considering the diffraction point as a point-source which, upon being hit by an incident wave, becomes an activated source that radiates waves in all directions. According to Huygens’ Principle, an obstacle hit by an incident wave becomes an energy-source from which seismic waves are generated and transmitted in all possible directions. If a plane seismic wave, for instance hits a point-diffractor embedded in a homogeneous medium, a diffracted wave with spherical wave fronts will be generated. The diffracted wave will move away from that source-point causing interference with the incident wave-train and all other waves that may be coexisting at the time (Figure 3.9).

---

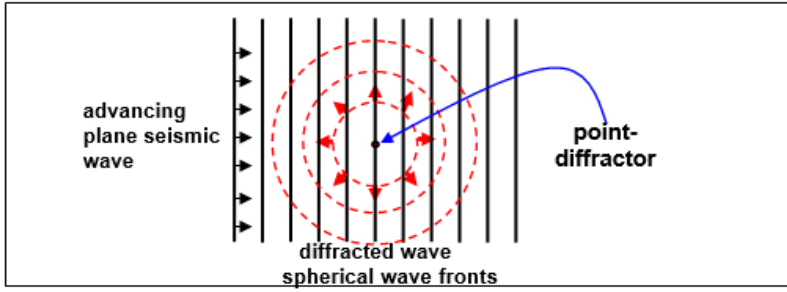


Figure 3.9 Generation of a diffracted wave with spherical wave fronts as an advancing plane seismic wave hits a small obstacle (point-diffractor).

### 3.5.2 Diffraction Travel-Time Function

Identification of diffraction is possible by use of its travel-time curve, which is, like reflection travel-time, of hyperbolic form but with larger normal move-out. To compare diffraction hyperbola with the reflection hyperbola for a given interface, let us consider the terminating reflector shown in Figure 3.10.

From the geometry of the reflection ray-path from a given interface and for diffraction ray-path from its termination edge, where the source-location is vertically above the diffraction point, we have for the same offset ( $\mathbf{x}$ ), the travel time function ( $\mathbf{TD}_x$ ) for diffraction and ( $\mathbf{TR}_x$ ) for the reflection are given by:

$$\mathbf{TD}_x = [(\mathbf{x}/\mathbf{v})^2 + (\mathbf{T}_0/2)^2]^{1/2}$$

$$\mathbf{TR}_x = [(\mathbf{x}/\mathbf{v})^2 + \mathbf{T}_0^2]^{1/2}$$

and,

$$\Delta\mathbf{T}_d = \mathbf{TD}_x - \mathbf{T}_0 = [(\mathbf{x}/\mathbf{v})^2 + (\mathbf{T}_0/2)^2]^{1/2} - \mathbf{T}_0/2$$

$$\Delta\mathbf{T}_r = \mathbf{TR}_x - \mathbf{T}_0 = [(\mathbf{x}/\mathbf{v})^2 + \mathbf{T}_0^2]^{1/2} - \mathbf{T}_0$$

where, ( $\Delta\mathbf{T}_r$ ) and ( $\Delta\mathbf{T}_d$ ) are the normal move-outs for the reflection and diffraction respectively, and ( $\mathbf{v}$ ) is the propagation velocity. For small offset-to-depth ratio ( $\mathbf{x}/\mathbf{v}\mathbf{T}_0 < 1$ ), these equations can be approximated by:

$$\Delta\mathbf{T}_r \approx \mathbf{x}^2/2\mathbf{T}_0\mathbf{v}^2$$

and,

$$\Delta\mathbf{T}_d \approx \mathbf{x}^2/\mathbf{T}_0\mathbf{v}^2$$

giving,

$$\Delta\mathbf{T}_d \approx 2\Delta\mathbf{T}_r$$

This shows that the normal move-out of a wave diffracted from a terminating reflector is approximately equal to double that of a wave reflected from the same

interface at the same offset. This feature is used in discriminating diffraction from reflection events.

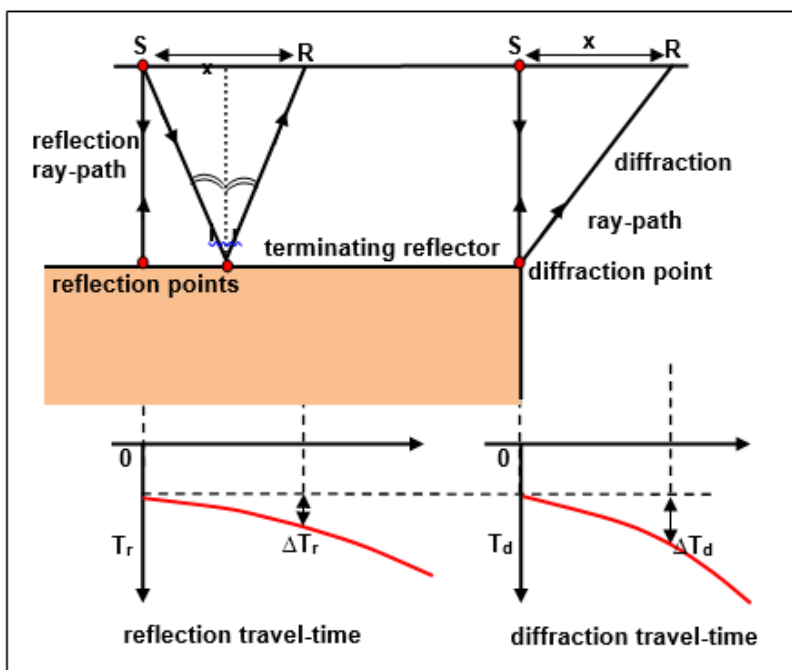


Figure 3.10 Reflection and diffraction ray-paths and their respective travel-time curves. The diffraction normal move-out ( $\Delta T_d$ ) is greater than the reflection normal move-out ( $\Delta T_r$ ) for the same offset ( $x$ ).

### 3.5.3 The Diffraction Hyperbola

The seismic image of the diffraction arrivals is (for constant velocity) a hyperbolic curve centered about the diffraction source-point. A diffraction event such as this is expected to appear on a seismic section made up of zero-offset traces. The seismic stack section is effectively a section of zero-offset traces (Figure 3.11).

In nature interfaces are not always plane and continuous surfaces. There are cases where these surfaces are irregular as reef bodies or discontinuous as faulted beds or pinchouts as found in angular unconformities. When a seismic wave is incident on such subsurface features, diffracted waves are generated and transmitted through the medium, interfering with, and distorting other co-existing waves such as reflection events, the main objective is normal seismic exploration.

On a seismic stack section, which is effectively made up of zero-offset traces, the diffraction arrivals (diffraction event) appear as a hyperbolic curve whose apex is coincident with the causing diffraction point. Faulting is one of the principal sources of diffraction waves seen in stack sections. A reflector termination caused by faulting,

generates diffraction arrivals. Because of their interferences, these arrivals are distorting or masking the reflection events and causing smearing effects at the fault-zone leading to decrease in fault-resolution. Appropriate measures (seismic migration) are usually taken in the processing stage to remove the distorting effects of the diffraction hyperbolae.

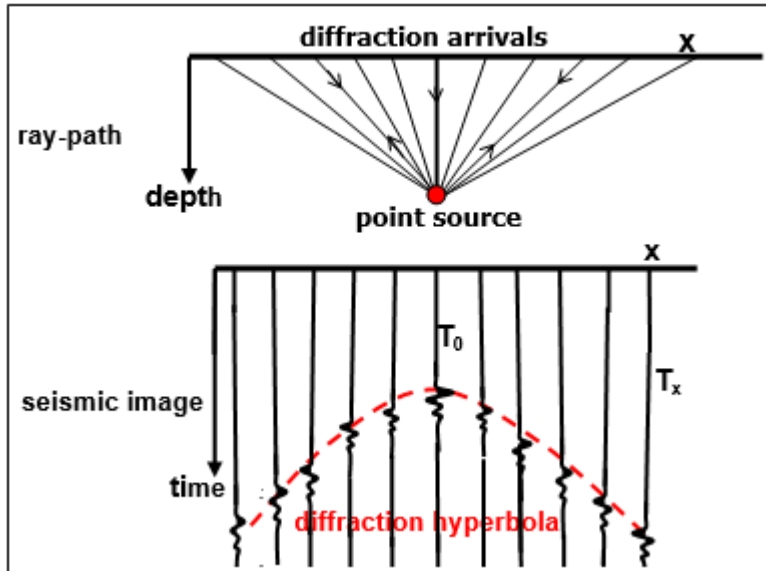


Figure 3.11 Point-source diffraction ray-path and its seismic image, which is a hyperbolic curve centered at the point diffractor



# 4. SEISMIC REFRACTION

## 4.1 Introduction

The first time the seismic refraction use of an artificial source in a seismic experiment is done by Irish physicist, Robert Mallett in 1846 and in 1910, L. Mintrop use for the first-time seismic waves transmit through the earth subsurface. At the same year the scientist Mohorovicic, identified and separated P and S waves on travel-time plots and associates them with base of the crust, (the Moho discontinuity). In 1916, the method developed to locate artillery guns by measurement of recoil and in 1919 applied it to determine depths and types of subsurface formation.

Seismic refraction was the first seismic technique to be used in petroleum exploration, and in the 1920's, E. V. McCollum used it in the USA. In 1925 the refraction method was well established as a tool in applied geophysics. In the early days the method was used for oil exploration and for detecting hidden salt domes. At the beginning of the 'thirties the refraction technique was also seen to be applicable to civil engineering problems. (Sjogren, Bengt, 1984).

Refraction seismology is applied to a very wide range of scientific and technical problems, from engineering site investigation surveys to large-scale experiments designed to study the structure of the entire crust or lithosphere (MOHO). Refraction measurements can provide valuable velocity information for use in the interpretation of reflection surveys, and refracted arrivals recorded during land reflection surveys are used to map the weathered layer (Kearey, et al)

The depth of investigation depended on the size of the source and the length of the seismic spread, which needs to be 4-5 times the depth of investigation.

For shallow investigation can be use in;

- Civil engineering for geotechnical work to determine the strength of a material and its composition, calculate of elastic moduli, assessment of rock quality. Determine tunnels and their entrances, oil and petrol storage depots, air raid shelters, military installations, factories, mines and sewage treatment plants
  - Hydrogeological investigations, depth of groundwater, determination of the water table. The seismic rock velocities are used for evaluating the risk for possible future water leakages under dam constructions or pollution of the groundwater.
-

- Environmental studies such as environmental audits and site assessments, seismic risk assessment, archeology, etc.
- Correction of lateral, near-surface, and Measuring the depth and thickness of the weathering zone, and erosion problems, mapping depth and topography of bedrocks
- Characterization and lithology of near surface material, evaluates soil, sand & gravel deposits, delineation of sedimentary layers, locating, identifying and mapping the fractures and faults, mapping thickness of landslides

Used to study large scale crustal layering: thickness and velocity large scale structure of earth (using earthquakes) such as Crustal structure and tectonics and Locates Geological Structures. (Redpath, 1973).

## 4.2 Advantages and disadvantages Seismic Refraction

Advantages of seismic refraction is that the refraction observations generally employ fewer source and receiver locations and are thus relatively cheap to acquire (Simple layout), low manpower requirements and limited Equipment Requirements. Also, rapid data reduction and little processing is done on refraction data with the exception of trace scaling or filtering to picking the arrival times and in addition, interpretations is easier than other geophysical methods. On the other hand, the method has some limitation and disadvantages such as: Relatively long layout (10 times depth), limited number of model layers, limited velocity differences and limited interface geometry (assume smooth). Refraction seismic observations require relatively large source-receiver offsets (distances between the source and where the ground motion is recorded, the receiver). In addition, the refraction seismic *only* works if the velocity at which motions propagate through the Earth increases with depth.

## 4.3 Wave Refraction and Snell's Law

When a seismic wave transmitted through the earth subsurface and reaches to boundary between two different mediums (layers), some of the energy is reflected and the others refracted and transmits into the earth with a different angle. (Figure 4.1).

A seismic wave incident on an interface is partly reflected and partly transmitted. In the general case where the wave is obliquely incident on the interface the transmitted wave changes direction (refracted). It will be bent either towards the normal line (normal to the interface at point of incidence) or away from that normal. The amount of bending (angle of refraction) and the sense of bending (towards or away from the normal) are governed by the velocities of the two layers separated by the interface. The refracted ray is bent away from the normal in case of the velocity in the medium in which the wave is refracted) is greater than that in the medium that hosts the incident wave. The bending of the refracted wave is towards the normal when the velocity of the medium, in which refraction occurs, is of lower value (Figure 4.2).

---

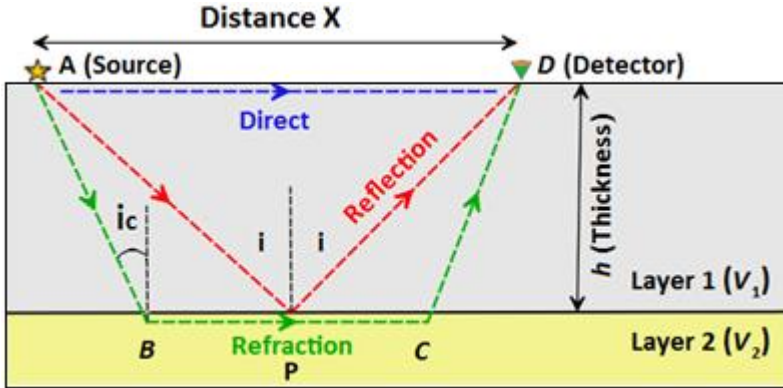


Figure 4.1. Reflection and refraction. Simple refraction occurs at P, critical refraction at B.

In essence, the phenomenon of ray bending (wave refraction) at an interface occurs only when the incidence direction is inclined to the interface.

Refraction of an incident seismic wave at an interface is governed by Snell's law which states that the ratio of the sine of angle of incidence ( $i$ ) to the sine of angle of refraction ( $r$ ) is equal to the ratio of velocity in the first medium (in which the wave is incident) to that of the second medium (in which the wave is refracted). In reference to (Figure 4.2), Snell's law takes the following form:

$$\frac{\sin i}{\sin r} = \frac{V_1}{V_2}$$

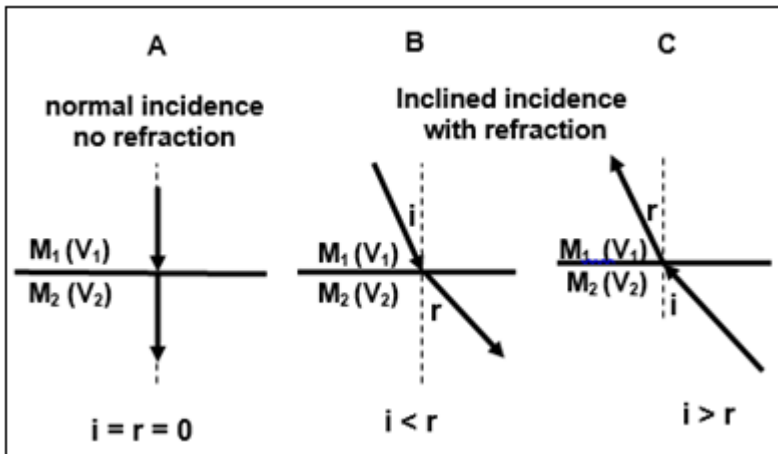


Figure 4.2 Occurrence of refraction in case of oblique incidence. (A) Normal incidence, no refraction, (B) Oblique incidence, from medium  $M_1$  to medium  $M_2$  (C) Incidence direction reversed. The velocities of the two media are  $V_1$  and  $V_2$ , where  $V_1 < V_2$ .

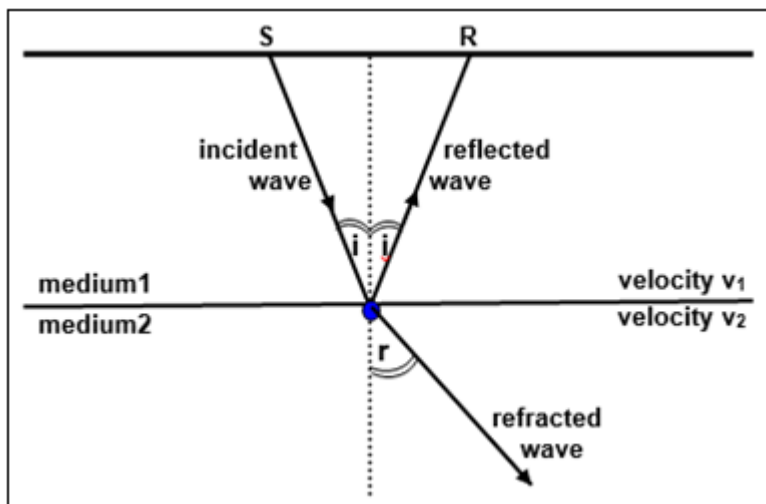


Figure 4.3 Reflection and refraction of a seismic wave at an interface separating media ( $M_1$ , velocity  $v_1$ ) and ( $M_2$ , velocity  $v_2$ ) where  $v_2 > v_1$ .

Referring to (Figure 4.4), the wave front (AB) of a plane seismic wave is hitting an interface existing between the two media ( $M_1$  and  $M_2$ ), at an incidence angle ( $i$ ). Point (B) requires an interval of time ( $\delta t$ , say) to reach the interface after point (A) has reached it. During this interval, the wave front would have travelled the distance of ( $v_1 \cdot \delta t$ ) into the medium ( $M_1$ ) and ( $v_2 \cdot \delta t$ ) into the second medium ( $M_2$ ). Being a plane wave, the wave front is plane surface which is represented by the line (AB) for the incident wave, (DE) for the reflected wave in medium ( $M_1$ ) and line (CD) for the refracted wave in medium ( $M_2$ ).

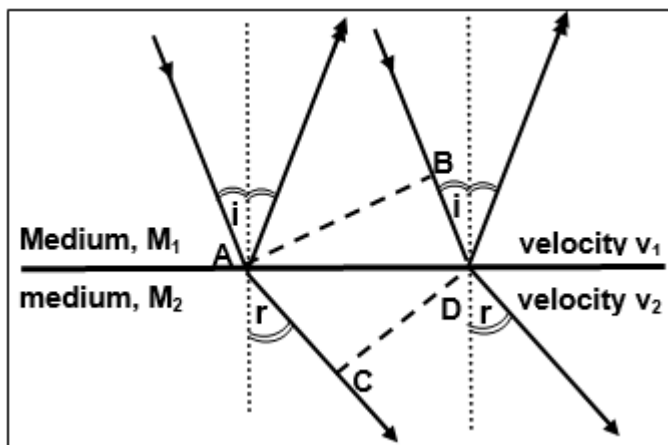


Figure 4.4 Refraction geometry of a seismic plane wave at an interface separating two media;  $M_1$ , velocity  $v_1$  and  $M_2$ , velocity  $v_2$ .

From the geometry of the wave path we note that the two right angle triangles (ABD) and (AED) are equal, giving equal reflection and incidence angles in support of the law of reflection. In the same figure 4.4, by examining the two right-angle triangles (ABD and ACD), we can write ( $\sin i = BD / AD$ ) and ( $\sin r = AC / AD$ ), giving the relation, which is Snell's law:

$$\frac{\sin i}{\sin r} = \frac{BD}{AC} = \frac{V_1 \cdot \delta t}{V_2 \cdot \delta t} = \frac{V_1}{V_2}$$

that is,

$$\frac{\sin i}{\sin r} = \frac{V_1}{V_2}$$

At each source point (shot point), three types of the seismic arrival waves are detected by the detectors (geophones) are;

- 1. Direct wave:** the waves (energy) travelling through the top layer (no refracted waves here). The travel-time curve for the direct wave is simply a linear function of the seismic velocity (Figure 4.5). Direct ray path to a detector at (R), with a distance (X) from the source (shot point). The direct ray travels horizontally through the top of the upper layer from (A) to (R) at velocity ( $V_1$ ) and the travel time determine by using this equation:  $t = X / V_1$ .

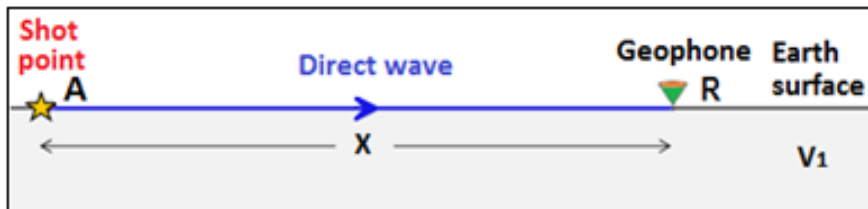


Figure 4.5. Path of direct wave near the earth surface from the source to geophone

- 2. Reflected wave:** The second type of waves appears on the seismograms are reflection waves as subsequent arrivals. Nevertheless, the relatively high reflection coefficients associated with rays incident on an interface at angles near to the critical angle often lead to strong wide-angle reflections which are quite commonly detected at the greater recording ranges that characterize large-scale refraction surveys (Kearey, ).

The seismic wave reflecting at the interface, the angles of incidence and reflection are equal, the wave reflects halfway between source and receiver (detector/geophone) and the reflected wave arrival time is never a first arrival (figure 4.6).

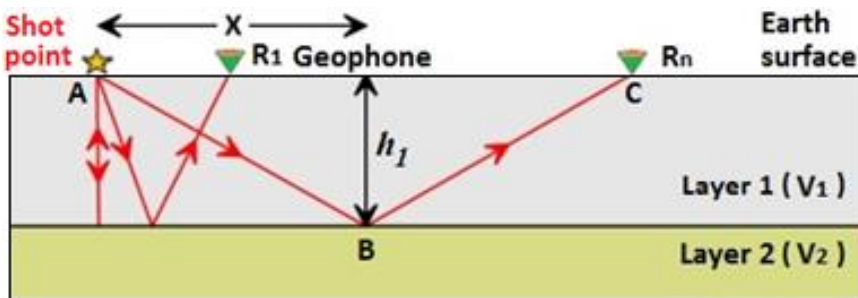


Figure 4.6. Path of reflected waves from the source to geophones (R<sub>1</sub>...R<sub>n</sub>)

**3. Head wave or Refracted wave:** where the travel waves refracting across the boundary between layers (interface), only arrives after critical distance and it is the first arrival only after crossover distance. The seismic refraction method depends on head waves (called refracted waves) arrive time to receivers (geophones) on the ground surface (Figure 4.7).

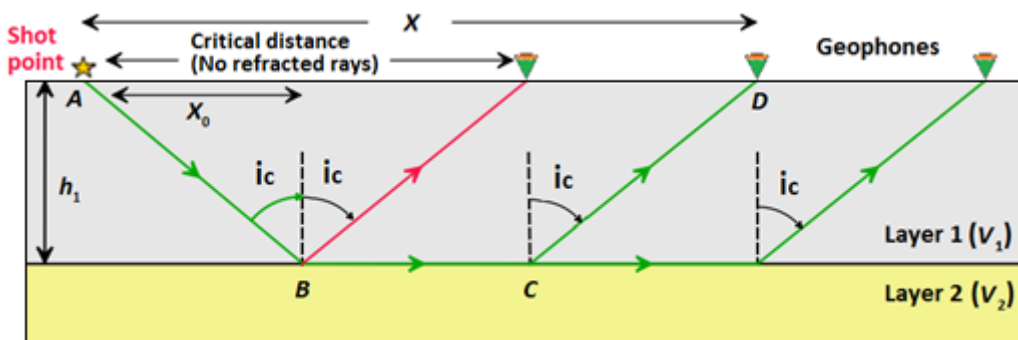


Figure 4.7. Path of head waves (refracted waves) from the source to geophones.

#### 4.4 Seismic ray Paths in the subsurface layers

The seismic refraction method applied to get information about the velocity, geometry and subsurface geologic layers. To apply and study the seismic refraction it is important to assuming that: -

- a. The subsurface layers separated by horizontal planes or dipping interfaces.
- b. The velocity of the seismic waves in each layer is constant.
- c. The subsurface layer velocities increase with depth.

In seismic refraction method the ray paths through two main cases which are horizontal and dipping layers.

#### 4.4.1 Case of horizontal reflectors:

There are three subsurface horizontal cases that are taken in consideration in analyses the seismic refraction data that are; a single horizontal subsurface interface, two or multiple horizontal layers and dipping layers.

##### 1. A Single Horizontal case (Interface)

There is only one geologic boundary between two different layers refract waves to the surface. The refraction based on Snell's law, critical angle, and critical refraction.

##### 2. Two-layered horizontal case (one refracted Interface)

The refracted waves travel within the earth and at the interface between the two layers having different velocities ( $V_1$  and  $V_2$ ) reflect to the surface at velocity  $V_1$  along AD path (along these three segment paths; AB, BC and CD that are inclined at the critical angle  $i_c$ , and travels along the interface between B and C at the higher velocity  $V_2$  (Figure 4.7).

The travel-time along the refracted ray path ABCD is

$$T_h(x) \text{ or } T_{AD} = T_{AB} + T_{BC} + T_{CD}$$

and when reflected to the surface so that:

$$T_h(x) = \frac{AB}{V_1} + \frac{BC}{V_2} + \frac{CD}{V_1}$$

or, (using  $\sin i_c = V_1/V_2$  from Snell's law and the sine-cosine relationship)

$$T_h(x) = \frac{x \sin i_c + 2h_1 \cos i_c}{V_1}$$

That is

$$T_{AD} = \frac{2h_1}{V_1 \cos i_c} + \frac{(x - 2h_1 \tan i_c)}{V_2} = \frac{x}{V_2} + \frac{2h_1}{V_1 \cos i_c} \left(1 - \frac{V_1}{V_2} \sin i_c\right)$$

or,

$$T_h(x) = \frac{x}{V_2} + 2h \frac{\sqrt{V_2^2 - V_1^2}}{V_1 V_2}$$

Where ( $i_c$ ) is the critical angle, and ( $h$ ) is depth of the interface. The two velocities, ( $V_1$  and  $V_2$ ) are velocities of the two layers. These are equal to the reciprocals of the slopes of the direct and refracted travel-time curves respectively.

It is readily noted that refraction travel-time function is linear in ( $x$ ), and its curve is straight line of slope equal to ( $1/V_2$ ) and its intercept ( $T_0$ ) is given by:

$$T_0 = 2h \frac{\sqrt{V_2^2 - V_1^2}}{V_1 V_2}$$

The depth ( $h$ ) can be calculated from this equation, where:

$$h_1 = T_0 \frac{V_1 V_2}{2\sqrt{V_2^2 - V_1^2}}$$

Thus, with the velocity ( $V_1$ ) which is obtained from the travel-time of the direct wave, and ( $V_2$ ) from the refraction travel-time, the interface depth ( $h$ ) can be calculated.

An alternative way of computing the depth ( $h$ ) of the refractor is by use of the cross-over distance ( $x_{cr}$ ). By definition, the travel-time of the direct wave, at the cross-over distance, is equal to that of the refracted. Thus, by equating the two travel times at the cross-over distance

$$\frac{x_{cr}}{V_1} = \frac{x_{cr}}{V_2} + 2h \frac{\sqrt{V_2^2 - V_1^2}}{V_1 V_2}$$

to give:

$$h_1 = \frac{x_{cr}}{2} \sqrt{\frac{(V_2 - V_1)}{(V_2 + V_1)}}$$

### **Travel-time curve**

As we mentioned above, on seismic shooting records, three main waves (direct, refracted, and reflected) arrivals are usually observed. The travel-time for direct and refracted arrival waves are straight (linear), but hyperbolic for the reflected arrival wave. At the critical distance ( $x_c$ ), where the incidence is at the critical angle ( $i_c = \sin^{-1}(v_1/v_2)$ ), a head wave is generated which is refracted to surface at an angle equal to the critical angle. The distance ( $0$  to  $x_c$ ), no refraction arrivals exist, hence it is a (shadow zone) for refracted waves (Figure 4.8).

---

After plotting the time-distance curve (Figure 4.8), the following steps are used to determine the velocities of the subsurface layers and their thickness: -

- a. Plot the of first wave versus the distance between shot point (source) and receivers (geophones).
- b. The arrival time of direct waves are lie along a straight line joining the origin. The slope of this line is  $(1/V_1)$ , where  $(V_1)$  is the velocity of the first layer (layer 1).
- c. The arrival time refracted wave also appears as a straight line with smaller slope equal to  $(1/V_2)$ , where  $(V_2)$  is the velocity of the second layer (layer 2).

From the time-distance curve (Figure 4.9), we can calculate of direct arrival and critical refraction, we can find velocities of two layers and depth to interface; determine the velocity of first layer  $(V_1)$  from the slope of direct arrival, velocity of second layer (layer 2) from the slope of critical refraction, estimate  $(t_i)$  from plot and the thickness  $(h_1)$  of the top layer  $(V_1)$  and the second layer  $(V_2)$  by using the following relation:

$$h_1 = \frac{x_c}{2} \sqrt{\frac{(V_2 + V_1)}{(V_2 - V_1)}}$$

Where;  $(x_c)$  is critical distance,  $(h_1)$  and  $(V_1)$  are the thickness and velocity of top layer, respectively.  $(V_2)$  is the velocity of bottom layer and  $(t_i)$  is the intercept time from the time-distance plot for each shot.

The axis **intercept time** is found by projecting the travel time curve back to  $(X = 0)$ . The intercept time allows a depth estimation.

$$t_i = 2h_1 \sqrt{\left(\frac{1}{V_1}\right)^2 - \left(\frac{1}{V_2}\right)^2}$$

**Critical distance**  $(x_c)$ : is a distance beyond which critical incidence first occurs.

$$x_c = 2h_1 \tan i_c$$

$$x_c = 2h_1 \sqrt{\frac{(V_2 + V_1)}{(V_2 - V_1)}}$$

At the critical distance the direct wave arrives before the head wave. At some point, the travel time curves cross, and beyond this point the head wave is the first arrival.

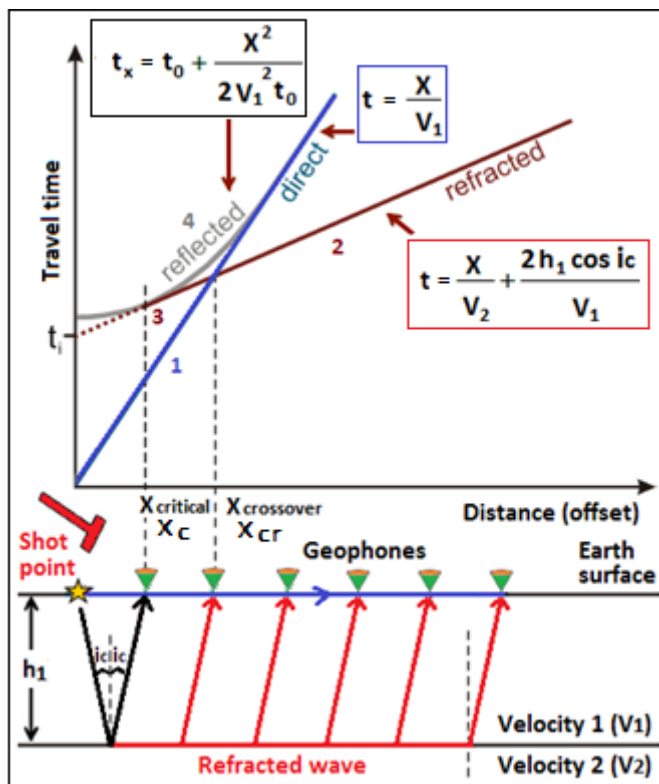


Figure 4.8 Ray-paths and travel-time curves of direct, critically-refracted, and reflected waves, with critical distance (0 to  $x_c$ ) and cross-over distance (0 to  $x_{cr}$ ). This is a two-layer case, the travel-time curve for direct waves, critically refracted waves (head waves), late refracted arrivals. Travel-time curves, and reflected waves are shown by numbers 1-4, respectively. Note that critically refracted waves start arriving after a critical distance  $X_{critical}$  but they overtake the direct waves at a crossover distance  $X_{crossover}$ . The break in slope of the above travel-time curve, which occurs at the “crossover distance”, marks the point at which travel-times refracted from  $(V_2)$  overtake direct arrivals traveling through  $(V_1)$  (modified from Sharma\_P\_Environmental\_and\_Engineering.pdf)

The depth can be determined from the crossover distance ( $X_{crossover}$ ). The thickness ( $h_1$ ) of the upper of the two layers can be determined from the crossover distance and the velocities or from the intercept time and the velocities.

$$h_1 = \frac{x_{cross}}{2} \sqrt{\frac{(V_2 - V_1)}{(V_2 + V_1)}}$$

The crossover distance determines the length of the refraction line.

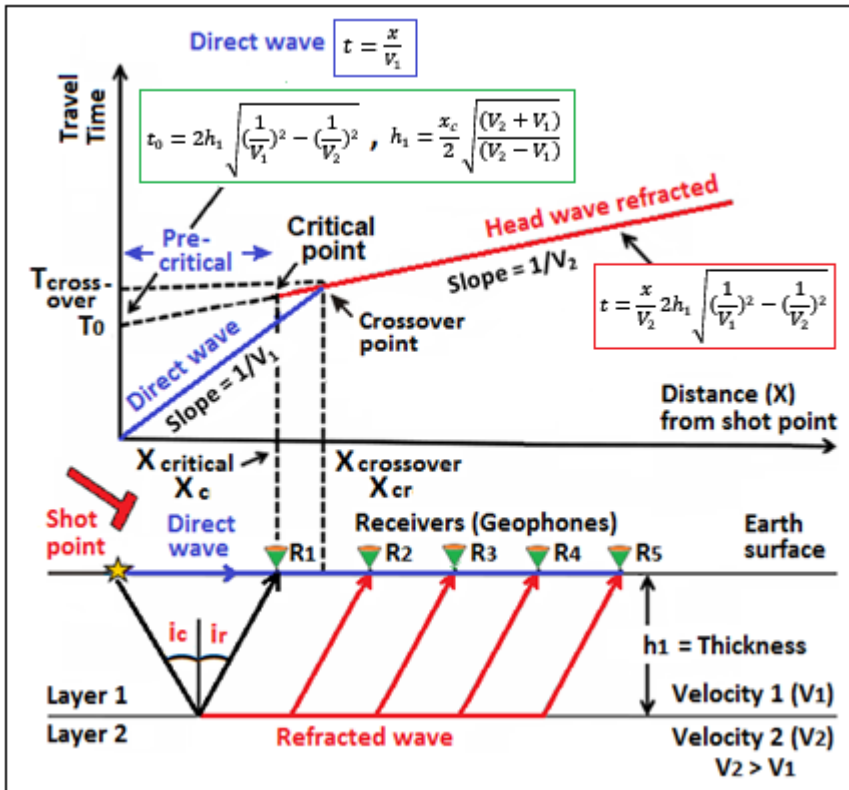


Figure 4.9. Propagation of the waves underground surface and travel-time curve for direct and refracted waves, a two-layer subsurface structure. Then, in two-layer problem, only, one reflection and one refraction. At pre-critical offsets, record direct wave and reflection, and in post-critical domain, record direct wave, refraction, and reflection. (Modified from Preliminary Seismic Refraction Survey of the Cannon River Wilderness Park, Kort H. Butler. Senior Integrative Exercise. March 11, 2009)

### 3. Three and multiple horizontal layers (interfaces)

The calculation of the velocities ( $V_1$  and  $V_2$ ) and thickness ( $h_1$ ) of the first layer in multiple horizontal layers case is the same as in the two layers case. We calculate the velocity of the third layer ( $V_3$ ) from the slope of the third layer (layer 3). Intercept time ( $T$  or  $t_i$ ) and thickness of the second layer ( $h_2$ ) could be calculate by using the following equations assuming that ( $V_3 > V_2 > V_1$ ).

$$T = \frac{x}{V_3} + 2 \frac{h_1 \cos i_{c1}}{V_1} + 2 \frac{h_2 \cos i_{c2}}{V_2}$$

Where  $i_{c1} = \sin^{-1} \frac{V_1}{V_3}$  and  $i_{c2} = \sin^{-1} \frac{V_2}{V_3}$

$$h_2 = (t_{i2} - \frac{2h_1 \sqrt{(V_3^2 - V_1^2)}}{V_3 V_1}) \frac{V_3 V_2}{2 \sqrt{(V_3^2 - V_2^2)}}$$

Where (T or  $t_i$ ) is the intercept time on the time-distance curve the for each shot.

Now, for multiple layers (n-layer) case: n-1 intercept times, then

$$T_n = \frac{x}{V_n} + \sum_{i=1}^{n-1} \frac{2h_i \cos i_{ci}}{V_i}$$

Where

$$i_{ci} = \sin^{-1} \frac{V_i}{V_n}$$

This gives the travel time, ( $T_n$ ) of a ray critically refracted along the top surface of the (n th) horizontal layer.

---

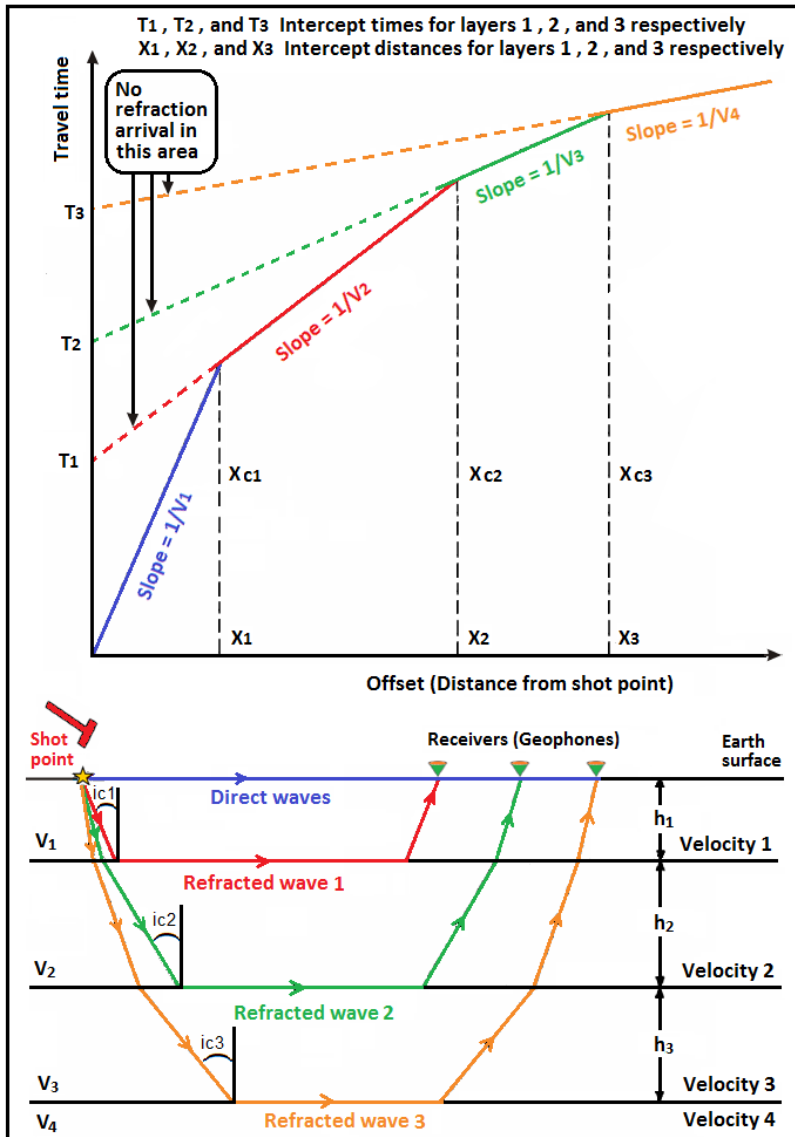


Figure 4.10. Time - distance curve for a simple multi-layer case.

#### 4.4.2 Case of Dipping refractors (layers)

When the underground layers (refractors) are dipping, the slope of the travel-time curve does not represent the true layer velocity and the velocities are called "apparent velocities". When the forward and reverse shooting survey acquired, the travel time plots for refracted rays of both shooting will differ in their gradients, apparent velocity and intercept times. Apparent velocity of the refractor at Shooting up dip become higher and when the shooting down dip then the apparent velocity of the

refractor is lower. Then, to determine both the layer velocity and the interface dip, forward and reverse refraction profiles must be acquired (figure 4.11).

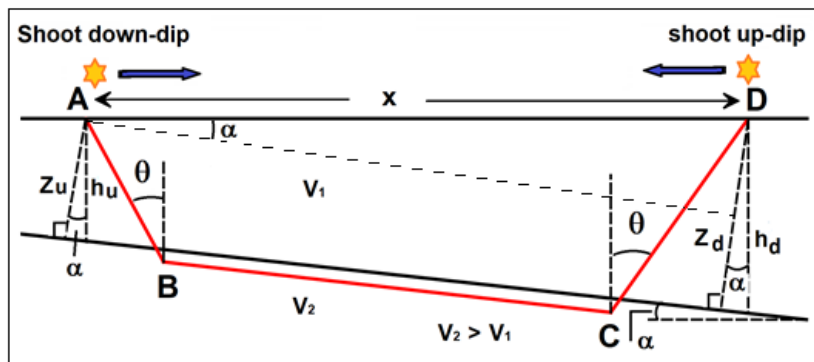


Figure 4.11 Ray-path geometry of a wave refracted from a dipping interface

By using  $(V=x/t)$  equation, it can be calculated critical angle  $(\theta)$  and the dip angle  $(\alpha)$  of the layer, velocity of first layer  $(V_1)$ , and the velocity of the second layer at the down-dip  $(V_{2d})$  and the up-dip  $(V_{2u})$  positions. Then,  $(Z_u)$ ,  $(Z_d)$ ,  $(h_u)$  and  $(h_d)$  can be calculated. It is important to know that the travel times are equal in forward and reverse directions for switched, reciprocal, source and receiver positions.

As it is with the case of horizontal (non-dipping) refractor consists of three segments; AB, BC, and CD, but the ray-path in the case of dipping refractor (dip angle,  $\alpha$ ) rotated, with extra time delay at D (Figure 4.11).

The travel time  $T(x)$ , in down-dip shooting, is given by

$$T(x) = \frac{AB}{V_1} + \frac{BC}{V_2} + \frac{CD}{V_1}$$

$$\frac{AB}{V_1} = \frac{Z_u}{V_1 \cos \theta}$$

where:

$$\frac{BC}{V_2} = \frac{x \cos \alpha - Z_u \tan \theta - (Z_u + x \sin \alpha) \tan \theta}{V_2}$$

$$\frac{CD}{V_1} = \frac{(Z_u + x \sin \alpha)}{V_1 \cos \theta}$$

$z_u$  is the perpendicular distance from the source at point (A) to the interface and  $z_d$  is the perpendicular distance from the receiver at point (D) to the interface.

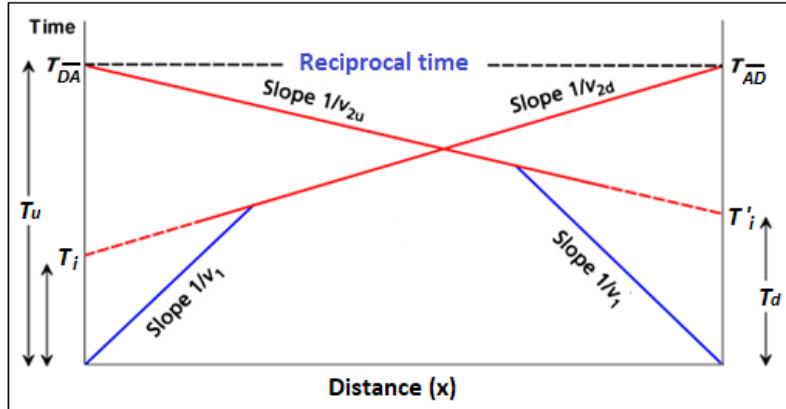


Figure 4.12 Same type of time-distance curve as for the horizontally layered case, but observation of two different apparent velocities ( $V_{2d}$ ), ( $V_{2u}$ ) for the refracted wave that propagates at true velocity ( $V_2$ ).

For down-dip shooting, the refraction travel-time function is given by:

$$T_{(x)} = \frac{x \sin(\theta + \alpha) + 2Z_u \cos \theta}{V_1}$$

and for up-dip shooting, ( $\theta$ ) is given negative sign, and the function becomes:

$$T_{(x)} = \frac{x \sin(\theta - \alpha) + 2Z_u \cos \theta}{V_1}$$

For down-dip shooting, the refraction travel-time function is given by:

$$t_2(x) = \frac{x \sin(\theta + \alpha)}{V_2} + \frac{2Z_u \cos \theta}{V_1}$$

and for up-dip shooting, ( $\alpha$ ) is given negative sign, then, the travel-time is:

$$t_2(x) = \frac{x \sin(\theta - \alpha)}{V_2} + \frac{2Z_d \cos \theta}{V_1}$$

Where the critical ( $\theta$ ) and dip ( $\alpha$ ) angles can be obtained by using the following formulas:

$$\theta = \frac{1}{2} \left( \sin^{-1} \left( \frac{V_1}{V_{2d}} \right) + \sin^{-1} \left( \frac{V_1}{V_{2u}} \right) \right)$$

$$\alpha = \frac{1}{2} \left( \sin^{-1} \left( \frac{V_1}{V_{2d}} \right) - \sin^{-1} \left( \frac{V_1}{V_{2u}} \right) \right)$$

Then, the intercept time ( $t_i$ ), ( $Z_u$ ), ( $Z_d$ ), ( $h_u$ ) and ( $h_d$ ) can be calculate:

$$t_i = \frac{2Z_u \cos \theta}{V_1}, \quad t'_i = \frac{2Z_d \cos \theta}{V_1}$$

The intercepts ( $t_i$ ) and ( $t'_i$ ) can be used to calculate the slant depths ( $Z_u$ ) and ( $Z_d$ ):

$$Z_u = \frac{V_1 t_i}{2 \cos \theta}, \quad Z_d = \frac{V_1 t'_i}{2 \cos \theta}$$

Finally, true depths ( $h_u$ ) and ( $h_d$ ) can be calculate using these slant depths ( $Z_u$ ) and ( $Z_d$ ) and for dip  $\alpha$  using the following relations

$$h_u = \frac{Z_u}{\cos \alpha}, \quad h_d = \frac{Z_d}{\cos \alpha}$$

The general form of the equation for the travel-time  $t_n$  of a ray critically refracted in the  $n$ th dipping refractor (Johnson 1976)

$$t_n = \frac{x \sin \beta_1}{V_1} + \sum_{i=1}^{n-1} \frac{h_i (\cos \alpha_i + \cos \beta_i)}{V_i}$$

where  $h_i$  is the vertical thickness of the  $i$ th layer beneath the shot,  $V_i$  is the velocity of the ray in the  $i$ th layer,  $\alpha_i$  is the angle with respect to the vertical made by the down-going ray in the  $i$ th layer,  $\beta_i$  is the angle with respect to the vertical made by the up-going ray in the  $i$ th layer, and  $x$  is the offset distance between source and detector (Jones, F., 2007).

The angle of dip ( $\alpha$ ) can be computed from two refraction-experiments; one down-dip giving a straight-line having slope ( $S_d$ ) and the other is up-dip which gives a straight line of slope ( $S_u$ ). From the travel-time functions for the two experiments, we have:

$$Z_d = \frac{\sin(\theta + \alpha)}{V_1}$$

$$Z_u = \frac{\sin(\theta - \alpha)}{V_1}$$

Hence,

$$\theta + \alpha = \sin^{-1}(V_1 Z_d)$$


---

and

$$\theta - \alpha = \sin^{-1}(V_1 Z_u)$$

giving:

$$\alpha = \frac{\sin^{-1}(V_1 Z_d) - \sin^{-1}(V_1 Z_u)}{2}$$

In order to calculate ( $\alpha$ ) from this formula, we need to know the velocity ( $V_1$ ). This is obtained from the slope of the direct wave which is always available in such experiment. The travel-time curve of the direct wave is straight line passing through the origin ( $T(x) = x/ V_1$ ) and its slope is equal to the inverse of the wave propagation velocity. We may further note that ( $\alpha$ ) is the apparent angle of dip in the direction of the shooting-line ( $x$ -axis direction).

### 4.2.3 Faulted Planar Interface

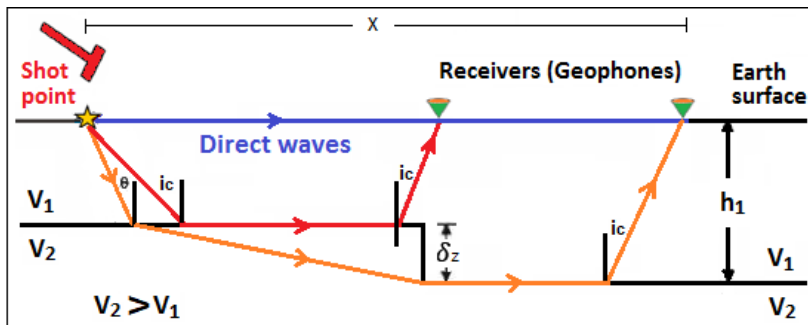


Figure 5.13 Faulted reflector path.

In case of the faulted refractor, there will be a sharp offset in the travel time curve:

The throw on fault can be estimate from offset in curves, (difference between two intercept times), using the formula:

$$\delta = \frac{\delta V_1 V_2}{\sqrt{V_2^2 - V_1^2}}$$

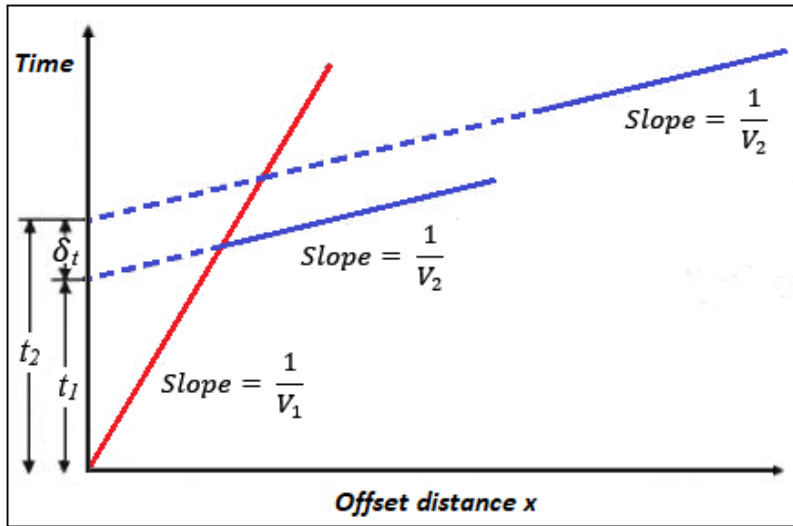


Figure 4.14 show the offset in the travel time curve due to the fault.

---

# 5. 2D SEISMIC REFLECTION SURVEYING

## 5.1 The Shot-point

A seismic survey of a certain seismic line starts with deployment of the spread elements (shot and receivers) along that line. The designed spread, which consists of linear array of receiver-points which are co-linear with the shot-point, is laid down along the line to be surveyed. When activating the energy source (as firing a dynamite charge), a seismic wave-front advances through the medium in the form of spherical surfaces (spherical when the medium is homogenous and isotropic). The seismic energy is reflected from intervening interfaces, back to the surface to be detected by the geophone groups planted on the surface. The reflection arrivals are then fed in to the recording system via the electrical channels which are displayed in a trace-gather (called the shot-gather).

An actual shot record of a center-spread, 48-trace shot-point, is given here-below (Figure 5.1). It is showing clear reflection arrivals as well as direct and refracted arrivals.

## 5.2 Seismic Trace Modes of Display

There are three common modes of trace-display. These are:

- (i) Wiggly-trace, when a wiggly line represents the amplitude variation recorded.
- (ii) Variable-area trace, when the peak-parts of the wiggly trace are blacked in.
- (iii) Variable-density trace, when the amplitude variation is represented by an appropriate shade-intensity

Usually field shot-records are displayed in a wiggly-trace mode (Figure 5.2), whereas stack sections are displayed by superimposing the wiggly- and variable-area modes of display.

---

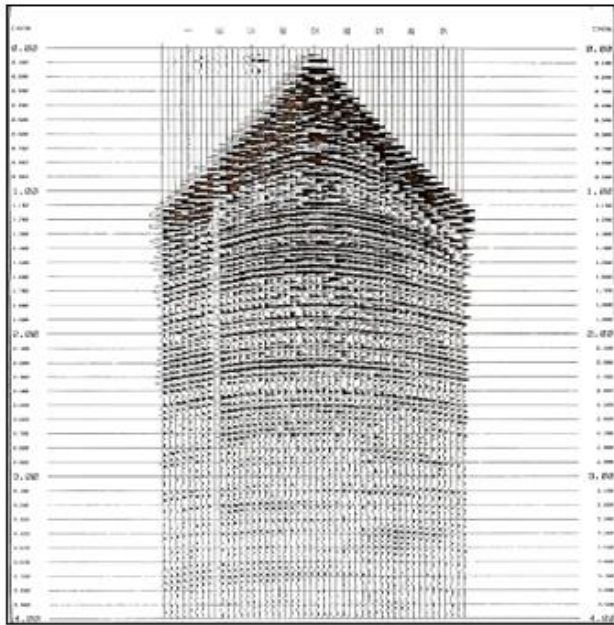


Figure 5.1 An actual 48-trace shot record showing clear reflection arrivals with relatively high-amplitude direct and refracted arrivals. Traces are displayed in variable-area modes of display.

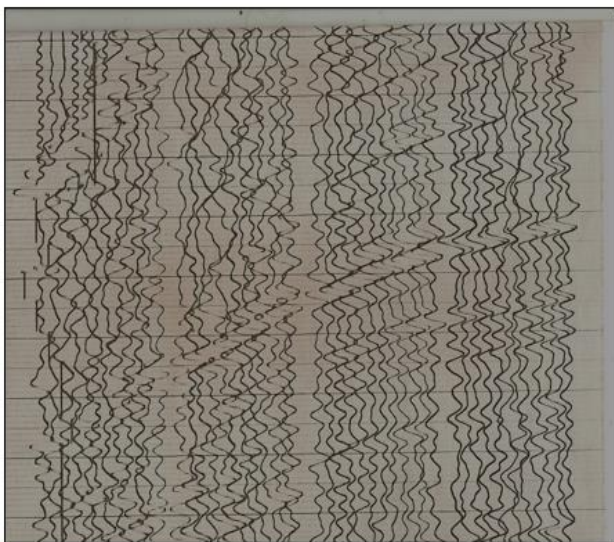


Figure 5.2 Part of 48-channel shot-record showing reflection arrivals and random seismic noise. Traces are displayed in wiggly-trace mode.

---

### 5.3 The Spread Configuration

The shooting spread used in seismic surveying, is defined as the geometrical relationship between the *source-point* and the *receiver-point* which are kept unchanged during surveying a seismic line. The main elements of a spread are the source-point (commonly known as the *shot-point*), and number and inter-spacing of the receiver-points. In practice, shot-points and receiver-points are not points but sets of points. Thus, a receiver point is usually made up of a group of detectors (geophones) and the shot-point consists of a group of source-points. For this reason, shots and receivers are usually referred to as geophone-groups and shot patterns respectively. For computation purposes, their geometrical centers are used to represent the shot-point and receiver-points respectively.

Based on the position of the shot-point in relation to the receiver-point, there are three types of spread configuration in common use. The shot-point may be located at one end of the receiver linear array giving a type called *end-on spread*. Another type of spread is the one in which the shot-point is located within the spread, it is called *split- or unbalanced-spread*, and when it is located exactly at the center of the receiver array-line, it is called *center spread*. The three common spread types are shown in Figure 5.3.

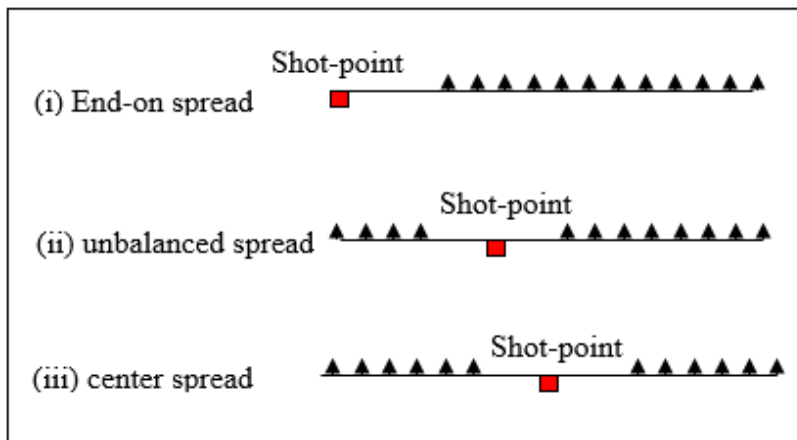


Figure 5.3 Types of commonly used shooting spreads.

The number of the active receiver points (or seismic channels) per spread is customarily fixed at a whole-number which is customarily taken as multiple of the number (12). In 2D seismic surveying, the number of spread-channels used has increased from 48 in the early 1970s to 240; and 360 channels in the following forty years. In 3D surveying the number may exceed 1200.

### 5.4 The CDP Concept

A shot-gather is the group of traces recorded by the spread channels of that shot. Likewise, the CDP-gather is a group of seismic traces which belong to one CDP. Naturally, the number of traces belonging to a certain CDP is equal to the fold of coverage for that CDP. By definition, the CDP is a subsurface point located vertically below the source-receiver midpoint. This means that each receiver-point of a spread will receive a seismic arrival reflected from a CDP located below the source-receiver midpoint. In fact, shooting of one spread, the reflector will be sampled by a number of reflection points (CDPs) equal to the number of the spread active receivers. From the geometry of the spread ray-path, the CDP spacing will be half that of the receiver spacing. Thus, the subsurface coverage (CDP-line) covered from shooting one shot will be about half the spread length (Figure 5.4).

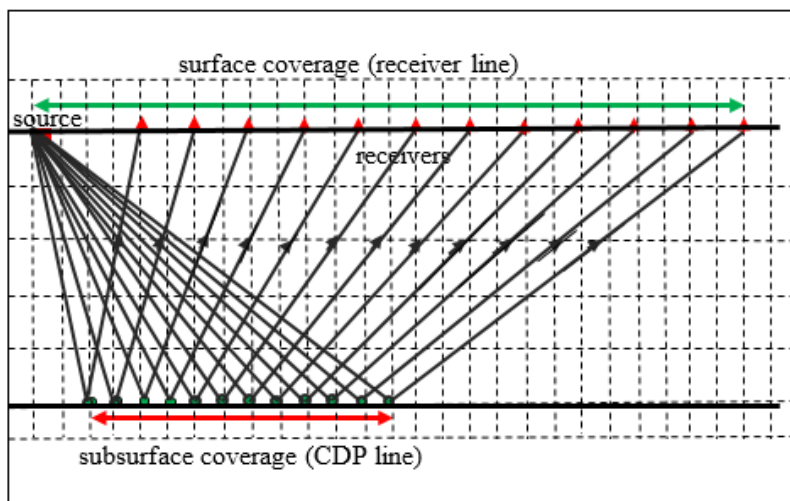


Figure 5.4 Shooting spread surface-coverage, reflection ray-path, and CDP subsurface coverage, as realized from one seismic shot-point.

### 5.5 The Seismic Profiling Technique

Seismic surveying along a linear track is carried out by a technique known as (multi-channel profiling technique). The survey procedure involves the use of a fixed-shape spread that moves along a linear profile at a constant move-up shift. The first shot-record is obtained from the spread which is laid out at the start-point of the line. In the following step, the second shot is recorded after shifting the spread location by a certain step-up distance.

This process (shift-and-shoot process) is repeated from the start point to the end point of the line. The move-up distance is normally made to be integral multiple of the receiver-point spacing. A map of all surface locations which have been occupied in

surveying the entire line is called *surface coverage*. An example is shown in Figure 5.5.

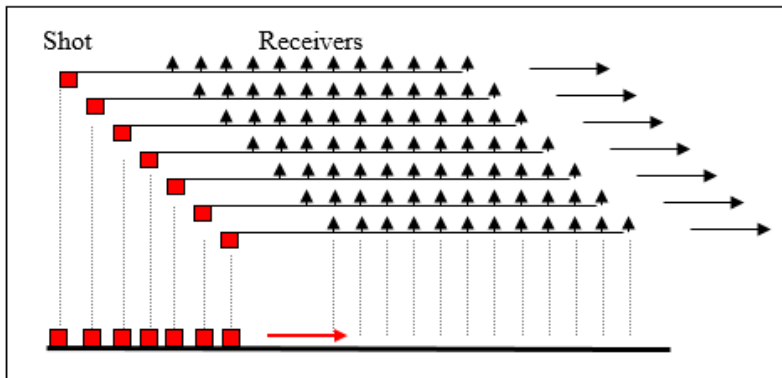


Figure 5.5 The surface coverage of a seismic line made up of 7 shot points, with 12 receivers each. The move-up is 1 receiver-station.

Seismic profiling process is accomplished by repeating the shooting process (shot firing and reflection-arrivals recording) at a series of equally spaced shot-point locations along a defined line. By making the spread move-up distance equal to half of the spread length, one reflection per one CDP will result for the entire line. The resulting seismic section, in this case, is commonly known as (single-fold section). For larger move-ups, gaps will result in the sampled reflector. That is, certain CDPs will not have reflections at all. On the other hand, if the move-up distance is smaller than half the spread length, then CDPs will get more than one reflection, giving the case of multi-fold profiling technique. The number of reflections realized per CDP is called the fold of coverage, (or just, fold). Of course, the shorter the move-up, the greater the fold will be.

## 5.6 The Coverage Diagram

The diagram which shows the geometry of the shot and receiver's locations in a profiling survey is customarily called the coverage diagram. This diagram shows the surface and subsurface coverage of the survey. An example of the coverage diagram is presented in Figure 5.6.

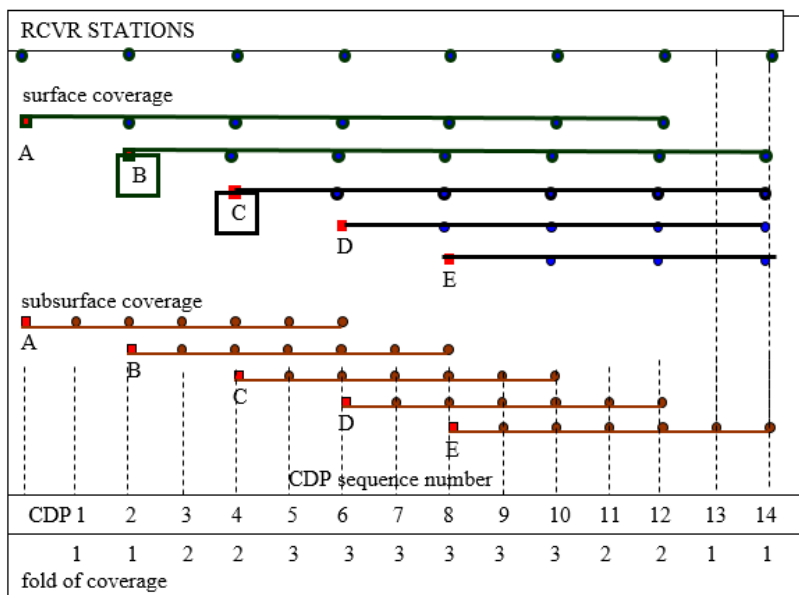


Figure 5.6 Surface and subsurface coverage of an example of a profiling survey for a spread made up of an end-on spread of six-channel shots moving at one receiver move-up motion.

In this example we have a survey made up of five shots (A, B, C, D, and E). Shot-A traces are  $(a_1, a_2, \dots, a_6)$  and Shot-B traces are  $(b_1, b_2, \dots, b_6)$ , and so on for the rest of shots. The complete surface coverage is occupying a total of 11 receiver-stations with one receiver-station for the spread move-up distance. Corresponding to this surface coverage, is a subsurface coverage made up of 14 CDPs,  $(CDP_1, CDP_2, \dots, CDP_{14})$ .

The trace gathers for  $CDP_1$  (CDPG-1) consists of one trace ( $a_1$ ). For the second CDP (CDPG-2) the gather has also one trace ( $a_2$ ). The CDPG-3 has two traces ( $a_3 + b_1$ ), and so on. The number of traces per CDP is representing the fold of coverage.

### Trace Re-sorting

In the example shown by the last figure, let the traces belonging to the shotpoint (A) be called  $(a_1, a_2, \dots, a_6)$  and those traces belonging to shotpoint (B) be called  $(b_1, b_2, \dots, b_6)$  and so on. In this case the CDP gathers for the CDPs will be as follows (Figure 5.7).

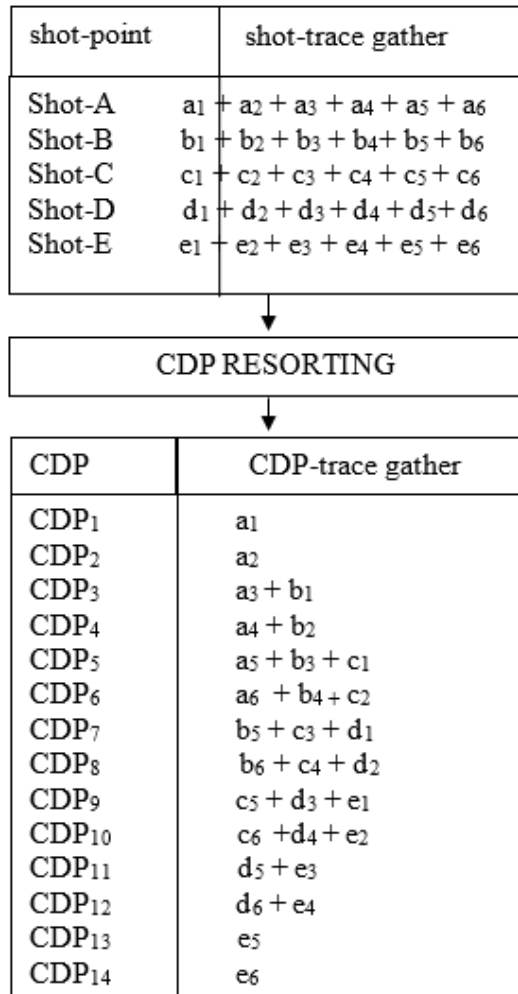


Figure 5.7 The CDP sorting process of the profiling case, given in the example shown in Figure 5.6.

## 5.7 The Fold of Coverage

The set of traces which belong to a CDP is normally referred to as the CDP trace gather (CDPG) and the number of reflections that occur from that CDP represents the fold of coverage. 6.6 The Fold of Coverage in a regular shooting, which is normally applied in seismic profiling, the fold of coverage (F) can be calculated from the following formula:

$$F = N / 2n$$

where, (N) is the total number of the spread active receiver-channels and (n) is the move-up distance expressed in receiver-station spacing, i.e. spacing measured in

number of receiver-stations. This equation shows that the fold is directly proportional to the number of channels and inversely proportional with the move-up distance.

## 5.8 Seismic Reflection Data Acquisition

In seismic reflection data acquisition, we are, in general, dealing with generating and detecting P-waves which are propagating from the source region and getting reflected from subsurface interfaces. The complete data acquisition process involves seismic source generation, reflected wave detection, and digitally data recording.

In order to record the reflection arrivals with minimum distortions, optimum operation parameters (called field parameters) are determined and applied in conducting the seismic survey. The seismic field-crew usually carries out certain field activities directed towards determination of the optimum survey parameters and optimum survey procedures. Optimization of survey parameters and survey procedures are collectively referred to as *survey design* which is normally outlined in the work plan.

## 5.9 Seismic Energy Sources

The traditional method applied in generating seismic waves is exploding dynamite in shot-holes. There are, however other methods which have been introduced as alternative seismic energy sources. Choice of the source-type depends on the surface conditions prevailing in the given survey area. The main criteria considered in evaluating a particular source-type are the following:

- strong enough to generate strong seismic signal that can be reflected from deep interface and be detectable at the farthest receiver (receiver of maximum offset).
- the generated seismic signal is rich in high frequency components to be able to resolve closely spaced reflectors'
- the generated noise is of least energy level.

Depending on the surface environments, the source types are classified into land- and marine-sources. Here-below are brief definitions of these types.

### 5.9.1 Land Seismic Sources

#### (i) Dynamite

This is one of the most common type of seismic source used in land seismic surveying. Normally, a certain dynamite charge is exploded inside a drilled hole at a depth ranging from few meters to several tens of meters. Typically, the drilled hole is of diameter of about 10 cm and depth of about 5m - 15m. Ideally the charge depth

---

should be placed deeper than the base of the weathered layer (low-velocity layer, LVL, as it is often called), in order to avoid high-frequency filtering and seismic pulse weakening caused by that layer (Figure 5.8).

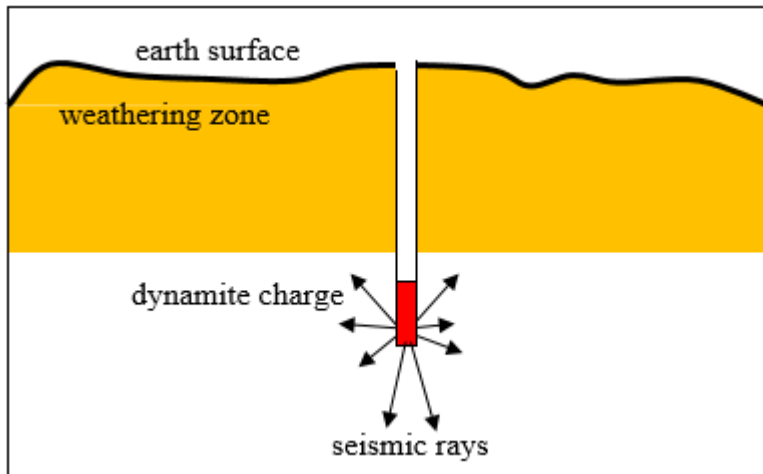


Figure 5.8 Dynamite seismic-energy source.

To increase the charge-coupling with the surrounding medium, the hole is filled with water or with mud.

The most common way of using this method is placing the dynamite charge at the bottom of a drilled hole. However, the charge, under certain conditions, may be placed in shallow holes or even at a height above the ground. A method called Air-shooting or Poulter method (Poulter, 1950) involves simultaneous firing of a number of charges placed on poles in the air. This is not an efficient method since the ground surface is of high reflection coefficient and thus a relatively small portion of the generated energy is transmitted into the earth, and most of the energy is reflected back from the surface and in generating surface waves. This method (Poulter method) is not in common use at present.

In general, the dynamite source is characterized by its high energy level, and of wide frequency band, though it involves a certain degree of danger and needs special storage conditions and strict safety measures.

### **(ii) Weight Dropping**

The Weight Dropping method (also called *Geograph* or *Thumper*) involves dropping a weight of about 3 tons from a height of about 3 meters on to the ground (Figure 5.9).

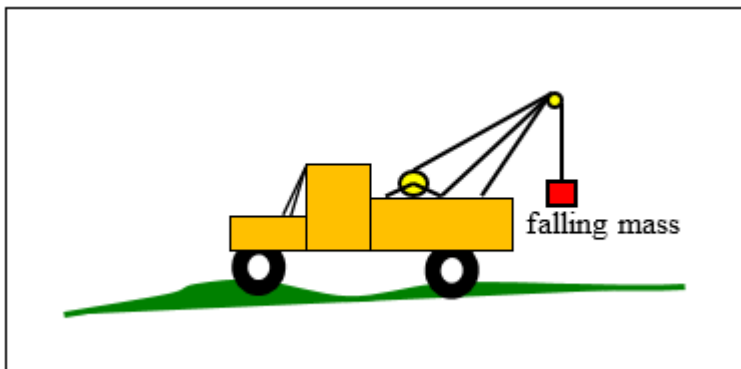


Figure 5.9 Weight-Dropping seismic-energy source

The seismic energy generated from the impact of the falling mass with the ground is considered to be weak in comparison with the dynamite explosion. In order to strengthen the generated seismic signal, the dropping shot is repeated number of times (30-60) shots done at the same location and electronically summed up to produce one shot-record. This technique of summing corresponding traces of shots of common location (called vertical stacking) is normally applied in cases of weak energy sources.

Compared with the other energy sources, weight dropping gives fairly high frequency, but less than dynamite-generated pulses. It is safe, fast, and cheap in operation. The draw-back of the method is the development of strong surface waves and, because of the filtering effect of the surface LVL zone, the high frequency components are severely attenuated. This method is rarely applied at present.

### **(iii) Gas Exploding**

This is another impulsive source (known as Dinoseis) in which the energy is created by exploding a mixture of oxygen and propane gases contained in a confined chamber, the bottom of which is a moveable plate resting on the ground surface. The so-designed chamber is attached to the bottom of a heavy vehicle to increase coupling of its plate with ground surface (Figure 5.10).

On detonating the gas mixture, a sudden pressure impact occurs which is transmitted through the base-plate to the ground surface. By hydraulic system the plate is locked into position after the impact to prevent repeated impacts.

Being weak-energy source, more than three units are fired simultaneously by a control signal sent from the recording system, and the shot is repeated many times, then vertical stacking is applied to get improved S/N ratio.

---

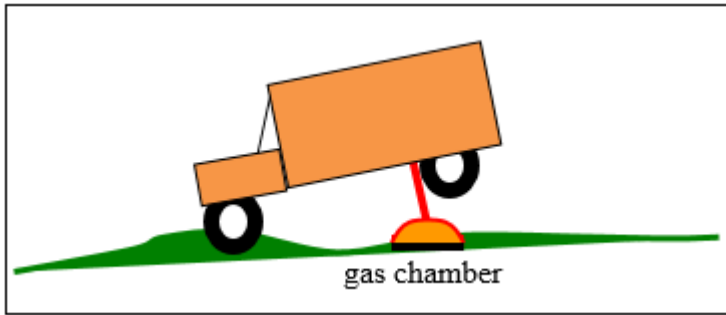


Figure 5.10 Gas exploding seismic-energy source.

The general features of Dinoseis are similar to the Weight Drop method. Both are surface sources which are generating relatively weak seismic energy, developing strong surface waves, and producing low-frequency seismic pulses. The method is rarely applied these days.

#### **(iv) Dynamite Cords Exploding**

This seismic source, well known by the name (Geoflex), consists of an explosive cord which is buried in the ground at a shallow depth (about half a meter depth). It is laid down by a hydraulically-operated plough which is especially designed for this purpose.

#### **(v) Vibroseis**

This is a non-impulsive seismic-energy source which was introduced in early 1950s and rapidly gained popularity as an acquisition tool. In 1982, over 40% of worldwide seismic surveys were using it (Mcquillin, et. al, 1984, p. 38). Unlike impulsive sources, Vibroseis method creates mechanical energy which is continuously vibrating for certain time duration. A mechanical, truck-mounted vibrator is hydraulically driven, produce electronically controlled vibration. The generated energy is conveyed to the ground by a metal pad (about one-meter square) attached beneath the truck (Figure 5.11).

---

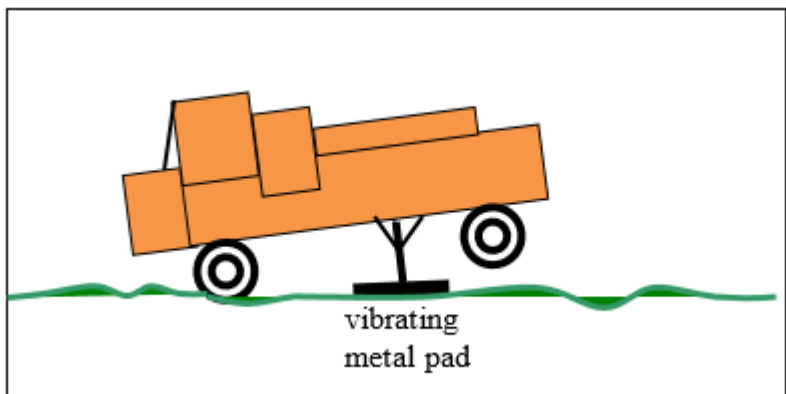


Figure 5.11 Vibroseis seismic energy source.

When in operation, the Vibroseis system transmits into the earth a seismic signal vibrating at a frequency which is varying linearly with time. This electronically-controlled vibration function is called the Sweep. In practical application, the sweep duration (called sweep length) is normally within the range (10 to 20) seconds over this time-span the sweep-frequency applied is (10 – 50) Hz. Apart from the taper imposed at both ends of the sweep (about half a second), the amplitude is kept constant during operation time. Further, we may note that the sweep may be started at low frequency then it is linearly increased (up-sweep) or started by high frequency (down-sweep). The up-sweep vibration is the more commonly applied method. A schematic representation of the sweep is shown in Figure 5.12.

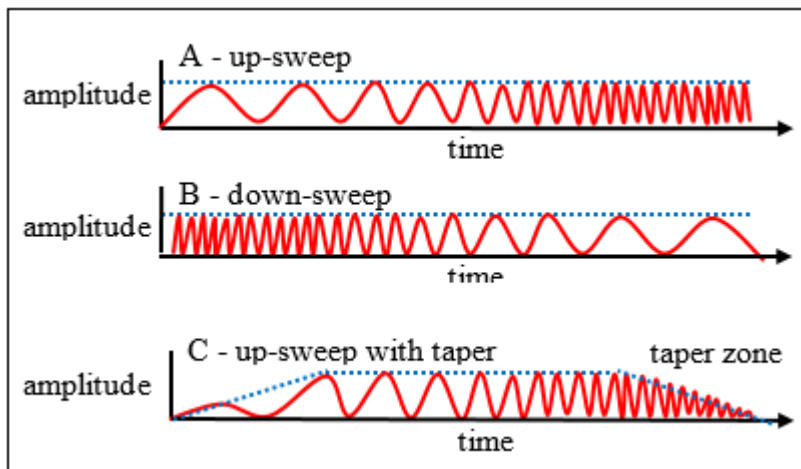


Figure 5.12 Vibroseis sweep signals. A- Up-sweep, B- Down-sweep, C- Up-sweep with taper applied at sweep ends.

As it is expected, the output reflection signals of Vibroseis-generated energy are not short wavelets, as normally seen with impulsive sources. The reflection signal, in

case of Vibroseis sources, is as long as the sweep-length used in the survey operation. In consequence, we get overlapping of the long reflection signals, and in this case, it will be very hard to distinguish individual reflection events on Vibroseis records. Comparison between outputs of vibroseis and impulsive sources is shown in Figure 5.12.

The main advantages of the Vibroseis method are being fast, safe, and comparatively cheap to run. It can be applied along roads and even in cities since it causes no damaging effects on environments. Technically, it has the advantage of having the source-function being under control. The sweep parameters (time duration, frequency range, and taper) can be changed at will. The main problem with the method is the low source energy-level. Like other weak surface sources, vertical stacking is carried out at the same time as the recording is going on. In normal surveying work, several Vibroseis-trucks (typically 4) are operating at the same time, and about 20 to 60 vibrations are conducted per each shot-point location.

### 5.9.2 Marine Seismic Sources

The most common types of seismic energy sources are:

- (i) **The Air-Gun** is a widely used energy source in marine seismic surveying, which generates energy by discharging highly compressed air into the water. A variation of this method is the (Unipulse), where the air continues flowing into the generated bubble for some time after the initial discharge. This is done to lessen the effect of the sudden bubble collapse which results in bubble oscillation.
- (ii) **The Steam-Gun** (also called Vaporchoc) utilizes hot steam instead of air. It is considered to be better than the Air-Gun, because with using hot steam, the effect of bubble oscillation is reduced
- (iii) **The Gas-Gun** is still another similar marine source which uses explosion of a mixture of propane and oxygen contained in a steel chamber. The pressure pulse created by the explosion of the propane-oxygen mixture is passed to the water via a flexible seal which forms a part of the chamber. The *Aqua pulse* works on this principle.

### 5.10 Seismic Detectors

The seismic detection process is based on conversion of the ground vibration to an electrical signal by a special transducer which can respond to seismic amplitude and frequency ranges completely and without distortions. Seismic detectors are of two

---

main types, the geophones for use in land and hydrophones used in marine environments.

**(i) The Geophone**

Detection of reflection arrivals in land surveying is done by geophones (seismometers as they are sometimes called). The geophone is a seismic-detection instrument which can transform the ground vibration motion into an electrical voltage. The most commonly applied geophones in seismic reflection surveys are the electromagnetic type. It operates on the principle of voltage generation in a coil moving within a magnetic field. The generated voltage is proportional to the velocity of the motion of the coil relative to the magnet. For this reason, geophones of this type are normally referred to as *velocity geophones*.

The geophone is made up of a permanent cylindrical magnet and a coil suspended by leaf-springs inside a circular slit made in the magnet. The slit is separating the magnetic south-pole (inner part of the magnet) from the north-pole (outer part). The magnet is firmly attached to the case, which is provided with a spike for easy fixing on the ground in an upright position (Figure 5.13).

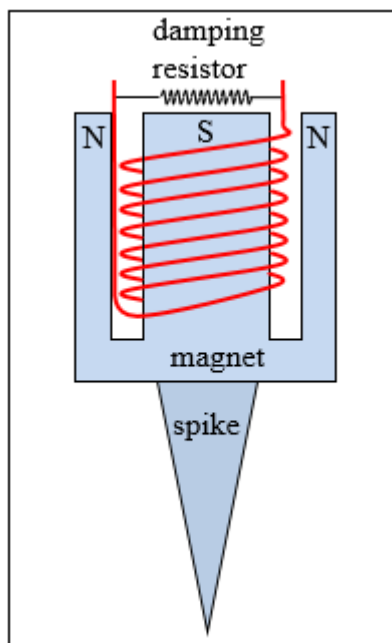


Figure 5.13 Schematic representation of the electromagnetic geophone.

For operation, the geophone is planted vertically into the ground. In this position the magnet will vibrate in vertical direction when the ground is seismically activated, and the coil stays stationary because of its inertia. The generated voltage in

---

the coil is function of the vibration rate and the coil parameters (number of turns, radius, and magnetic-field intensity).

### **(ii) The Hydrophone**

This is a geophone-equivalent detector used in detecting seismic waves in marine surveying environments. The hydrophone is a pressure-sensitive detection device that uses substances that generate electrical voltage proportional to pressure caused by the arrival of a seismic signal. Such a substance (called piezoelectric substance) has a property of generating an electric voltage when subjected to pressure. Piezoelectric transducers are also called *electrostrictive devices* (Sheriff, 2002, p263). The pressure changes, caused in a water medium due to the passage of a seismic wave, are proportional to the velocity of the water particles set into motion by the signal (Dobrin and Savit, 1988, p63).

## **5.11 The Seismic Data Recording**

For about 30 years after seismic exploration was introduced, seismic shot-records were directly recorded on paper as wiggly traces. In the early 1950's however, recording of seismic data on magnetic tapes were introduced in an analogue mode. After about ten years, more superior digital recording techniques were introduced. Soon after mid-1965, the analogue method was completely superseded by the digital method. Despite the fact that analogue recording is now considered to be obsolete no more in application. A brief description of the analogue system is presented here-below. This will be useful as the digital system involves some of the components of the analogue system.

### ***The Digital Recording System***

The main feature of the digital recording instrument is that it converts the incoming analogue seismic signal to a digital form. In this process the signal is converted into a series of discrete values at uniform time-intervals. This technique proved to give higher fidelity output than the analogue method. In the digital form, the seismic signal can be subjected to various mathematical analyses to achieve improvement in accuracy and resolution.

## **5.12 Field Measures for Signal Enhancement**

Before commencing a seismic reflection survey, certain field procedures are normally carried out to determine the nature of the dominant noise in the area in order to be able to design the source and receiver parameters that can output the strongest reflection signal and the least possible noise level. For noise analysis, a special seismic experiment is done in the field, called the *noise test* (called also *walk-away* or *micro-*

---

*spread test*). Analysis of the resulting seismic record will lead to determination of coherent noise parameters such as apparent wavelength, velocity, periods, and frequency, which are necessary in the design process for both of the receiver and the source.

### The Noise Test

There are two types of field procedures that can be followed in conducting the noise test in the field. These are the fixed-spread method and the fixed-shot method. The fixed spread method is done by using end-on spread which is made up of geophones spaced at short distances (typically, 5-meter spacing). After recording the first shot, the shot is moved along the spread line by a distance equal to the spread length and the second shot-record. This shift-and-record action is repeated a number of times such that the resulting combined record will have its maximum offset to be about equal to the maximum offset planned for that survey.

An alternative method (called, the fixed-shot method) is conducted by fixing the shot location and move the receiver spread (along the spread line) away, hence, the term walk-away test.

### Experimental Shooting

The source parameters depend on the type of the source used to generate the seismic energy. For the dynamite source, there are three main parameters. These are: charge depth, charge weight, and shot-hole pattern. The optimum charge depth and charge weight are determined through direct experimental shooting. For the charge depth, several trial shots are conducted such that the charge weight is fixed while varying the depth. The same approach is followed in optimizing the charge weight, that is by fixing the depth and varying the weight of the charge (Figure 5.14).

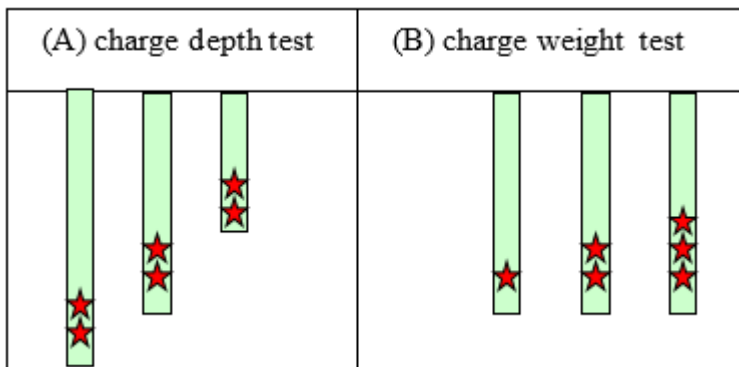


Figure 5.14 Experimental shooting for determination of: (A) charge depth and (B) charge weight.

---

As for the shot-hole pattern, the suitable number of shot-holes is determined by applying the same principles applied in the case of the receiver geophone array. However, very often and for economic reasons, this is determined by the experimental shooting method alongside with the determination of optimum charge depth and charge weight. Conducting multi-shot sources is another approach for increasing the signal-to-noise ratio. This is normally done in case of surface-sources as in the case of vibroseis and weight dropping techniques.

### **5.13 Determination of the LVL Properties**

The earth surface is characterized by its non-uniform topography (variable elevation), and the surface layer is, in general, made up of loose low-velocity materials. This layer, (commonly referred to as the low-velocity layer, LVL) is made-up of one or more layers of velocity and thickness that can vary with location within the survey area. The LVL thickness and velocity are typically of ranges (10-to-50) m and (500-to-1500) m/sec respectively.

Because of the large velocity contrast at the base of the LVL, its base acts as a strongly efficient reflector and refractor. Multiple reflections (reverberation and ghosts) can develop in such environments. Effect of the LVL is not restricted to the travel-time changes, but also on the reflection waveform. In particular, high-frequency components of the travelling seismic waves experience severe attenuation due to absorption.

An integral part of the field activity in a seismic reflection survey is determination of the properties of the surface layer. In particular, the thickness and velocity which are essential information needed in correction-computations of the reflection and refraction travel times (the static correction). Along with the normal reflection shooting, special field activities are conducted for determination of the depth and velocity of the surface layer. The commonly applied methods are the up-hole surveying and specially designed refraction surveying.

#### ***(i) LVL Characterization by Up-hole Surveying***

The up-hole survey involves drilling a borehole of depth exceeding the expected LVL thickness, normally within the range (50m-100m). Small charges (dynamite capsules) are fired at a series of points arranged at certain depths inside the borehole. These charges are fired in sequence starting at the base of the hole and continuing upward till the last shot which is nearest to surface. For recording the arrivals at the surface, a group of geophones are usually planted at equal distances from the surface location of the hole (Figure 5.15).

---

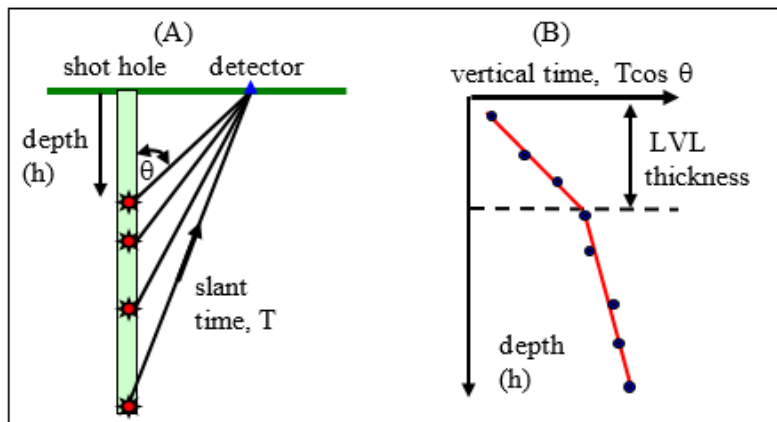


Figure 5.15 Up-hole survey: (A) travel-path and (B) plot of vertical travel time ( $T \cos \theta$ ) against depth ( $h$ ), where ( $T$ ) is the slant time and ( $\theta$ ) is the angle between travel-path and the borehole.

For analysis and interpretation of the recorded data, travel times (reduced to vertical travel-path) are plotted against depth. From the slope of the resulting plot, and the depths of the points at which slopes show abrupt changes, the velocity and thickness of the LVL layer (or layers) are calculated.

**(ii) LVL Characterization by Refraction Surveying**

Because the surface weathered-layer (LVL) is of velocity lower than that of the underlying bedrock, the refraction method lends itself as a tool for determination of the thickness and velocity of the LVL. The refraction survey is conducted using a special short spread, typically (150 m-250 m) provided with 24 channels.

There are two alternative field methods to conduct the survey; fixed-spread method, and fixed-shotpoint method. In the first method, two shot-points are recorded, one on either end of the fixed-in-place spread. This is, in effect, two end-on shots which are implemented for the fixed spread. In the second method two shots, fixed at the same point, are fired. For the first shot, the spread is located on one side of the shot-point, and for the second shot, the spread is moved to the other side of the shot-point location. This is a spread set-up similar to center-spread shooting. The two methods are shown as follows (Figure 5.16).

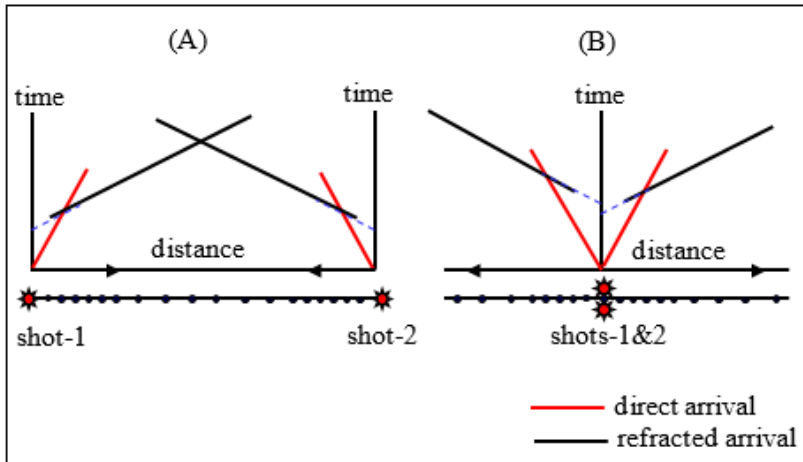


Figure 5.16 Two methods of refraction survey specially designed for determination of the LVL properties (thickness and velocity), (A) fixed spread, and (B) fixed shot-point method.

From travel-time curves, both of the velocity and thickness are computed from the slopes and time intercept of the produced curves. It is worth noting here that the travel-times of both of the direct- and refracted-arrivals are linear functions of distance. The velocity ( $v_0$ ) of the direct wave and that of the refracted wave ( $v_1$ ) are given by the reciprocal of the corresponding slopes. Thickness ( $z$ ) can be measured from its relation to the intercept time ( $t_i$ ), where  $t_i = 2z[(v_2)^2 - (v_1)^2]^{1/2} / v_1v_2$ . The LVL parameters (thickness and velocity) are computed from the data obtained from the two implemented shots.

## 5.14 The Seismic Field Crew

Survey work of an area is carried out by a team of workers made up of professionally prepared personnel who are technically equipped to cope with all of the activities needed to complete the seismic survey. This is the seismic crew, or seismic party as it is sometimes called.

A seismic crew consists of a number of sections each of which is specialized in one of the field survey activities. The main sections are:

### (i) Data Recording Section

This section is under the management of the Observer, who is responsible of the technical management of the recording system (recording station) and magnetic tape recording. Under this section is the group of workers for geophone planting and control of the activities taking place over the seismic line during shooting. The Observer usually submits complete daily documented reports.

***(ii) Topographic Surveying Section***

Fixing on the ground of the survey points (shots and receivers) and measuring coordinates (x, y, & z) of each of these points. These data, in addition to data concerning geographical nature and surface environments, are documented and reported.

***(iii) Drilling Section***

This is concerned with drilling the shot-holes, and other holes needed by the survey, such as the deep holes needed for up-hole surveys.

***(iv) Shooting Section***

Workers in this section do all the necessary steps needed to prepare a shot-hole. This involves preparation of the right charge and placing it at the required depth and filling the hole with water and mud mixture to secure coupling. The section is also responsible for the dynamite storage and transport taking all the safety and security precautions.

***(v) Mechanical Engineering Section***

This section is responsible for mechanical work needed by the crew as maintenance of drilling machines, trucks, electricity generators and the Vibroseis systems.

***(vi) Administration and Finance Section***

This section is responsible for personnel recruitment, living requirements, transport, communications, material storage and all finance affairs.

These are the main sections of a typical crew using dynamite for the seismic energy source. All the sections are headed by the party chief who is managing the crew work through direct contacts with the crew and through the daily meetings held every night with the sections' heads.

---

# 6. 3D SEISMIC REFLECTION SURVEYING

## 6.1 Nature is Three Dimensional

The sub-surface geology targeted by seismic exploration is, in essence, three-dimensional in nature. The seismic field created in seismic reflection surveys is likewise, three-dimensional. In an ideal homogeneous medium, the wave-front of the advancing seismic wave is of three-dimensional shape, which is spherical, in a homogeneous medium. In reality, the geological medium is made-up of different rock layers of different properties and different geometrical shapes. With this realistic type of environments, the advancing wave-front, is still having the three-dimensional form but no more perfectly spherical. The created seismic rays travel in every direction in the space surrounding the source zone. In other words, the geological field, as well as the seismic field in which it is created, is 3D in nature (Figure 6.1).

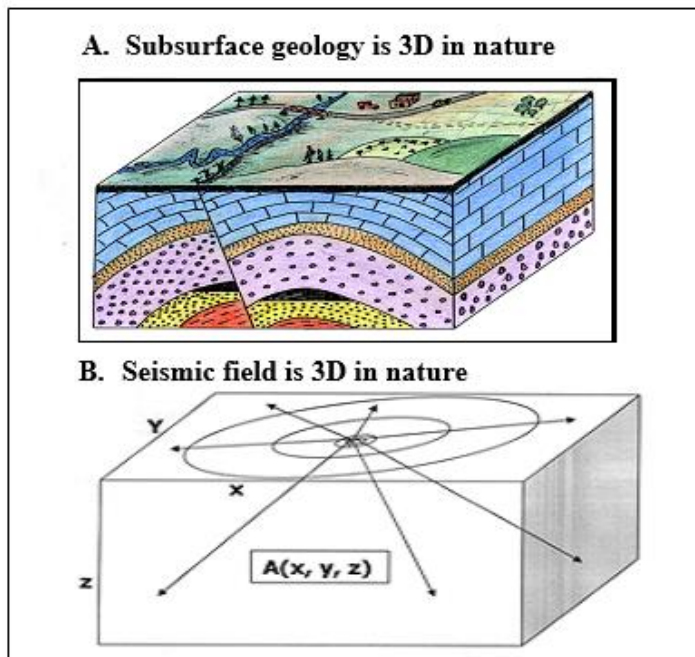


Figure 6.1 By nature, both of the subsurface geology (A) and the seismic field (B) created to explore it, are three dimensional.

In the conventional 2D shooting, the seismic field is created as three-dimensional wave-field, but detected by two-dimensional array of detection-points. Thus, the 2D surveying is concerned with a limited portion of the reflected energy, leaving out the rest of the reflected energy, with all the useful information they carry, to pass undetected.

## 6.2 1D - 2D - 3D Terminology

A seismic trace can be viewed as a time function of the seismic amplitude which is normally representing variation of vibration-velocity as function of recording time. If we disregard its position information (that is neglecting the x-y coordinates of the CDP location), the seismic trace is represented as a one-dimensional (1D) function of amplitude with time  $f(t)$ , or with depth  $f(z)$ . The synthetic seismogram is another example of the 1D seismic function which represents reflection-amplitude variation with the depth of the drill-hole. The sonic log expresses variation of the transit-time with the depth of the well which is also a 1D function.

In the conventional 2D seismic surveys, where the shot-point and receiver-points are co-linear, the resulting stack section consists of a series of seismic traces each of which belongs to a CMP location. The stack traces of a stack section are uniformly spaced along the distance coordinate (x). Thus, the seismic amplitude in the produced section is function of both trace-position (x) on the seismic line and the two-way reflection time (t). This means that the amplitude in the produced seismic section, is represented by the two-dimensional (2D) function  $f(x,t)$ , or  $f(x,z)$  when time is scaled by the propagation velocity.

With the 3D shooting technique, the produced CMP-locations form a two-dimensional array over the surveyed reflectors. In this case, we have a seismic trace for each of these CMPs, forming a data volume in which the seismic amplitude is represented as a function of its position in space, defined by the three-dimensions x, y, t (or x, y, z). Thus, the amplitude is expressed as a three-dimensional (3D) function,  $f(x, y, t)$  or  $f(x, y, z)$ . The three terminology definitions are shown in Figure 6.2.

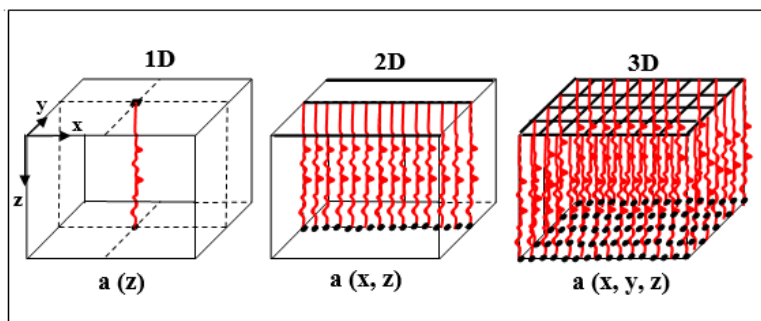


Figure 6.2 Seismic data output represented as 1D-function (seismic trace), as 2D-function (seismic section), or as 3D-function (seismic data volume). The corresponding functions are  $a(z)$ ,  $a(x,z)$ ,  $a(x,y,z)$ .

The end product of the 3D seismic surveying is a seismic data volume which represents a three-dimensional function expressing the variation of seismic amplitude with the three coordinates; x, y, and z.

### 6.3 Merits of the 3D Technique

#### (i) Providing the data volume

The 3D data processing provides the stack data-volume, which allows displaying vertical sections at any direction and horizontal sections (time-slices) at any level within the data-volume (Figure 6.3).

#### (ii) Capability of Surveying Inaccessible Areas:

As far as seismic surveying is concerned, an area is considered to be inaccessible, when no seismic energy-sources nor receivers are allowed to be located within the area boundary. An inaccessible area can be surveyed by deploying the receivers on the boundary of the area and shooting at source-points which are also distributed over the area boundary while the receiver spread is kept fixed throughout the shooting process. For each shot there will be a number of CMPs located at the source-receiver's midpoints, which will be located within the surveyed area (Figure 6.4).

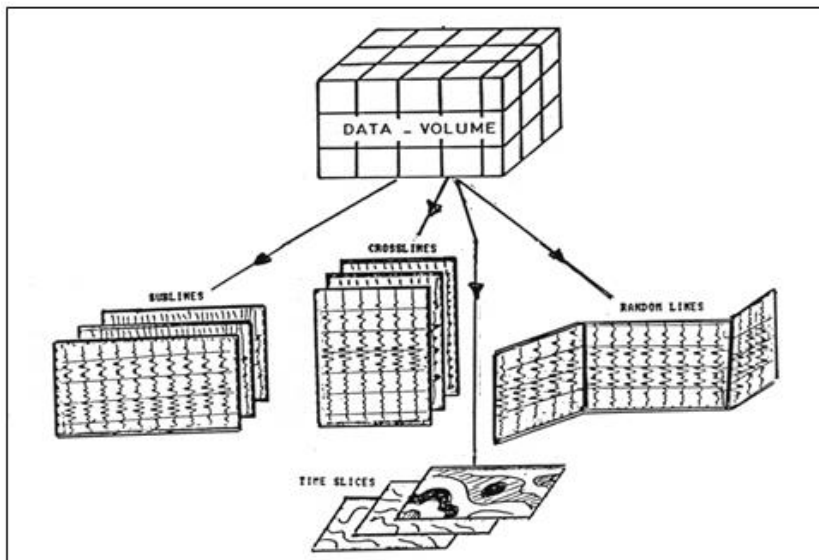


Figure 6.3 Types of sections which can be extracted from the 3D data box



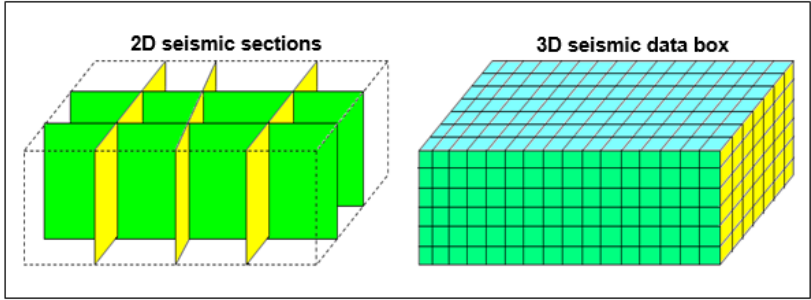


Figure 6.5 Sketch showing that the 3D data provides more dense sampling points of the subsurface geological space than the 2D data.

### 6.4 3D Field Surveying

What makes a survey 2D or 3D is the way the receivers are deployed on the surface. In 2D surveying, receivers are laid down in line with the source point, and the used spread is linear, made up of one-dimensional array of receivers. In this case, the reflection points will fall on a subsurface straight line.

In case of 3D surveying, the spread consists of receivers which are distributed over an area, rather than on a straight line, and the used spread consists of a two-dimensional array of receivers. The reflection points in this case will be distributed over a subsurface area of the reflector-plane (Figure 6.6).

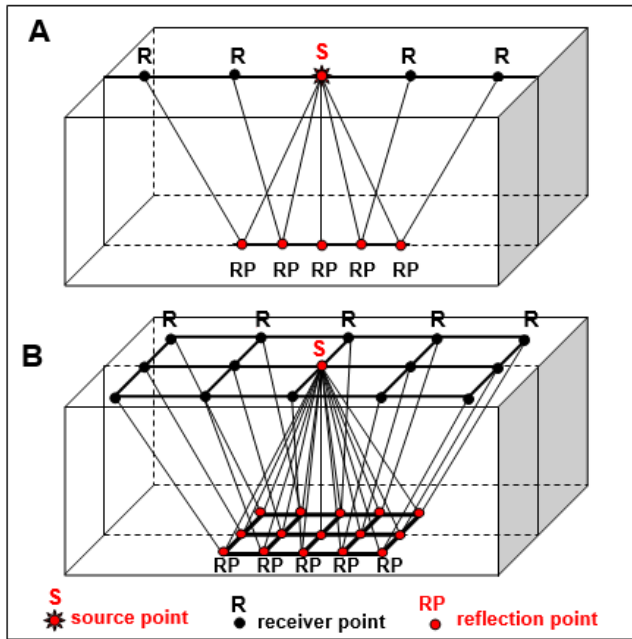


Figure 6.6 Type of spread decides whether the survey is 2D or 3D. One-dimensional array spread for 2D survey, Two-dimensional array spread for 3D survey

Shot-records, obtained from 2D and 3D spreads are shown schematically in the following figure (Figure 6.7)

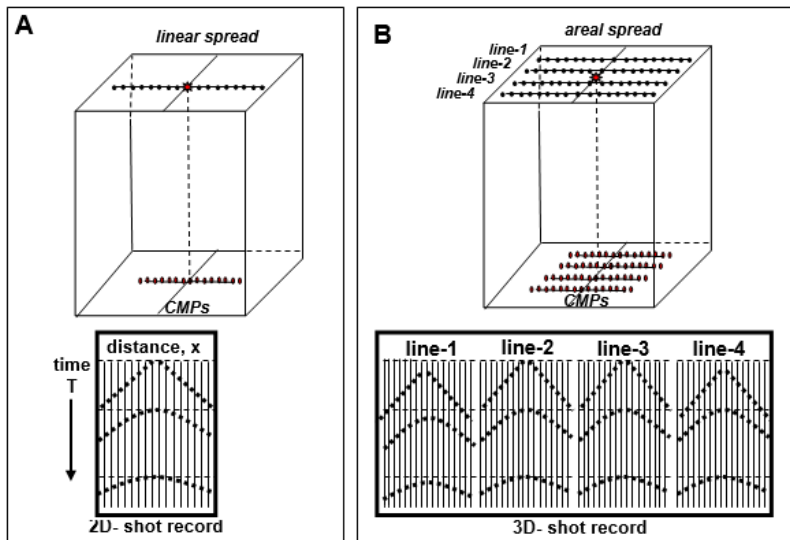


Figure 6.7 Sketch showing 2D and 3D shot-records. A. 2D Case: surface linear spread, mapping line of CMPs, and B. 3D Case: surface areal spread, mapping an area of CMPs

### 6.5 The CDP-Bin Concept

Considering horizontal plane reflectors, all the reflection ray-paths, of the CDP trace-gather (in 2D surveying) are coincident on one common vertical plane (the ray-path vertical plane). In the 3D method, however, each reflection ray-path may fall in its own vertical plane. These ray-path planes are generally not coinciding on each other, because of the varying source-receiver directions (azimuths) of the CDP gather-traces. Thus, the receiver azimuth (source-receiver bearing) in 2D surveying is constant which is along the seismic line, whereas the corresponding azimuth, in 3D surveying, is variable (Figure 6.8).

In the normal profiling technique followed in 2D surveying, the spread moves (at an equal move-up rate) along the uniformly-spaced station-points. In this way, the reflection points of each CDP trace-gather are all coinciding at the CDP. Sometimes, due to a shifted placement of a shot-point, one (or more than one) reflection-point falls outside the CDP. In CDP sorting, a search distance (usually defined to be equal to half of the CDP-spacing) is set in processing. All traces found within the search distance of a CDP are included in the trace gather of that CDP.

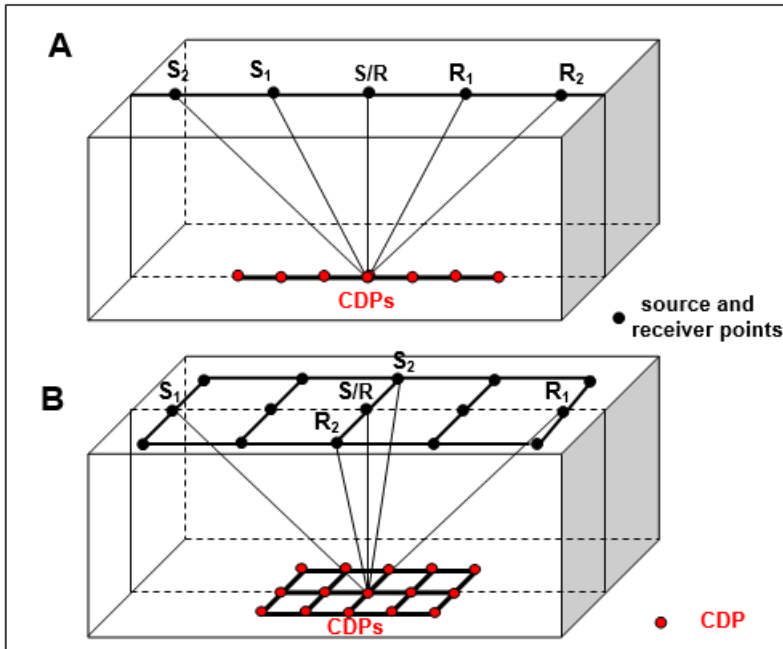


Figure 6.8 Reflection ray-paths of the CDP trace-gather in 2D are all coinciding on one common plane (A). These planes are generally not all coincident on one plane in 3D surveying (B).

This same principle is applied to the CDP-grid in case of 3D surveying, except that in 3D, we have a search area instead of the 2D search distance. The search area is having a rectangular shape (or square shape) centered about the CDP. The width and length of this search area are equal to the CDP spacing in the two perpendicular directions of the survey station-grid. This search area is called the (CDP-bin) and the traces included within it, form the bin-gather. The process of sorting of traces into the appropriate bin is called bin-gridding or binning. These concepts are shown in Figure 6.9.

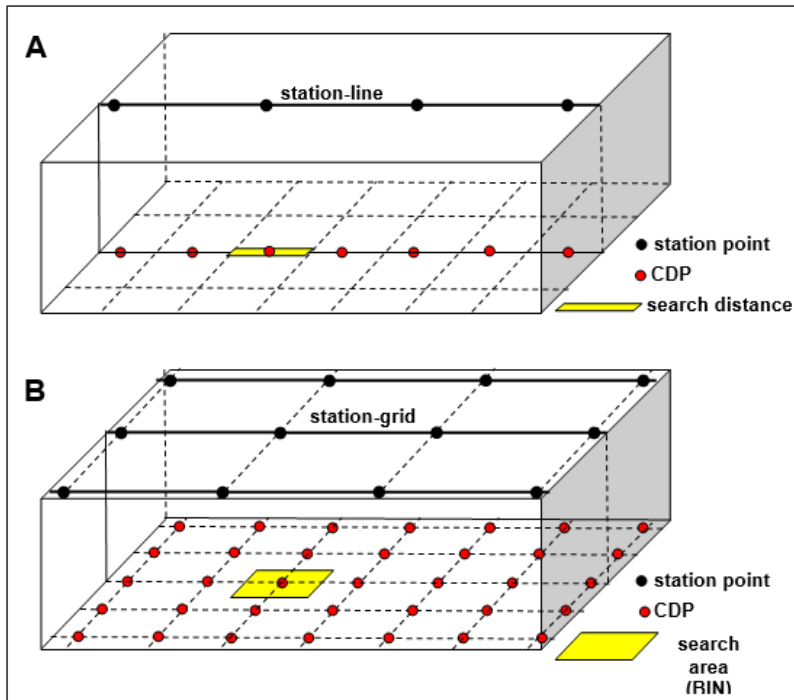


Figure 6.9 Definitions of the search distance in 2D surveying (A), and search area (Bin) in 3D surveying (B).

The bin is normally specified by bin shape (square or rectangular), bin size (bin dimensions), and bin attributes (offset, azimuth, and fold), which are shown in a special diagram, called “spider diagram”. For a 7-fold bin gather, the diagram is as follows (Figure 6.10):

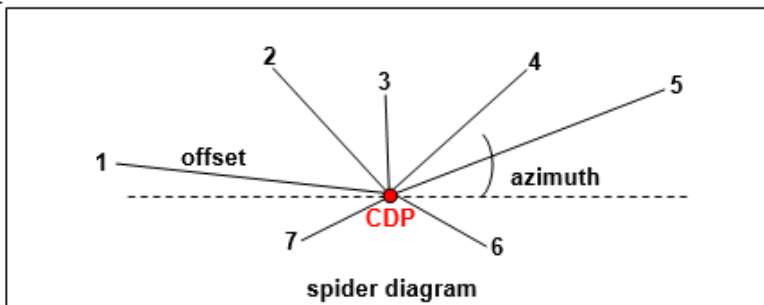


Figure 6.10 spider diagram, 7-fold bin gather.

## 6.6 The Seismic Data Volume

The end-product of a 2D-data processing, is the 2D seismic stack section. In case of the 3D seismic surveying, the corresponding end-product is a three-dimension stacked traces; the "data volume" or the "data box" as it sometimes called. The data volume represents a three-dimensional function in which the seismic amplitude varies with the three coordinates; (x,y,t). The reflection-time (t) may be replaced by the depth dimension (z), where ( $z=tv/2$ ), v is velocity.

The data volume is in digital form, composed of discrete volume-elements, called the (resolution cells) defined by the three dimensions ( $\Delta x$ ,  $\Delta y$ ,  $\Delta t$ ). This volume element is also termed as the *voxel* in analogy to the term *pixel* used for the unit of a digital picture. The data volume is a subsurface data-set, made up of voxels bounded by the sublines (SL) and crosslines (XL) as shown in Figure 6.11.

With the help of special processing software, it is possible to extract a variety of seismic sections from the data-volume. Normally, three types of mutually perpendicular sections, can be extracted. A vertical section may be obtained along any subline, or along any crossline, and a horizontal section (called a "time slice") can be obtained at any reflection-time. It is also possible to obtain a vertical section connecting points at arbitrary locations as for example, sections along distances connecting several well locations. A section which is not a subline or a crossline is normally referred to as a crooked, oblique or diagonal section (Figure 6.12).

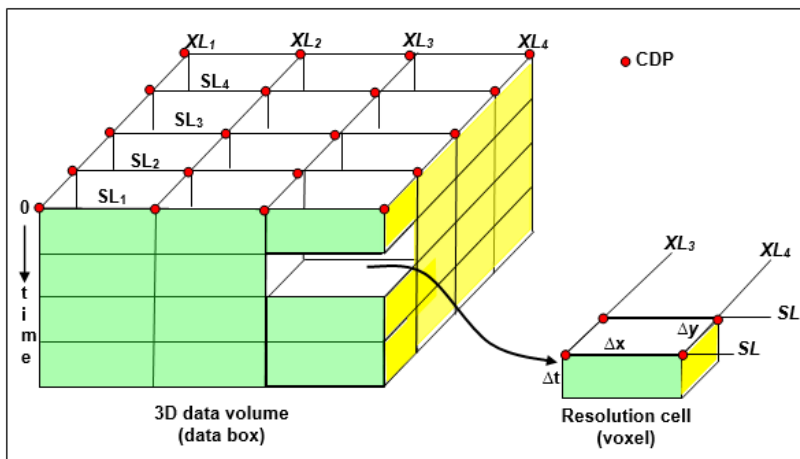


Figure 6.11 The 3D data volume (data box) and the definition of the resolution cell (voxel).

The horizontal section, called seiscrop section, or more often called (time slice), is a representation of the seismic amplitude values which fall on the same reflection-time. In fact, it is the locus of equal-time amplitudes existing in the data volume. In color displays, the time-slice plots are given in color-coded amplitude-values with clear distinctions between peak- and trough-values.

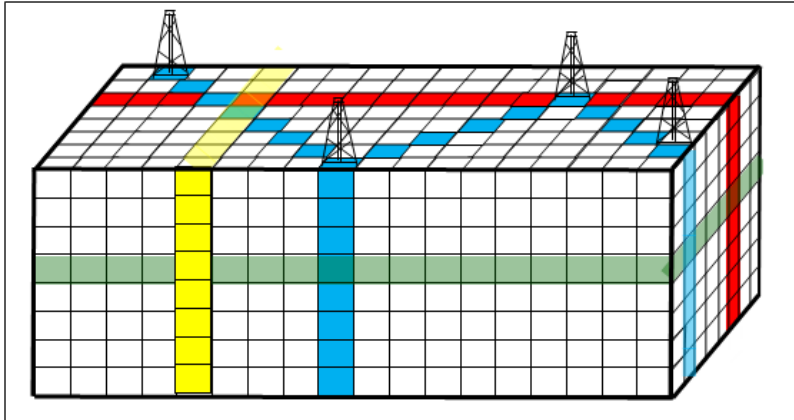


Figure 6.12 The 3D data volume, showing the four possible sections obtainable from the data volume. These are: subline (red), crossline (yellow), crooked line passing through 4 wells (blue), and time-slice (green).

## 6.7 Types of 3D Spread

Since the introduction of the 3D technique in seismic exploration, in the 1970s, several types of areal spreads were developed. According to the surface conditions, spreads can be divided into two main groups; the marine spreads and the land spreads.

### 6.7.1 Marine 3D Surveying Spreads

Conventionally, marine 3D surveying is conducted by using spreads similar to those used in land (and marine) 2D surveying. The boat and the towed-behind streamer are recording as they move along straight-line courses. The technique differs from the normal 2D surveying in that the survey shooting is conducted along closely spaced parallel lines. Line spacing (typically, 100 m-200 m), is kept constant throughout the survey area. The basic elements of the spread used in marine surveying consists of an energy source (such as an air-gun) and the streamer which is a sleeve containing the hydrophones. The streamer is equipped with a depressor and a depth controller to keep the streamer at the required depth. A tail buoy carrying equipment for radio communications is connected to the end of the streamer.

To increase survey efficiency, multi-source and multi-streamers have been used in the marine surveying. Examples of spreads which can be configured are; single source-single streamer, dual source-single streamer, single source-dual streamer, and dual source-triple streamer (Figure 6.13).

---

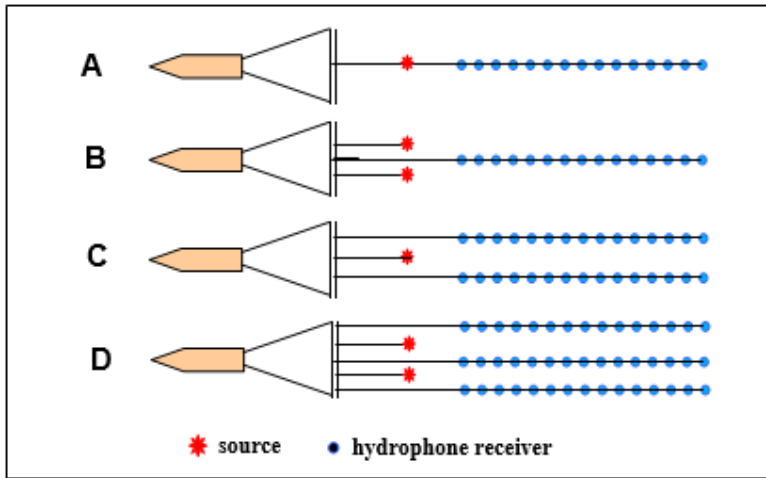


Figure 6.13 Types of spreads used in marine 3D surveying. (A) single source-single streamer, (B) dual source-single streamer, (C) single source-dual streamer, (D) dual source-triple streamer.

Spread movement during recording, is done normally along parallel straight lines (parallel linear paths). Because of the long streamer-line towed behind, the boat needs to turn with a relatively large steering radius in order to record the following line. A variation of this method is shooting along circular paths. The boat moves along overlapping or spiral circular paths. The advantages of the circular type of spread is that the survey is completed with no times lost due to turns of the boat needed in case of straight-line surveying. These types of spread-movements are shown in Figure 6.14.

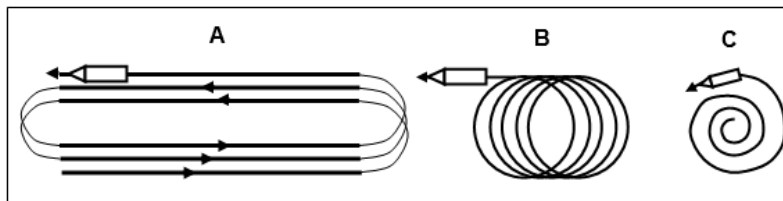


Figure 6.14 Types of spread movements used in marine 3D surveying. (A) Parallel linear path, (B) Overlapping circular path, (C) Spiral circular path.

It should be noted here that deviation of the streamer course-line from the linear form (caused by the circular spread or by the feathering effect) gives certain amount of azimuthal variation. This makes the marine surveying to be approaching the proper 3D surveying.

### 6.7.2 Land 3D Surveying Spreads

The normal spread used in land 3D surveying consists of source-lines perpendicular to receiver lines. Examples of these types of spread (not in common use

at present) are X-spread, L-spread, T-spread, square-spread (called Seis-square), and Seis-loop (Figure 6.15).

### 6.7.3 The Spread Template

The most commonly applied shooting spread, used in land 3D surveying, is the rectangular-shaped spread normally referred to as the spread template. This type of spread is used in the technique called the swath-shooting technique. It consists of a number of parallel receivers lines perpendicular to the shot-line. In some surveys, the shot-line is inclined with respect to the receiver lines, usually at an angle of 45°. The group of shots per spread is normally referred to as the salvo. A typical form of the spread used in swath shooting is shown in Figure 6.16.

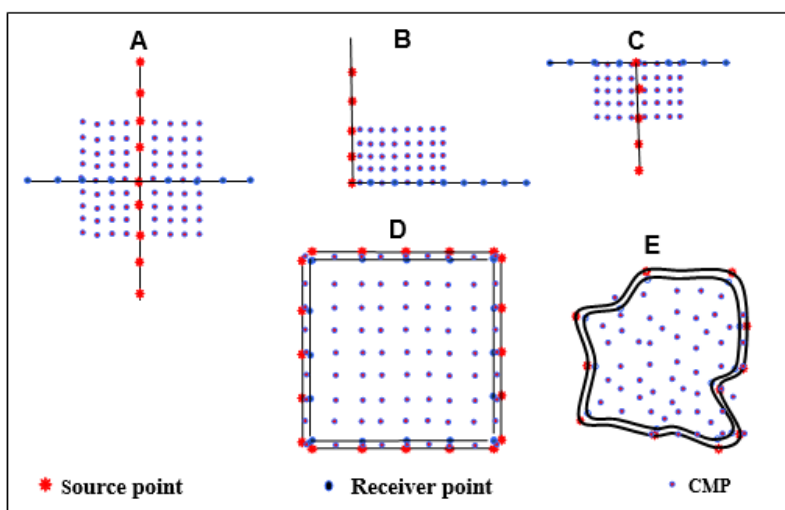


Figure 6.15 Types of land 3D spreads: (A) X - Spread, (B) L - Spread, (C) T - Spread, (D) Square - Spread, (E) Loop - Spread.

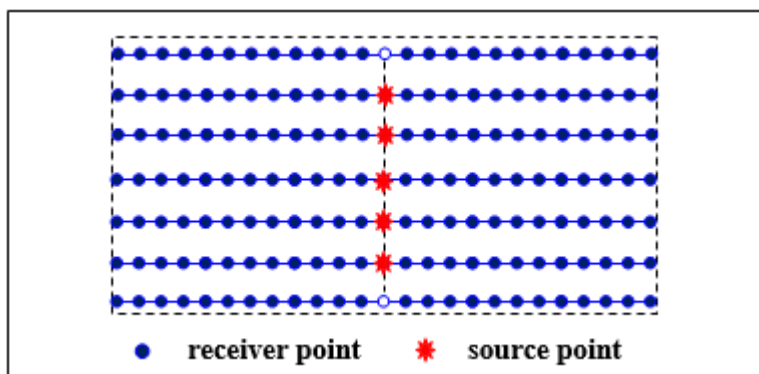


Figure 6.16 Spread template commonly used in Swath shooting. Source line is perpendicular to receiver lines. Spread is made up of 7 receiver lines and 5-shot salvo.

### 6.7.4 The Swath Shooting Technique

The swath is defined to be a strip of the survey area of width equal to the width of the used spread which moves along the defined strip in a roll-along movement similar to the “shift-and-shoot” technique used in conventional 2D surveying (Figure 6.17).

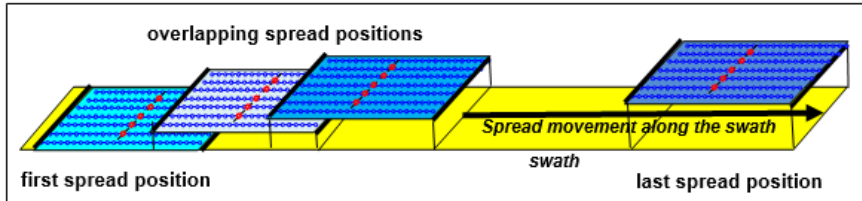


Figure 6.17 Spread movement (shift-and-shoot movements) over the swath, with overlapping shooting spreads.

In practice, when the template reaches the end of the first swath, the template is re-configured at the near-by end of the adjacent swath, then carrying out the “shift-and-shoot” process from end to end. In this way all the rest of swaths are sequentially covered. It should be remembered that swaths are not laid down side by side, but laid down with overlap to obtain fold build-up (Figure 6.18).

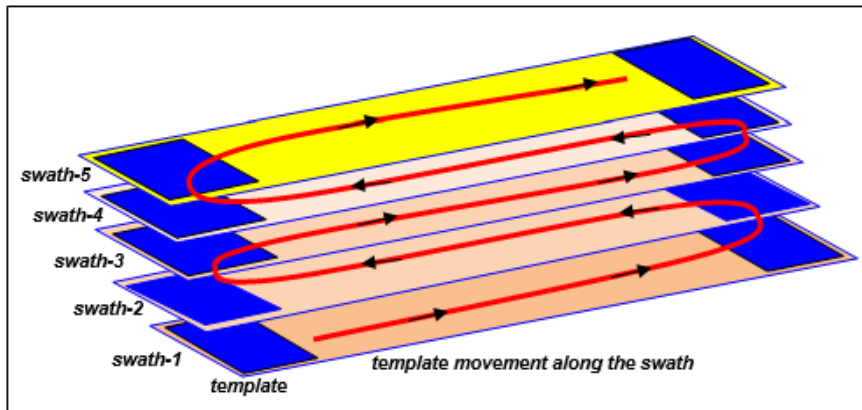


Figure 6.18 Template movements along the sequence of five overlapping swaths.

Swath shooting is a common acquisition technique implemented -in today's land 3D surveys. It has the advantages of being simple to configure, and efficient to execute in the field. It gives uniform bin fold and adequate offset and azimuth variation. On the other hand, swath shooting requires land with fully accessible space, and type of surface conditions which allow the appropriate freedom for the survey maneuvering.

## 6.8 3D Data Display

The ultimate end-result of the processing sequence is a data-volume, which is also, called data box (Figure 6.19).

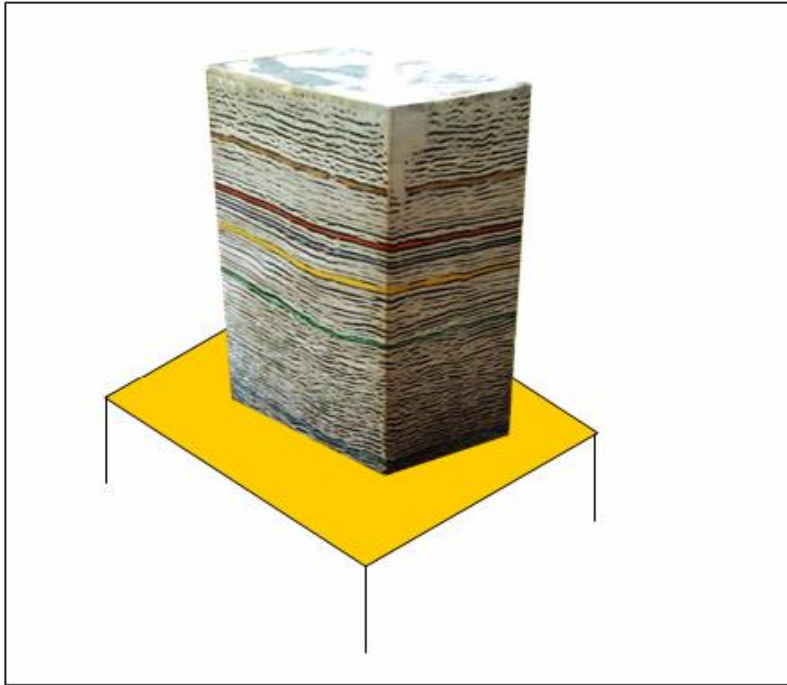


Figure 6.19 The 3D data volume obtained from processing of a 3D data-set of an area of (10 by 20) sq. km.

The data volume consisting of an amplitude value at the point  $(\mathbf{x}_i, \mathbf{y}_i, \mathbf{t}_i)$ , where  $(\mathbf{x}_i)$  and  $(\mathbf{y}_i)$ , are the bin-center coordinates in the in-line and cross-line directions respectively. The coordinates  $(\mathbf{t}_i)$  are the time values of the trace samples. Three types of displays are usually extracted from the produced data volume; an in-line, cross-line vertical-sections, and horizontal sections (time-slices). At each sample-time, a time-slice can be displayed. Examples of vertical and horizontal sections are shown in Figure 6.20 and Figure 6.21.

---

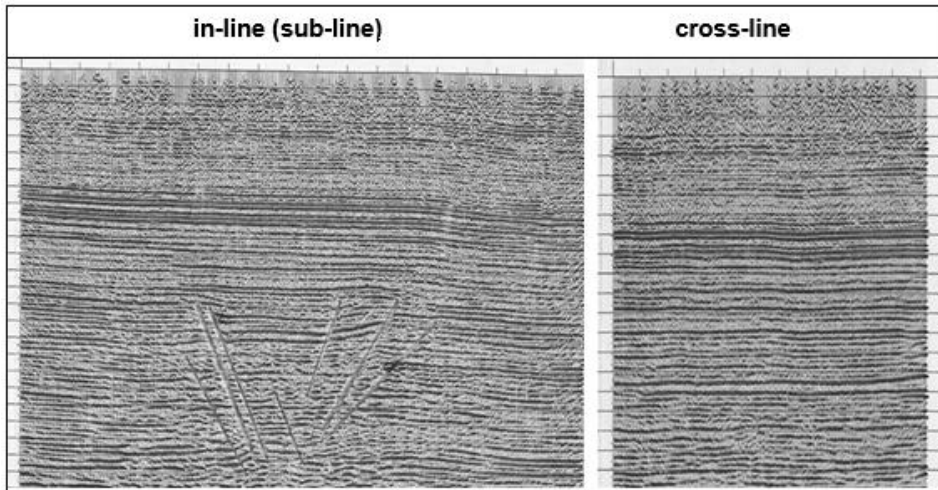


Figure 6.20 Examples of vertical sections (in-line and cross-line) obtained from a 3D data volume

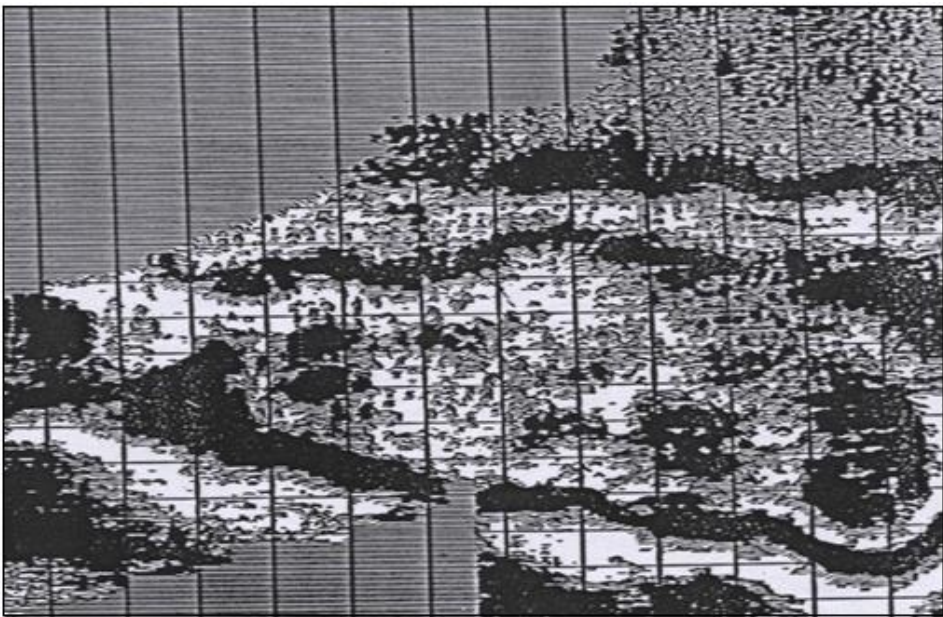


Figure 6.21 Example of a time slices obtained from the 3D data volume.

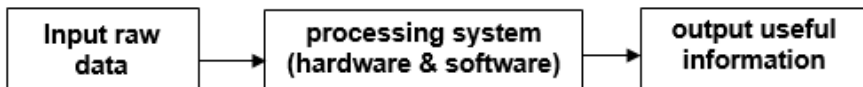
---



# 7. REFLECTION DATA PROCESSING

## 7.1 Processing Definition and Objectives

Seismic data processing is a sequence of mathematical and statistical processes carried out on the acquired raw seismic data in order to extract more readily interpretable data to give useful geological information. The whole processing activities can be represented as an input-output system in which the seismic recorded data represent the input and the final stack data represent the output. The processing system involved in this operation is made up of two main parts; the processing computer system (the hardware) and the computer operation programs (the software). This is summarized as follows:



The processing operations include a group of steps (processing tools) which are mathematical and statistical manipulations aiming at achieving the following main objectives:

1. Enhancement of signal-to-noise ratio.
2. Correct reflection travel-times relative to a defined datum plane.
3. Correct shape and position of the reflector seismic image

Summary of the processing objectives is expressed by the Figure 7.1.

To achieve these three main objectives, the input data provided by the field crew, is subjected to a series of processes, called the processing sequence. In more details, the main processes carried out by a processing system can be summarized as follows:

1. Reformatting of the recorded data
  2. Removal of noises and interferences
  3. True amplitude recovery
  4. True spectrum recovery
  5. Equalization of the seismic traces
-

6. Correction of the travel time of shot traces to a defined datum level (static correction)
7. Correction of the travel time of shot-traces to the zero-offset positions (NMO correction)
8. CDP-gather sorting and trace-stacking
9. Correction of shape and position of reflector images (seismic migration)
10. Display and storage of the final seismic stack-data

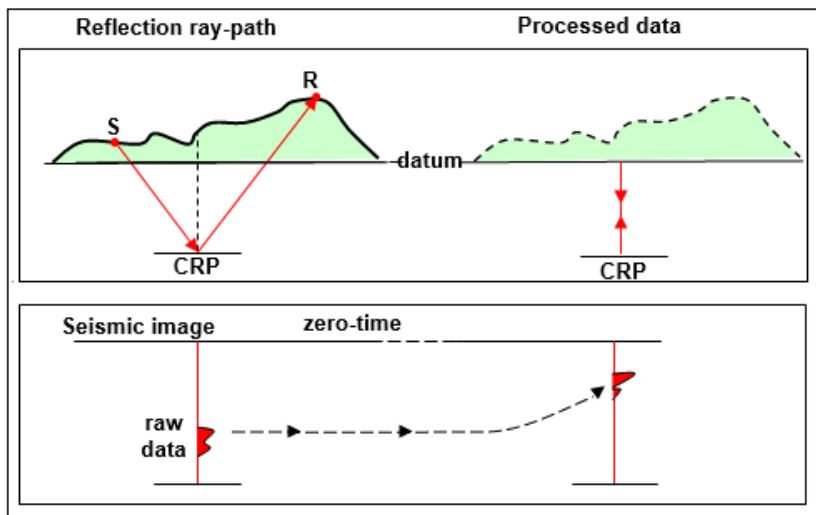


Figure 7.1 Summary of seismic data processing and objectives

Starting with the raw seismic shot-records (the basic input-element), a series of processing steps are performed to produce the stack section (the ultimate output-element); which is the corrected seismic image of the geological reflectors in the surveyed area (Figure 7.2).

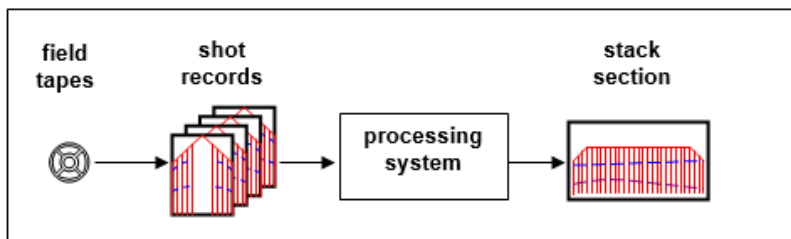


Figure 7.2 Input (field shot records) to the processing system.

## 7.2 Main Processing Activities

To achieve the objectives that are required from processing, the raw field data are passed through a sequence of steps (the processing sequence) using certain processing-controls (the processing parameters) for each step of the sequence. The standard processing sequence normally followed in processing of the field data, involves a sequence of activities starting with preconditioning of the field data, carrying out certain measures to enhance the S/N ratio, correcting arrival times and ending with the stacked data to be handled to the interpreter. These activities are summarized as follows:

### ***(i) Data Preconditioning***

In this step, all corrupted data found within the raw data are removed or corrected by a process called (data editing). Recovery of the original signal amplitude and the original signal waveform are carried out in this stage also. Frequency filtering, inverse filtering (deconvolution) and other such-like processes are applied in the preconditioning work to get a data-set free of corrupted data. Preconditioned data are then inputted for the following processes.

### ***(ii) Travel-Time Corrections***

There are two main corrections to be carried out to reflection travel-time. These are the static and dynamic (NMO) corrections. In the static correction, the effect of surface topography on the reflection travel-time is removed; whereas, the NMO correction removes the effect of the receiver offset (receiver distance from the source point). The outcome of these two processes are making the reflection travel-time of each reflection event as it would be if both of the source and receiver were occupying a common position at a point located on a fixed datum level.

### ***(iii) Signal Enhancement***

The most effective process in signal enhancement is what is called CDP-stacking. In this process several seismic traces generated from the same reflection point (i.e. same CDP trace-gather) are algebraically summed-up. The result of this sum is a new trace (the stack-trace), it is representing the mean of the traces in the CDP-gather. In this process, reflection signals on the individual traces are summed constructively producing stronger (larger amplitude) reflection signal. The seismic noise, being of random nature, is destructively summed, and hence gets reduced.

Application of digital filters is another option for reducing noises and other unwanted interferences and enhancing the reflection signal. There are several types of filters. The most commonly applied type is the frequency filters which discriminate seismic events on the basis of frequency. Another well-known filter is the velocity

---

filter (also called F-k filter) which discriminates events on the basis of their apparent velocity. Frequency filters and F-K filters are powerful tools in seismic signal enhancement.

#### ***(iv) Structural Amendment***

In certain cases, where there are structural complexities (folds and faults) in the subsurface geological structure, the seismic image of the corresponding seismic stack section will have structural distortions of magnitude depending on the degree of the structural complexities. This type of distortion occurs because of shifting of the location of the reflection point due to dipping of the reflectors. Another type of distortion results from the diffraction phenomenon which is associated with terminating reflectors like faults and pinch-outs. Restoration of seismic sections affected by such distortions is made by a special process (the seismic migration).

#### ***(v) Data Storage and Display***

For quality control purposes, paper displays (or on-screen displays), after each processing step is normally produced. The final product, which consists of stack sections of seismic lines (or stack data-volume, in case of 3D surveying) is recorded on a certain storage medium. This is an important processing step in which the final processing product is recorded on a permanent storage medium (usually on magnetic tapes) ready to be delivered to the interpretation geophysicist who will load it in his interpretation system.

In addition to the conventional seismic stack sections, other types of sections may be produced according to special requests from the interpreter. Examples of such data are seismic-attribute sections in which parameters other than amplitudes (such as frequency, phase or propagation velocity) are displayed in the form of seismic sections (seismic attribute sections). Such sections are additional tools helping in the interpretation process, especially in stratigraphic interpretation.

### **7.3 The Processing Sequence**

In order to get a seismic section made up of traces containing reflection wavelets which are corrected with respect to shape and corrected with respect to travel-time, a sequence of processing steps are normally performed. These steps are taken in sequence, where some are mandatory (compulsory) and others are optional, decided by the processing geophysicist according to certain needs.

There is no fixed sequence for the processing steps. Details of seismic data processing differ with different processing centers, and may vary from data-set to data-set in the same center. However, there is a kind of a standard form for the basic

---

processing steps normally followed in all processing activities. This shall be briefly described in this section.

To simplify discussions, the processing sequence is divided into four stages of processing. These are: Data re-organization, pre-stack processing, post-stack processing, and parameter optimization processing (Figure 7.3).

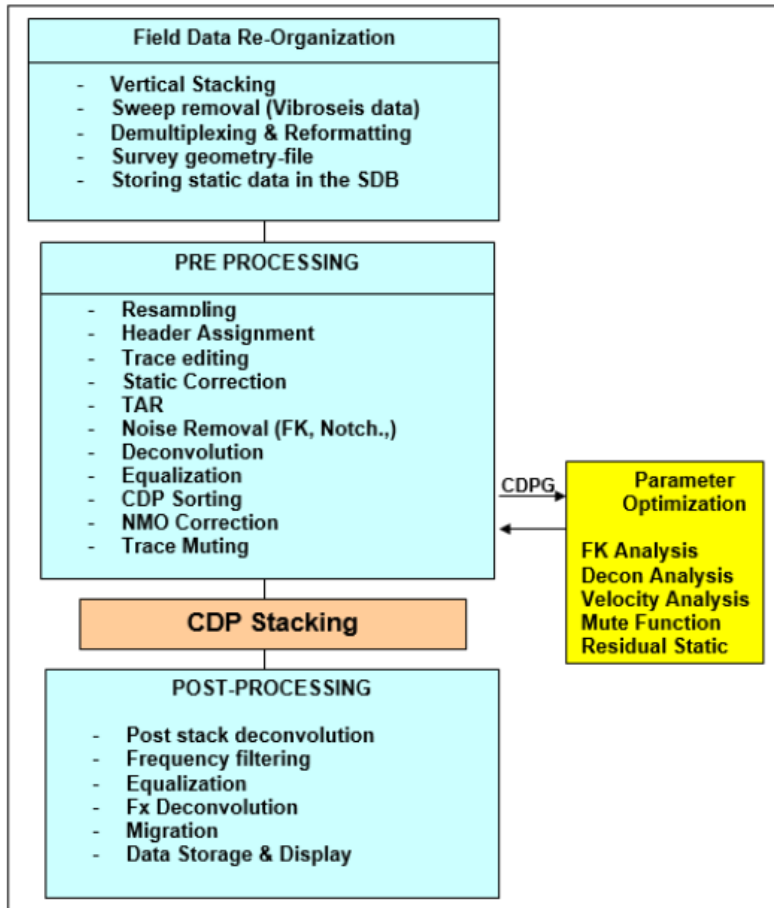


Figure 7.3 A standard form of a sequence normally applied in processing 2D seismic reflection data.

The input data are subjected to a sequence of processing steps which can be grouped into four major stages. These are:

The raw data provided by the field crew, which form the input data to processing, consist of two sets of data: the seismic shot records (normally recorded on magnetic tapes) and the support "statistics" data (normally recorded on CDs or magnetic tapes). The shooting statistics include the observer report in which complete descriptions and notes on the recorded shots are documented. The report also includes

the shooting geometry and, often, the field statics computed with respect to a defined datum level.

The input to the processing system comprises basically of seismic traces sorted into shot-gather records. Each seismic trace contains a series of seismic events representing the reflection wavelets recorded at their respective arrival times. In this state (raw-data state), the reflection wavelets are generally weak and distorted seismic signals. The travel-times of the arrived reflection wavelets need to be corrected to be relative to a constant-elevation datum level. Corrections and data rectification are done in the processing center, using specialized computer software.

## 1. The Final Product

For QC'ing purposes, section display is normally produced after each processing step. The final product, which consists of stack sections of seismic lines (or stack data-volume in case of 3D surveying) is recorded on magnetic tapes. This is an important processing step in which the final processing product is recorded on a permanent storage medium (usually on magnetic tapes) ready to be delivered to the interpretation geophysicist who will load it in his interpretation system.

In addition to the conventional hard-copy displays, other types of sections may be produced according to special requests from the interpreter. Examples of such data are seismic-attribute sections in which parameters other than amplitudes (such as frequency, phase or propagation velocity) are used for the stack traces. Such sections are helpful in the interpretation process, especially in stratigraphic interpretation.

Brief description on the main processing steps of the processing sequence is cited here-below:

### The Input Raw Data

The raw data furnished by the field crew, which form the input data to processing, consist of two sets of data:

- (i) **The seismic shot records** which are normally recorded on magnetic tapes.
- (ii) **The support “statistics” data** (recorded on CDs or magnetic tapes) include shooting report (observer report) in which complete descriptions and notes on the recorded shots are documented. The report includes the shooting geometry and, often, the field statics computed with respect to a defined datum level.

## 7.4 Data Re-Organization

In this phase of data processing, the seismic data received by the processing center, is subjected to some re-organization together with certain preparations done

---

prior to the signal enhancing processing. These operations which are collectively referred to as data re-organization, are explained as follows:

***(i) Tape Copying, Reformatting, and Data Loading***

Before starting with any processing step, a copy of the field tapes is made. The original tapes are stored in a safe place, while the copy-tapes are used in the processing. This is a necessary procedure for safety purposes. The copy-tapes are reformatted into a format that complies with the particular processing software employed in the processing center. After being reformatted, the data is loaded to the system, ready to be used in the subsequent steps.

***(ii) Data De-multiplexing***

This is a compulsory step to be taken if the field seismic data is in multiplexed form. In such cases, the trace-samples are sorted in sample-sequential mode. Demultiplexing is a process whereby the samples are re-sorted into trace-sequential mode. The demultiplexed data is a series of traces each of which consists of its own sequence of samples.

The necessity of demultiplexing comes from the fact that computer programs deal with seismic traces in the form of time-series of sample values, sequenced per each trace (trace sequential mode, that is in demultiplexed mode). Very often, recorded data received by processing centers are already in demultiplexed form and thus application of this processing step is not needed.

***(iii) Sweep Removal***

In case of vibroseis shooting, the source function (the applied sweep) must be removed before any processing step. This process can be done in the field by the Vibroseis recording system, or later by the processing software.

***(iv) Vertical Stacking***

Vertical stacking, involves summing corresponding traces from several shot-records, executed in the same location. This is done normally with weak surface-sources (such as weight dropping and Vibroseis) to get enhanced reflection signals. Vertical stacking is applied without doing any time-corrections to the traces before being summed together. (Figure 9.8).

---

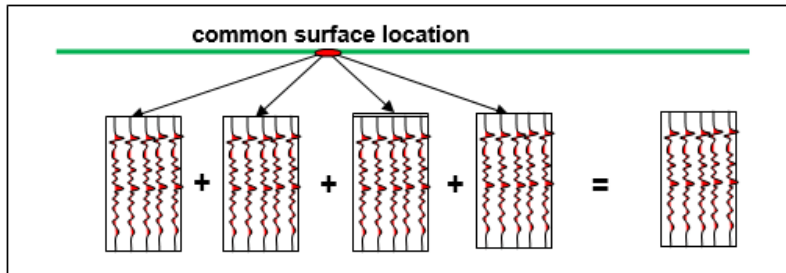


Figure 7.4 Principle of vertical stacking. Four shot records having one common surface location are vertically stacked to produce one record.

Vertical stacking is normally done in the field where the recording system is equipped with the appropriate software to perform the process. However, it can be done in the processing center when the need arises.

#### **(v) Geometry Data and Field Statics Loading**

Survey-geometry data give all information pertinent to the geometrical layout of all survey points (source- and receiver-points) used in the seismic survey. Essential elements of the surface layout are the following:

- Spread parameters (Total live seismic channels, trace offset, and receiver spacing)
- Coordinates (x, y, z) of each source and receiver points
- Shot identification number, shot spacing, shot coordinates
- Receiver sequence number, receiver spacing, receiver coordinates
- Geometrical shape of the seismic line

With these shooting statistics, which describe the surface positions of survey elements, the corresponding subsurface data are determined. This is achieved by running a special module of the processing package (the Geometry Module). The subsurface elements worked out in this processing step are:

- CMP sequence numbers, coordinates, and CMP-spacing,
- CMP gather-traces, and number of traces in each gather (fold of coverage).

#### **(vi) Trace Header Assignment**

The seismic trace is considered as a record of seismic amplitude variation with reflection time, in addition to various types of noise. In short, it is amplitude time-function. In order to be able to direct the processing system to a particular trace, each trace is provided with identification information called the (Trace Header). Among

---

other things, trace header of a particular trace will specify to what shot-point or to what CMP any trace belongs.

### ***(vii) Data Re-sampling***

In its digital form, the trace consists of a series of regularly-spaced sample-values. Normally, the field trace is sampled at 2 millisecond sampling period and re-sampled into 4 millisecond sampling period, before being input to processing. In order to avoid possibility of aliasing, a digital anti-alias filter is applied to the data prior to the re-sampling process. The type of the anti-alias filter is a high-cut filter that removes frequency components higher than the Nyquist frequency. Since Nyquist frequency ( $f_N$ ) is tied up to the sampling frequency ( $f_s$ ), by the relationship ( $f_N = f_s/2$ ), there will be no need to specify the anti-alias filter. The software is designed to identify the filter system-function, once the sampling period (or the sampling frequency) is specified by the user.

## **7.5 Pre-Stack Processing**

The output from the re-organization phase is still in shot-gather, where the data is in de-multiplexed (trace –sequential) form. These shot records are used as input to the following phase of processing, the pre-stack processing phase which includes a sequence of steps, which are the following;

### ***(i) Trace Editing***

Together with the observer report, all shot records are inspected for data quality. There may be some shots which are very weak, or, for some reasons, corrupted to the extent of being useless to include in the processing. Weak traces or traces which are abnormally noisy are, likewise, omitted from processing or just zeroed altogether. Traces with reversed polarity, if any, are rectified. The process of trace editing is normally done manually on the shot records.

### ***(ii) Noise Attenuation***

There are several types of noise that may be found recorded alongside with the reflection signal. Measures to attenuate noise and lessen its effect on the signal resolution are taken in processing as well as those measures taken during the acquisition activities. The objective of noise attenuation at this stage of processing is to attenuate, as much as possible, the two types of noise which are the coherent (systematic) and the incoherent (random) noise.

The coherent noise which is commonly observed in field shot records is the low-frequency, high energy surface waves, known as the ground roll. This type of noise can

---

be attenuated by the application of a low-cut frequency filter or by the application of (F-K) filter. In either of these two techniques, processing tests are done to determine the noise spectrum and to find the appropriate filter to be applied on the data to remove the noise or lessen its effects.

The other type of noise, the random noise, is normally of broader frequency-band and lower energy and of random nature. It is more difficult to attenuate than the coherent noise, because of the overlap between its spectrum and that of reflection signals. Because of its random nature, this type of noise is very effectively attenuated in the stacking process, as with the application of vertical stacking and CMP stacking.

### **(iii) True Amplitude Recovery**

True amplitude Recovery (TAR) is a processing step which aims at adjustment of the amplitude of reflection-wavelet, leading to recovery of the true amplitude which represents the reflection coefficient. This is achieved by corrections for these three factors, namely, removal of the imposed gain and compensation for the geometrical spreading and inelastic attenuation effects.

#### **- Gain Recovery**

The gain-value applied during recording to each sample of the seismic trace is recorded alongside that sample. As a first step in TAR, the software is made to remove the effect of the recorder-applied gain from the sample value, recovering the true amplitude as detected by the geophone group. The correction factor  $F_G$ , due to the time-variant gain  $G(t)$ , may be represented by:

$$F_G = 1/G(t).$$

#### **- Geometrical Spreading**

This is amplitude attenuation caused as a result of spreading of the wave front as it travels away from the source region. Since the attenuation is inversely proportional to travelled distance, the correction factor ( $F_{GS}$ ) is of the form:

$$F_{GS} = v(t).t$$

Where  $v(t)$  is the velocity time-function for the reflection travel-path medium.

#### **- Inelastic Attenuation**

Inelastic attenuation takes place because of energy-absorption due to dissipation of seismic energy into heat due to friction. Studies has shown that this is a frequency-dependent effect and given by the exponential function,  $\exp(-\alpha x)$  where  $(\alpha)$  is the

---

attenuation factor which varies linearly with frequency, and ( $\mathbf{x}$ ) is the travelled distance (Sheriff, 2002, p.2). The travelled distance ( $\mathbf{x}$ ) can be substituted for by  $\mathbf{v}(\mathbf{t}) \cdot \mathbf{t}$

The correction factor ( $\mathbf{F}_{IA}$ ) is of the form:

$$\mathbf{F}_{IA} = \mathbf{e}^{+\alpha \mathbf{v}(\mathbf{t}) \cdot \mathbf{t}}$$

Inelastic attenuation is the third and last step in the TAR correction. The three steps can be combined in one compact correction factor ( $\mathbf{F}_{TAR} = \mathbf{F}_G \cdot \mathbf{F}_{GS} \cdot \mathbf{F}_{IA}$ ), hence:

$$\mathbf{F}_{TAR} = [\mathbf{v}(\mathbf{t}) \cdot \mathbf{t} \cdot \mathbf{e}^{+\alpha \mathbf{v}(\mathbf{t}) \cdot \mathbf{t}}] / \mathbf{G}(\mathbf{t}).$$

As this formula shows, there are two parameters that need to be inputted; the attenuation factor ( $\alpha$ ) and the velocity function  $\mathbf{v}(\mathbf{t}) \cdot \mathbf{t}$ . The first step is applying the gain recovery, then the geometrical spreading using a velocity function  $\mathbf{v}(\mathbf{t})$ , which is representative of the area. For the third TAR- correction, the parameter ( $\alpha$ ) is estimated from the slope (expressed in db) of the decay-line of a trace after being corrected for gain and geometrical spreading.

#### ***(iv) Field Static Correction***

Static correction is a travel-time correction which reduces the reflection travel-time to what it would be, if both the source and receiver were located on a defined horizontal datum-level. It is essentially a time bulk-shift made to each trace, making reflection travel-time to be measured from the fixed datum plane. Each sample of the trace is shifted in time by an amount which is constant to all the samples of the trace, hence the name **static correction** as opposed to another correction, the **dynamic correction**, in which the shift varies with the sample-time. The dynamic correction is referred to as **NMO correction**.

The principle of static correction is shown in Figure 7.5. In this figure it is shown that static correction is virtually placing both of the source and receiver on the defined datum plane and the correction is the same time shift (static) for all of the reflection events.

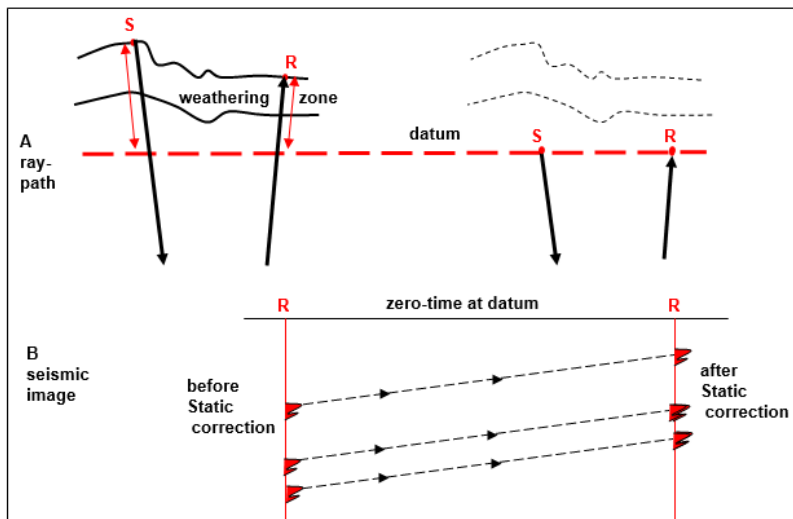


Figure 7.5 Principle of static correction. A-Ray-path, and B- seismic image of the seismic trace, before and after static correction.

The datum plane is chosen to be slightly below the base of the weathering zone. It can be the sea mean level or any horizontal plane defined at a suitable elevation. With the datum plane defined, the time shift (static correction) can be easily calculated from knowledge of thickness and propagation velocity of the weathering zone, which can be determined in the field by up-hole surveying or by especially designed refraction surveys.

**(v) Deconvolution**

Deconvolution is a process which is made to reverse a prior convolution (filtering) process. For this reason, it is also called *inverse filtering*. In addition to the inverse frequency filtering, deconvolution process has another function, which is shifting of repeated wavelets, created in certain situations in the reflection shooting, back to the original wavelet. Removing of ghosts and reverberations are examples of applying deconvolution as well as the inverse filtering action.

There are two basic types of deconvolution: Spiking (or Whitening) deconvolution which results in equalizing of amplitudes of frequency components (spectrum whitening) and Gapped (or Predictive) deconvolution which is attenuating multiples from shallow reflectors (as in removing ghosts and ringing) and removing reverberations.

**(vi) Trace Equalization**

Trace equalization is normally included in the processing to get a reasonably balanced form of the trace. Processing software provides several alternative options of the way to equalize the trace. One way to equalize the trace is by applying an AGC-type of scaling. This is carried out by defining a gate-length (normally of about 500 ms length) which slides down the trace at one sample-interval at a time. In the first position, at the top of the trace, the mid sample of the gate is multiplied with a factor proportional to the inverse of the average power of all the sample-values found within the gate. This multiplication process is repeated in the second gate-position, and so on until the whole trace is covered.

**(vii) CMP-Sorting**

The field seismic data received by the processing center consists of a series of shot records recorded on a magnetic tape in the sequence of shooting implemented in the field. In other words, the received seismic traces are grouped in shot-gathers which are subjected to the re-organization and pre-processing steps. Since in the following processing phase the CMP-traces are going to be stacked, the traces which are sorted in shot-gathers are re-sorted into CMP-gathers in which the traces are normally arranged in sequence of increasing offset. In fact, the CMP-record looks like shot records shot in end-on type of spread. The number of traces per certain CMP-gather is equal to the fold of coverage for that CMP. The process is just regrouping of the traces such that all traces belonging to a CMP are grouped together under that particular CMP.

**(viii) NMO Correction**

Reflection travel time ( $T_x$ ) of seismic signal reflected from a horizontal reflector and received at a point on surface at distance ( $x$ ) from the source location is given by

$$T_x = [ (x/v)^2 + (T_0)^2 ]^{1/2}$$

where ( $T_0$ ) is the two-way reflection vertical time, and ( $v$ ) is propagation velocity assumed to be constant for the medium.

**The NMO Concept**

Normal moveout (NMO) is defined to be the difference ( $\Delta T$ ) between the slant reflection time ( $T_x$ ) and the vertical reflection time ( $T_0$ ) for the same CMP (Figure 7.6), that is:

$$\Delta T = T_x - T_0$$

---

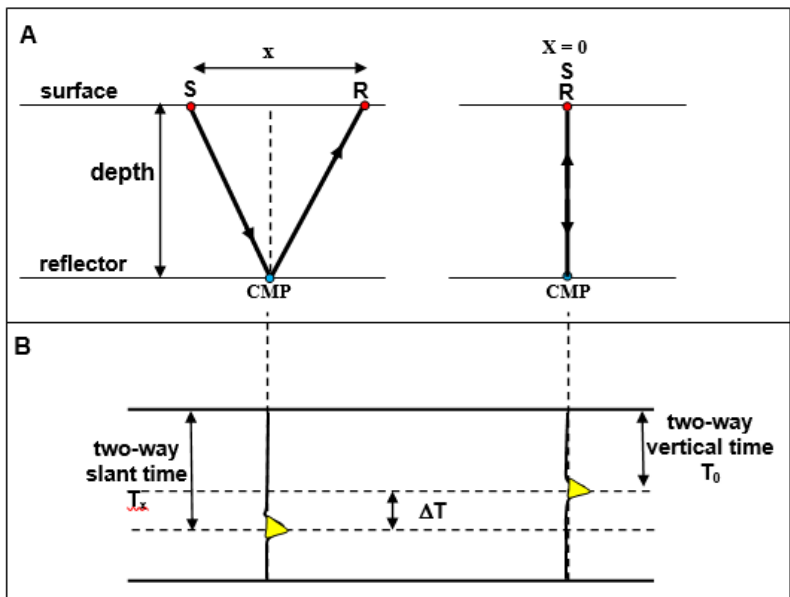


Figure 7.6 Definition of the Normal Move Out (NMO),  $\Delta T = T_x - T_0$ . (A) Reflection ray-path, and (B) Reflection image

For a horizontal reflector, the normal move out ( $\Delta T$ ) is given by:

$$\Delta T = T_x - T_0$$

That is,

$$\Delta T = [ (\mathbf{x}/\mathbf{v})^2 + (\mathbf{T}_0)^2 ]^{1/2} - \mathbf{T}_0$$

For a sufficiently small offset-to-twice the depth ratio ( $\mathbf{x}/\mathbf{v}\mathbf{T}_0 \ll 1$ ), normal move out ( $\Delta T$ ) can be approximated by expanding the square root in the ( $\Delta T$ ) formula with the Binomial Theorem to give:

$$\Delta T = \mathbf{x}^2 / 2\mathbf{T}_0\mathbf{v}^2$$

With this approximation, the formula was transformed from the exact hyperbolic function to the approximate parabolic form which can express, more clearly, the mathematical relationships of the NMO parameters ( $\mathbf{x}$ ,  $\mathbf{T}_0$ , and  $\mathbf{v}$ ). It is shown that ( $\Delta T$ ) is directly proportional to square of offset ( $\mathbf{x}$ ) and inversely proportional to vertical time ( $\mathbf{T}_0$ ) and to square of velocity ( $\mathbf{v}$ ). On a seismic reflection record, ( $\Delta T$ ) is clearly seen to increase as the trace-offset increases and decreases with increasing reflector's depth for the same offset (Figure7.7).

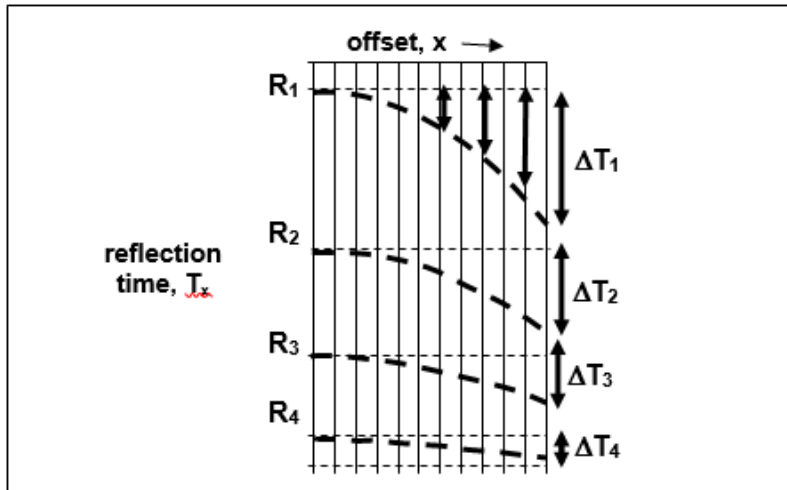


Figure 7.7 Variation of the NMO parameter ( $\Delta T$ ) as shown in a seismic record. ( $\Delta T$ ) increases with trace offset and decreases with depth of reflector.

### NMO Application

In processing of reflection data, seismic traces, before being stacked, must be NMO-corrected. This involves removing the extra time in the reflection travel-time from the reflection slant time. Arrival reflection times in each gather will be corrected to what it would be if the trace offset is zero. With this correction, the common-reflector events in the gather traces (from a given horizontal reflector) will all have the same arrival-times. Thus, when the gather traces are NMO-corrected, they will give boosted reflection amplitude after being stacked. As it is shown in Figure 7.7, the NMO value varies with the reflection time. It is decreasing with reflector depth. NMO correction, involves calculating ( $\Delta T$ ) accurately for each sample of the trace and then the sample is shifted up the trace by the calculated  $\Delta T$ -value.

Unlike static correction where the correction is constant (static) for all the trace samples, NMO correction varies with the sample time and that is why it is also called dynamic correction. Static correction is, effectively, placing both of the source and receiver on a common horizontal plane, the datum plane. Likewise, NMO correction, effectively, places the source and receiver on a common position on the datum plane. With the static and NMO corrections, reflection events from a horizontal reflector (on a CMP-gather), will be aligned on the same timing line, giving enhanced reflection on the CMP trace-gather stacking. These concepts are shown in Figure 7.8.

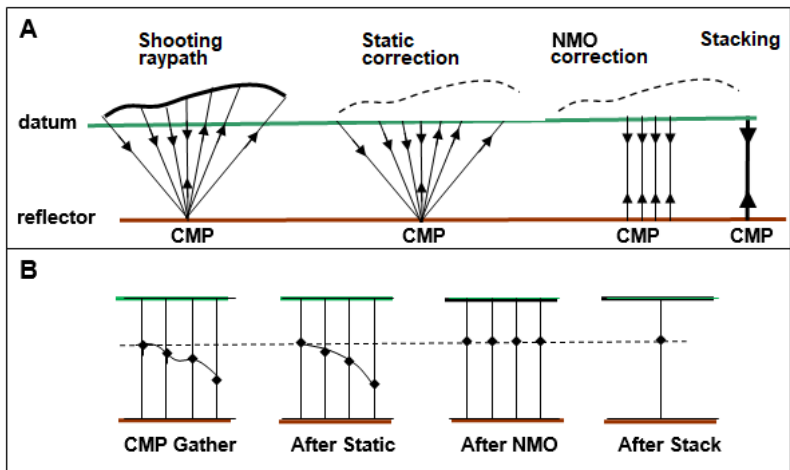


Figure 7.8 Concepts of static and NMO corrections. (A) ray-path of a CMP reflection (B) seismic image (seismic traces) of a CMP gather after NMO and static corrections

**(ix) Trace Muting**

The muting process is done by multiplying the trace by a scaling function which is of zero-value over the parts to be muted and unity over the rest of the trace. The change from zero to unity is usually made to change gradually and not abruptly, in order to avoid creating spikes or sudden breaks in the trace at the extremities of the mute-zone. For this purpose, a ramp-type of function is used in muting rather than a step-type of function. The time of the ramp part of the scaling function is called (ramp length). Trace muting is sometimes called ramping because of the use of ramp scaling function. The concept is shown in Figure 7.9.

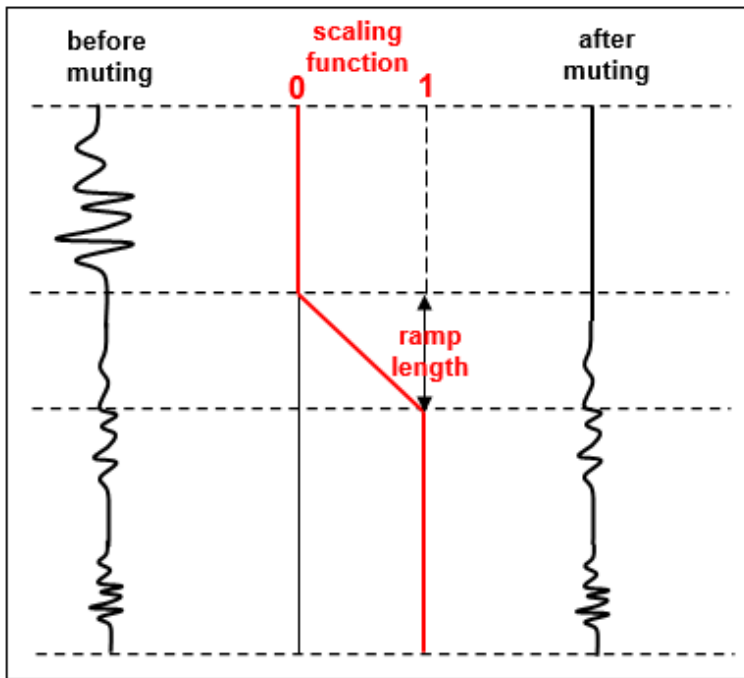


Figure 7.9 Concept of trace muting, using mute ramp-function.

## 7.6 Stack and Post-Stack Processing

Stacking of a group of seismic traces is a process by which seismic traces are summed up together to form one output trace, called the stack trace. The process involves finding the algebraic sum of the values of trace samples which have a common recording time. The output is normally divided by the number of traces entering in the summation to get the arithmetic mean of the traces. In seismic data processing, there are three main types of stacking. These are: CMP stacking, vertical stacking, and horizontal stacking.

### (i) CMP Stacking

The process of CMP-stacking, is summing the trace-gather of a CMP. This is done after both static and NMO corrections are applied to the gather-traces in order to bring reflection events in phase. The stack trace is normally subjected to a certain scaling process as finding the arithmetic mean of the summed traces with or without weighting. Thus, each CMP-gather will, after stacking, give one stack trace showing enhanced reflection wavelet with marked (S/N) enhancement of the reflection events (Figure 7.10).

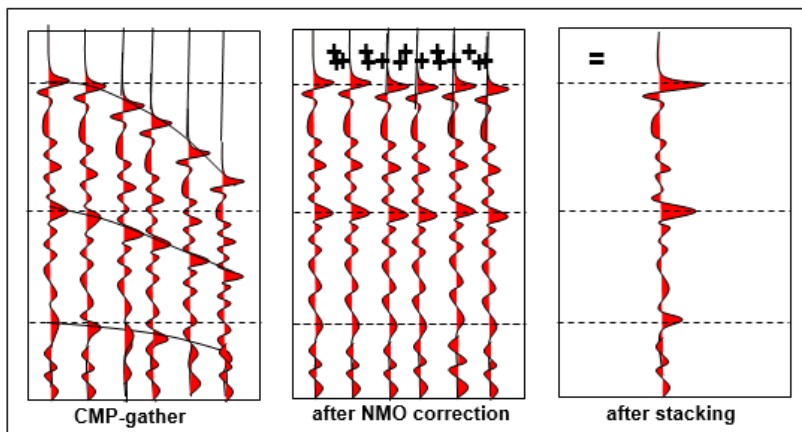


Figure. 7.10 CMP-stacking of CMP gather-traces after being NMO-corrected

The main advantage of the CMP stack is enhancing the seismic reflection signal. This is because reflection events are summed in phase resulting in constructive interference whereas the background noise, being of random nature, is destructively interfered with each other resulting with noise-cancellation. The increase in S/N ratio due to CMP stacking is estimated to be of the order of square root of the number of the traces in the CMP-gather (that is square root of the fold of coverage).

**(ii) The Stack Section**

The stack trace is obtained from summing of all NMO-corrected traces in the CMP-gather, a process which is repeated for all the CMP-gathers after being CMP sorted. From displaying these stack traces in the order of CMP sequence-number, the stack section is obtained.

A stack section represents a subsurface seismic image of the subsurface geological structure. Normally, the stack section is provided with top-label showing the CMP sequence numbers, elevation, and static correction drawn as function of distance along the seismic line. Another important label (normally drawn below the section) is the fold of coverage drawn as function of the CMP sequence number.

A typical stack section is shown in Figure 7.11.

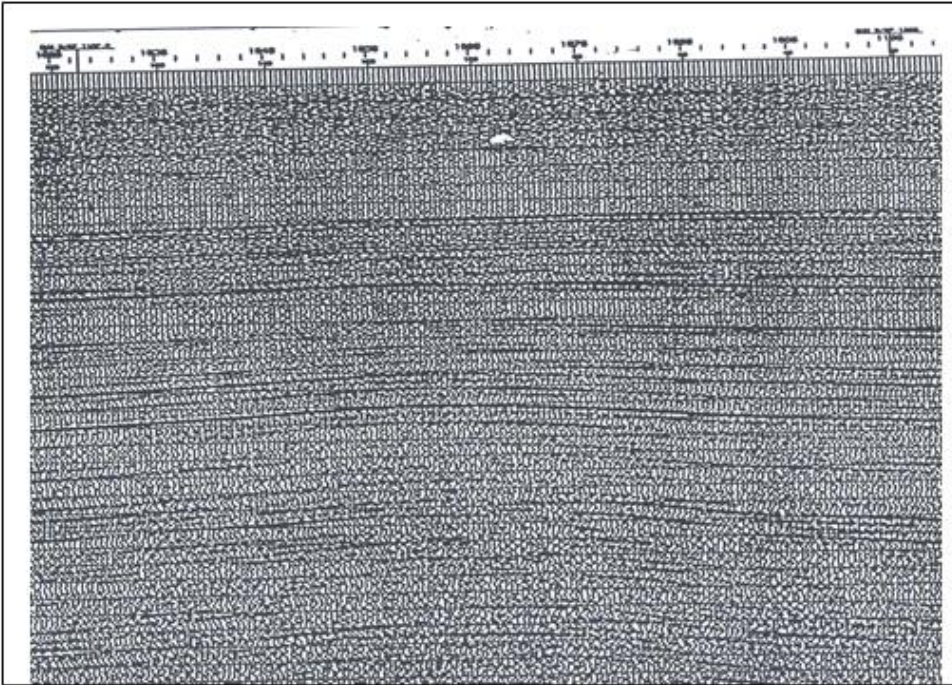


Figure. 7.11 A conventional seismic stack section

### **(iii) Seismic Post-Stack Migration**

The seismic stack section represents the undistorted seismic image of the subsurface geological structure only when it is made up of continuous horizontal reflecting interfaces. When we have folded formations (dipping reflectors) and faulted beds (terminated reflectors), the stack section is a distorted image of the subsurface geology.

#### ***Distortions in the Stack Section***

There are two cases in which distortions can occur in the seismic stack section:

**Case-1: Dipping reflector**, shifting of the reflection event horizontally and vertically from its true position, resulting in decrease of the dip-angle from its true value and shortening of the reflection segment (Figure 7.12).

---

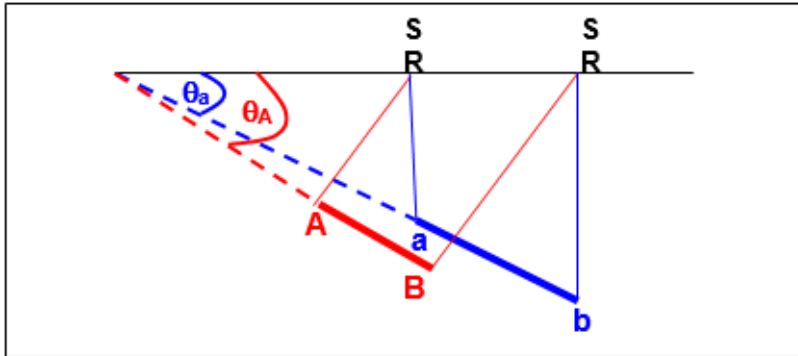


Figure 7.12 Distortions of a dipping reflection segment. The segment is misplaced, gets shortened and its dip is decreased.

**Case-2: Terminating reflector,** creation of diffraction arrivals in the form of hyperbolic events interfering with reflection events obscuring fault zones that caused the termination (Figure 7.13).

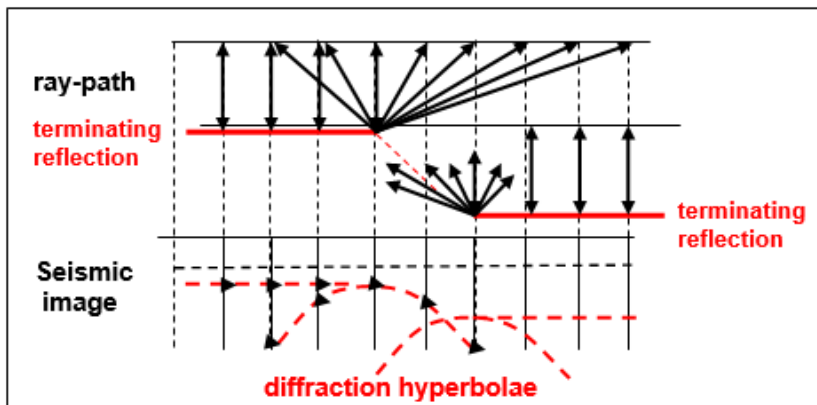


Figure 7.13 Distortions due to diffraction arrivals created by a faulted reflector. Two diffraction points were created by the fault.

Another case of distortions associated with folding is the presence of a too-tight syncline (curvature width  $\ll$  depth). We have, in this case, a reflector having dips in opposite directions allowing zero-offset receivers to receive more than one reflection event coming from different reflection points. The resulting seismic image shows what is called a *buried focus* or *bow-tie image* which is a reflection image having a shape, far from the real structure and thus, a very misleading stack-section feature (Figure 7.14).

A migration process would do the appropriate restorations whereby dipping reflection events are positioned in their correct positions and their dips are corrected to their true values, also it would remove the diffraction arrivals (diffraction hyperbolae).

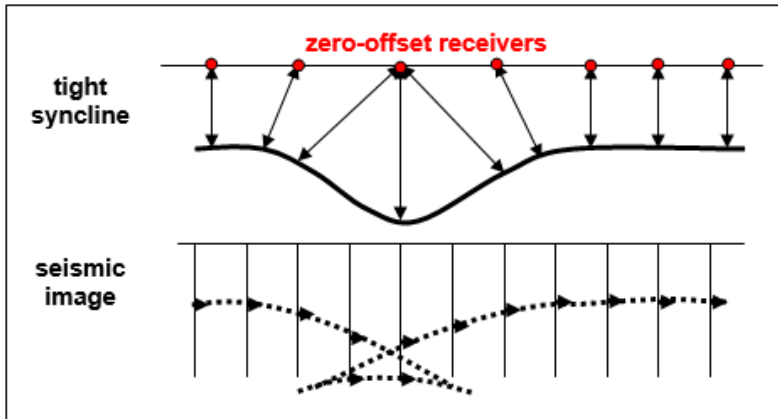


Figure 7.14 Distortions due to multi-reflection arrivals created by a too-tight syncline

#### (iv) Frequency Filtering

As we have mentioned in the processing objectives, processing aims at reflection travel-time corrections and reflection signal enhancement and at improving of resolution. One of the main factors that affect reflection wavelet is the filtering effect. This effect is in operation during the reflection journey through the earth (earth high-cut filter) and later in the detection, recording, and processing stages.

In general, a seismic trace shows reflection wavelets of frequency spectra that vary with the depth of the reflector. The frequency tends to decrease as the reflection travel-time increases. It is therefore, expected that the signal-noise interaction varies with reflection time. This phenomenon is the basis for the application of a time-variant filtering (TVF). If the area is large and showing complex geology, there may be a need for a distance-variant filtering as well. However, spatial variation of the filter is rarely applied.

Specification of the frequency band-pass filter is normally found through a special filter-test processing. With the aid of Fourier-spectrum analysis, the frequency changes with reflection-time can be investigated. Based on the spectrum analysis and the filter test, a time variant filtering system is designed and applied to the stacked and migrated data-set.

## 7.7 Parameter Optimization

The processing sequence, normally followed to process a set of seismic reflection data, consists of a sequence of procedures with special processing parameters. The efficiency of a certain process is mainly controlled by the parameter applied. Thus, for example, a frequency-filtering process depends on the band-width parameter adopted. Other parameters for the filtering process are, the operator-length, operator-truncation window, gate-length, TVF time-knees, and so on. The important

thing here is that the applied parameters must be optimum, producing the best results in terms of signal accuracy, clarity, and position correctness.

**(i) Velocity Analysis**

Velocity parameter is of prime importance in seismic processing. Its role is in controlling the quality of the stacking output. An optimum velocity value used for the NMO correction gives best stacking response in terms of signal-to-noise ration. For this reason, it is called stacking velocity. It might be more appropriate to be called *NMO-correction velocity*, since its direct application is in the NMO correction which precedes the stacking process.

To derive the optimum stacking velocity function (velocity as function of reflection time) a data-set made-up of a group of CMP traces is chosen at a location on the seismic line where the analysis is to be done (Figure 7.15).

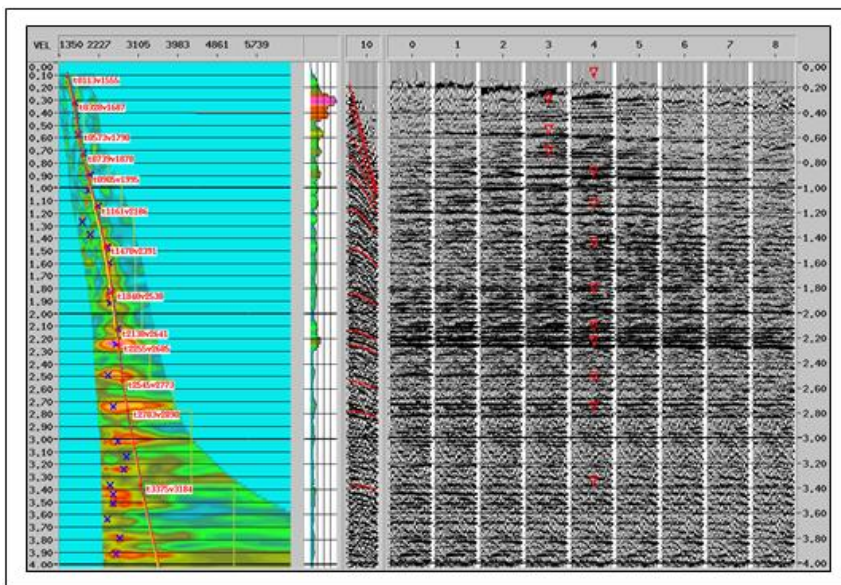


Figure 7.15 Typical velocity analysis output: Interpreted color-coded power display (velocity “spectrum”), NMO-uncorrected CMP gather of the central CMP, and a panel of stacked mini-sections for the selected set of CMPs corresponding to 9 different velocity functions.

# 8. SEISMIC REFLECTION DATA INTERPRETATION

## 8.1 The Two Interpretation Tools

There are two main tools commonly applied in seismic interpretation; the travel-time tool and the waveform tool (Figure 8.1).

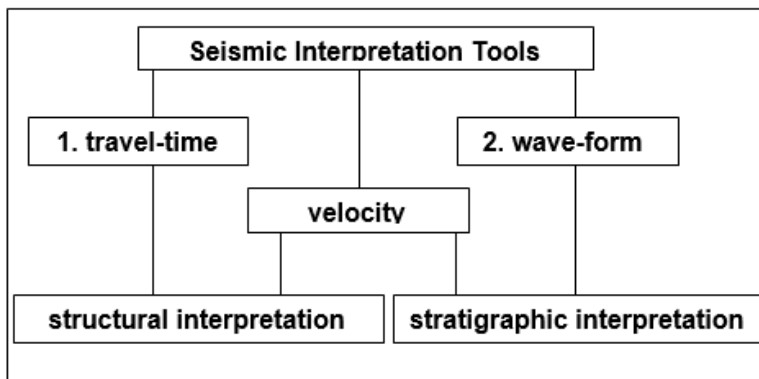


Figure 8.1 The two interpretation tools; the travel time for structural interpretation and the waveform tool for stratigraphic interpretation.

### (i) The travel-time tool:

Reflection travel-time computations lead to determination of the variation of the reflector depth along the seismic line. This means that this approach (travel-time analysis) would serve as a structural interpretation tool. In particular, the structural features; folding and faulting are mapped with this tool.

### (ii) The wave-form tool:

The wavelet energy level (expressed by the wavelet amplitude) is related to the reflection coefficient which is, in turn, related to the contrast in the acoustic impedance across interfaces. The other wavelet parameters (frequency and phase characteristics) are influenced by the physical properties of the rocks as lithology, porosity, and fluid contents. This means that wave-form changes can be used as stratigraphic interpretation tools.

---

## 8.2 Structural Interpretation Sequence

In a procedure similar to that normally followed in the seismic data processing, interpretation is carried out by a sequence of steps, the interpretation sequence. The standard sequence involves four main steps; reflection identification, the isochron map, the velocity map, and depth map. These steps are here, briefly described:

### ***(i) Reflection Identification and Picking***

Reflection times of the reflection horizon are read (manually or electronically) by a process called (reflection picking). The process is carried out for the same horizon in all of the sections in the area. Care is needed to be taken when the reflectors are affected by faults. A common difficulty met with is the mistie-phenomenon. In the process of tying horizons picked at intersecting sections, reflection times may not coincide. This problem, which may be due to anisotropy or other causes, needs special treatment to make the horizons at the intersections to tie well.

### ***(ii) The Isochron Map***

The picked reflection values are posted onto the seismic lines at regular intervals, then a contour map is drawn to produce the isochron map. Another set of contour map are drawn for iso-time interval for time interval between two adjacent reflectors. This time-interval contour map corresponds to the depth interval (or isopach) contour map. Interval changes may indicate true thickness changes or velocity changes, which both can give significant geologic information.

### ***(iii) The Velocity Map***

There are two main sources for the velocity data for the surveyed area. (1) The velocity functions obtained from well velocity surveys, or VSP surveys and (2) the stacking velocity functions used in processing stage. Well-survey velocities are more accurate but available only at the limited number of well locations. The normal procedure is to compute a smoothed contour map of the average velocity functions (derived from the stacking velocity) and get it calibrated with the well velocity functions.

### ***(iv) The Depth Map***

Based on the smoothed average velocity map and the isochron map (corrected for misties etc.), the depth contour map is computed. The resulting map represents the structural contour map, with the fault-lines clearly marked on.

The standard sequence normally followed in seismic structural interpretation is presented in Figure 8.2.

---

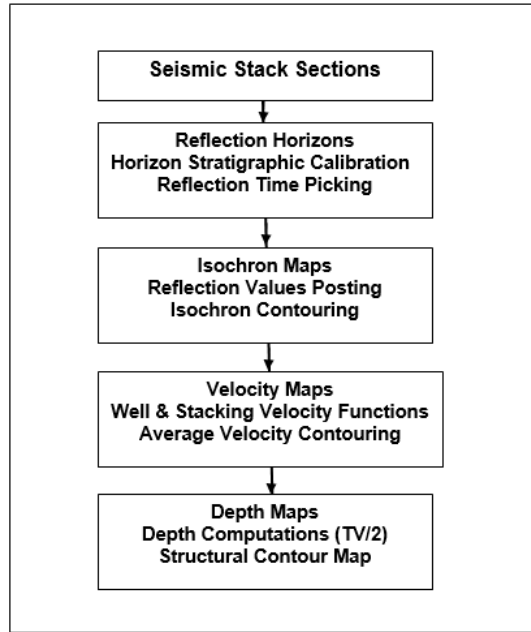


Figure 8.2 Standard sequence normally followed in seismic structural interpretation

### 8.3 Stratigraphic Interpretation Sequence

As in structural interpretation procedure, stratigraphic interpretation can be carried out through a sequence of steps; the stratigraphic interpretation sequence (Figure 8.3).

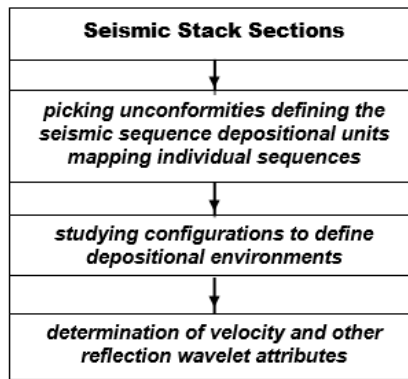


Figure 8.3 Standard sequence normally followed in seismic stratigraphic interpretation (modified after Sheriff, 1980, p.22).

The stratigraphic interpretation starts with the section of the major seismic sequences by marking the sequences bounding unconformity surfaces. From the events

configuration patterns, the stratigraphic units and sedimentary environments are determined. The last steps of the interpretation are applying inversion modeling and producing maps for the changes of velocity and other seismic attributes. The final interpretation work would be the determination of lithological changes, deposition environments, and hydrocarbon contents.

The main parameters used in seismo-stratigraphic interpretation and their geological significance may be summarized as follows (Vail et al., 1977).

### 8.4 Interpretation Example

An ideal example of a structural feature of semi-parallel horizontal layers, a simple anticline, fault picking as shown in Figures 8.4 - 8-9.

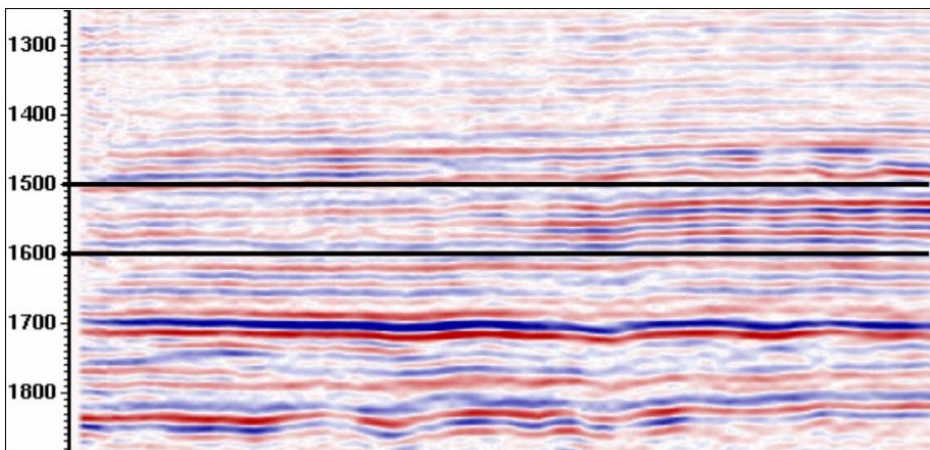


Figure 8.4. seismic stack section of the particularly horizontal layers.

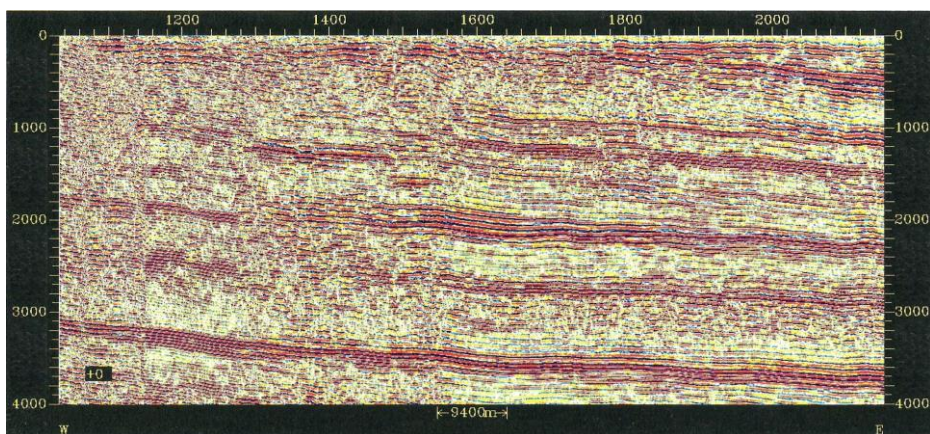


Figure 8.5 A seismic image of a semi parallel and dipping layers toward the east.

---



Figure 8.6 A seismic image of a structural feature (simple anticline).



Figure 8.7 A seismic image of structural features (unconformity, anticlines and synclines).

---

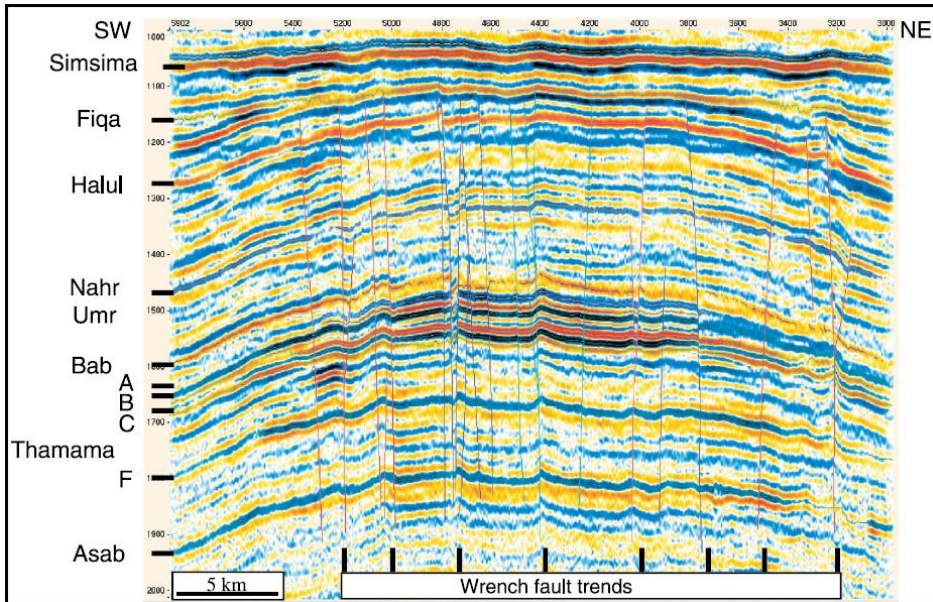


FIGURE 8-8. A seismic line along the crest of the anticline axis showing the Cretaceous section with interpreted horizons. The large anticline is cut by near-vertical Upper Cretaceous-aged wrench faults (Eberli et al, 2004).

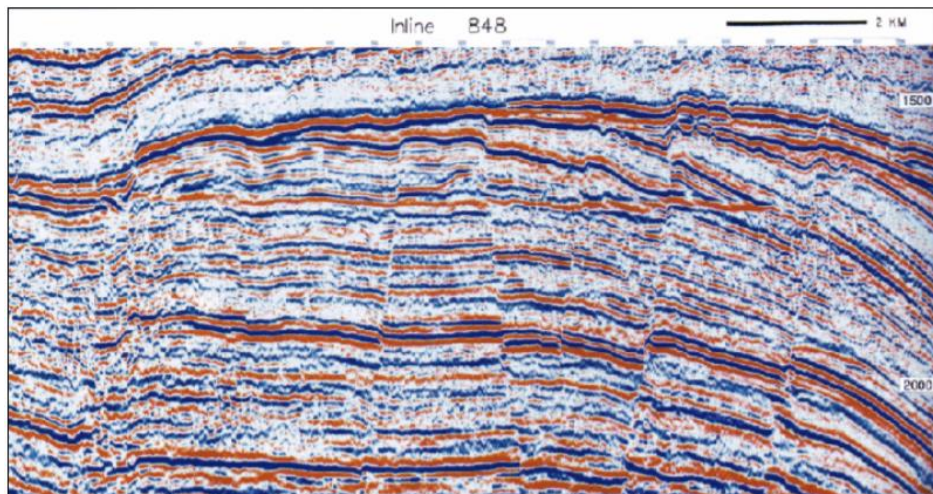


Figure 8.9 Vertical section across Troll gas field offshore Norway shows numerous faults and flat spots (Countesy Norsk Hydro a.s.).

Another example of a stratigraphic feature is an angular unconformity as shown in Figures 8.10 - 8.14.

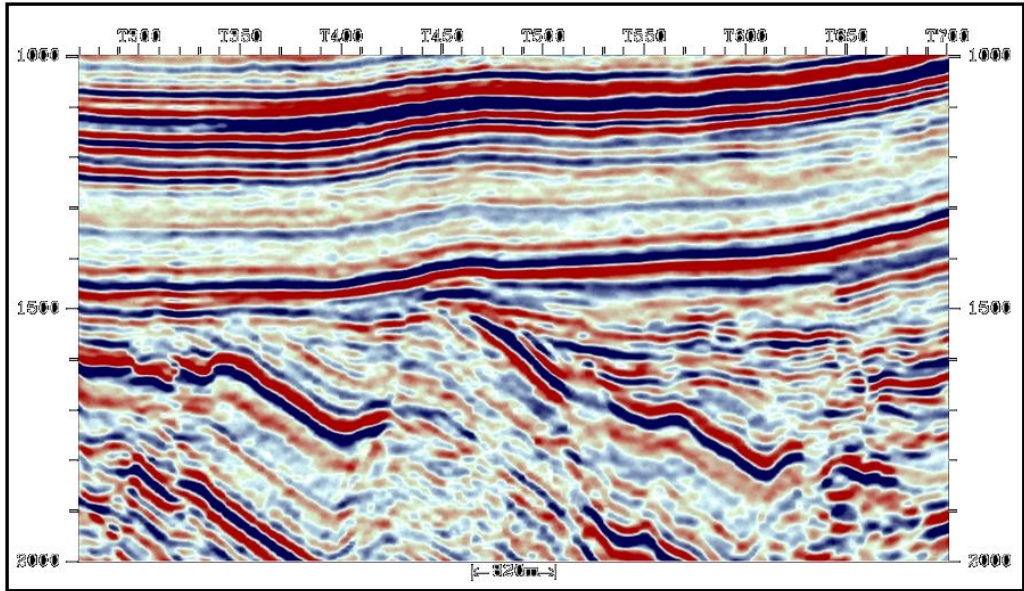


Figure 8.10 A seismic image of a stratigraphic feature (angular unconformity).

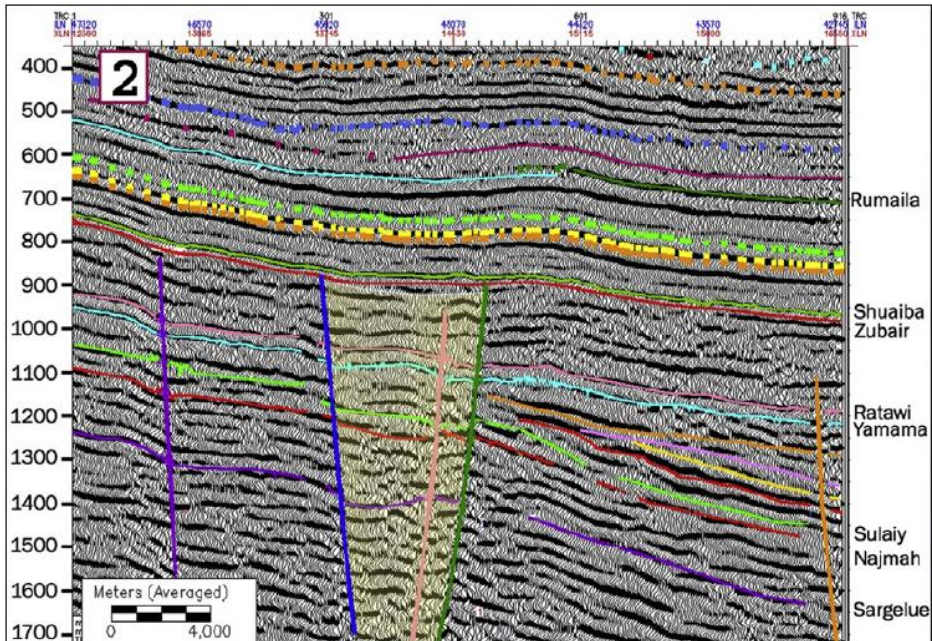


Figure 8.11 NE-SW seismic profiles across the picked fault system that affect Merjan field in Iraq, shows three normal faults affect Jurassic to lower Cretaceous succession. (after Fadhel and Al-Rahim, 2019).

Strictly speaking, an unconformity has both structural element (the beds tilting) and stratigraphic element (the erosion and deposition) processes.

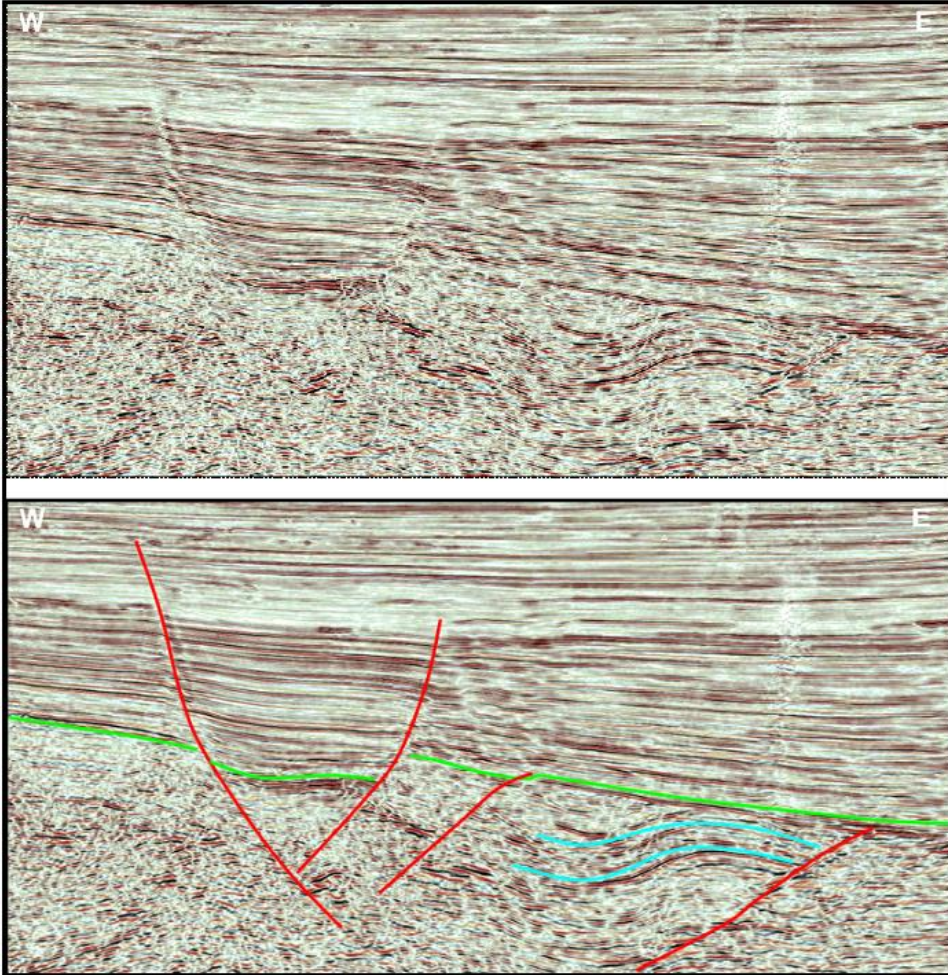


Figure 8.12 East-west seismic line with interpretation across the northern Dibba Zone showing Late Cretaceous “folding”. Post-unconformity structuring is limited to normal extensional faulting (Mokhtari, 2006).

---

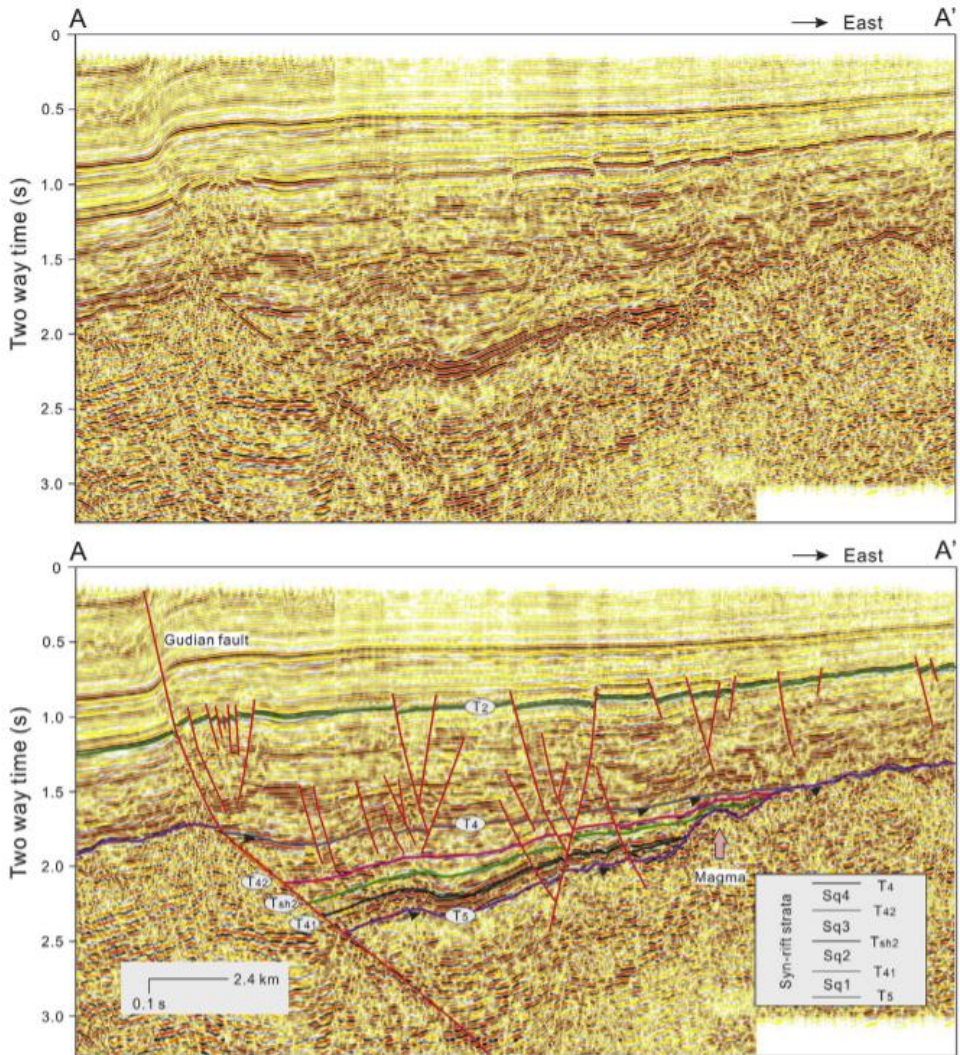


Figure 8.13 Seismic profile AA' showing the geological subsurface framework in the Gudian half-graben. Six sequence boundaries, four sequences, faults including the Gudian fault and some small secondary faults, are identified on the profile. T5 and T4 are angular unconformities showing truncation relationships with underlying seismic reflectors, and the strata between them belong to syn-rift deposition. Top: initial seismic profile; Bottom: interpreted seismic profile, (After Wang et al, 2018).

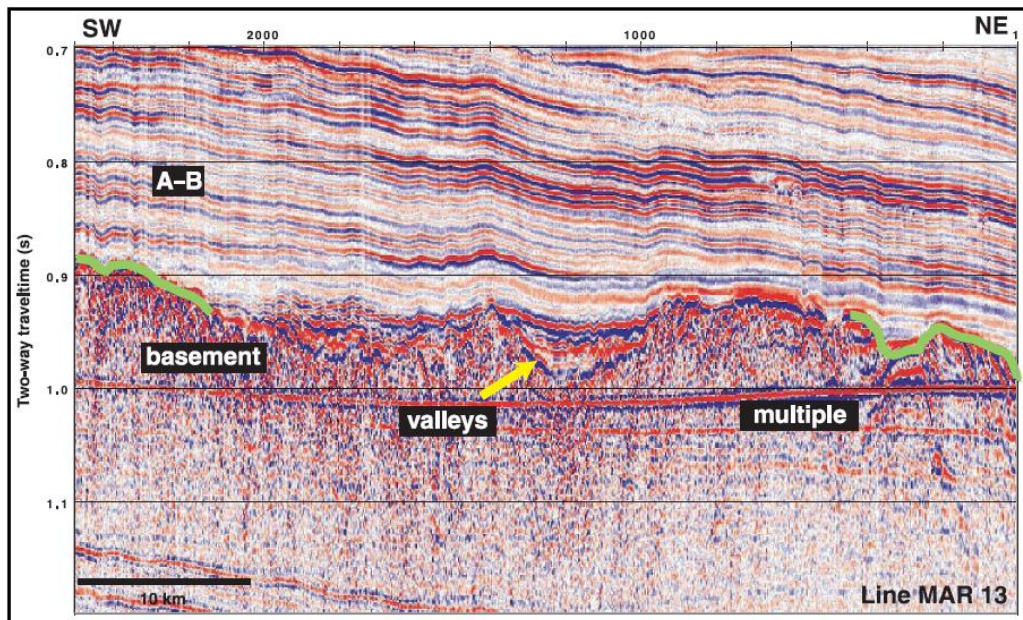


Figure 8-14 Detail of seismic line MAR 13 showing the nature of acoustic basement here overlain by sediments of megasequence A that transgressed over basement. These sediments are overlain by periplatform sediments of mega-sequence B that were shed from the adjacent NMP. Green lines indicate the location of the basement reflector. The sea-floor multiple is also indicated, (Isern, et al, 2004).

## 8.5 Seismic Attributes

In the geophysical literature, the term (attribute) is used to mean a property or a parameter attributed to a certain seismic element. It serves as a specific character related to a geophysical element. For example, it is said that the fold of coverage is a CDP attribute, and the azimuth (or, offset) is a bin attribute, because fold and azimuth are parameters of the CDP and bin respectively. In the field of the seismic stratigraphy, the term *Seismic Attribute* is used for calling one of the parameters of the seismic reflection wavelet. The attribute in this sense is a measured or computed value of a seismic parameter (data) of a (or, related to) the reflection wavelet. Typical seismic attributes are wavelet amplitude, frequency, phase, dip, and polarity. Attributes can be measured at one instant in time or over a time window and may be measured on a single trace, on a set of traces or on a surface interpreted from seismic parameters (data). A normal seismic trace is considered as a time function of the parameter (amplitude). After being converted into the attribute-domain, we get an attribute trace which is a function of the attribute value that varies with the reflection time. By converting all of the seismic traces of a stack section a seismic attribute-section is obtained.

Seismic attributes let the interpreter to obtain more information from seismic data such as to finding the geomorphologic insight using 3-D datasets.

Seismic attributes are used to check seismic data quality, creating seismic facies mapping for depositional environments, prospect identification, analysis of risk, reservoir characterization, and evaluation of hydrocarbon,

Taner et al. (1994) divide attributes into two general categories: geometrical and physical

- Physical attributes have to do with the physical parameters of the subsurface and so relate to lithology. These include amplitude, phase, and frequency.
- The objective of geometrical attributes is to enhance the visibility of the geometrical characteristics of seismic data; they include dip, azimuth, and continuity.

#### ***(i) The Instantaneous Attributes***

The three basic instantaneous attributes are usually derived from the seismic stack trace, using the time-domain Hilbert Transform (Taner, et al, 1979). The instantaneous frequency is more sensitive to changes in the inelastic absorption property of the rock medium and in studying sedimentary facies. The third and last attribute in this group, is the instantaneous phase which is considered to be a very active tool in showing reflection-termination phenomena as they happen with faults, unconformities, and pinch-outs.

#### ***(ii) Spectral Attributes***

Spectral attributes, were introduced in early 1970s (Båth, 1974, p 203-218). In a study based on earthquake P-waves spectra, several spectral attributes called then, *spectrum parameters*, were introduced to explore properties of the Earth Upper mantle (Al-Sadi, 1973). This attribute is considered to be one of the most efficient seismic attributes, because each of the Centroid coordinates is function of the distribution manner of the frequency components of the analyzed wavelet. Computation of this attribute is done by a sliding window with length and shift-step that are controlled by the processing geophysicist. The principle of deriving of the spectrum-centroid coordinates, is shown in Figure 8.15.

---

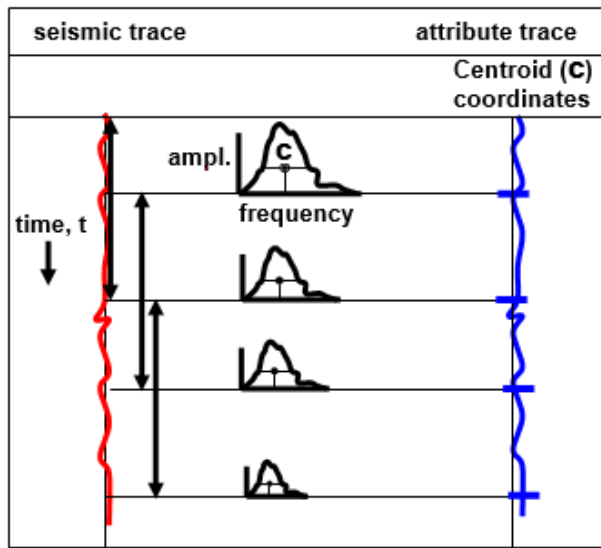


Figure 8.15 Sketch showing the definition of the attribute trace. Spectral attribute (spectrum centroid,  $C$ ) is presented as function of reflection time.

**(iii) Application of the Spectrum Centroid to Reflection Seismology**

In 1995, the Spectrum-Centroid attribute section was computed for a seismic stack section (Figure 8.16). In this figure both of the attribute sections (instantaneous amplitude, and Spectrum-Centroid sections) are presented for comparison purposes.

This figure shows that both of the attribute sections show the main general trends. However, the Centroid attribute section shows less noisy section and can be said to have a better feature resolution.

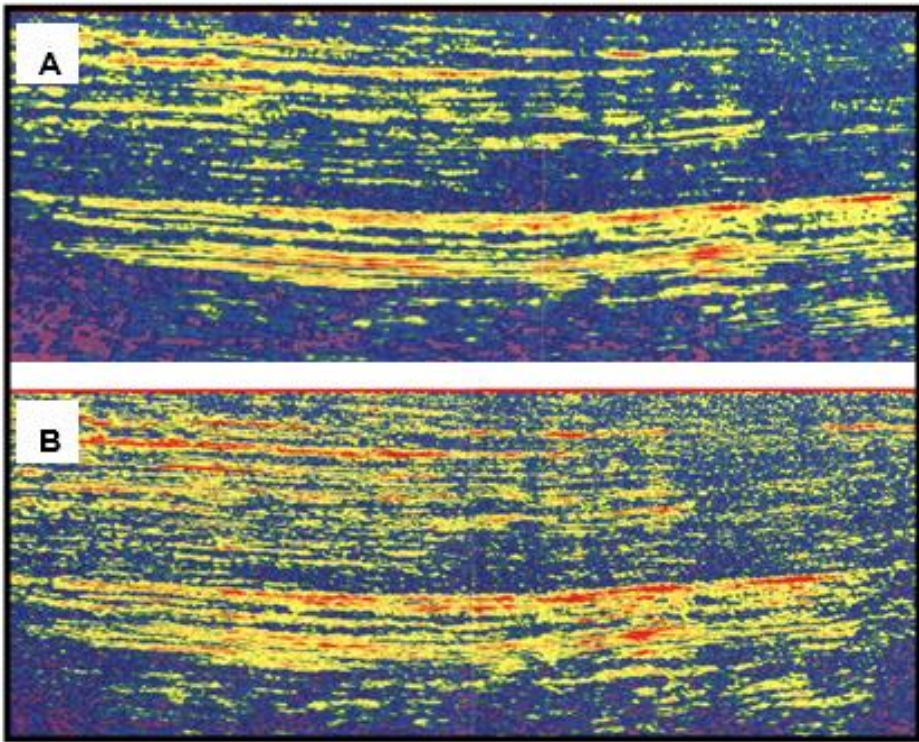


Figure 8.16 Seismic-Attribute color-coded sections: (A) Spectrum Centroid section and (B) Conventional Instantaneous amplitude section (Alsadi, 1995, 1998).

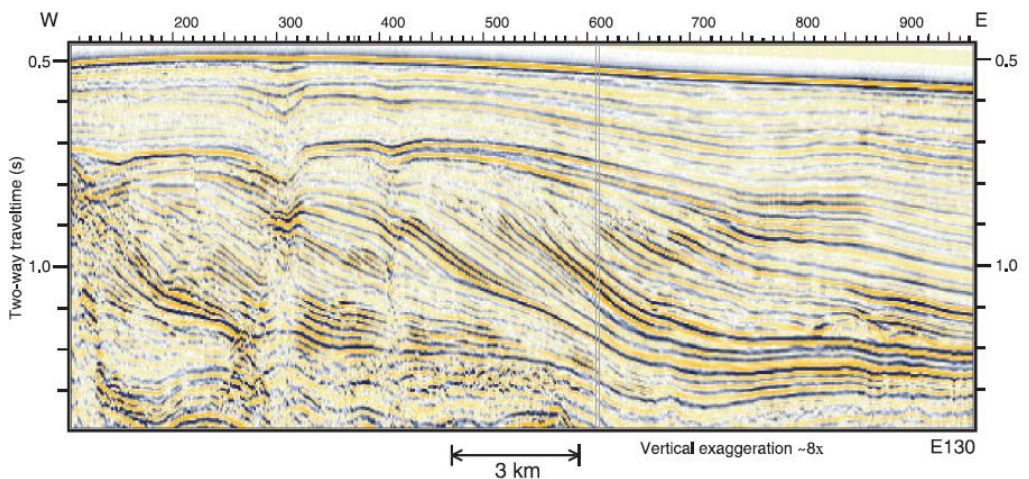


Figure 8.17 Seismic section indicate sequence boundaries. Each sequence is divided into strong-amplitude reflection package (SARP, shaded) and weak-amplitude reflection package (WARP, no color fill), (Belopolsky and Droxler, 2004).

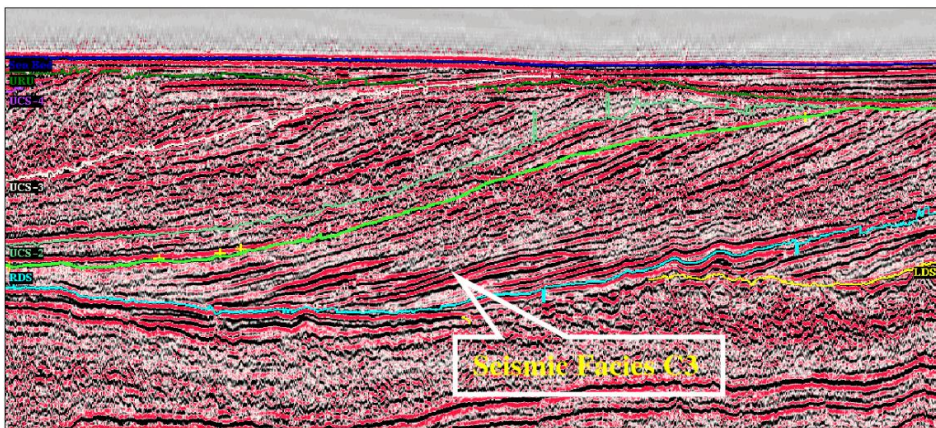


Figure 8.18 Seismic section showing seismic facies; as bottom sets of progradational clinothems. The units of these kind of seismic facies category are recorded in various parts of the Plio-Pleistocene prograding wedge system (after Abbas, 2006).

# 9. CASE STORIES

## 9.1 Seismic study of a regional line in the Western Desert of Iraq

Ezzadin Najmadin Baban, Basim R. Al- Hijab, Hamid N. Al-Sadi

2<sup>nd</sup> Conference of CAJG, 25-28 Nov. 2019, Sousse, Tunisia

### 9.1.1 Introduction

The study area is located in the Western Desert of Iraq. It is a strip that extends from the Iraqi-Saudi Arabia border at Longitudes  $41^{\circ} 30'$  -  $43^{\circ} 45'E$  and Latitudes  $32^{\circ} 00'$  -  $33^{\circ} 15' N$  toward the Euphrates river, southwest of Al Fallujah town crossing the Umm Anz, Thumaily, and Razzaza-Habbaniyah areas, (Figure 9.1).

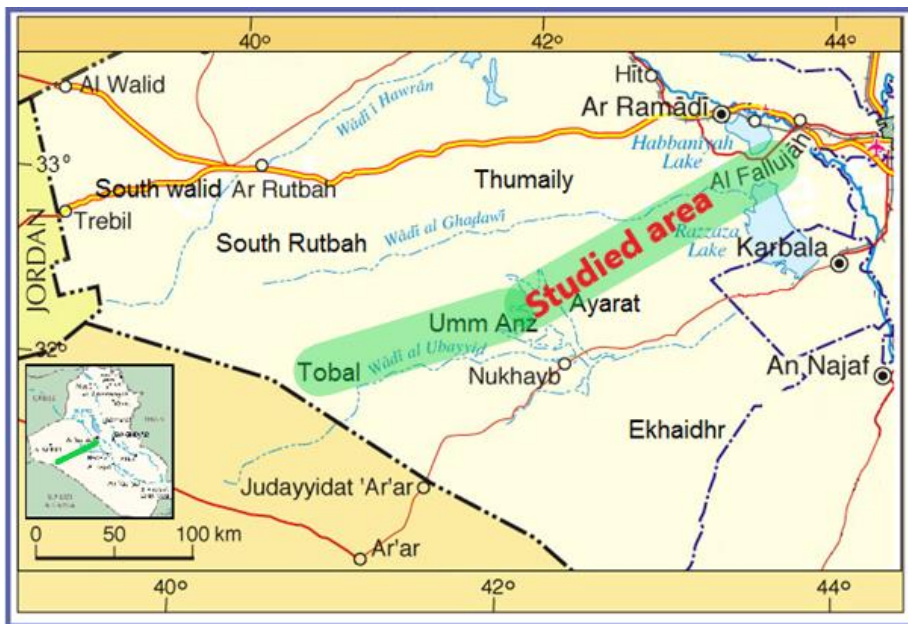


Figure 9.1 Location map of the studied area.

The surface geology, geomorphology, mineralogy, tectonic, geophysics and hydrogeology of the area are studied by numerous researchers, including: Al-Sayyab and Valek (1968), Abbas and Masin (1975), Al-Khatib (1976), Al-Bdaiwi (1982),

Abbas (1985 and 1995), Al-Rawi (1986), Baban (1983), Aziz (1986), Al-Husseiny (1989), Al-Banna (1992), Al-Yasi and Hijab (1995), Al-Khatib (1996), Hijab (1996), Hijab and Al-Khatib (1997), Al-Sheikh (1997), Al-Yassi (1997), Abdul Jalil (1998), Al-Banna (1999). However, no real subsurface studies have been carried out for this area. This is due to limited numbers of deep boreholes and restricted detailed geophysical survey. The aim of the present study was to better define the regional geological features within the Western Desert of Iraq based on a synthesis of a number of local seismic surveys. The study focused on subsurface structure and stratigraphy features along a constructed seismic regional line and sought to delineate and characterize the nature, depth, thickness, and type of Mesozoic, Paleozoic, and crystalline basement rocks in the area.

### **9.1.2 Geology and Tectonic setting**

The Western Desert of Iraq lies within the Al-Widyan physiographic subdivision and is characterized by relatively flat topography that exhibits a very gradual and gentle rise in elevation from east to west. The area is interspersed by a few depressions and hills and is cut by many wadies, most of which trend in SW-NE and E-W directions.

The surface geology of the study area, (Fig. 2), is represented by rock units ranging in age from Cretaceous to Quaternary-Pleistocene (Recent). The Umm Radhuma formation of Paleocene time outcrops in the west and southwest of the study area. In the central part of the study area, Middle-Upper Cretaceous formations are exposed, while in the eastern part of the study area outcrop exposures are dominated by the Euphrates, Zahra, Injana, Dibdibba / Middle and Injana (Upper Fars of Quaternary – Pleistocene age), Fatha (Lower Fars), and Najaf beds / Fatha (Middle and Lower Miocene) formations.

The subsurface rocks of the study area are mainly deduced through examination of exposed formations in neighboring countries, and from logs of some deep oil wells such as; Kf-3, Akkas-1 and Wkf-1, which are located to the north and south of the study area; Safra-1, RH-1, RH-3, and RH-6 in Jordan; and Turaif and Badanah in Saudi

---

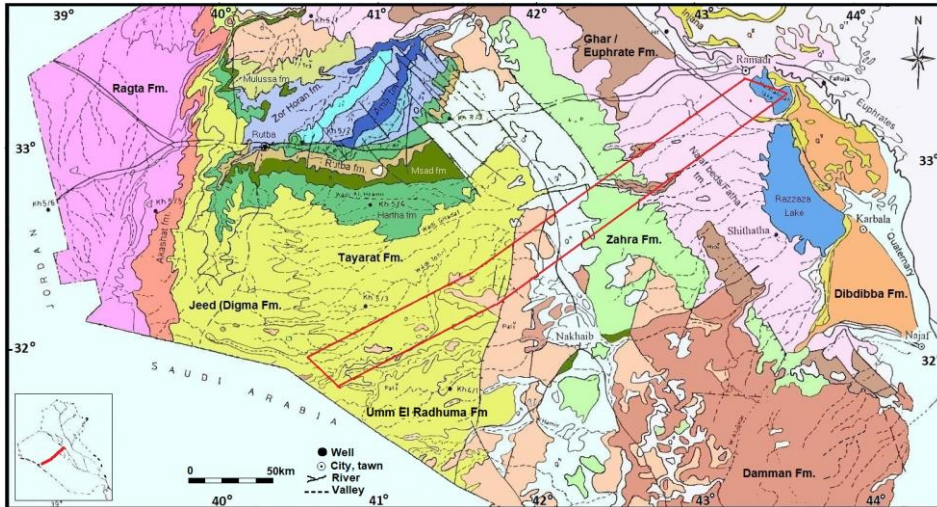


Figure 9.2. Surface geological map of the studied area (GEOSURV, 1996).

Tectonically, most of Iraq, lies in the Arabian Shelf. The Iraqi part of the Arabian Shelf is divided into Stable Shelf and Unstable Shelf. The study area is located in the Stable Shelf. It is bordered to the north and northeast by three geological zones (South Sinjar, east of Hatra, and Hit). It extends uniformly south-southeast toward Saudi Arabia.

Although the Iraqi Western Desert belongs, tectonically to the Stable Shelf, but the tectonic and structural effects have controlled the type of the exposed rocks, thickness and the extension of the formations. The Rutbah Uplift and Ga`ara Depression, located to the north of the study area, have exposed Permian rocks followed by Triassic and Jurassic rocks, which are absent in other parts of the Iraqi Western Desert and the surrounding areas, even in the nearby areas of the neighboring countries. In General, the structural axes are NE-SE, NW-SW, N-S, and E-W trends. These represent faults and the related folds.

### 9.1.3 Constructing of the regional line

Numerous localized seismic reflection surveys have been carried out in the study area by, Iraqi Oil Exploration Company (OEC) and others, using different types of spread (e.g. 24, 48, 60, 96, 120 channel spreads), both explosive and vibroseis energy sources and processing parameters. Using local seismic data, combined with knowledge obtained from surface outcropping is among the most powerful and cost-effective tools for revealing regional geological features and trends. For constructing our regional seismic line (profile), we selected proximate local seismic lines

(Az\_122A, Tm\_26C, Tm\_26, Tm\_26E, WRH\_30 and Rh\_17) that form a coherent transect roughly bisecting the area of interest (Reg124 line) as shown in Figure 9.3.

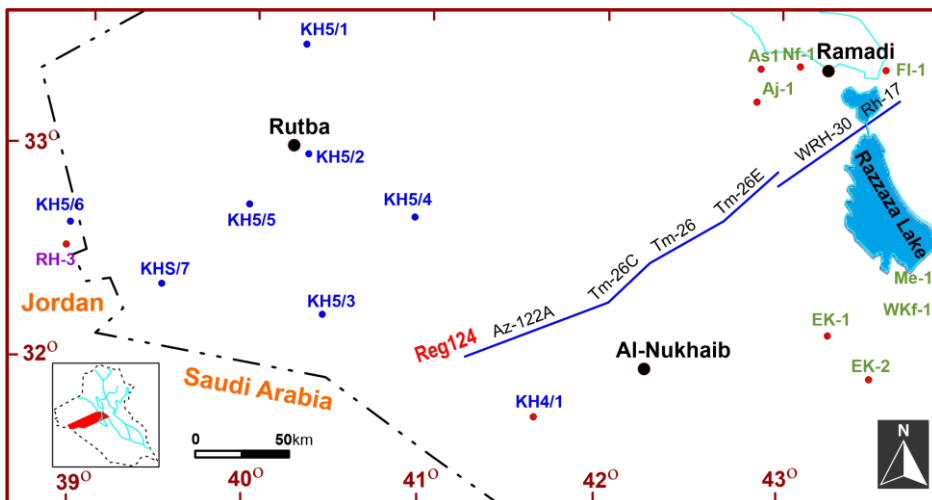


Figure 9.3 Show the local seismic sections used for construct the Regional line (Reg124).

In some cases, there are no local seismic lines intersecting the selected regional line path or the quality of the local lines is very poor. To address these data gaps, we have in some cases interpolated the nearest parallel line to the regional line path, while in others we have put a gap of blank traces. Considerable effort was made to choose the best intersection points when re-sorting the traces and to select, an optimal datum plane for the seismic regional line. Based on our review of available data, a datum plane, of 400m a.s.l. was used to prepare the seismic regional line. After unifying the datum plane, the regional line traces were re-sorted according to the CDP points using the Disco processing system. Under this system, each shot point is equivalent to two CDP points. After merging the selected local lines at intersecting adjacent points, at a unified datum plane, the regional seismic line data was reprocessed. The final stacked section was stored on disk or magnetic tapes in "SEGY" format for additional processing. The constructed regional seismic line here is called Reg124, (Figure 9.4). The Reg124 line trends southwest-northeast and is approximately 275km long.

The seismic data processing (design of sequence and parameters determinations) involved in producing regional lines was conducted by Dr. Hamid Alsadi, in the Iraqi Processing Centre of the Iraqi Oil Exploration Company using the mainframe computer (VAX11780) and (Disco-7.3) processing software.



Table (9-1) shows horizons code, name, age and composition of the formation.

Horizon	Age	Formation lithology
H1	Jurassic	<u>Najmah fm.:</u> Conglomerate, marl, sandstone, limestone, marly limestone. At east of Rutbah white quartzite sandstone, clayey siltstone and claystone, pink and violet dolomitic limestone, very rarely secondary gypsum occurs in fractures. <u>Gotnia Fm.:</u> anhydrite, shale and limestone.
H2	Triassic	<u>Kurra China;</u> carbonate-anhydrite with shaly-sandy carbonate & black shale. <u>Mallusa fm;</u> Limestone, silty and marly sandstone and sandy siltstone, dolomites and dolomitic limestones. <u>Zor Houran fm.:</u> Yellow gypsiferous clay, marl and siltstone, limestone, calcareous mudstone, marlstone, & yellowish green dolomitized limestone.
H3	Permian	Ga'ara Fm. (in the west part); Red and varicolored sandstones, shales and claystone, with plant remains (565-780m thick)
H4	Carbo/Devonian	Ora shale, Kaista; sandstone, limestone, dolomitic limestone and shale, and Harur; detrital limestone and calcareous shale
H5	Silurian	Akkas Thick Sandstone (source R.)
H6	Ordovician	Khabour quartzite (/hard sandstone & silty micaceous shales); strong reflector, sometime composed of 3 succession cycles, (thick reservoir R.)
H7	B. Ordovician / T Cambrian	Bottom of Khabour quartzite / top of the Cambrian” rocks; Thick reservoir R., See Figure (9-6)
H8	M. Cambrian	Represent the top of Burj limestone formation of Middle Cambrian age, which is identified in the Jordanian territory (west of the studied area) are identified using information obtained from the Jordanian Safra-1 well which lies at 42km southeast of Amman City, penetrated the Cambrian and Basement rocks. Burj limestone (Figure 9-6).
H9	Basement surface	Identified depending on the aeromagnetic basement structural map of the C.G.G, 1974-1975? (Figure 9-6).

Identifying the “top of basement” is still subject to question. To do this we considered the presence of numerous diffraction patterns over the irregular basement surface. Below the presumptive basement, no reflectors could be detected due to the complex structure of these rocks.

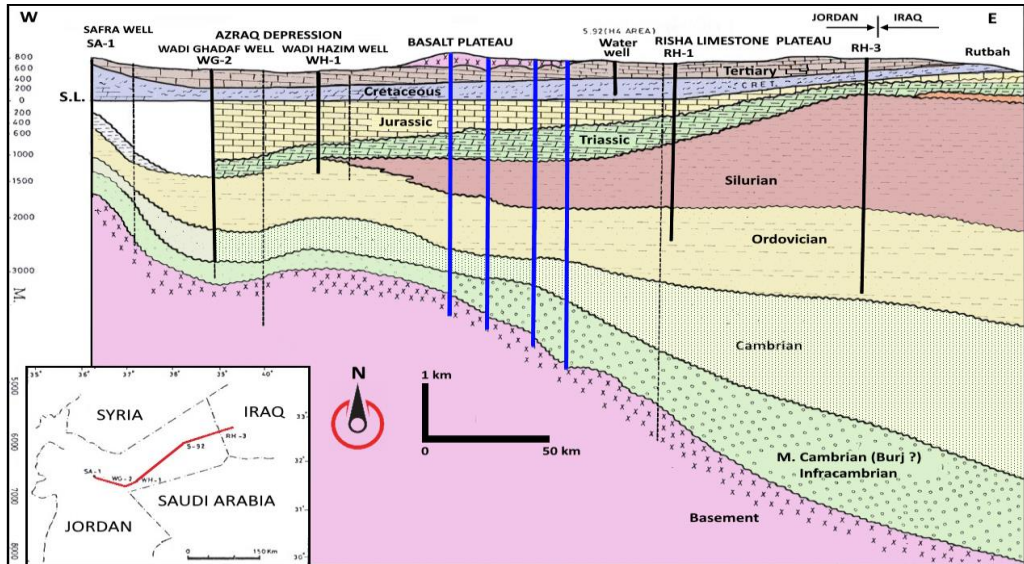


Fig.9.6 Generalized west to east geological profile across the Jordan territory.

Overall data, the quality of the selected reflectors along the regional line ranges from good to fair. Along the central part, data quality is relatively poor (at Umm Anz, and Thumaily areas), while data quality is much improved toward the east, especially for Cenozoic and Mesozoic reflectors. However, the quality of each reflector changes along the Reg124 line. These differences in reflectors quality may be due to:

1. The geological and surface conditions such as the presence of highly consolidated layers near the surface (such as limestone and dolomite or evaporate rocks) that hinder the penetration of energy and do not transmit the seismic signal effectively;
2. Static correction problem and geometry of the field layout;
3. Poor coupling caused by stony desert area where perfect contact of vibrator plate and the surface is not reached; and
4. Interference from boundaries of thin layers, lithology changes, presence of the fault and folds forming due to the uplifting of the basement rocks.

#### a. Regional Time section (line)

Generally, in the upper part of the line, the quality of the reflectors ranges from fair to good (Figure 9.7), while at the lower part (between H5 and H9), toward the northeastern part of the line approximately after the shot point 1275, the quality ranged from poor to fair.

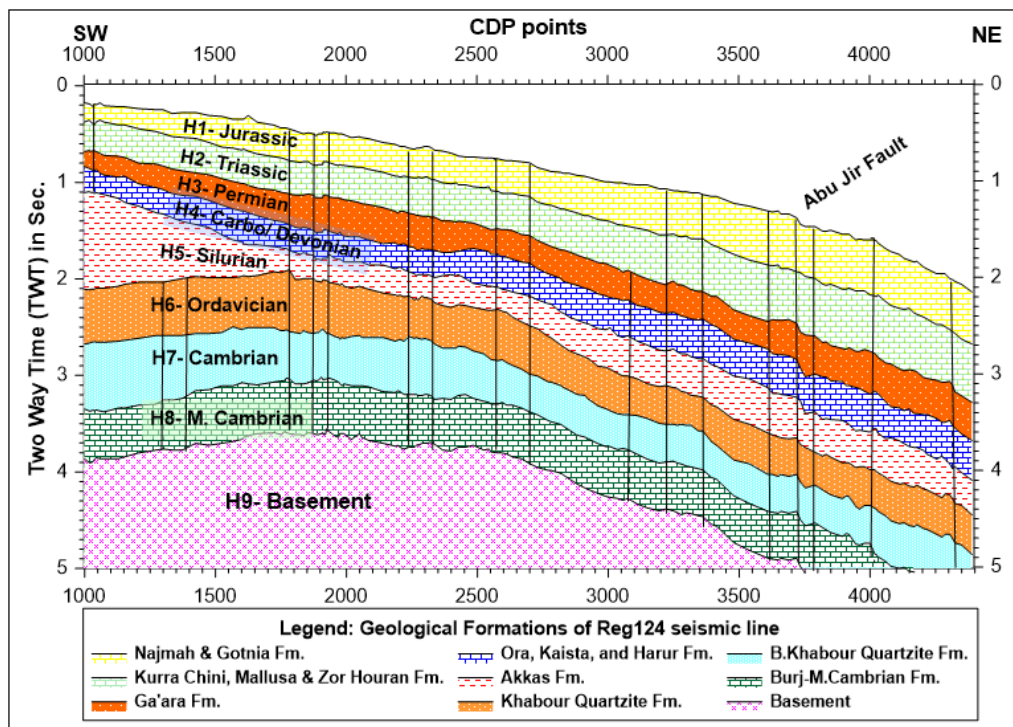


Figure 9.7 Show the picking of the reflectors (H1-H9) and distinguished faults on TWT Reg124 line.

**Structurally**, a Paleotime high (called *Anbar paleotime*) appears at the southwestern part of the line. The top of this paleotime lies between shotpoints 1600-1900. The amplitude of the Paleotime high decreases toward the south. The top and the northeastern part of the line is highly deformed, fractured, and more faulted. The two vertical faults at the western flank of the Anbar uplift at shot points 1275 and 1430 forming a time depression or a graben, affecting the lower part reflectors (H6-H9). Another two vertical faults lies at the shot points, 3680-3725. These two faults may be representing the Abu Jir fault zone. Some of these faults cross all the reflectors suggesting they occurred recently while others penetrate only the oldest rocks and represent among the oldest orogeny affecting regional geology. There were no indications or any trace of a broad high or low within the eastern part of the line.

From shot points 1275-1990, fractured and split reflectors can be observed particularly along the lower part of the line and toward the northeast. Propagation phenomena further suggest changing depositional conditions between reflectors H5 and H6. Moreover, from shot points 2720 to 3275 the character of all reflectors changes, with the appearance of some of strong reflectors and disappearance of others.

**Stratigraphically**, the upper reflectors, H1-H5, dip regionally toward the northeastern side. The reflectors on western side of the Paleotime high (*Anbar paleotime*), H6-H9, are dip toward the southwest at shot points 1700-1875. In general,

all the reflectors dip steeply toward northeast, from approximately shot point 1875 to the end of the line, forming an onlap feature on both side of the this paleotime. It appears that the Mesozoic reflectors thicken whereas the Paleozoic reflectors are thinner toward the northeast or east.

**b. Depth section of the regional line:**

Due to relatively smooth distribution velocity in the studied area, there is more similarity between time and depth regional lines. The depth regional line (Figure. 9.8) show regional dipping trends toward the east, and all the formations deepen more steeply toward the east (the southeastern part is steeper than the northeastern) of the regional line, the Mesozoic and upper Paleozoic formations thicken while the lower Paleozoic formations are thinning.

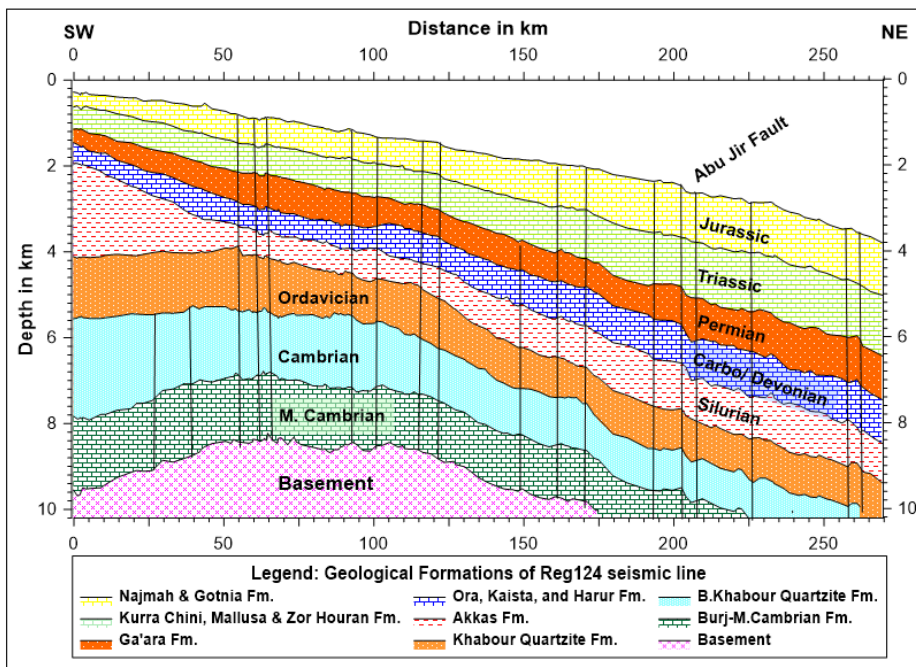


Fig.9.8 Depth cross section of Reg124 line showing more conspicuous faults and deformations.

Structurally; the eastern flank of the Anbar uplift appears on the southwestern part of the line (Fig. 9.8) sloping toward the northeast gently. The maximum amplitude of the uplift at this line is less than one kilometer, and may be formed through the Caledonian and Hercynian orogenies. The formations from the Jurassic down to the Basement, on the southwestern part of the line, appear at depths of about 261, 565, 1000, 1130, 1652, 3609, 4870, 6870, and 8261 meters successively. At the top of the

uplift (about 60km east of the western end of the line), the same formations appear at greater depths; 783, 1304, 1913, 2565, 3043, 3565, 4696, 6087 and 7391m respectively.

Al-Bassam *et al.*, (1997) believed that this uplift is a part of the Hail - Rutba arch in Iraq. Most workers that are studying the Saudi Arabian part of the Hail - Rutba arch believe that, this arch (uplift) occurred during the Hercynian orogeny (Late Devonian-Early Carboniferous).

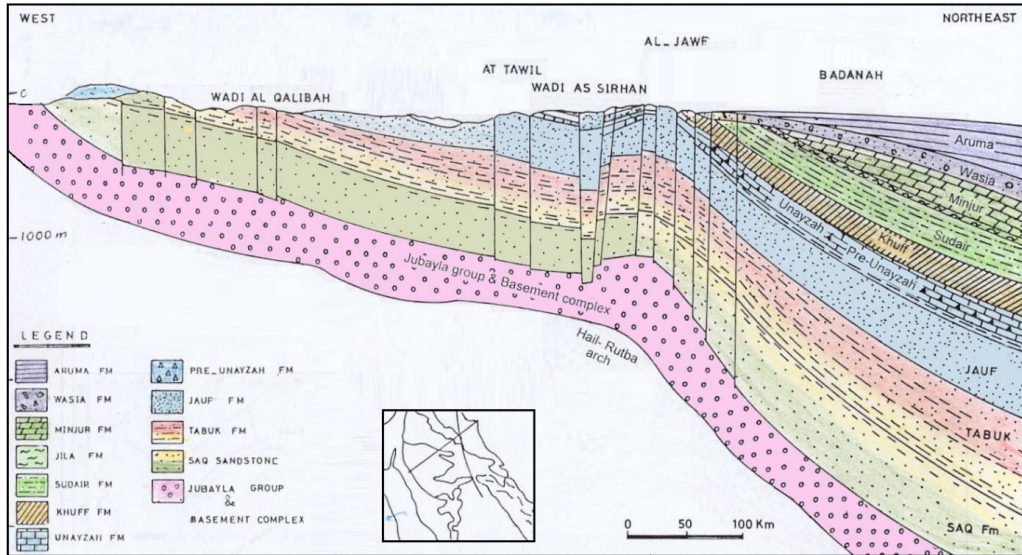


Figure 9.9 Structural cross section of Paleozoic relationship in the Tabuk-Widyan basin in part schematic (After Al-Laboun, 1986).

The formations from Cambrian to Lower Devonian (Jauf formation in Saudi Arabia) ages can be noticeable on this arch, while the formations of post-Devonian till Cenozoic are missing, as shown in Figure (9.9), and according to studies undertaken by Saudi Arabia workers, all the formations from the Paleozoic to Mesozoic (from Cambrian to Cretaceous) are penetrated by deep wells in Saudi Arabia near the southwestern part of the studied area. These two observations indicate that there was no uplifting in that area after Caledonian and Hercynian orogenies. In addition, the Silurian formation is very thin on the top of the Anbar uplift, therefore, we believed that creation of the Hail - Rutba arch occurred during the Caledonian orogeny and that the region was uplifted and subject to erosion for a relatively short time. At the end of this short time (period) the subsidence may have occurred again and then stabilized and/ or the transgression of the sea continued in the area.

However, to the east of Anbar uplift, there is no indication of any significant or large structural traps. Only a gentle northeastward monoclinial dip with several small anticline and synclines of small amplitudes (between 100-200m) are well-expressed on

the Reg124 time line. These small anticlines and synclines are of limited size, amplitude, and situated at different depths and probably related to the faults (Figure 9.9).

Several local low and high features are also observed on top of the Silurian and Basement rock formations. These features impose themselves on the main structural time features of the line.

A series of vertical or sub-vertical faults, most of them of small displacements, are also well-expressed on the regional line (Figure 9-8). The origin of most of these faults lies within the basement or deeper. Most of these faults penetrate the Paleozoic and Mesozoic rocks, with some reaching the surface, such as in the Abu Jir faults zone. These faults also often separate the blocks or sub-blocks forming horst and graben features. These up and down blocks indicate that the vertical forces acting on the area was quite variable during different time intervals.

Tamar-Agha (1993). believed that the vertical movements are a translation of the lateral movements, which are induced as a sequence of the interaction and differential movements of the adjacent basement blocks, however, our view is that the source of the movements are mostly isostatic vertical movements.

Stratigraphically, the formations are divided into two separate sequences (Figure 9.8). The basement to Ordovician rocks represents the lower sequence, are parallel to sub-parallel, and become progressively thin as you move from west to east (convergence). In the second sequence, Silurian to Jurassic aged rocks appear as the upper sequence, and show a reverse pattern, being progressively thicker from west to east (divergence). Each sequence may represent one cycle of depositions. The dipping, thickness, and deepening of the beds of the lower group are significantly different from those of the upper sequence. Stratigraphic traps can be expected in the eastern part of the line due to the transition stage from Arabian platform to the Mesopotamian basin. All the formations dip and deepen toward the northeast. The first sequence thickens as you move northeast, while the second sequence becomes thinner in that direction.

The angular unconformity surface (Top Khabour Quartzite of Ordovician time, thick reservoir rock for accumulation the hydrocarbon) which separates the two main sequences come in sight on this line. The thickness of the Silurian formation at the western side of the section is greater than that at the eastern side. It reaches 2250m (thick source rock for production of hydrocarbon) at the southwest, and at the highest point of the Anbar uplift flank, it becomes 600m, while at the northeastern side it reaches 900m. The onlap feature between Silurian and Ordovician rocks can be seen also in the western part of the line. The Silurian is thin on the top of the Anbar uplift as compared with other sides.

---

**c. Flattening of the regional line reflectors:**

During the Precambrian period most basins were formed due to the combination of wrenching faults acting and thermal sagging. These early basins filled with clastic sediments during the Lower Cambrian period, with carbonate sediments (such as Burj formation) in the Middle Cambrian and with clastic and marine deposits (such as Khabour Quartzite formation) through the upper Cambrian and Ordovician times. During the Silurian time shale, claystone, and sandstone rocks was deposited to form the Akkas formation. No evidence of large tectonic activity was observed in the data. However, during the post Silurian Caledonian orogeny, deposits beneath the Late Silurian time were subject to volcanic activity, deformation and uplifting.

To study the shape and situation of the sedimentary basin of the area during different period, the flattening method selected to return the shape of the reflectors to original shape at their time deposition. Depending on the fact that sedimentary rocks are always deposited on a horizontal surface in the sedimentary basin of the deep cliff or within a continental slope and deep open basins. Therefore, we try to return the original forms of reflectors to the initial state in which sediments began to settle.

Flattening method is a technique used to flatten seismic line reflectors by removing the effect of any orogenies or movements that happened in the area after or during the deposition of formations that have been deposited after depositing assigned reflector (surface/ formation) to be flatten from the basin gradually. This is done by reset (zeroing) the time values of the specified reflector (flatten reflector) and placing the resetting (zeroing) time values on the horizontal plane. Therefore, the shape of the reflectors lies under the assigned (flatten) reflector represents the shape of these reflectors and the basin during the deposition of the flatten reflector (Abdul Jalil, 1998). The flatten technique was applied to three reflectors: Jurassic capitals, Carbo / Devonian, Silurian, and highest Ordovician reflectors of Reg124 line.

Below are the descriptions of these flattening reflectors:

**1. Flattening of the Ordovician reflector:**

The Ordovician reflector represents the last reflector of the lower sequence. Figure (9.10) shows that the presence of parallel and near-horizontal reflectors indicate an extended period of geological stability, with negligible tectonic activity during Cambrian and Ordovician times (Figure 9-10). Sediments deposited under shallow marine conditions during this interval are now represented by near-horizontal clastic, carbonate, sandstone, Quartzite, and shale deposits. No trace of the main Paleohigh (Anbar uplift) is apparent within the Basement, Cambrian, and Ordovician seismic profiles.

---

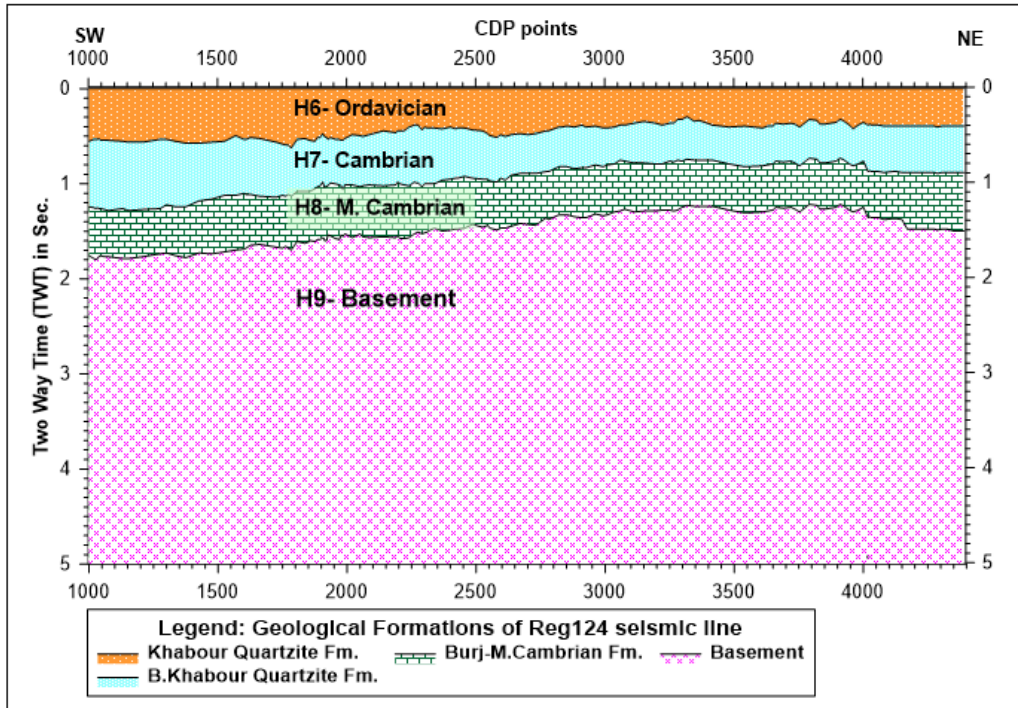


Figure 9.10 Flattening of Ordovician reflector of the regional line Reg124.

## 2. Flattening of the Silurian reflector:

The *Anbar uplift* which occurred as part of the Caledonian orogeny at the end of the Late Silurian-Early Devonian period is well expressed in the regional seismic profile (Figure 9.11). The effect of erosion on the Anbar Uplift is clearly evident in the center of this feature where the Silurian deposit is very thin yet thickens on both sides of the uplift, especially on the western side. It is apparent the Silurian transgression was interrupted by the Caledonian orogeny but had resumed before the Middle-Upper Devonian period and continued through the Carboniferous until Permian times. Furthermore, the onlap phenomena clearly appear on both sides of the uplift. This means the transgression of the sea occurred on both sides of this uplift after the Silurian time. The other reflectors (beneath the Silurian) are more parallel and arranged in semi-horizontal form, again suggesting this deposition occurred in a tectonically quiet environment that included the creation of the Akkas formation with its marine derived shales and sandstones.

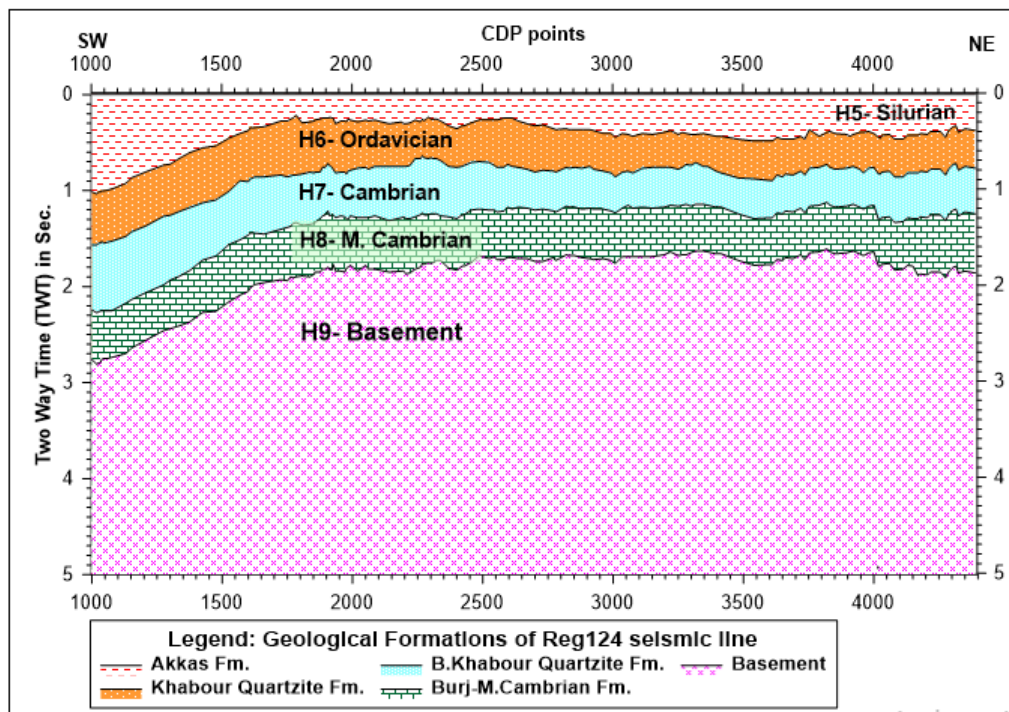


Figure 9.11 Flattening of Silurian reflector of the regional line Reg124.

### 3. Flattening of the Jurassic reflector:

During the Early Permian time, clastic sediments associated with the Ga'ara Formation were deposited in the western part of the study area while, in the eastern part, materials later forming the carbonate rocks of the Chia Ziri formation were deposited. From the Early Triassic period through to the Jurassic, transgression and regression of the sea resulted in the deposition of carbonate and evaporate sediments particularly in the eastern part of the study area.

However, the Jurassic reflector is the first picked reflector on the regional line (Figure 9.12). The observation of flattening line representing the Jurassic period suggests that the Paleohigh Anbar Uplift and the Silurian-Ordovician onlap uplifting occurred before this time. The surface of the reflector is more undulate and is more faulted. The onlap phenomena between the Silurian and Ordovician reflectors are clear too. At any rate, the transgression of the sea covered all the central and eastern parts of the study area while the western and southwestern parts exhibit positive areas (regression). On the eastern flank of the Anbar uplift, the deposition of the intertidal foreshore and subtidal shore face is also apparent.

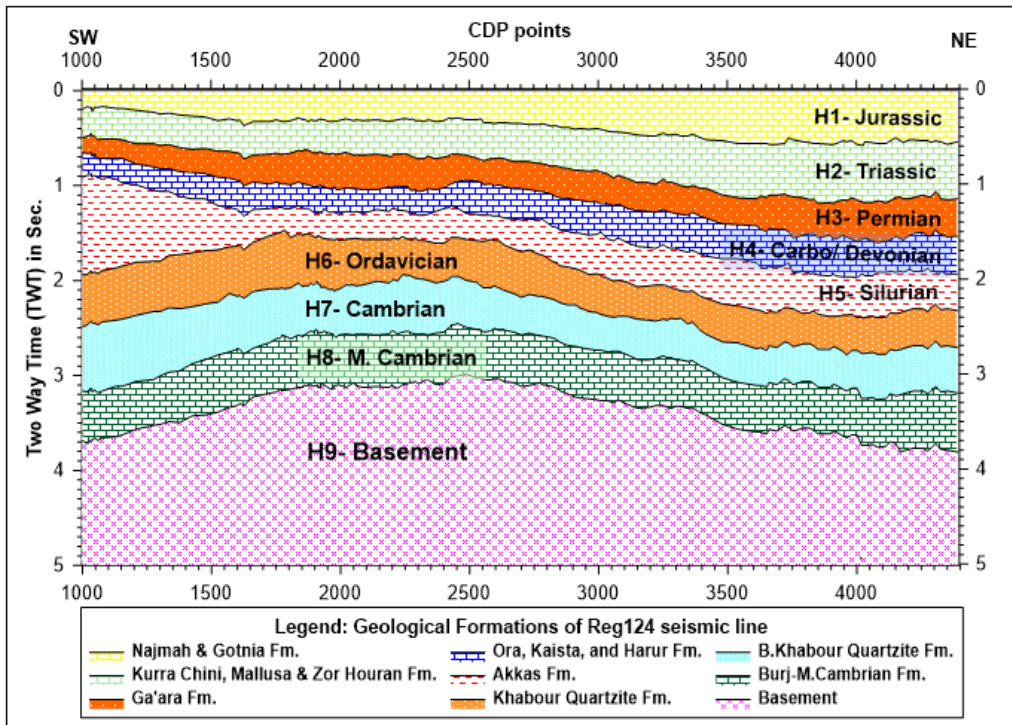


Figure 9.12 Flattening of Jurassic reflector of the regional line Reg124.

The important factor affecting the depositional condition during the Jurassic and Triassic times is the restricted faulting that resulted in the creation of Graben and Horst features comprised of Evaporate or Carbonate rocks. The Anbar uplift was the source of clastic facies that feeding the basins lies at the west and east of it such as South Rutbah Depression and the eastern part of the studied area toward the Mesopotamian basin.

### 9.1.5 Conclusions

- Nine Horizons (H1-H9) are evident on the seismic regional line sections analyzed. Those horizons delineate the presence of Jurassic Triassic, Permian, Carbo/Devonian, Silurian, Ordovician, “Bottom of Ordovician” or “top of Cambrian”, Middle Cambrian and “Basement” and rocks respectively. All these reflectors show a dipping configuration that deepens toward the East.
- Two groups of reflectors can be recognized on the regional line sections formed as two sequences or cycles, particularly on the western part of the Anbar uplift. The first group consists of Jurassic, Triassic, Permian, Carbo/Devonian, and Silurian reflectors. All these reflectors are sub-parallel, and diverge or prograde in a

parallel oblique configuration that dips towards the east, and progressively thins toward the West. The second group consists of Ordovician, “Bottom of Ordovician or top of Cambrian”, Middle Cambrian and “basement” reflectors. The reflectors characterize by parallel and thick sediment of clastic and carbonate rocks which are important as a reservoir rocks of hydrocarbon.

- c. The data reviewed suggests the Silurian formation decreases in thickness towards the east, and that some reflectors within it are missing, are mixed with others, or are terminated at another reflector surface, particularly near the top of Anbar uplift forming onlap with the Ordovician reflector. To the east of this uplift the thickness of the Silurian increases again.
  - d. On the eastern part of the studied area, the presence of stratigraphic features such as clinoform, delta, divergence? and reef structures characterize the transition from Platform geology? to sedimentary basin (Mesopotamian basin).
  - e. The most important result of the study was the detection of the Paleohigh (*Anbar uplift*) in the western and central parts of the study area. Analysis of reflector geometry suggests this uplift most likely occurred during the Caledonian orogeny in the Late Silurian-Early Devonian.
  - f. The most observed faults are vertical or sub-vertical, generated from the basement and cutting most of the Paleozoic and Mesozoic rocks. This means that the area was affected by another uplift movement probably at the Cretaceous time due to the effect of upwelling hot material coming up from deep sources within the mantle. The vertical faults indicate that the area was affected by vertical movements forming upwelling and subsidence blocks that have created horst and graben systems in the basement.
  - g. Changes during the Jurassic period have resulted in formations dipping and deepening toward the east (toward the Mesopotamian basin). At the same time, the lower Paleozoic rocks became thinner while the Mesozoic and Cenozoic rocks thicker.
-

## **9.2 Study of subsurface structures using seismic reflection data for Kalar–Khanaqin area / Kurdistan region, Iraq**

Ezzadin N. Baban & Bakhtiar Q. Aziz & Nawzad H. Aziz

### **9.2.1 Introduction**

The studied area is located in Iraqi Kurdistan Region, north-eastern part of Iraq, about 97.0 km south of Sulaimani city. It is bounded by coordinates easting points (500000– 541134) and northing points (3800768–3857412). It covers an area of 1,752.0 km<sup>2</sup> (Figure 1).

The first seismic exploration was started in the northeastern part of Iraq in 1928 by the Turkish oil company in the Pulkhana area. During 1951–1952, the USSR Technoexport company carried out the seismic reflection survey in the Jaria Pika area near the studied area. The studied area surveyed by seismic exploring companies USSR, Hungarian and Iraqi National Oil Company (INOC) during 1975 to 1976.

### **9.2.2 Geology and tectonic setting**

The surface and subsurface geological formations in the studied area deduced from exposed rocks and stratigraphic sections of the Chia Surkh-9 and Qumer (Qr-1) deep wells

(Figures. 9.11 and 9.12) which were drilled at the surrounding area. These formations as described by Jassim and Goff (2006) are: Jeribe formation (lower Miocene) which is composed of limestone and dolomite; lower Fars (Fatha) formation (middle Miocene), composed of alternations of thick gypsum beds and limestone, with few thin beds of green marl and red clay stone; upper Fars (Injana) formation (upper Miocene), which is characterized by alternations of sandstones and clay stone with siltstones, lower Bakhtiari (Mukdadiya) formation; (uppermost Miocene–Pliocene), which is composed of alternation of pebbly sandstones and light brown clay stone in fining upward cycles; and upper Bakhtiari (Bai Hassan) formation (Pliocene) is largely composed of coarse and thick fluvial and estuarine conglomerate. The formation is usually unconformably covered by recent deposits.

Tectonically, the studied area is situated on the northeastern part of the Arabian plate. It is considered as a part of the Zagros fold-belt, which is the result of the collision between the Arabian plate and Iranian plate (Ameen 1992). Depending on (Ditmar and Iraqi–Soviet team 1979) tectonic subdivision, the study area belongs to the central faulting zone. It is characterized by the fact that this zone is complicated by the system

---

of faults of northwest to southeast trend during lower Miocene and by overthrust of NW-SE (Zagros) trending in the middle Miocene sediments.

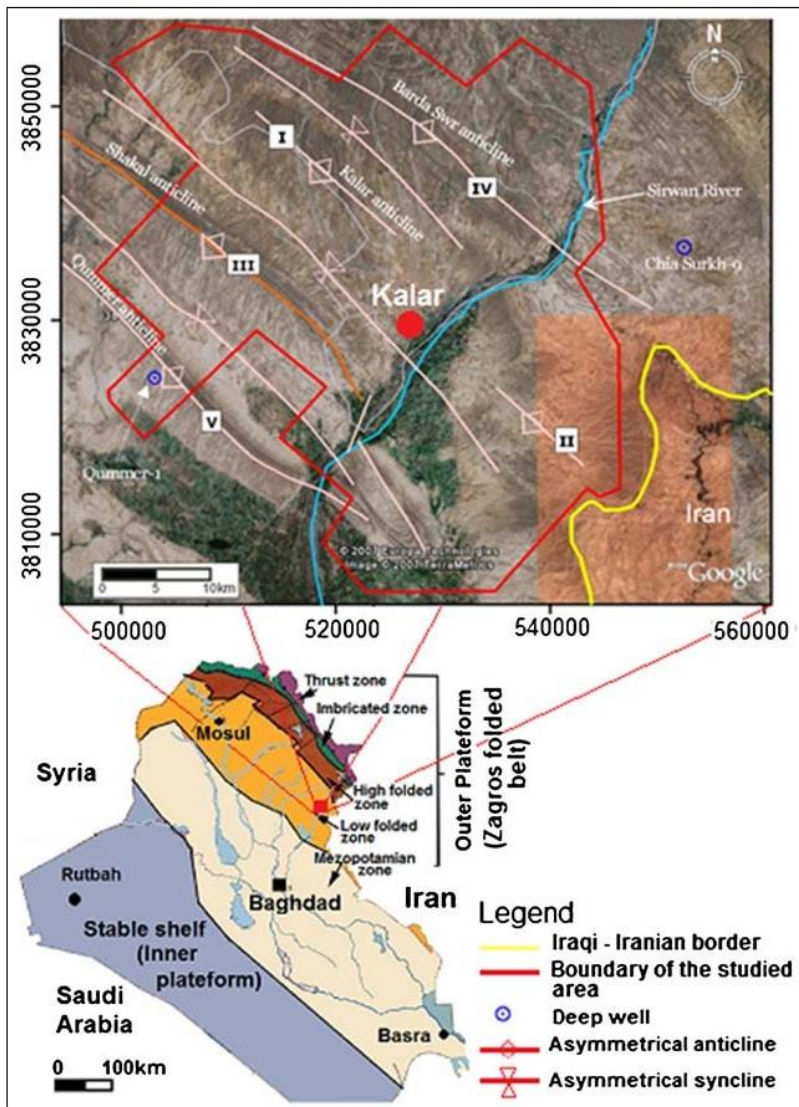


Figure 9.11 Satellite image (Google earth) of the studied area shows location and the major geological structures.

### 9.2.3 Seismic data and methodology

Twenty-five seismic lines parallel and perpendicular to the axis of the major structures were used in this study (Figure 9.13). The seismic lines named, Qasri Shirin (QS), Khanaqin (X), and Qumer (QR). They were surveyed by seismic exploring

companies (USSR, Hungarian, and INOC). The total lengths of the surveyed seismic lines are about 650.4 km.

Depending on the geological column and synthetic seismogram of the Qr-1 well, the reflectors are identified (Figure 9.13). The geological data of the deep well were correlated with the seismic line QR-5 at the intersection point.

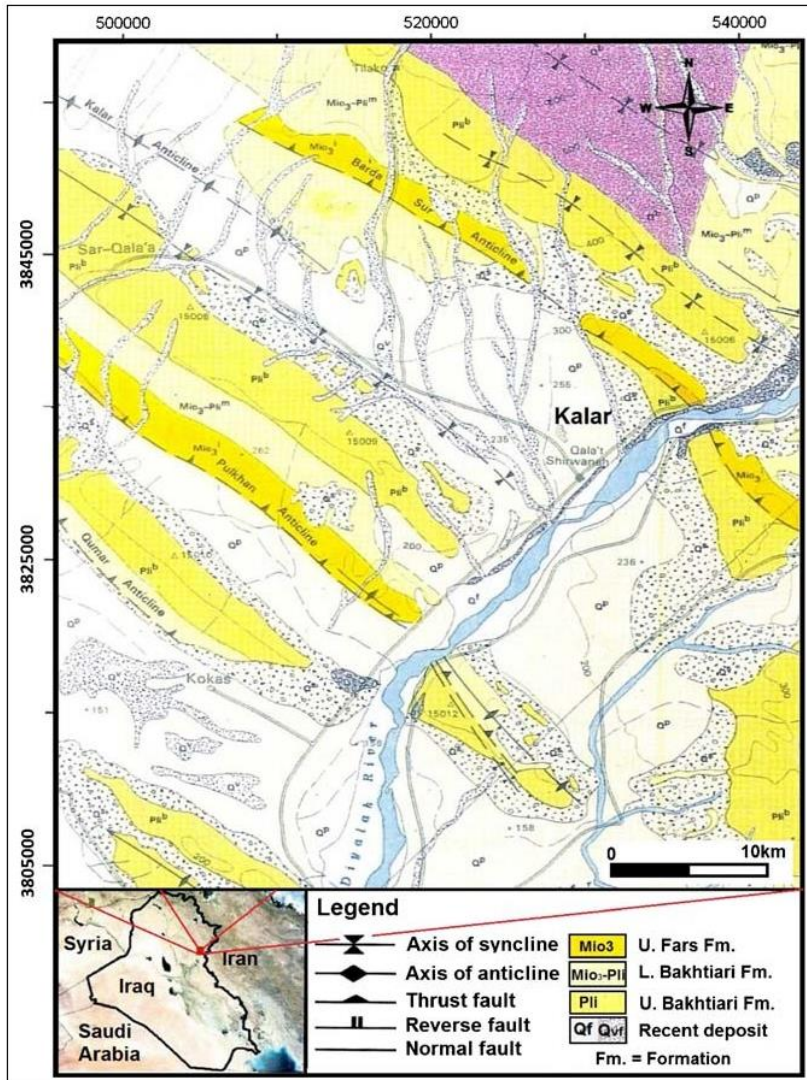


Figure 9.12 Geological and structural map of the area (Sissakian, 2000).

At the intersection point between Qr-1 well and seismic line QR-5, directly from the synthetic seismogram of the well, the geological column at the time domain translate to the seismic line. The top of both interested reflectors of lower Fars and Jeribe

formations were identified. Then, the seismic line QR-5 correlated with the seismic line QS-9 and so on.

The picking has focused on both the lower Fars and Jeribe formations because the deeper formations have very bad qualities and over most parts of the seismic sections are invisible, so picking them were impossible. The bad reflection qualities of the deeper formations may be due to the existence of evaporate beds within the lower Fars formation, which is a good reflector and absorbed large amount of the seismic waves (Figure 9.14).

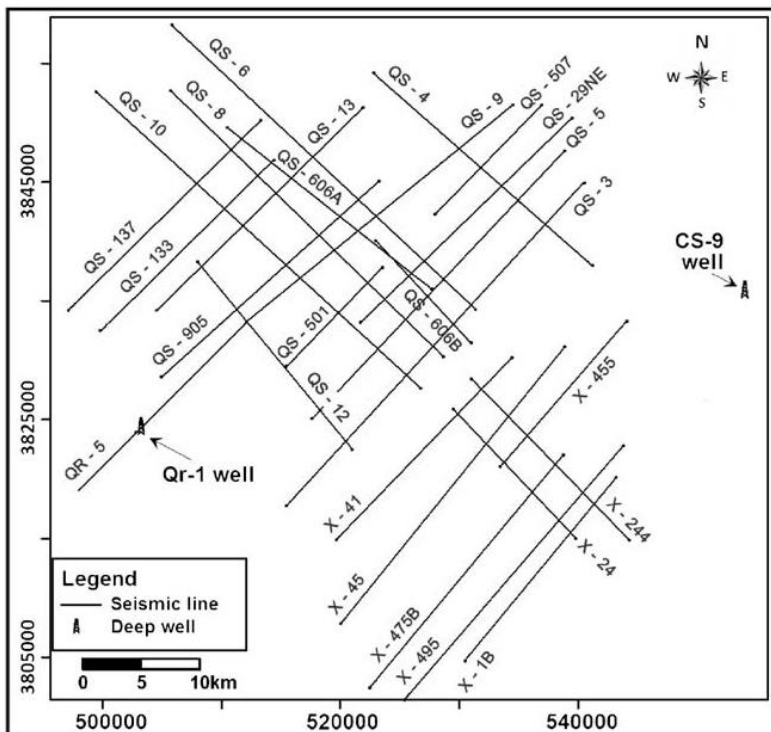


Figure 9.13 A distribution map of the seismic lines in the studied area

### 9.2.4 Interpretation and discussion

Several structural phenomena were detected during the study of these seismic sections, such as faults and folds, as shown in Figure 4. Most of the detected faults are associated with the folds simultaneously, which generally intersect the SW limb of the anticlines. The definition of shapes, types, and geographical distributions of these structures is of great importance because they have a great role on accumulation of the oil and gas. The good quality of the seismic sections is facilitated by the description of some of the structural properties on the seismic sections, such as fault types with the vertical displacements and the fold types.

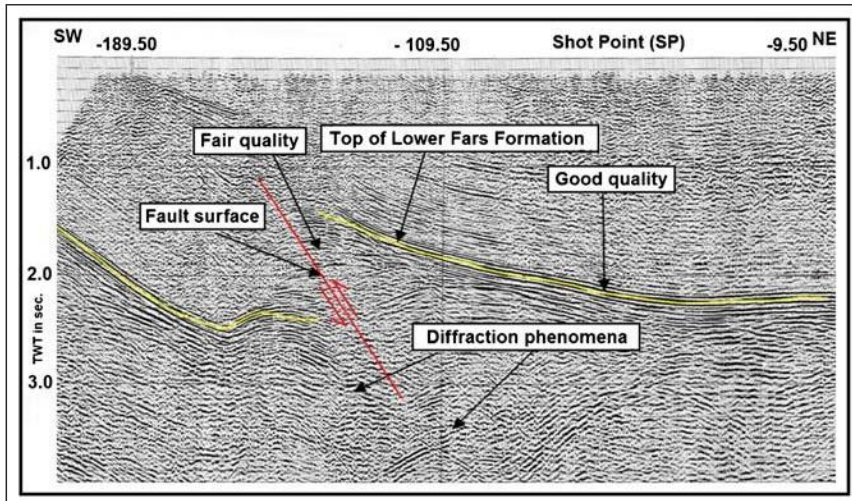


Figure 9.14 The different qualities of seismic data through line QS-3

### **Isochrone maps**

The isochrone maps of both lower Fars and Jeribe formation reflectors (Figures 9.15 and 9.16) show the existence of many structural features of time domain such as closure contours of high and low values and faults.

The isochrone map for the near to top of Lower Fars (Figure 9.15) shows two-way time (TWT), ranging between 0.1 to 2.6 s. The map also shows the existence of several structures at time domain such as:

The closure no. (1): It is an elongated structure located at NE of Kalar district and extended from the shot point (SP) (230) on the line QS-13 to SP (75) on the line QS-3. There are three small closures near the crest of this structure of different dimensions. The highest point locates around SP (1048) on line QS-507.

The closure no. (2): It is an elongated structure located at west of the Kalar district and extended from the SP (1130) on the line QS-137 to SP (82) on the line X-45. This structure consists of four small closures, its TWT increases toward the SE. The minimum amount of the TWT occurs around SP (1130) on the line QS-137.

The closure no. (3): It is located at NW of the Kalar district around the SP (150) on the line QS-13 and around SP (1130) on the line QS-137.

The closure no. (4): It is located at SE of the Kalar district around the SP (1559) on the line 475-B with the closure amount of 0.1 s and dimensions of 1.66×5.3 km.

The closure no. (5): It is an open structure located at the west of the studied area around the deep Qr-1 well.

The isochrone map for the top of Jeribe formation shows that the TWT is ranging between 1.0 to 2.7 s (Figure 9.16). More or less, it is similar to the isochrone map of lower Fars formation except the closure no. (3), which is at the NW part of the Kalar district, has larger closure amount equal to 0.2 s, and its dimensions are equal to 4.4×9.7 km. Also, the closure no. (4), is detected in the south of Kalar district and within lower Fars reflector.

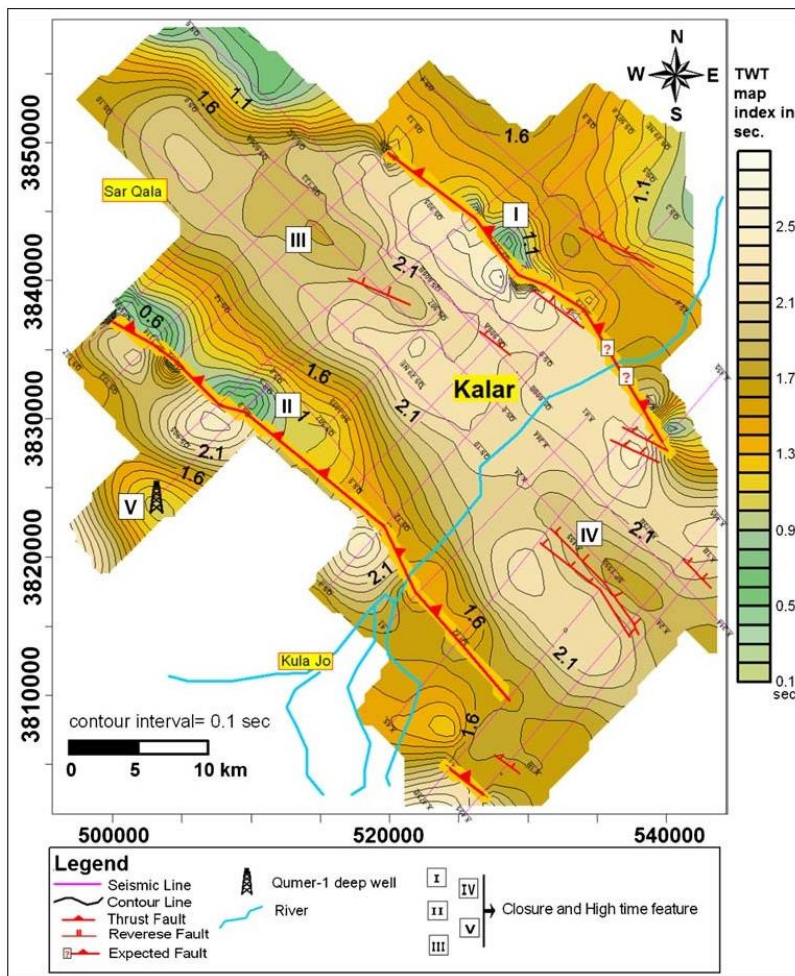


Figure 9.15 The isochrone map of the near top of lower Fars formation shows the major closures and faults detected in the area.

### Velocity maps

In the present study, absence of the deep wells with the velocity survey over the studied area compels to be dependent on the RMS velocities. There are about (149) stacking velocity boxes which are distributed on the seismic lines and also depend on

sonic log of Qr-1 deep well at the west of the studied area for calculating the average velocity and its distribution over the studied area.

The isochrone map for the top of Jeribe formation shows that the TWT is ranging between 1.0 to 2.7 s (Figure 9.16). More or less, it is similar to the isochrone map of lower Fars formation except the closure no. (3), which is at the NW part of the Kalar district, has larger closure amount equal to 0.2 s, and its dimensions equal to 4.4×9.7 km. Also, the closure no. (4), which is detected in the south of Kalar district and within lower Fars reflector.

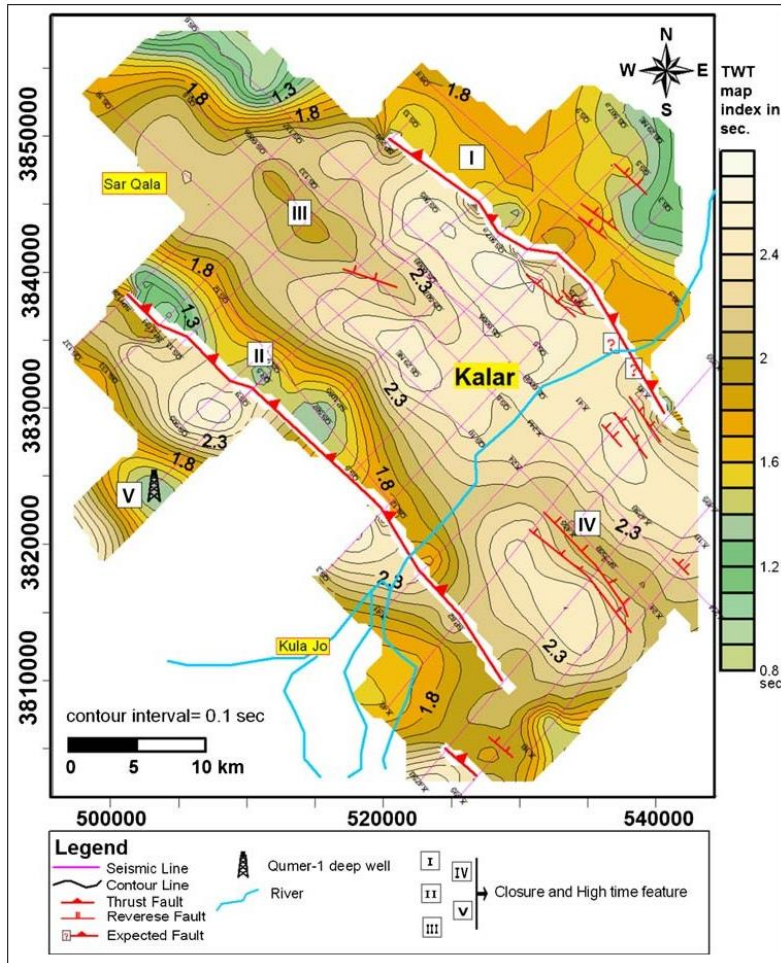


Figure 9.16 The isochrone map of the top of Jeribe formation shows the major closures and faults detected in the area.

### **Depth maps**

The depth map to the top of both lower Fars and Jeribe formations are shown in Figures. 9.17 and 9.18. There is no significant difference in all major geological structures that appear in the depth maps for lower Fars and Jeribe formations.

The depth of the lower Fars formation in the studied area ranges between 100.0 to 4,800.0 m. The description of the lower Fars depth map (Figure 9.17) is briefly given in the following points:

The Barda Sur anticline (no. 1) exist at the east of the Kalar district and extends from the NW of the area [at SP (230) on the line QS-13] toward the SE [to SP (75) on the line QS-3] and extends outside the area toward the NW direction. The length of this structure within the area is about 20.0 km. It has variable width reduction toward the SE. The maximum width at the NW is about 1.15 km around the SP (230) on line QS-13 and becomes 2.0 km approximately at the SE of the area and exactly around the SP (75) on line QS-3. There are sequences of crests along the top of this structure. They appear as the elongated domes shape of different heights, which decreases toward the SE of the area. This structure is completely similar to the structure that exists at the western part of the area. Also, longitudinal thrust fault extends beside this structure and intersects its SW limb, as the result of this, the anticline appears as monocline structure. The throw of this thrust fault is variable and generally decreases toward the SW of the area.

The Shakal anticline (no. 2) lies at the west of the Kalar district, which is elongated and extended from the NW [at SP (1132) on line QS-137] to the SE [SP (82) on line X-45]. Part of this structure extended outside the studied area toward the NW. Its length inside the study area is about 36.5 km. The structure shows variable width, the maximum amount appears at the NW of the area around the SP (1115) on line QS-133, it reaches a b o u t 7.1 km. This amount decreases toward the SE of the area and it reaches 2.85 km around the SP (82) on the line X-45 and disappears gradually at the lower most part of the area. There are four crests along this structure, which appear as the elongated dome shape. They show different vertical height, and their values reduce toward the SE of the area. The longitudinal thrust fault is extended beside this structure and intersects its SW limb; as a result, the anticline appears as a monocline structure. The thrust fault has different throw amounts, and its amount decreases toward the SE of the area. This thrust fault may be responsible for the entity of this elongated structure, as well as the difference in its throw amount may be responsible for the change of the elevation along the anticline.

The Sawz Blakh anticline (no. 3) is located NW of the Kalar district around the SP (150) on the line QS-13 with the closure amount of 400.0 m. It has a dimension of about 5.3×10.3 km, and it is buried below the depth of 3,200.0 m. This structure appears as asymmetrical double plunged anticline, it is plunging in both NW and SE direction.

---

The Kalar nose structure (no. 4), which is asymmetrical nose, is located at the south of the Kalar district. The dip angle at the SW limb is more than the NE limb. It is plunging toward the NW, and there are two sets of reverse faults intersecting the SW limb of the structure. At the west of the area, exactly around the Qr-1 deep well, anticline (no. 5) appears on the map, which represents a part of Qumer anticline. This structure extends outside the studied area toward both NW and SE direction.

The Jeribe formation is buried at the depth ranging between 1,700.0 to 5,000.0 m in the studied area. The description of Jeribe formation depth map as shown in Figure 8 is briefly shown in the following points:

The elongated Barda Sur anticline (no. 1) exists at the east of the Kalar district, which extends from NW at the SP (230) on the seismic line QS-13 toward the SE to SP (75) on the line QS-3. The length of this structure is about 21.5 km, and it has different width which is reduced toward the SE of the study area. The maximum width of it is about 5.0 km around the SP (1115) on line QS-13 at the NW and is reduced to about 1.53 km at the SE near the SP (235) on the line QS-5. Along its top, there are four crests with different heights. At the SW limb of this structure, longitudinal thrust faults extend and intersect its SW limb. This structure appears as a monocline structure because of this thrust fault. This fault has different throws, and its amount decreases towards the SW, and may be responsible of the existence of this anticline.

The elongated Shakal anticline (no. 2) is located at the west of the Kalar district. This anticline extended from the NW at SP (1132) on the line QS-137 to the SE to SP (82) on line X-45 and may extend outside the studied area toward the NW. The maximum length of the structure inside the study area is about 38.4 km. The width of this structure is different and its value gradually decreases towards the SE of the area. The maximum width of it around the SP (1115) on seismic line QS-133 at the NW is about 9.2 km and is reduced to about 3.4 km at the SE around the SP (82) on seismic line X-45. There are four crest points along the top of this structure, which appear as dome shapes. The heights of these crests differ, and their values decrease towards the SE of the area. There is a longitudinal reverse fault intersecting the SE limb of this structure and as a result, the structure appears as a monocline structure. The throw of this thrust fault differs and its amount reduces toward the SE. The existence of this anticline may be due to that fault, as well as the difference in fault throw may be responsible for the change of the elevation of those crests along the top of the anticline.

---

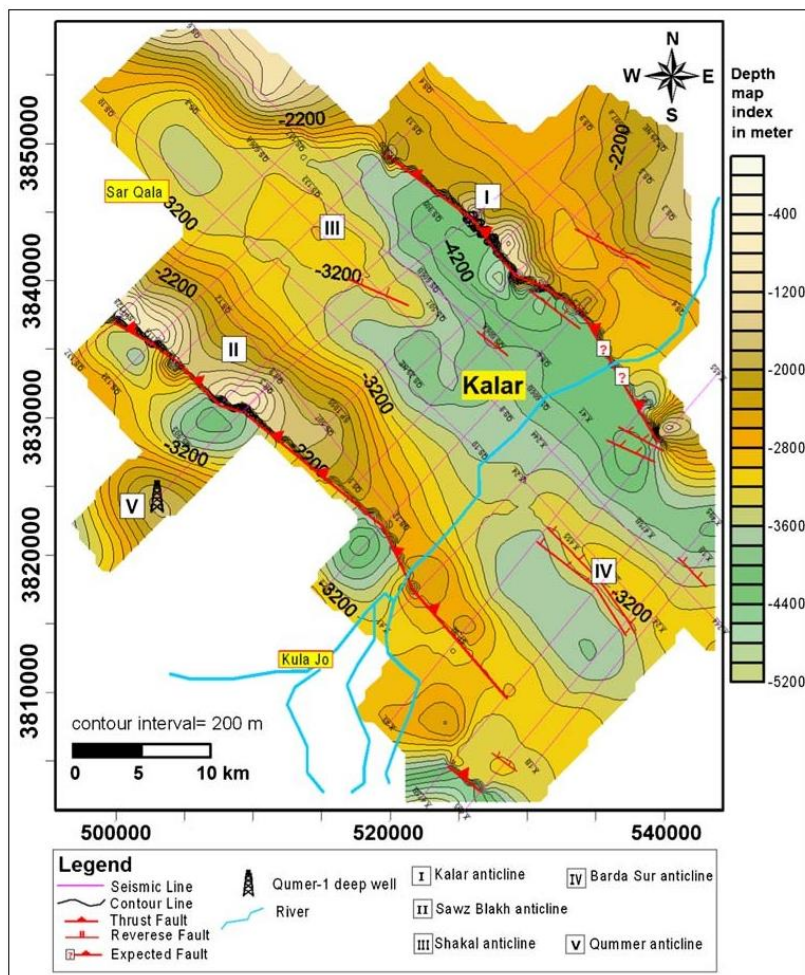


Figure 9.17 The depth map of the lower Fars formation showing the major structures and faults detected in the area.

The Sawz Blakh anticline (no. 3) is located NW of the Kalar district around the SP (150) on the line QS-13 with the closure amount of 400.0 m. It has a dimension about 5×8.82 km and depth of 3,400.0 m. This structure appears as asymmetrical double plunge anticline, plunges in both NW and SE directions.

The Kalar anticline (no. 4), which is asymmetrical double plunging, is located at the South of the Kalar district around the SP (1559) on the line QS-475B. It is buried below depth of 3,600.0 m. This structure is plunged in both NW and SE directions, and the dip angle at the SW limb is more than the NE limb. There are two sets of reverse faults intersecting the SW limb of this structure.

Part of Qumer anticline (no. 5) appears around the Qr-1 well at the west of the area. This structure is buried below the depth of 2,400.0 m and extends outside the area towards both NW and SE direction of the area.

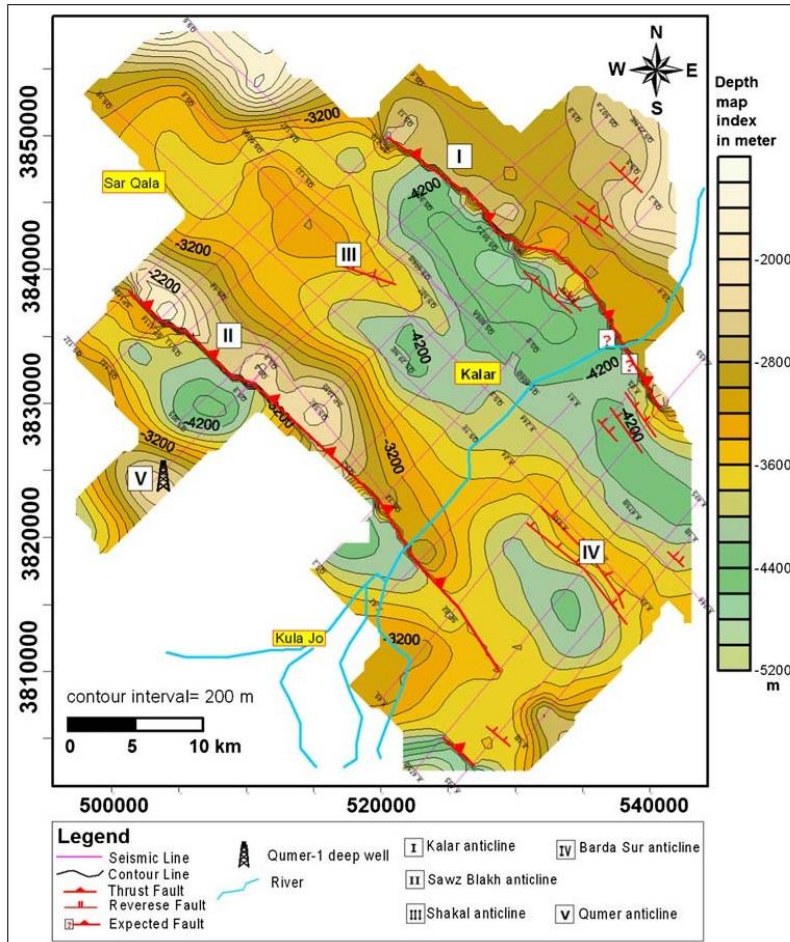


Figure 9.18 The depth map of the Jeribe formation showing the major structures and faults detected in the area.

### Fault distribution maps

There are three major faults and several minor faults within the studied area (Figure 9), which are trending generally in NW-SE direction.

The first major fault (named Barda Sur Fault) is located at the north and the NE of the Kalar district, which ranges between reverse and thrust fault. It also has different throws, which is approximately ranging between 700.0 to 1,600.0 m. This amount decreases toward the SE of the area (Figure 9.20). This fault is extended outside of the

study area in both NW and SE direction, and its length inside the study area is about 36.0 km.

The second major fault (named Shakal Fault) is located at the west and the southwest of Kalar district. This fault has the same situation as the first major fault. Its throw amount is approximately ranging between 600.0 to 1,700.0 m and decreases towards the SE. It extends outside of the study area towards the NW part of the area, its length inside the studied area is about 45.5 km.

The third major fault (named Rahamla) is located in the south part; it may be a part of the larger thrust fault extended outside of the studied area to the SE direction. The maximum length of this fault inside the studied area is about 5.7 km.

The minor faults presented in the studied area have a small throw amount, and most of them are located at the east and southeastern parts of the area.

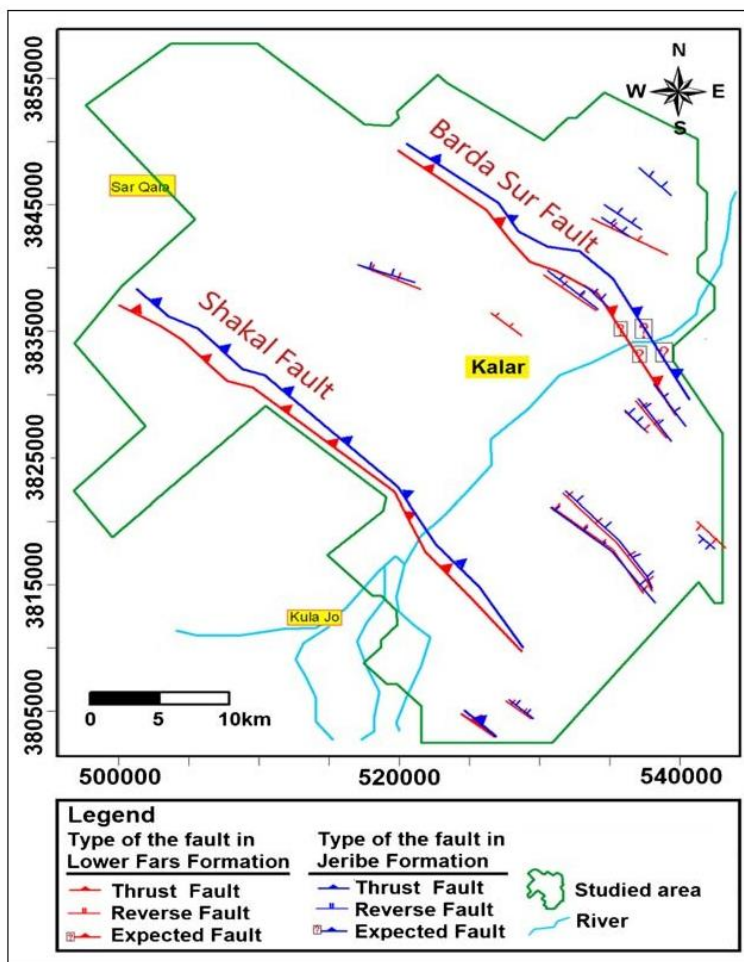


Figure 9.19 Subsurface distribution of the types of the faults (thrust, reverse and expected faults) of lower Fars and Jeribe formations in the study area.

Two sets of the reverse faults are located 7.6 km south of the Kalar district, they are running parallel to semi-parallel to each other. Their length is about 15.0 km. There are two other small reverse faults to the east of these faults, which may be parts of the larger fault outside the area, and they are extending into the study area from the southeastern part.

At a distance of about 11.36 km at the north of the Kalar district, there is a longitudinal reverse fault, which has a length of about 5.0 km. It has a throw ranging between 70.0 to 100.0 m.

At the NE of the studied area, there are three sets of the faults, two of them are intersecting the Jeribe formation and not reach to the lower Fars formation. Also, near the Kalar district exactly at the north of it, there is a small fault. This fault intersects the lower Fars formation and not downward to the Jeribe formation.

---

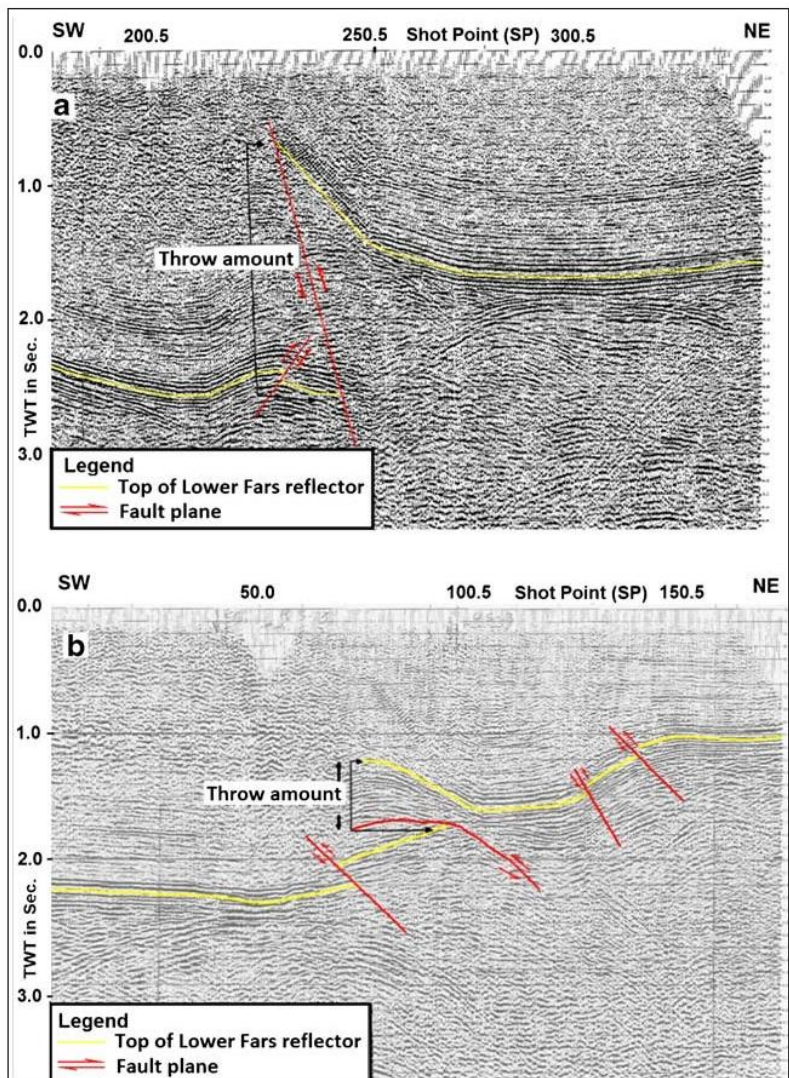


Figure 9.20 a Large throw reverse fault (QS.9). b Small throw thrust fault (QS-3)

**Subsurface structural maps**

The maps (Figures. 9.21 and 9.22) show that the major anticlines axis is intersected by a major fault. This note is also mentioned by Jassim and Goff (2006) that the Zagros folded zone can be distinguished from the rest of the orogeny by NW-SE trend parallel folds and thrust core anticline.

Due to the fact that the fold axis is mostly affected by thrust fault, the structures can be said thrust fold or fault related fold as mentioned by Bahroudi and Koyi (2004). The decollement surface and the reactivated preexisting basement

faults after the collision led to the deformation accommodated by fault related fold. As a result, they appear as monocline or homoclinal structures (Figures. 9.22 and 9.23).

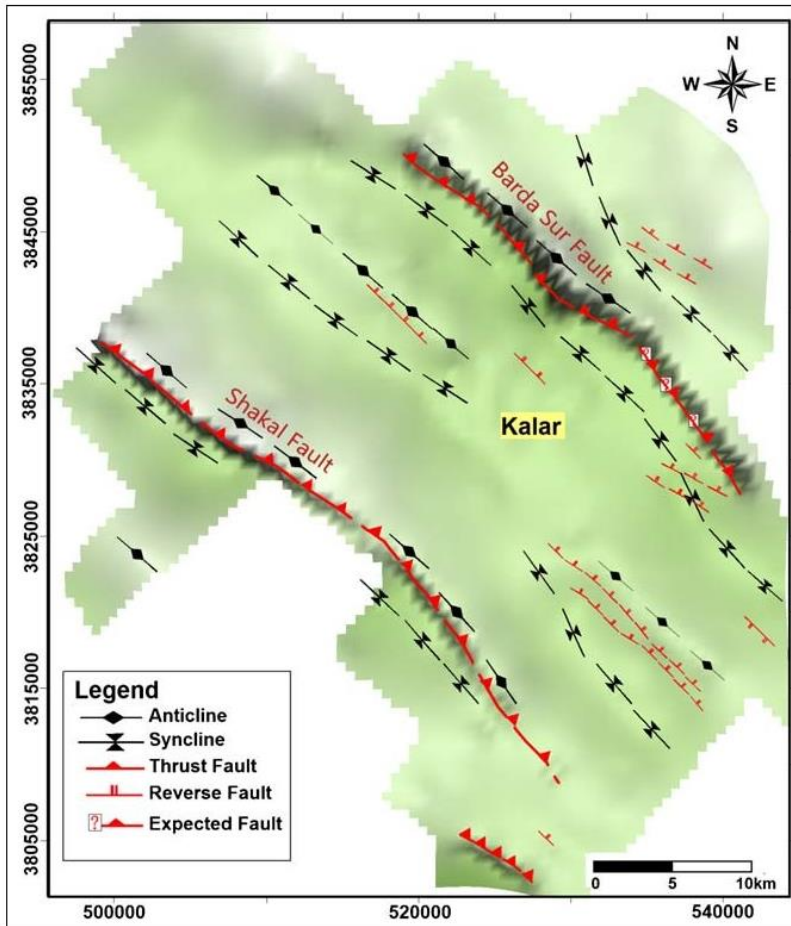


Figure 9.21 The subsurface structure map of the near top of the lower Fars formation in the studied area. It shows anticlines, synclines, and the three types of the faults.

It is observed from the study of the seismic sections that the amount of the vertical and horizontal displacement of the lower Fars formation is greater than of the Jeribe formation, this most probably referred to the evaporated beds of the lower Fars formation that acts as a decollement surface. (Letouzey et al. 2002); (Blanc et al. 2003); (Sherkati and Letouzey 2004); (Inger and Hassani 2004) and (Koyi et al. 2005) studied the Zagros foreland in Iran, they suggested that the effect of the basement blocks movement is also controlled by the stratigraphic position of the decollement levels. The reactivation of this decollement surface during the collision of the Arabian and Iranian plate during the Alpine Orogeny caused the displacement of the lower Fars formation over the underlain formations, as shown in Figures. 9.22 and 9.23. Shakal and Barda Sur structures are the best examples for such structure; they are usually

associated either by bitumen seepages or sulfuric spring (e.g., Na Saleh village bitumen seep). On the surface, the diagnostic topographic changes or variation on both the sides of the thrust fault is quite clear, as well as its effect on the geomorphological feature.

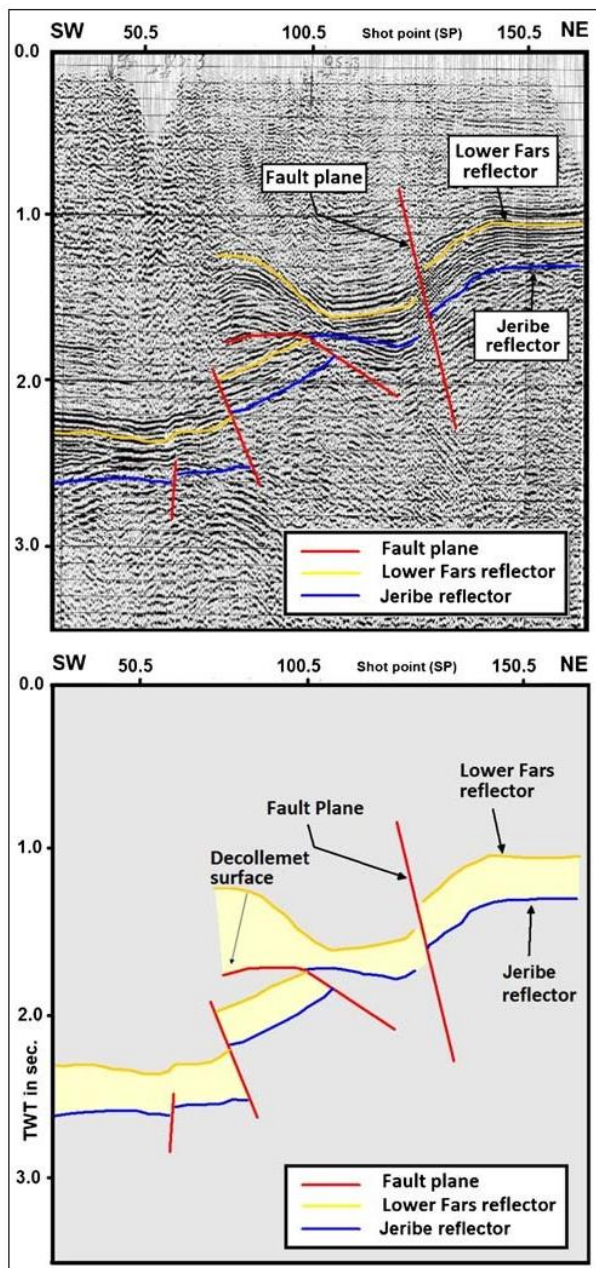


Figure 9.22 The decollement surface phenomena within lower Fars formation on seismic section QS-3.

The horizontal displacement of the lower Fars formation over the Jeribe formation is estimated between 150.0 to 1,500.0 m (Figure 9.21). The displacement to southwest direction. The amount of the displacement along the Barda Sur fault is greater than Shakal fault. This is because Barda Sur fault location is close to the Zagros thrust zone.

### **9.2.5 Possibility of hydrocarbon occurrences**

The presence of the several significant structures in the studied area such as Barda Sur, Shakal, Sawz Blakh, and Kalar anticlines, which lies to the south of Kirkuk and Jambur oil fields and to the east of Qumer oil field, and the presence of oil seepages in Na Salih village near Kifri town, in addition to the result of this study and the dimensions of the discovered structures, all increase the possibility of oil and gas occurrences in the Oligocene, Eocene, and Cretaceous reservoirs rocks in the area. Therefore, it will be a very high prospective area and expected to contain several billion barrels of oil equivalent.

### **9.2.6 Conclusions**

The two reflectors of the top of both lower Fars and Jeribe formations were picked from seismic sections show several geological structures on depth maps such as Kalar, Sawz Blakh, Shakal, and Barda Sur anticlines. The structures of both formations show the same structural picture and having the same NW-SE (Zagros) trend. Shakal and Barda Sur anticlines appeared as monoclinal structures because longitudinal reverse fault intersects their SW limbs, while other structures appear as asymmetrical anticlines with SW limbs of greater slope.

Several reverse and thrust faults were detected. They intersect both formations, and they have different throw amounts ranging from 50.0 to 1,700.0 m.

The study concluded that the lower Fars formation and overlay beds are thrust over the underlain beds. This most probably related to the existence of the evaporate beds within the lower Fars formation, which act as decollement surface. The amount of displacement along the Barda Sur fault is greater than the displacement along the Shakal fault.

---

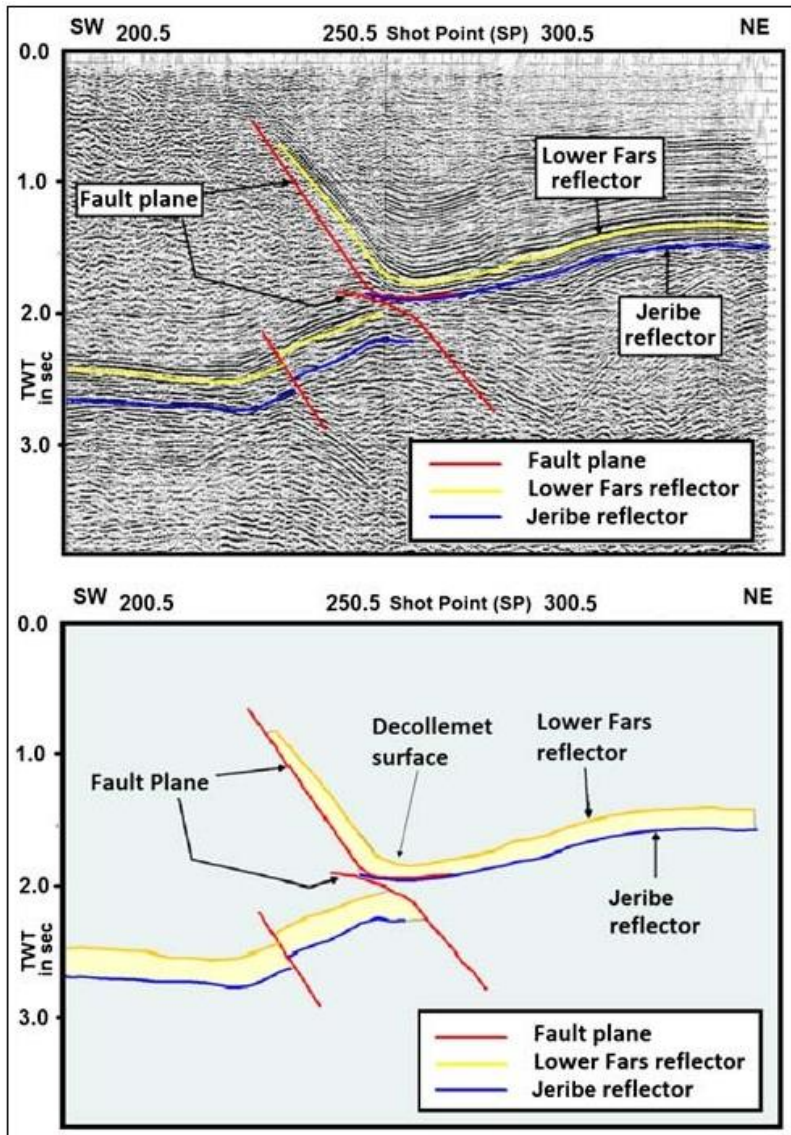


Figure 9.23 The decollement surface phenomena within lower Fars formation on seismic section QS-5.

## REFERENCES

- Abbas, M.J, 1985. Analysis of gravity lineaments in Western Desert. Jour. Geol. Soc. Iraq, V18(1), pp37-46.
- Abbas, M.J, and Masin, J., 1975. New geophysical aspects of the basement structure in Western Desert. Jour. Geol. Soc. Iraq. Special Issue pp1-13.
- Abbas, M.J., 1995. A new proposed northeastern boundary position of the stable shelf in Iraq based on geophysical data. Iraqi, Geol. Jour. V28(1), pp1-13.
- Abbas N., 2006. Late Cenozoic sedimentary outbuilding offshore mid-Norway: sequence stratigraphic analysis, Semantic Scholar, Geology.
- Abdul Jalil, L.A., 1998. Geological variations of Middle Cretaceous from regional seismic section at Middle Iraq. Al-Maaniya - Khanaqin. M.Sc. thesis, dept. of geology, college of science, University of Baghdad, Iraq, (Unpublished).
- Acheson, C. H., 1963, Time depth and velocity depth relations in Western Canada. Geophysics, vol. 28.
- Al-Banna, A.S., 1992. Gravity lineaments, fault trends and depth of the basement rocks in Western Desert Iraq. Iraqi Geol. Jour. V33(1-2), pp63-79.
- Al-Banna, A.S., 1999. The main lithological basement regions inferred from geophysical data, in Western Desert of Iraq. Iraqi Geol. Jour. V40C (4), pp8-22.
- Al-Bassam, K.S., Al-Bdaiwi, J.M., and Al-Kadhimi, J.A., 1997. A study about the extending of the Ha'il arch inside Iraq: A new data from Nukhaib area at the southern Iraq. Geoscience and Arab development, No. 1-2, pp12-23.
- Al-Bdaiwi, J.M., 1982. Detailed magnetic survey of Al-Waled area Western Desert. GEOSURV Library, report no. 1240, (unpublished).
- Al-Chalabi, M., 1979, Velocity determination from seismic reflection data: In Developments in Geophysical Exploration methods, Vol. 1, Fitch, ed., pp 1-68, Amsterdam: Elsevier.
- Al-Husseiny, M.M., 1989. Gravity and magnetic investigation along regional profiles in Iraq. M.Sc. thesis, dept. of geology, college of science, University of Baghdad, Iraq, (Unpublished).
- Al-Khatib D.A., 1996. Two dimensional modeling of the gravity and magnetic anomalies a profiles south of Al-Qaim City, Western Desert. M.Sc. thesis, dept. of geology, college of science, University of Baghdad, Iraq, (Unpublished).
-

- Al-Khatib H.H., 1976. Downward analytical continuation of the gravity field in central Iraq between latitudes (32 -33), M.Sc. thesis, dept. of geology, college of science, University of Baghdad, Iraq, (Unpublished).
- Al-Rawi, F.R., 1986. Basement depth estimation in the Western Desert of Iraq using the power spectrum technique. *Jour. Geol. Soc. Iraq*, V19(2), pp11-25
- Al-Sadi, H. N., 1973, Dependence of the P-wave amplitude spectrum on focal depth. *Pure and Applied Geophysics*, vol. 104, p439-452.
- Al-Sadi, H. N., 1994, Use of the loop spread in seismic surveying of a rugged mountain (text in Arabic Language), presented to the twelfth geological conference, May, 1994. 12p.
- Al-Sadi, H. N., 3D surveying of inaccessible areas (text in Arabic Language), presented to the tenth geological conference, December, 1992. 17p.
- Al-Sadi, H. N., and Baban, N., 2014, Introduction to Gravity Exploration Method. 203p, Sulaymaniyah University, Kurdistan Region, Iraq, Sulaymaniyah.
- Al-Sayyab, A. and Valek, R., 1968. Patterns and general properties of gravity field of Iraq. 23th International geological congress, Czechoslovakia, Sec.5: pp129-42.
- Al-Sheikh, Z.D., 1997. A contribution of the basement question in Iraq, *Raf. Jour. Sci.*, V8(2), pp71-87.
- Al-Yasi, A.I. and Hijab, B.R., 1995. Gravity transects of Western Desert in Iraq and its tectonic applications. *Jour. Geol. Soc. Iraq*. V28(2), pp27-35.
- Al-Yasi, A.I., 1997. Use of the potential methods in studying deep geological structures in the Western Desert-Iraq. Ph.D. thesis, dept. of geology, college of science, University of Baghdad, Iraq, 128p, (Unpublished).
- Ameen MS (1992) Effect of basement tectonics on hydrocarbon generation, migration, and accumulation in northern Iraq. *AAPG* 76(3):356-370
- Aud, B. W., 1974, Abnormal pressure zones can be predicted by seismic data. *World Oil*, Aug-74, pp. 37-39.
- Aziz, B.K., 1986. Study of thickness distribution of the Paleozoic sediments and basement depths in parts of the Western Desert based on seismic reflection data. M.Sc. thesis, dept. of geology, college of science, University of Mosul, Iraq, (Unpublished).
- Baban, E.N., 1983. Analysis of the geophysical data of the Abu Rassain area. M.Sc. thesis, dept. of geology, college of science, University of Mosul, Iraq, (Unpublished).
- Bahroudi A, Koyi HA (2004) Tectono-sedimentary framework of the Gachsaran Formation in the Zagros foreland basin. *Marine Petroleum Geol* 21:1295-1310
-

- Barnes, A., 1993a, When the Concepts of Spectral Frequency and Instantaneous Frequency Converge, *Leading Edge*, Oct-1993, P.1020-1023.
- Barnes, A., 1993b, Instantaneous spectral bandwidth and dominant frequency with applications to seismic reflection data, *Geophysics*, vol. 58, P.119-428.
- Barnes, A., 2001, Seismic attributes in your facies: *CSEG Recorder*, 26, Sept., pp. 41-47.
- Båth, M., 1971, Average crustal structure of Sweden., *Pur. Appl. Geophys*, vol. 88, p. 75-91.
- Båth, M., 1973, *Introduction to Seismology*. Birkhäuser Verlag, Basel, 395p.
- Båth, M., 1974, *Spectral Analysis in Geophysics*. 563p., Elsevier Scientific Publishing Company, Amsterdam.
- Båth, M., 1979, *Introduction to Seismology*, Birkhauser Verlag, 428p, Basel, Switzerland.
- Belopolsky, A. V., and Droxler A. W., 2004, Seismic expressions of prograding carbonate bank margins: Middle Miocene, Maldives, Indian Ocean, in *Seismic imaging of carbonate reservoirs and systems: AAPG Memoir 81*, p. 267 – 290.
- Birch, F., 1966, Compressibility, Elastic Constants, in *Handbook of Physical Constants*, by S. P. Clark, Geological Society of America, Memoir 97, p. 97-173
- Birch, F., 1966, Compressibility, Elastic constants, in S. P. Clark, ed *Handbook of Physical Constants*, geological Society of America, Mem. 97, p. 97 - 173.
- Blanc EJP, Allen MB, Inger S, Hassani H (2003) Structural styles in the Zagros Simple Folded Zone, Iran. *J Geol Soc* 160:401-412
- Brown, A. R., 2011, *Interpretation of three-dimensional seismic data*, 7th. edition, AAPG Memoir 42 (9), 646p.
- Bullen, K. E., 1965, *An Introduction to the Theory of Seismology*, The University Press, 381p, Cambridge, England.
- Chapman, R., E., 1976, *Petroleum Geology*, Elsevier, Amsterdam.
- Chen, Q. and Sidney, S., 1997, Seismic attribute technology for reservoir forecasting and monitoring: *The Leading Edge*, 16, no. 05, 445,447-448,450,453-456.
- Chopra. S. and Marfurt. K., J., 2005, Seismic attributes-a historical perspective, *Geophysics*. Vol 70(3) p.3SO-28SO.
- Deregowsky, S. M. 1986, What is DMO? *First Break*, vol. 4, No. 7, P. 6-24.
- Ditmar V and Iraqi- Soviet team (1979) *Geological conditions and hydrocarbon prospects of Republic of Iraq*, OEC Library, Baghdad, (Unpublished Technoexport).
- Dix, C., 1955, Seismic Velocities from Surface Measurements. *Geophysics*, vol. 20, p. 68 - 86.
-

- Dobrin, M. B., 1960, Introduction to Geophysical Prospecting. McGraw Hill Book Company, 446p. New York.
- Dobrin, M. B., and Savit, C. H., 1988, Introduction to Geophysical Prospecting. McGraw Hill Book Company, 867p., New York.
- Dobrin, M., 1977, Seismic Exploration for Stratigraphic Traps, AAPG Memoir, P329-352.
- Eberli, G. P., Masaferrro J. L., and Rick Sarg J. F., 2004, Seismic imaging of carbonate reservoirs and systems, in Seismic imaging of carbonate reservoirs and systems: AAPG Memoir 81, p. 1 - 9.
- Evenden, B. S., and Stone, D. R., 1971, Instrument Performance and Testing. in Seismic Prospecting Instruments, 195p, Gebruder Borntraeger, Berlin, Germany.
- Ewing, M., Jardetzky, W., and Press, F., 1957, Elastic Waves in Layered Media, McGraw-Hill, 380p., New York.
- Fadhel M.S. and Al-Rahim A.M., 2019, 3D seismic model of faulting systems of a Jurassic - Cretaceous sedimentary packages in Merjan, west Kifl oil fields - Central Iraq, Heliyon 5 (2019) e02507, pp1-11.
- Faust, L. Y., 1951, Seismic Velocity as a Function of Depth and Geologic Time, Geophysics, vol. 16, pp. 192-206.
- Galperin, E. I., 1973, Vertical seismic profiling, SEG, Tulsa, Oklahoma, USA.
- Gardner, G. H., Gardner, L. W., and Gregory, A. R. 1974, Formation velocity and density-the diagnostic basics for stratigraphic traps, Geophysics, 39, 770-780.
- Gardner, L. W., 1939, An aerial plan of mapping subsurface structure by refraction shooting. Geophysics, vol. 4, pp. 247-259.
- Gassman, F., 1951 Elastic waves through a packing of spheres. Geophysics, vol. 16, p. 673-685.
- GEOSURV, 1996. Geological and tectonical maps of the Iraq, (unpublished maps), scale, 1:1000000.
- Grant, F. S., and West, G. F., 1965, Interpretation Theory in Applied Geophysics. McGraw-Hill, 584p., New York.
- Green, C. H. 1938, Velocity determination by means of reflection profiles. Geophysics, vol. 3, p: 295 - 305.
- Gregory, A. R., 1977, Aspects of rock physics from laboratory and log data that are important to seismic interpretation, AAPG memoir 26, p. 15-46.
- Gurvich, I., 1972, Seismic Prospecting (translated from Russian by Jean Agrell). 463p., Mir publications., Moscow.
-

- Gutenberg, B., 1959, *Physics of the Earth's Interior*. 240p., Academic Press Inc., New York.
- Hardage, B. A., 1983, *Vertical Seismic Profiling. Handbook of Geophysical Exploration*. Geophysical Press, London.
- Hijab, B.R. and Al-Khatib, D.A., 1997. Subsurface igneous activity at the Western Desert of Iraqi and its tectonic implication. *Jour. Geol. Soc. Iraq*, V30(2), pp68-76.
- Hijab, B.R., 1996. Structural evolution history of Gaara sedimentary basin- Western Desert-Iraq. *Jour. Geol. Soc. Iraq*, V29(1).
- Holmes, A., 1975, *Principles of Physical Geology*, 1288p., Nelson, London.
- Inger S and Hassani H (2004) Tectonic evolution of the Zagros mountain belt: new approaches and their hydrocarbon implications, University of Cambridge, UK, report. 6 P.
- Isern, A. R., F. S. Anselmetti, and P. Blum, 2004, A neogene carbonate platform slope, and shelf edifice shaped by sea level and ocean currents, Marion Plateau (northeast Australia), in *Seismic imaging of carbonate reservoirs and systems: AAPG Memoir 81*, p. 291 – 307.
- Jassim SZ and Goff JC (2006) *Geology of Iraq*. Dolin, Prague and Moravian Museum, Brno, 341p.
- Jones F., 2007 *UBC Earth and Ocean Sciences*,  
[https://www.eoas.ubc.ca/courses/eosc350/content/methods/meth\\_6/dipping.html](https://www.eoas.ubc.ca/courses/eosc350/content/methods/meth_6/dipping.html)
- Kanasewich, E. R., 1973, *Time Sequence Analysis in Geophysics*. 352p., The University of Alberta Press, Edmonton.
- Kaufman, H., 1953, Velocity functions in seismic prospecting. *Geophysics*, vol. 18, pp. 289-297.
- Kearey, P., Brooks, M., and Hill, I., 2002, *An Introduction to Geophysical Exploration*, Blackwell Science Ltd., Oxford, 262p.
- Koyi HA, Sans M, Bahroudi A and Lawa F (2005) Modeling the role of multiple salt horizons on deformation in fold-thrust belts. *Abstracts Volume, AAPG 2005, Annual. Convention, Calgary, Canada*. P. A75
- Krehbiel, S. C., 1999, Trivariate Attribute Displays, *Leading Edge*, Nov.-1999, pp. 1248– 1257
- Lavergne, M., 1989, *Seismic Methods*. 172p., Editions Technip, Paris.
- Letouzey J, Sherkati S, Mengus J, Motiei H, Ehsani M, Ahmadnia A and Rudkiewicz JL (2002) A regional structural interpretation of the Zagros mountain belt in northern Fars and high Zagros (SW Iran), *AAPG annual meeting, Houston, Texas*.
-

- Liner, C. L., 2004, Elements of 3D Seismology, PennWell, Tulsa, Oklahoma, 526p.
- Lombardi, L. V., 1955, Notes on the Use of Multiple Geophones, Geophysics, vol. 20.
- Louden, L. R. et al, 1971, Ultra deep drilling guided by seismic data. World Oil, May-71, pp. 67-71.
- Maton, A., Hopkins, J, Johnson, S., LaHart, D., Warner, M., Wright, J., 1995, Exploring Physical Science, Prentice Hall, 818p, Englewood Cliffs New Jersey, USA.
- Mayne, W. H., 1962, Common reflection point horizontal stacking techniques, Geophysics, vol. 27, p.927-938.
- Mayne, W. H., 1967, Practical considerations in the use of common reflection point technique, Geophysics, vol. 32, p.225-229.
- McQuillin, R., Bacon, M., Barclay, W., 1984, An Introduction to Seismic Interpretation. Graham & Trotman, 287p., London.
- Mitchum, R. M. & Vail, P. R., 1977, Seismic Stratigraphy Interpretation Procedure, AAPG Memoir 26, p. 135-144.
- Mokhtari M., 2006. Seismicity, Major Structural Elements and Required Tsunami Early Warning System for Makran (Sea of Oman) Region. National Center for Earthquake Prediction. International Institute of Earthquake Engineering and Seismology (IIEES) Iran, Gulf seismic forum, Oman.
- Nafe, J. E. and Drake, C. L. 1963, Physical properties of marine sediments, The Sea, Interscience, New York, 794-815.
- Nestvold, E. O., 1987, The use of 3D seismic in exploration, appraisal and field development, Proc. 12th World Petroleum Congress, Houston, 1987, 2, 125-132, Wiley, Chichester.
- Nettleton, L. L., 1940, Geophysical Prospecting for Oil., McGraw Hill Book Company, 440 p., New York.
- Newman, P., 1973, Divergence effects in a layered earth, Geophysics, vol. 38, p.481-488.
- Papaulis, A., 1962, The Fourier Integral and its Applications. 318p., McGraw-Hill New York.
- Parasnis, D. S., 1971, Physical Property Guide for rocks and minerals. Geoph. Mem. 4/71, (ABEM,) Stockholm, Sweden.
- Parr, J. O., Jr., and Mayne, W. H., 1955 A New Method of Pattern Shooting, Geophysics, vol. 20, p. 539-565.
- Peacock, K. L., and Treitel, S., 1969, Predictive deconvolution, Theory and practice. Geophysics., vol. 34, p. 155-169.
-

- Pennebaker, E. S., 1968, Seismic data indicate depth magnitude of abnormal pressures. World Oil, June 68, pp. 73-78.
- Peterson, R. A., Fillipone, W. R., and Coker, F. P., 1955, The synthesis of seismograms from well log data. Geophysics, vol 20, pp. 516-538.
- Pickett, G. R., 1963 Acoustic character logs and their application in formation evaluation, J. Petrol Tech., Geophysics, vol. 15, p. 650-667.
- Poulter, T. C., 1950, The Poulter seismic method of geophysical exploration, Geophysics, vol. 15, p.181-207.
- Redpath B.B., 1973. Seismic refraction exploration for Engineering site investigations. Technical report e-73-4 U. S. Army engineer waterways experiment station Explosive excavation research laboratory Livermore, California.
- Reynolds, E. B., 1970, Predicting over pressured zones with seismic data. World Oil, Oct- 70, pp. 78-82.
- Richardson, E. G., 1953, Sound, Edward Arnold & Co., 352p, London, England.
- Richter, C. F., 1958, Elementary Seismology, Freeman and Company Inc., 768p.
- Robinson, E. A., 1967, Statistical Communication and Detection with Special Reference to Digital Data Processing of Radar and Seismic Signals. Hafner, New York, USA. 362p.
- Robinson, E. A., 1983, Seismic Velocity Analysis and the Convolutional Model. IHRDC., Boston, USA. 290p.
- Robinson, E. A., and Treitel, S., 1967, Principles of Digital Wiener Filtering. Geophys. Prospect., vol. 15, p. 311-333.
- Robinson, E. A., 1954, Predictive deconvolution of time series with applications to seismic exploration. Cambridge, MIT, Geophysical Analysis Report no. 7, (reprinted in Geophysics, v32, (pp. 418-484, 1967).
- Robinson, E. A., 1983, Migration of Geophysical Data, IHRDC, Boston, USA, 208p..
- Sharma, P., 1976, Geophysical Methods in Geology. Elsevier, Amsterdam.
- Sheriff, R. E., 1969, Addendum to Glossary of Terms used in Geophysical Exploration Geophysics, vol. 34, p. 255-270.
- Sheriff, R. E., 1973, Encyclopedic Dictionary of Exploration Geophysics, Society of Exploration Geophysicists (SEG), Tulsa, Oklahoma, USA.
- Sheriff, R. E., 1977 Limitations on resolution of seismic reflections and geologic detail derivable from them. In seismic Stratigraphy-Applications to Hydrocarbon Exploration, AAPG, Memoir 26, pp. 3-14.
- Sheriff, R. E., 1980, Seismic Stratigraphy, International Human Resources Development Corporation (IHRDC), 227p, Boston, USA.
-

- Sheriff, R. E., 2002, *Encyclopedic Dictionary of Exploration Geophysics*, Society of Exploration Geophysicists (SEG), Tulsa, Oklahoma, USA.
- Sheriff, R. E., and Geldart, L. P., 1995, *Exploration Seismology*. Cambridge University Press., 592p., UK.
- Sheriff, R.E., 1975, Factors affecting amplitudes. *Geophysical Prospecting*, Vol. 23, P.125-138.
- Sherkati S, Letouzey J (2004) Variation of structural style and basin evolution in the central Zagros (Izeh zone and Dezful Embayment), Iran. *Mar Pet Geol* 21:517-640
- Sissakian VK (2000) *Geological Map of Iraq*, 3<sup>rd</sup> edit., scale 1: 1 000 000. GEOSURV, Baghdad, Iraq.
- Sjogren, Bengt, 1984, *Shallow refraction seismic*, 1st Ed., Chapman and Hall Ltd, 270p
- Tamar-Agha, M.Y., 1993. *Exploration and processing in the Ga'ara depression, part one, general geology*, GEOSURF, report no. 1899, Baghdad. 145p.
- Taner, M. T., 2001, *Seismic attributes: CSEG, Recorder*, 26, 48–56.
- Taner, M. T., and Sheriff, R. E., 1977, Application of amplitude, frequency and other attributes to stratigraphic and hydrocarbon determination. *AAPG Memoir* 26. P301-328.
- Taner, M. T., Schuelke J. S., O'Doherty R., and Baysal E., 1994, *Seismic attributes revisited: 64th Annual International Meeting, SEG, Expanded Abstracts*, 1104–1106
- Taner, M. T., Koehler, F., and Sheriff, R. E., 1979, *Complex seismic trace analysis*. *Geophysics*, vol. 44, P1041-1063.
- Telford, W. M., Geldart, L. P., Sheriff, R. F., 1990, *Applied Geophysics*. Cambridge University Press., Cambridge, 770p.
- Vail, P. R., Mitchum, R. M., et al ,1977, *Seismic Stratigraphy and global changes of sea level, Application to hydrocarbon exploration*, Payton, C., E., ed., AAPG Mem-26, Tulsa, Oklahoma, 516p.
- Walton, G. C. 1972, *Three-Dimensional Seismic Method*. *Geophysics*, vol. 37, No. 3, p. 417.
- Wang R., Shi W., Xie X., Tang D., Mangerd W., Busbeyc A. B., and Xub L., 2018. Boundary fault linkage and its effect on Upper Jurassic to Lower Cretaceous sedimentation in the Gudian half-graben, Songliao Basin, northeastern China, *Marine and Petroleum Geology* J. 98, pp33–49.
- West, S. S., 1950, Dependence of seismic wave velocity upon depth and lithology. *Geophysics*, vol. 15, pp. 653-662.
-

Wuenschel, P. C., 1976, The vertical array in reflection seismology, *Geophysics*, vol. 41, p.219-232.

Wyllie, M. R. J., A. R. Gregory, and G. H. F. Gardner, 1958, An Experimental Investigation of Factors Affecting Elastic Wave Velocities in Porous Media, *Geophysics*, vol. 23, pp. 459-493.



# INDEX

- (F-K) filter, 128  
 2D seismic reflection, vi, 83  
 2D surveying, 104, 107, 108, 110, 112, 115  
 2D-data processing, 111  
 3D data processing, 105  
 3D data-volume, 106  
 3D seismic reflection, 1  
 3D seismic reflection surveying, vii, 103  
 3D spreads, 108, 114  
 3D surveying, iii, 85, 106, 107, 108, 109,  
 110, 112, 113, 114, 122, 124, 184  
 7-fold bin gather, 110  
 Acceleration, 3  
 Acoustic impedance, 45, 46, 55, 56, 141  
 Aeromagnetic surveying, 5  
 AGC-type, 131  
 Air-gun, 112  
 Air-Gun, 95  
 Alpha, Beta, and Gamma, 10  
 Amendment, 122  
 Amplitude, 40, 41, 42, 49, 50, 51, 54, 55,  
 83, 84, 94, 95, 104, 105, 111, 116, 119,  
 121, 126, 128, 133, 141, 145, 146, 147,  
 156, 158, 184, 190  
 Anbar uplift, 156, 157, 158, 160, 161, 163,  
 164  
 Angle of dip, 80, 81  
 Anti-alias filter, 127  
 Apparent velocities, 77, 79  
 Apparent velocity, 77, 122  
 Apparent velocity, 77  
 Apparent wavelength, 98  
 Aqua pulse, 95  
 Arrival times, 58, 66, 121, 124  
 Arrivals, 23, 24, 41, 53, 56, 62, 65, 69, 72,  
 74, 83, 84, 87, 90, 96, 99, 101, 138, 139  
 Attenuation, 48, 49, 50, 99, 127, 128, 129  
 Attenuation, vi, 50, 127, 128  
 Attenuation factor, 129  
 Attribute, 122, 124, 145, 146, 147, 185  
 Audio-Frequency Magnetic, 10  
 Azimuth, 25, 108, 110, 115, 145  
 Azimuthal variation, 113  
 Azimuths, 108  
 Band-pass filter, 139  
 Bin-gridding, 109  
 Binning, 109  
 Bit, 12  
 Blowout prevention, 27  
 Body Waves, v, 38  
 Borehole, 14, 22, 23, 25, 99, 100  
 Burj formation, 160  
 Caledonian orogeny, 158, 160, 161, 164  
 Caliper logs, 25  
 CDP, vi, vii, 59, 60, 86, 87, 88, 89, 104,  
 108, 109, 120, 121, 145, 152  
 CDP-bin, 109  
 CDP-Gather, 60  
 Center spread, 85  
 Channels, 83, 85, 86, 89, 100, 126, 151  
 Check-shot survey, 23  
 Chia Ziri formation, 162  
 Christmas tree, 27  
 CMP, vi, 59, 60, 104, 106, 126, 127, 128,  
 131, 133, 134, 135, 136, 140  
 CMP gather-traces, 126, 136  
 CMP sequence number, 136  
 CMP-gather, 131, 133, 135, 136  
 CMP-gathers, 131, 136  
 CMP-record, 131  
 Coefficient, 37, 48, 50, 54, 55, 56, 91, 128,  
 141  
 Coherent noise, 98, 128  
 Coherent noise, 42  
 Coherent Noise, 42  
 Common depth point., 59  
 Common mid-point, 59  
 Common reflection point, 59, 187  
 Compressibility, 36, 185  
 Contour map, 142  
 Convergence), 159  
 Convolution, 50, 130  
 Convolutional model, 50, 51  
 Coverage, 1, 86, 87, 88, 89, 106, 126, 131,  
 136, 145  
 Coverage, vii, 87, 89  
 Critical distance, 70, 72, 73, 74  
 Critical distance, 73

- Crosslines (XL), 111
  - Crossover distance, 70, 74
  - CRP, vi, 59, 60
  - Cubical Dilatation, v, 33
  - Data acquisition, 43, 90
  - Data Acquisition, vii, 90
  - Data box, 105, 111, 116
  - Data Loading, 125
  - Data Preconditioning, 121
  - Data Recording, vii, 97, 101
  - Data Re-sampling, 127
  - Data volume, 104, 105, 111, 112, 116, 117
  - Datum level, 3, 120, 121, 124
  - Decibel unit (or db), 51
  - Deconvolution, 130
  - Deepening, 160, 164
  - Demultiplexed, 125
  - Demultiplexing, 125
  - Density Log, 20
  - Depth map, 142, 172, 173, 174, 175
  - Detector, 19, 20, 23, 24, 43, 50, 53, 69, 80, 97
  - Detectors, 43, 69, 85, 95
  - Detectors, vii, 20, 95
  - Diffraction, iii, 46, 47, 48, 53, 60, 61, 62, 63, 122, 138, 156
  - Diffraction, vi, 2, 60, 61, 62
  - Diffraction Arrivals, 2
  - Diffraction point, 60, 61, 62
  - Digital recording, 1, 97
  - Digital Recording System, 97
  - Dip-angle, 137
  - Dip-meter logs, 25, 26
  - Dipping reflector, 137
  - Dipping reflectors, 137
  - Direct (Transmission) Arrivals, 2
  - Direct wave, 24, 69, 72, 73, 75, 81, 101
  - Direct wave, 69
  - Discontinuities, 7
  - Divergence, 49, 159, 164
  - Down-dip shooting, 78, 79
  - Down-sweep, 94
  - Drilling, v, 10, 11, 12, 14, 26, 102
  - Drilling rig, 11, 12, 13
  - Dual source-single streamer, 112, 113
  - Dual source-triple streamer, 112, 113
  - Dynamic correction, 129, 133
  - Dynamite, 90, 91, 93
  - Dynamite capsules, 99
  - Earthquake, 1
  - Elastic Moduli, v, 35
  - Elasticity, v, 29
  - Electrical conductivity, 6
  - Electrical Induction Logging, 16
  - Electrical Logging, v, 15
  - Electrical Method, v, 6
  - Electrical resistivity, 6, 15
  - Electrical Resistivity Logging, 15
  - Electrode-configuration, 16
  - Electromagnetic, 2, 6, 7
  - Electrostrictive, 97
  - End-on spread, 85, 88, 98
  - Energy Sources, vii, 90
  - Equalization, 119, 131
  - Equalizing, 130
  - Equipotential, 6, 7
  - Evaporate, 163
  - Exploration drilling, 11
  - Filtering, 24, 48, 66, 91, 92, 121, 130, 139
  - Filters, 121
  - Fixed spread, 98, 100
  - Flattening, 160, 161, 162, 163
  - Fluid injection, 26
  - Formation Evaluation, 25
  - Forward, 6, 77, 78
  - Forward and inverse, 6
  - Frequency, 9, 10, 40, 43, 49, 91, 92, 93, 94, 95, 98, 99, 121, 122, 124, 127, 128, 130, 139, 141, 145, 146, 185, 190
  - Frequency Filtering, 139
  - Frequency range, 42, 95
  - Frequency ranges, 95
  - Gain recovery, 129
  - Gain Recovery, 128
  - Gal, 3
  - Gamma ray, 18, 19, 20, 21
  - Gamma-gamma logging, 19
  - Gamma-ray, 18, 19, 21, 26
  - Gapped, 130
  - Gas Exploding, 92
  - Gas-Gun, 95
  - Gate-length, 131, 139
  - Geiger counter, 10
  - Geoflex, 93
  - Geograph, 91
  - Geometrical spreading, 48, 49, 128, 129
  - Geometrical Spreading, vi, 49, 128
  - Geometry Module, 126
-

- 
- Geophone, 41, 69, 83, 85, 96, 97, 99, 101, 128  
Geophone, 96  
Geophones, 69, 70, 73, 85, 96, 98, 99, 156  
Geophysical element, 145  
Geophysical Exploration, v, 1, 2, 183, 186, 187, 189  
Geophysical logging, 11, 14  
Geophysicist, 41, 122, 124, 146  
Ghost, 56, 57  
Ghosts, 99, 130  
Gravimeter, 3  
Gravimeters, 3, 25  
Gravity anomaly, 3, 4  
Gravity attraction, 3  
Gravity Method, v, 3  
Hard-copy, 124  
Hardware, 119  
Head wave, 70  
High frequency, 90, 92, 94  
High-cut filter, 127, 139  
Hole-drift angle, 25  
Homogeneous, 43, 44, 45, 47, 49, 60, 103  
Horizons, 142, 187  
Horizontal stacking, 135, 187  
Huygens' Principle, vi, 44, 45, 60  
Hydrocarbon, viii, 2, 12, 14, 21, 144, 181, 184, 185, 187, 190  
Hydrocarbons, 10, 22  
Hydrophone, 97  
Hydrophones, 96, 112  
Hyperbola, 56, 61  
Hyperbolic form, 61  
Impulsive sources, 93, 94  
Incidence, 48, 54, 55, 60, 66, 67, 68, 69, 72, 73  
Incident, 46, 48, 50, 54, 55, 56, 60, 62, 66, 67, 68, 69  
Incoherent noise, 42  
Induced Polarization, 6, 7  
Inelastic, 48, 128, 145  
Inelastic, vi, 50, 128, 129  
Inhomogeneous, 45, 46  
Intercept time, 73, 74, 76, 80, 101  
Interface, vi, 45, 46, 71, 81  
Interpretation, iii, 1, 2, 4, 5, 19, 25, 57, 65, 100, 122, 124, 141, 142, 143, 144, 160, 186, 187  
Interval transit time, 22, 23  
Intervals, 50, 97, 142  
Iraq, i, ii, viii, 149, 150, 158, 165, 183, 184, 185, 186, 187, 189  
Isochron, 142  
Isochron Map, 142  
Isopach, 142  
Kalar, viii, 165, 169, 170, 171, 172, 173, 174, 175, 176, 177, 181  
Khabour Quartzite, 160  
Khanaqin, viii, 165, 166, 183  
Kurdistan region, viii, 165  
Land Seismic Sources, vii, 90  
Land spreads, 112  
Lateral-sonde configuration, 16  
Laterolog, 16  
Laterologging, 16  
Longitudinal Waves, 38  
Loop-shooting, 106  
Love Waves, 41  
Love-waves, 38  
Low frequency, 6, 15, 42, 94  
Low-cut frequency filter, 128  
Low-velocity, 99  
L-spread, 114  
LVL, vii, 91, 92, 99, 100, 101  
Magnetic anomaly, 5  
Magnetic field, 4, 5, 7, 9, 16, 96  
Magnetic Method, v, 4  
Magnetic tapes, 1, 2, 97, 122, 123, 124, 153  
Magnetic-field, 5, 97  
Magneto-telluric Currents, 9  
Marine spreads, 112  
Mesopotamian basin), 160, 163, 164  
Midpoint, 86  
Mintrop Seismos Company, 1  
Mistie, 142  
Modulus, 36  
Moho discontinuity, 65  
Multi-fold profiling, 87  
Multiple, 41, 56, 57, 71, 75, 76, 85, 86, 187  
Multiple, vi, 56, 57, 99, 187  
Multiples, 24, 57, 130  
Multiples arrival, 24  
Multiplexed, 125, 127  
Multiplication process, 131  
Natural Gamma-Ray Logging, 19  
Neutron Gamma-Ray Logging, 20  
Neutron log, 21
-

- NMO, vi, 58, 59, 120, 121, 129, 131, 132, 133, 134, 135, 136, 140
  - NMO correction, 120, 121, 129, 133, 140
  - NMO-correction velocity, 140
  - Noise, 41, 42, 43, 84, 90, 97, 98, 99, 119, 121, 126, 127, 128, 136, 139, 140
  - Noise test, 97, 98
  - Noise-cancellation, 136
  - Noises, 43, 119, 121
  - Non-impulsive, 93
  - Normal move-out, 61, 62
  - Normal Move-Out (NMO), vi, 58
  - Nyquist frequency (fn), 127
  - Oersted, 5
  - Oil-Well Drilling, v, 10
  - Parallel linear paths, 113
  - Parameter optimization, 123
  - Petroleum exploration, 5, 65
  - Phase, 1, 10, 55, 56, 122, 124, 127, 131, 135, 136, 141, 145
  - Picking, 142
  - Piezoelectric, 97
  - Pinch-outs, 122, 146
  - Point-Diffractor, vi, 60
  - Poisson's Ratio, 35
  - Post-stack processing, 123
  - Post-Stack Processing, viii, 135
  - Potential Methods, 2
  - Poulter method, 91
  - Preconditioned data, 121
  - Predictive, 130, 188, 189
  - Pre-stack, iii, 123, 127
  - Pre-Stack, viii, 127
  - Processing computer, 119
  - Processing parameters, 121, 139
  - Processing Sequence, vii, 122
  - Processing system, 119, 120, 124, 126
  - Production drilling, 11
  - Pulse, 24, 43, 46, 50, 91, 95
  - P-wave, 23, 37, 38, 39, 46, 48, 54, 55, 184
  - P-waves, 48
  - QC'ing purposes, 124
  - Radioactivity, v, 2, 10, 18, 26
  - Radioactivity Logging, v, 18
  - Radioactivity Method, v, 10
  - Ramp, 134, 135
  - Ramp scaling function, 134
  - Raw Data, vii, 124
  - Ray, vi, 19, 21, 24, 26, 43, 44, 46, 47, 48, 58, 60, 61, 62, 63, 66, 67, 69, 70, 71, 76, 78, 80, 86, 108, 109, 132, 134
  - Rayleigh, 38, 40, 41
  - Receiver, 2, 7, 8, 16, 22, 54, 58, 59, 66, 69, 78, 83, 85, 86, 87, 88, 89, 90, 97, 98, 99, 104, 105, 106, 108, 113, 114, 121, 126, 129, 133
  - Receivers, 16, 22, 70, 73, 83, 85, 86, 87, 102, 105, 106, 107, 138
  - Recording, ii, 1, 2, 10, 20, 23, 24, 69, 83, 87, 90, 92, 95, 97, 98, 99, 101, 104, 112, 113, 125, 126, 128, 135, 139
  - Reflected wave, 69
  - Reflection, iii, viii, 1, 2, 3, 38, 41, 42, 43, 46, 47, 48, 50, 53, 54, 55, 56, 57, 58, 59, 60, 61, 62, 63, 65, 69, 75, 83, 84, 86, 87, 90, 91, 94, 96, 97, 99, 103, 104, 107, 108, 111, 119, 121, 122, 123, 124, 125, 126, 127, 128, 129, 130, 131, 132, 133, 134, 135, 136, 137, 138, 139, 140, 141, 142, 145, 146, 151, 165, 168, 183, 184, 185, 186, 187, 190
  - Reflection Arrivals, 2
  - Reflection coefficient, 50, 55, 56
  - Reflection data processing, vii, 119
  - Reflection picking, 142
  - Reflection surveying, 1
  - Reflections, 24, 41, 56, 57, 60, 69, 87, 89, 99, 106, 189
  - Reformatting, 119, 125
  - Refracted wave, 70
  - Refraction, iii, 1, 2, 3, 38, 41, 46, 47, 48, 53, 55, 57, 65, 66, 67, 68, 69, 70, 71, 72, 73, 74, 75, 78, 79, 80, 99, 100, 101, 130, 186, 188, 189
  - Refraction Arrivals, 2
  - Resistivity logs, 16
  - Resolution cells, 111
  - Re-sorted, 125, 131, 152
  - Restoration, 122
  - Reverberation, 99
  - Reverberations, 130
  - Reverse, 77, 78, 130, 173, 174, 175, 176, 177, 178, 181
  - Reverse shooting, 77
  - Rotary Drilling, 12
  - S/N enhancement, 43
  - S/N ratio, 42, 43, 92, 121, 136
-

- 
- Sampling frequency, 127  
Second gate-position, 131  
Seis-loop, 114  
Seismic, ii, iii, viii, 1, 2, 3, 22, 23, 24, 25, 26, 29, 32, 33, 38, 41, 42, 43, 44, 45, 46, 47, 48, 49, 50, 51, 53, 54, 55, 56, 57, 58, 59, 60, 61, 62, 63, 65, 66, 67, 68, 69, 70, 71, 72, 83, 84, 85, 86, 87, 89, 90, 91, 92, 93, 94, 95, 96, 97, 98, 99, 101, 102, 103, 104, 105, 106, 108, 111, 112, 119, 120, 121, 122, 123, 124, 125, 126, 128, 130, 131, 132, 133, 134, 135, 136, 137, 138, 139, 140, 141, 142, 143, 144, 145, 146, 150, 151, 152, 153, 155, 156, 160, 165, 166, 167, 168, 169, 170, 173, 179, 180, 181, 182, 183, 184, 185, 186, 187, 188, 189, 190  
Seismic Attribute, 145  
Seismic Attributes, viii, 145  
Seismic exploration, ii, iii, 1, 2, 43, 46, 53, 62, 97, 103, 112, 165, 189  
Seismic Field, vi, vii, 43, 101  
Seismic Method, v, 2, 190  
Seismic migration, 63, 120, 122  
Seismic Noise, v, 41  
Seismic profiling, 87  
Seismic Reflection, vii, 90  
Seismic refraction, vi, 65  
Seismic stratigraphy, 145  
Seismic Trace, vi, 50, 83  
Seismic Waves, v, 43  
Seismic waves, v, 29  
Seismogram, 25, 104, 155, 167  
Seismograms, 23, 38, 40, 41, 50, 69, 188  
Seismology, 1, 146, 185, 187, 188, 189  
Seismometers, 96  
Seismo-stratigraphic, 144  
Seis-square, 114  
Self Potential (SP), 8  
Shear, 30, 31, 32, 35, 36, 37, 39  
Shear, v, 32, 36, 37  
Shift-and-shoot, 86, 115  
Shift-and-shoot process, 86  
Shooting, 24, 59, 72, 77, 81, 85, 86, 87, 89, 91, 98, 99, 100, 101, 104, 105, 106, 112, 113, 114, 115, 123, 124, 125, 126, 130, 131, 186  
Shooting, vii, 77, 86, 98, 102, 115, 188  
Shooting updip, 77  
Shooting-spread, 59  
Short wavelets, 94  
Shot records, 41, 42, 120, 123, 124, 126, 127, 131  
Shot-gather, 83, 86, 124, 127  
Shot-gathers, 131  
Shot-hole, 98, 99, 102  
Shotpoint, 88, 100  
Shot-point, 83, 85, 86, 87  
Shot-point, 95  
Shot-point, 100  
Shot-point, 101  
Shot-point, 104  
Shot-point, 108  
Shot-point, 127  
Shot-traces, 120  
SH-wave, 39, 41, 48  
Signal, iii, 1, 41, 42, 43, 48, 50, 90, 92, 94, 95, 97, 99, 119, 121, 125, 127, 131, 136, 139, 140, 156  
Signal Enhancement, vii, 97, 121  
Single source-dual streamer, 112, 113  
Single source-single streamer., 112, 113  
Single-fold, 87  
Snell's law, 67, 69, 71  
Snell's Law, vi, 66  
Software, 106, 111, 119, 124, 125, 126, 127, 128, 131, 153  
Sonde, 14, 15, 16, 17, 19, 20, 21, 22, 23  
Sonic logging, 22  
Sonic Logging, 22  
Sorting, 131  
Source-receiver, 66, 86, 105, 108  
Spectra, 42, 139, 146  
Spectral attributes, 146  
Spectrum parameters, 146  
Spectrum-Centroid, 146  
Spherical wave-fronts, 44, 49  
Spider diagram, 110  
Spike, 96  
Spiking, 130  
Split, 85  
Spontaneous Potential (SP) Logging, 17  
Spread, iii, 16, 44, 65, 83, 85, 86, 87, 88, 89, 98, 100, 101, 105, 107, 108, 112, 113, 114, 115, 131, 151, 184  
Spread Configuration, vii, 85  
Spread movement, 113, 115  
Spread Template, vii, 114
-

- Square-spread, 114
  - Stack, viii, 135, 136, 137
  - Stack trace, 135, 136, 145
  - Stacking velocity, 140, 142, 170
  - Stack-trace, 121
  - Static correction, 99, 120, 121, 129, 130, 133, 136
  - Static correction, 129, 133, 156
  - Static Correction, 129
  - Statistics, 123, 124, 126
  - Steam-Gun, 95
  - Strain, 29, 30, 31, 32, 33, 34, 35, 36, 37, 39, 43
  - Strain, v, 30, 31, 32, 34
  - Stratigraphic interpretation, 122, 124, 141, 143
  - Stratigraphic interpretation sequence, 143
  - Stress, 29, 30, 31, 32, 34, 35, 36, 37
  - Stress, v, 29, 34
  - Structural contour map, 142
  - Structural Interpretation, viii, 142
  - Sublines (SL), 111
  - Surface coverage, 88
  - Surface waves, 38, 40, 41
  - Surface Waves, v, 40
  - Surface-reflector, 53
  - Survey design, 90
  - Susceptibility, 5
  - SV-wave, 39, 48
  - SV-waves, 40, 48
  - Swath shooting, 114, 115
  - S-waves, 37, 39, 41
  - Sweep Removal, 125
  - Synthetic, 23, 25, 50, 104, 155, 167
  - Taper, 94, 95
  - TAR, 128, 129
  - Telluric Currents, 6, 9
  - Template, 114, 115
  - Terminated reflectors, 137
  - Terminating reflector, 138
  - Thickness, 41, 66, 73, 74, 75, 80, 99, 100, 101, 130, 142, 149, 159, 160, 163, 164, 184
  - Three Dimensional, vii, 103
  - Thumper, 91
  - Tie well, 142
  - Time slice, 111
  - Time-distance curve, 73, 76, 79
  - Time-slices, 105, 116
  - Topographic Surveying, 102
  - Trace Editing, 127
  - Trace Header Assignment, 126
  - Trace Muting, 134
  - Trace Re-sorting, 88
  - Trace-gather, 83, 108, 109, 121, 133, 135
  - Traction, 29
  - Transgression, 158, 161, 162, 163
  - Transverse Waves, 39
  - Travel-time, 2, 23, 24, 43, 49, 50, 56, 57, 58, 61, 62, 65, 69, 71, 72, 74, 75, 77, 79, 80, 81, 99, 101, 121, 122, 129, 133, 139, 141
  - Travel-Time Corrections, 121
  - Travel-time curve, 72
  - Travel-time curves, 62, 72, 74, 101
  - Travel-times, 22, 74, 101, 119, 124
  - True Amplitude Recovery, 128
  - T-spread, 114
  - Unbalanced-spread, 85
  - Unipulse, 95
  - United States of America, 1
  - Up-dip shooting, 79
  - Up-hole, 99, 102, 130
  - Up-hole Surveying, 99
  - Up-sweep, 94
  - Vaporchoc, 95
  - Variable-area trace, 83
  - Variable-density trace, 83
  - Velocity, 2, 22, 23, 24, 26, 37, 38, 39, 40, 41, 42, 43, 45, 46, 49, 50, 55, 56, 58, 59, 61, 62, 65, 66, 67, 68, 69, 70, 71, 72, 73, 75, 77, 78, 79, 80, 81, 91, 96, 97, 98, 99, 100, 101, 104, 111, 121, 122, 124, 128, 129, 130, 131, 132, 140, 142, 144, 158, 170, 183, 186, 190
  - Velocity Analysis, 140, 189
  - Velocity Map, 142
  - Vertical Seismic Profiling (VSP), 24
  - Vertical stacking, 92, 95, 126, 128, 135
  - Vertical stacking, 125, 126
  - Vertical Stacking, 125
  - Vertical travel-path, 100
  - Vibration, 41, 46, 50, 93, 94, 95, 96, 97, 104
  - Vibroseis, 95, 99, 125, 151
  - Vibroseis, 1, 93, 94, 95, 102, 125
  - Vibroseis-trucks, 95
  - VSP, 22, 24, 25, 26, 142
-

- VSP surveying, 22
  - Walk-away test, 98
  - Wave arrivals, 2, 53, 57
  - Wave scattering, 60
  - Waveform, 43, 46, 48, 99, 121, 141
  - Wave-fronts, 49
  - Wavelet, 2, 48, 50, 128, 130, 135, 139, 141, 145, 146
  - Waves, 1, 2, 10, 22, 24, 29, 37, 38, 39, 40, 41, 42, 43, 44, 45, 48, 53, 54, 55, 60, 62, 65, 69, 70, 71, 72, 73, 74, 75, 90, 91, 92, 93, 97, 99, 127, 146, 168, 186
  - Weak traces, 127
  - Weathered-layer, 100
  - Weathering zone, 56, 66, 130
  - Weight dropping, 92, 99, 125
  - Weight Dropping, 91
  - Weight-dropping, 1
  - Well Casing, v, 12
  - Well completion, 26
  - Well logging, 14, 15, 25
  - Well logs, 12, 15, 25, 26
  - Well Rotary Drilling, v, 12
  - Well shooting, 22
  - Well Velocity Surveying, 23
  - Well-depth, 14, 23
  - Wenner configuration, 6
  - Western Desert, viii, 149, 150, 183, 184, 186
  - Whitening, 130
  - Whole trace, 131
  - Wiggly-trace, 83
  - Wildcat drilling, 11
  - Window, 139, 146
  - Xcrossover, 74
  - X-spread, 114
  - Young's Modulus, 35
  - Zero-offset positions, 120
-

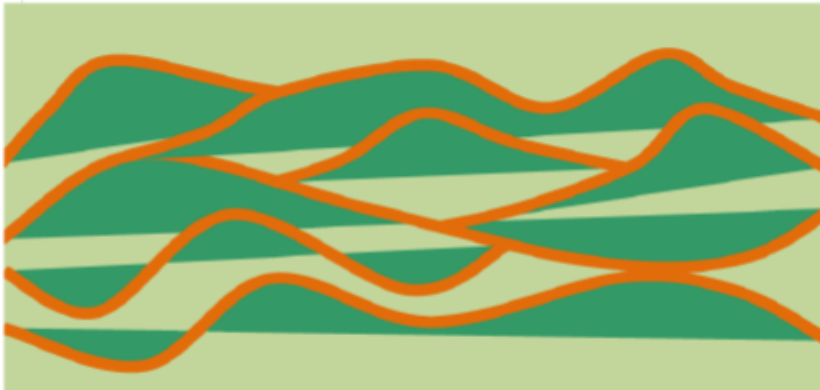


ھەرئىمى كوردستانى عىراق  
وھزارەتى خويىندى باﻻو توپزىنەھەى زانستى  
زانكۆى سلېمانى  
كۆلچى زانست / بەشى جىۋلۇجى

سەرەتايەك بۆ

# لېگەرانى لەرزەىى

حامد نىار السعدى (شارمزا؛ دكتورا لە جىۋفېزىك)  
عزالدىن نىم الدىن بابان (پروڧېسور؛ دكتورا لە جىۋفېزىك)  
بىداچوونەھە:  
بختىار قادر عزيز (پروڧېسور؛ دكتورا لە جىۋفېزىك)



چاپى يەكەم ۲۰۲۰

لەسەر ئەركى زانكۆى سلېمانى لە ھەرئىمى كوردستانى عىراق چاپكراوھ